

Norfolk Boreas Offshore Wind Farm

Appendix 17.8

Norfolk Boreas Offshore Wind Farm Stage 4 Palaeoenvironmental Assessment

Environmental Statement

Volume 3

Applicant: Norfolk Boreas Limited
Document Reference: 6.3.17.8
RHDHV Reference: PB5640-006-0178
Pursuant to APFP Regulation: 5(2)(a)

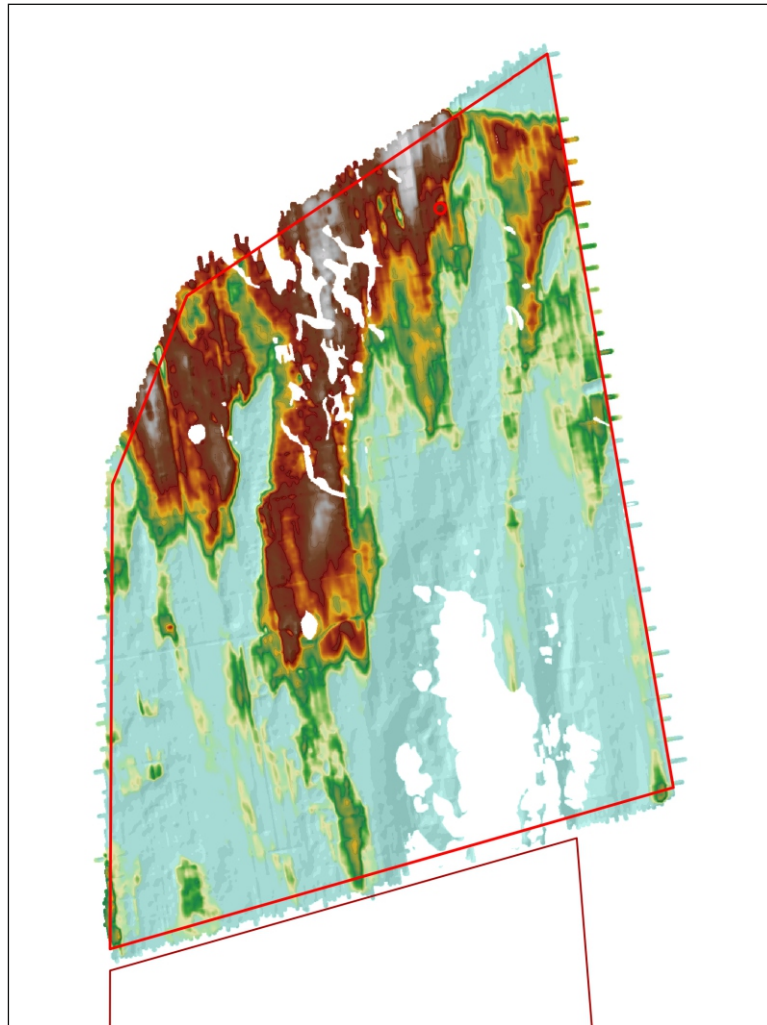
Date: June 2019
Revision: Version 1
Author: Wessex Archaeology

Photo: Ormonde Offshore Wind Farm



Norfolk Boreas Offshore Wind Farm

Stage 4 Palaeoenvironmental Analysis



Ref: 117122.01
March 2019



© Wessex Archaeology Ltd 2019, all rights reserved.

Portway House
Old Sarum Park
Salisbury
Wiltshire
SP4 6EB

www.wessexarch.co.uk

Wessex Archaeology Ltd is a Registered Charity no. 287786 (England & Wales) and SC042630 (Scotland)

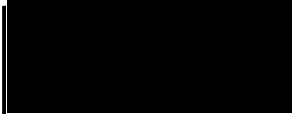
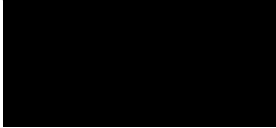
Disclaimer

The material contained in this report was designed as an integral part of a report to an individual client and was prepared solely for the benefit of that client. The material contained in this report does not necessarily stand on its own and is not intended to nor should it be relied upon by any third party. To the fullest extent permitted by law Wessex Archaeology will not be liable by reason of breach of contract negligence or otherwise for any loss or damage (whether direct indirect or consequential) occasioned to any person acting or omitting to act or refraining from acting in reliance upon the material contained in this report arising from or connected with any error or omission in the material contained in the report. Loss or damage as referred to above shall be deemed to include, but is not limited to, any loss of profits or anticipated profits damage to reputation or goodwill loss of business or anticipated business damages costs expenses incurred or payable to any third party (in all cases whether direct indirect or consequential) or any other direct indirect or consequential loss or damage.

Document Information

Document title	Norfolk Boreas Offshore Wind Farm
Document subtitle	Stage 4 Palaeoenvironmental Analysis
Document reference	117122.01
Client name	Royal HaskoningDHV
Address	2 Abbey Gardens Great College St Westminster London SW1P 3NL
On behalf of	Norfolk Boreas Limited.
Address	First Floor 1 Tudor Street London EC4Y 0AH
Site location	Southern North Sea
Planning authority	Marine Management Organisation
WA project name	Boreas Geoarchaeology Stage 4
WA project code(s)	117122 (117120; 117121)
Project management by	David Norcott
Document compiled by	Claire Mellett
Contributions from	Alex Brown, Ines Lopez-Doriga, Dave Howell, Megan Metcalfe, Andrew Shaw, Louise Tizzard, Nigel Cameron and Phil Toms
Graphics by	Kitty Foster

Quality Assurance

Issue and date	Status	Author	Approved by
1	28/02/2019	External draft	CLM
			DRN 
2	14/03/2019	Revised after client comments	CLM
			DRN 

DATA LICENCES

This product has been derived in part from material obtained from the UK Hydrographic Office with the permission of the UK Hydrographic Office and Her Majesty's Stationery Office.

© Crown copyright, [2019]. Wessex Archaeology Ref. HA294/007/316-01.

The following notice applies:

NOT TO BE USED FOR NAVIGATION

WARNING: The UK Hydrographic Office has not verified the information within this product and does not accept liability for the accuracy of reproduction or any modifications made thereafter.

This product has been derived in part from material obtained from the UK Hydrographic Office with the permission of the Controller of Her Majesty's Stationery Office and UK Hydrographic Office (www.ukho.gov.uk).

Contains Ordnance Survey data © Crown copyright and database rights [2019]



Contents

Summary	iii
Acknowledgements.....	i
1 INTRODUCTION	1
1.1 Project background.....	1
1.2 Summary of previous works.....	1
1.3 Scope of report.....	3
2 AIMS AND OBJECTIVES.....	4
3 GEOARCHAEOLOGICAL BACKGROUND.....	5
3.1 Geological baseline	5
3.2 Archaeological record	6
4 METHODS.....	9
4.1 Stage 4 analysis	9
4.2 Diatom analysis	10
4.3 Pollen and charcoal analysis.....	10
4.4 Plant macrofossils.....	11
4.5 Radiocarbon dating and chronological modelling.....	12
4.6 Optical dating.....	12
4.7 Palaeogeographic reconstructions.....	15
5 RESULTS.....	16
5.1 Deposit model.....	16
5.2 Diatom analysis	18
5.3 Pollen and charcoal analysis.....	19
5.4 Plant macrofossils.....	23
5.5 Radiocarbon dating and chronological modelling.....	25
5.6 Optical dating.....	27
5.7 Palaeogeographic reconstructions.....	29
6 DISCUSSION	30
6.1 Introduction.....	30
6.2 Middle to Upper Palaeolithic (Early-Mid Devensian) [MIS 5e – MIS 3]	30
6.3 Late Upper Palaeolithic to Mesolithic (Late Devensian to Holocene) [MIS 2-1]	34
7 CONCLUSIONS	40
8 RECOMMENDATIONS	41
REFERENCES	42
APPENDICES	1
Appendix 1 – list of sub-samples.....	1
Appendix 2 – raw pollen data.....	1
Appendix 3 – radiocarbon dating reports.....	1
Appendix 4 – OSL dating report.....	1
Appendix 5 – Norfolk Boreas site stratigraphy (deposit model)	2

List of Figures

Figure 1	Location of the Norfolk Boreas Project Area
Figure 2	Chronostratigraphic framework for the last 1 MA
Figure 3	Norfolk Boreas extent and location of deposits and palaeolandscape features mapped from geophysical data



-
- Figure 4** Pleistocene ice limits
Figure 5 Location of geotechnical vibrocores showing stages of geoarchaeological assessment/analysis
Figure 6 Vibrocore log and geophysical palaeolandscape assessment showing palaeoenvironmental and dating, results and interpretation, for VC016
Figure 7 Vibrocore log and geophysical palaeolandscape assessment showing palaeoenvironmental and dating, results and interpretation, for VC028
Figure 8 Vibrocore log and geophysical palaeolandscape assessment showing palaeoenvironmental and dating, results and interpretation, for VC032
Figure 9 Vibrocore log and geophysical palaeolandscape assessment showing palaeoenvironmental and dating, results and interpretation, for VC039
Figure 10 Vibrocore log and geophysical palaeolandscape assessment showing palaeoenvironmental and dating, results and interpretation, for VC047
Figure 11 Diatom species percentage counts, for VC032
Figure 12 Percentage of total diatoms within each halobian (salinity) group, for VC032
Figure 13 Pollen diagram VC028
Figure 14 Pollen diagram VC032
Figure 15 Pollen diagram VC039
Figure 16 Composite diagram showing relationship between pollen assemblages in VC028, VC032 and VC039, and key vegetation phases
Figure 17 Bayesian modelling of radiocarbon dates
Figure 18 Palaeogeography of Norfolk Boreas during the Early Devensian
Figure 19 Horizons mapped from seismic data (Fugro 2018)
Figure 20 Middle to Upper Palaeolithic sea-level and palaeolandscape history of Norfolk Boreas
Figure 21 Schematic cross section of site stratigraphy (deposit model)
Figure 22 Upper Palaeolithic to Mesolithic sea-level and palaeolandscape history of Norfolk Boreas

List of Tables

- Table 1** Previous marine archaeological works in support of the Norfolk Boreas project area
Table 2 Stages of geoarchaeological assessment and recording.
Table 3 Parameters used in Early Devensian palaeogeographic model
Table 4 Shallow-stratigraphy of the Norfolk Boreas site (deposit model)
Table 5 Plant macrofossils
Table 6 AMS radiocarbon dates
Table 7 Bayesian modelling of Vegetation Phases
Table 8 Dose Rate (D_r) and Equivalent Dose (D_e) and resulting OSL age estimates. Age estimates expressed in ka relative to year of sampling. Uncertainties in age are quoted at 1 σ confidence and include combined systematic and experimental variability.
Table 9 Palaeogeography of the Norfolk Boreas site during Early to Mid-Devensian
Table 10 Archaeological potential of deposits studied within the Norfolk Boreas site



Summary

Wessex Archaeology (WA) were commissioned by Royal HaskoningDHV to undertake Stage 4 paleoenvironmental analysis and dating of vibrocore samples retrieved from within the Norfolk Boreas site.

The results presented in this report build upon previous geoarchaeological and geophysical works that included a review of geotechnical vibrocore logs, geoarchaeological recording, deposit modelling, palaeoenvironmental assessment, dating and palaeolandscape feature mapping from seismic data (WA 2018a; 2018b; 2018c; 2018d). Additional results presented here for the first time include Infra-red Stimulated Luminescence (IRSL) dating of sub-samples from Upper Brown Bank deposits, and high-resolution pollen and diatom analysis and radiocarbon dating of Late Devensian to Early Holocene sediment sequences comprising peat and over/underlying minerogenic deposits.

The principal aim of this report is to assess the submerged palaeolandscape resource within the Norfolk Boreas project area by integrating the results from all stages of marine geoarchaeological and geophysical works. The report focusses on two key periods; Middle to Upper Palaeolithic, and late Upper Palaeolithic to Mesolithic, which are represented by deposits belonging to Upper Brown Bank (Unit 5) and Elbow Formation (Unit 7), respectively.

The age and depositional history of Upper Brown Bank deposits is of archaeological interest, as establishing whether the southern North Sea was marine or terrestrial during the early parts of the last glacial period can help address questions regarding the lack of evidence for hominins in Britain at this time.

The results suggest Upper Brown Bank was deposited in an outer estuarine environment within a shallow embayment between 83.2 ± 9.5 and 69.8 ± 7.7 ka (MIS 5a-4), during a period of climatic instability and fluctuating sea levels in the Early Devensian. Palaeogeographic modelling shows that at times of low sea level there is potential for parts of Norfolk Boreas to become partially exposed, creating a coastal plain along the margins of an estuary or restricted embayment/lagoon. The Brown Bank embayment appears to have been a persistent feature in the landscape until ~57 ka, when sea levels fell low enough to fully expose the southern North Sea. Interestingly, this broadly correlates to the timing of reoccupation of Britain (~60 ka). Therefore, it could be argued that the presence of the Brown Bank embayment created a significant geographic barrier to migration pathways through the southern North Sea during the Middle Palaeolithic.

Doggerland, the area of the southern North Sea that was previously sub-aerially exposed, is known for its potential to preserve prehistoric archaeology. Reconstructing environmental change using samples from submerged palaeolandscapes is important for identifying where archaeology may be most likely to be preserved, but also for providing a landscape context for any prehistoric activity. For this reason, Late Devensian to Early Holocene minerogenic and peat deposits belonging to the Elbow Formation (Unit 7) were targeted for palaeoenvironmental analysis and dating.

An extensive submerged palaeolandscape characterised by a network of meandering river channels fringed by wetland and woodland areas has been identified within Norfolk Boreas. Unit 7a represents deposition in an active river environment during the Late Devensian (10435 ± 66 BP; UBA-39472; 12550-12080 cal. BP). Peat development commenced at the start of the Early Holocene at 9992 ± 51 BP (UBA-38190; 11710-11260 cal. BP) and continued for a period of up to ~700 years.

Unit 7 documents up to ~3,000 years of environmental history and shows the landscape of the Norfolk Boreas site was initially open grassland with localised reed and fen wetlands. During the early Holocene, woodland returned dominated initially by pine and later by hazel with some oak and



elm. Inundation of the landscape is marked by an increase in vegetation tolerant to increased salinity marking a shift to saltmarsh and mudflat environments. The presence of charcoal in peat deposits provides evidence of repeated fire-events, which may have been caused by human activity or natural processes.

The results from one new sea-level index point points suggest Norfolk Boreas was flooded by rising sea levels at ~9700 cal. BP. Rates of sea-level rise were rapid at this time, which is thought to be a significant factor in the exceptional preservation observed. Modern seabed processes appear to play a role in both preserving, through burial, and exposing, through erosion, palaeolandscape features.

By integrating marine geoarchaeological and geophysical techniques, we have identified an extensive, previously unknown submerged palaeolandscape resource within the Norfolk Boreas site. The results have been used to reconstruct vegetation and environmental history over a period of up to 3,000 yrs, from the late Upper Palaeolithic to early Mesolithic. They have also been used to reappraise the formation history of Middle to Upper Palaeolithic deposits in relation to southern North Sea palaeogeography at a time when humans are apparently absent from Britain. To maximise the impact of this work, it is recommended the results are published as two period-specific articles in a peer-reviewed journal.



Acknowledgements

This work was commissioned by Royal HaskoningDHV on behalf of Norfolk Boreas Ltd. We would like to thank Victoria Cooper and David Tarrant of Royal HaskoningDHV for their support during production of this report, as well as Fugro and Joseph Hine of Vattenfall for provision of seismic interpretations.

This report was compiled by Dr Claire Mellett, Wessex Archaeology (WA). Diatom analysis was carried out by Dr Nigel Cameron of University College London. Optical dating was undertaken at University of Gloucestershire by Prof. Phil Toms. Radiocarbon dating was carried out at 14 Chrono Centre, Queens University, Belfast. Pollen analysis was undertaken by Dr Alex Brown (WA), plant macrofossil assessment and chronological modelling was undertaken by Dr Ines Lopez Doriga (WA) and Nicki Mulhall (WA) carried out sub-sampling and macrofossil extraction. Geophysical data assessment was undertaken by Megan Metcalfe (WA) and Dave Howell (WA). Palaeogeographic modelling was carried out by Dr Claire Mellett (WA). Dr Louise Tizzard (WA) and Dr Andrew Shaw provided technical review. Illustrations were prepared by Kitty Foster (WA). Quality control and project management was provided by Dave Norcott (WA).

Norfolk Boreas Offshore Wind Farm

Stage 4 Palaeoenvironmental Analysis

1 INTRODUCTION

1.1 Project background

1.1.1 Wessex Archaeology (WA) have been commissioned by Royal HaskoningDHV on behalf of Norfolk Boreas Limited. to undertake Stage 4 paleoenvironmental analysis and dating of vibrocores within the proposed Norfolk Boreas offshore project area (**Figure 1**).

1.1.2 The Norfolk Boreas offshore project area comprises the offshore wind farm array (the site), the offshore cable corridor and area of project interconnectors cables. The Norfolk Boreas site is located approximately 73 km (39 nautical miles) northeast of Great Yarmouth within the southern North Sea (**Figure 1**).

1.1.3 The Norfolk Boreas site lies within a region of the southern North Sea known to preserve nationally and internationally important archaeological and geoarchaeological records from the last one million years (Bicket and Tizzard 2015), which formed part of a vast habitable plain connecting Britain with the rest of the European continent at the end of the last ice age. This landscape was later submerged by rising post-glacial sea levels with full marine conditions occurring across the southern North Sea basin by ca. 8,000 yrs before present (BP) (**Figure 2**).

1.2 Summary of previous works

1.2.1 Marine archaeological works in support of the Norfolk Boreas Offshore Wind Farm project have been ongoing since 2017 (**Table 1**) and include assessment of marine geotechnical (WA 2018a; 2018b; 2018d) and geophysical Norfolk Boreas site specific surveys (WA 2018c) undertaken in support of the proposed development.

1.2.2 An assessment of geophysical data, principally sub-bottom seismic data, identified 190 features with palaeogeographic potential within the Norfolk Boreas site. These included extensive areas of intermittent high amplitude reflectors representing organic rich deposits, possibly peat, and associated buried palaeochannels (WA 2018c; **Figure 3**).

1.2.3 A geotechnical survey campaign was undertaken in October 2017 during which a total of 61 vibrocores were recovered from 50 locations within the Norfolk Boreas site reaching depths of up to 6 m below sea floor (mbsf). These vibrocores provided a continuous record of the deposits within ~6 m of the seabed. Preliminary geotechnical logs and associated test results were subsequently provided to WA for a Stage 1 geoarchaeological review (WA 2018a).

1.2.4 The Stage 1 geoarchaeological review identified deposits of potential archaeological interest in thirteen vibrocores, assigning them a high or medium priority status, with a further 48 vibrocores assigned low priority geoarchaeological status with no further work recommended (WA 2018a).



- 1.2.5 Eight vibrocores (VC003, VC005, VC005a, VC010, VC013a, VC024, VC029 and VC033) were assigned medium priority status and were opened under supervision of a suitably trained geoarchaeologist at Fugro House, Wallingford (31st October - 1st November 2017). No deposits of geoarchaeological significance were noted during the monitoring of these medium priority vibrocores and no further work was recommended.
- 1.2.6 Five vibrocores (VC016, VC028, VC032, VC039 and VC047) were assigned high priority status due to the presence of organic material and thick sequences of fine-grained deposits. These vibrocores were not split or subsampled for geotechnical testing and were delivered to WA for Stage 2 geoarchaeological recording. Descriptions of these high priority vibrocores, along with all vibrocore geotechnical logs, were used as a basis to construct a deposit model for the Norfolk Boreas project area (Wessex Archaeology 2018b).
- 1.2.7 Stage 2 geoarchaeological recording and deposit modelling identified two units of geoarchaeological interest: Early Devensian sandy clays and silts of the Brown Bank Formation, and; Early Holocene pre-transgression peats and associated under/overlying minerogenic sediments. It was recommended that Stage 3 sub-sampling and palaeoenvironmental assessment be undertaken on these deposits of interest.
- 1.2.8 Five vibrocores were subject to Stage 3 palaeoenvironmental assessment (VC016, VC028, VC032, VC039 and VC047). Upper Brown Bank deposits were targeted in VC016 and VC047 for Optical Stimulated Luminescence (OSL) dating and accompanying assessment of foraminifera, ostracods and diatoms, to determine age and palaeoenvironment. To help establish the depositional environment of an Undifferentiated unit, samples from VC016 and VC047 were submitted for foraminifera and ostracod assessment. Holocene pre-transgression peat deposits in VC028, VC032 and VC039 were selected for radiocarbon dating as they showed the greatest potential for preservation of pollen and plant macrofossils which would provide information on landscape development. Diatoms, foraminifera and ostracod assessment was also undertaken on these cores across transitions between peat and the over/underlying minerogenic sediments. The key results of the Stage 3 palaeoenvironmental assessment are summarised in Section 5 and 6 of this report.

Table 1 Previous marine archaeological works in support of the Norfolk Boreas project area

Report type	Title	Report no.	Reference
Stage 1	Norfolk Boreas Offshore Wind Farm Stage 1 Geoarchaeological Review	117120.01	WA 2018a
Stage 2	Norfolk Boreas Offshore Wind Farm Stage 2 Geoarchaeological Review	117120.02	WA 2018b
Geophysics	Norfolk Boreas Offshore Wind Farm Archaeological Assessment of Geophysical Data	117120.03	WA 2018c
Stage 3	Norfolk Boreas Offshore Wind Farm Stage 3 Geoarchaeological Assessment	117121.01	WA 2018d

- 1.2.9 Concurrently, a series of geophysical and geoarchaeological works were undertaken in support of the proposed Norfolk Vanguard Offshore Wind Farm project area which lies directly south, and west of the Norfolk Boreas site (**Figure 1**). A palaeolandscapes assessment of geophysical data was undertaken and identified features of archaeological interest that included buried palaeochannels and areas of possible organic deposits (WA 2017a). A total of 65 vibrocores were recovered from the Norfolk Vanguard project area and after Stage 1 geoarchaeological recording (WA 2017b), 22 vibrocores were recommended



for Stage 2 geoarchaeological recording (WA 2018e), of which five vibrocores were selected for Stage 3 and Stage 4 palaeoenvironmental works WA 2018f; WA 2019).

- 1.2.10 The results from Stage 4 palaeoenvironmental analysis (WA 2019) reveal the deposits at the Norfolk Vanguard site are contemporaneous with those in the Norfolk Boreas site, suggesting the features and deposits identified are part of a much larger submerged landscape that has not been identified to date.

1.3 Scope of report

- 1.3.1 To help frame geoarchaeological investigations of this nature, WA has developed a five-stage approach, encompassing different levels of investigation appropriate to the results obtained, accompanied by formal reporting of the results at the level achieved. The stages are summarised below (**Table 2**).
- 1.3.2 This report presents the results of Stage 4 palaeoenvironmental analysis and integrates the results of the previous geoarchaeological and geophysical assessments to reconstruct palaeoenvironmental evolution of the Norfolk Boreas site in relation to the submerged palaeolandscapes resource.

Table 2 Stages of geoarchaeological assessment and recording.

Stage	Method	Description
1	Review	A desk-based archaeological review of the borehole, vibrocore and CPT logs generated by geotechnical contractors. Aims to establish the likely presence of horizons of archaeological interest and broadly characterise them, as a basis for deciding whether and what Stage 2 archaeological recording is required. The Stage 1 report will state the scale of Stage 2 work proposed.
2	Geoarchaeological recording and deposit modelling	Archaeological recording of selected retained or new core samples will be undertaken. This will entail the splitting of the cores, with each core being cleaned and recorded. The Stage 2 report will state the results of the archaeological recording and will indicate whether any Stage 3 work is warranted.
3	Sampling assessment and	Dependent upon the results of Stage 2, sub-sampling and palaeoenvironmental assessment (pollen, diatoms and foraminifera) may be required. Subsamples will be taken if required. Assessment will comprise laboratory analysis of the samples to a level sufficient to enable the value of the palaeoenvironmental material surviving within the cores to be identified. Subsamples will also be taken and/or retained at this stage in case scientific dating is required during Stage 4. Some scientific dating (e.g. radiocarbon or Optically Stimulated Luminescence (OSL)) may be undertaken at this stage to provide chronological context. The Stage 3 report will set out the results of each laboratory assessment together with an outline of the archaeological implications of the combined results, and will indicate whether any Stage 4 work is warranted.
4	Analysis dating and	Full analysis of pollen, diatoms and/or foraminifera assessed during Stage 3 will be undertaken. Typically, Stage 4 will be supported by scientific dating (e.g. radiocarbon or OSL) of suitable subsamples. Stage 4 will result in an account of the successive environments within the coring area, a model of environmental change over time, and an outline of the archaeological implications of the analysis.



Stage	Method	Description
5	Final report	If required Stage 5 will comprise the production of a final report of the results of the previous phases of work for publication in an appropriate journal. This report will be compiled after the final phase of archaeological work, whichever phase that is.

2 AIMS AND OBJECTIVES

2.1.1 The principal aim of this report is to assess the submerged palaeolandscape resource within the Norfolk Boreas site by integrating the results from all stages of marine geoarchaeological and geophysical works (see section 1.2).

2.1.2 This will be achieved through the following objectives;

- Present the results from Stage 4 palaeoenvironmental analysis and dating;
- Refine the deposit model, outlining the stratigraphy, depositional environment, age, extent and depth of deposits;
- Reconstruct palaeogeographic and palaeoenvironmental evolution, and;
- Assess the archaeological resource, its preservation potential, and the implications for prehistoric archaeology.

2.1.3 A series of period-specific research questions are proposed below, building upon previous works (WA 2018a; 2018b; 2018c; 2018d) and taking into account the regional research framework (Medlycott 2011) and the national maritime research framework (Ransley et al. 2013).

Middle to Upper Palaeolithic

- What is the age and depositional history of Brown Bank Formation?
- What is the palaeogeography of the area during deposition of Brown Bank Formation?
- How do the findings relate to the presence or absence of hominins in Britain during the Middle Palaeolithic?

Late Upper Palaeolithic to Mesolithic

- What is the age and formation history of the preserved peat deposits?
- What is the landscape and vegetation history?
- Is there evidence for hominin activity?
- What is the timing and nature of landscape inundation?



3 GEOARCHAEOLOGICAL BACKGROUND

3.1 Geological baseline

- 3.1.1 Geoarchaeological assessments are typically undertaken with reference to geological periods (e.g. Quaternary), epochs (e.g. Pleistocene) and sub-epochs (e.g. Devensian) that reflect major climate, sea-level or environmental changes. Here we adopt British nomenclature correlated to the Marine Isotope Stage (MIS) record to distinguish between different climatic periods, with dates given as ka (thousands of years before present). Marine Isotope Stages are deduced from marine palaeoclimatic records and reflect alternating warm (interglacial) and cold (glacial) periods throughout the Quaternary. Some Marine Isotope Stages can be subdivided into sub-stages reflecting relatively warmer (interstadial) or cooler (stadial) periods within a single stage.
- 3.1.2 The Norfolk Boreas offshore project area is located in a region characterised by Pleistocene and Holocene sediments (Cameron et al. 1992), comprising clays, silts, sands and gravels with occasional organic-rich deposits (peats), overlain by recent unconsolidated marine shelly sands.
- 3.1.3 The Pleistocene geological history of the North Sea basin is dominated by repeated glacial/interglacial cycles, resulting in rising and falling sea levels (**Figure 2**) and deposition of terrestrial, marine and glacially-derived sediments. The Norfolk Boreas offshore project area, and southern North Sea in general, is known to contain an important sedimentary archive including material dating from the earliest occupation of North Western Europe (Parfitt et al. 2010) up to more recent post-glacial reoccupation of Britain (Waddington 2015).
- 3.1.4 Only one glacial episode is thought to have directly affected the area. This was during the Anglian period (MIS 12, 480-423 ka) when ice extended into the southernmost North Sea (**Figure 4**). During subsequent glacial episodes, ice sheets terminated further north so did not directly affect the region. However, indirect affects resulting from changing sea levels and cold periglacial conditions will have influenced the region. The exact southern extent of the Anglian glaciation is debatable. However, bathymetric data suggests part of the Anglian ice sheet may have extended as far south as offshore from Felixstowe (Emu 2009), and Dix and Sturt (2011) argue for an Anglian glacial origin for over-deepened valleys (tunnel valleys) identified within the Outer Thames estuary.
- 3.1.5 As the area off East Anglia, including the offshore project area, has only experienced one glacial advance during the Pleistocene (**Figure 4**), palaeolandscape features from periods of low relative sea level are more likely to be preserved here rather than further north (approximately north of the north Norfolk coast), where they have been removed during the subsequent Saalian and Devensian glacial advances. Any surviving Pleistocene deposits may have been reworked or redeposited to a certain extent during subsequent marine transgressions (Cameron et al. 1992), but there is potential for them to survive on the seabed.
- 3.1.6 Potential superficial deposits of geoarchaeological significance likely to be encountered within the Norfolk Boreas site area include the Brown Bank Formation, tentatively dating from the late Ipswichian interglacial to early Devensian glaciation (Limpenny et al. 2011).
- 3.1.7 The Brown Bank Formation includes deposits of silty sand, sandy silt and sandy silty clay, which is in places up to 20 m thick. The sandy silty clay deposits are here termed the Upper Brown Bank, to distinguish them from the underlying deposits of silty sand and sandy silt

that characterise both the Lower Brown Bank (Early Devensian) and underlying Eem Formation (Ipswichian) (Limpenny et al. 2011; Bicket and Tizzard 2015).

- 3.1.8 The Brown Bank Formation is present as a blanket deposit across the general area and has traditionally been interpreted to represent a shallow lagoon environment, comprising clayey silty sands (Cameron et al. 1992; Limpenny et al. 2011).
- 3.1.9 Brown Bank Formation has been previously dated using OSL (WA 2008; Limpenny et al. 2011; Tizzard et al. 2014; 2015) and ages fell into two broad ranges: MIS 3 and MIS 5d-5c. Based on this evidence, it is not clear if Brown Bank Formation was deposited over the duration of the early Devensian, or if deposition was more episodic punctuated by periods of hiatus and sub-aerial exposure (Tizzard et al. 2015). The date of the Brown Bank Formation therefore has significant implications both for our understanding of the palaeogeographic development of the North Sea as well as the nature and significance of any archaeology, if preserved.
- 3.1.10 In places across the southern North Sea a sequence of early Holocene deposits are mapped overlying Pleistocene sediments. The Holocene sediments include organic-rich peats along with more minerogenic fluvial and alluvial sediments, most often infilling channels (Limpenny et al. 2011; Tappin et al. 2011; Tizzard et al. 2015; Gearey et al. 2017; Brown et al. 2018), but also preserved on the Brown Bank Formation or overlying periglacial aeolian sediment. The peats are of high geoarchaeological potential, preserving a range of palaeoenvironmental remains and material suitable for radiocarbon dating.
- 3.1.11 Pleistocene and early Holocene sediments are capped by post-transgression marine sands. The progressive inundation of the North Sea occurred over an extended time scale, with particularly rapid sea-level rise during the early Holocene (11.5-7 ka), and with fully marine conditions occurring by around 6 ka (Sturt et al. 2013). However, limitations in the availability of reliable sea-level index-points (Hazell 2008, WA 2013a), combined with uncertainty around the glacio-isostatic response of the southern North Sea, make it difficult to accurately reconstruct sea-level history and the timing of inundation across the Norfolk Boreas project area.

3.2 Archaeological record

- 3.2.1 The southern North Sea off the east coast of East Anglia is known to contain relatively well preserved palaeolandscape features such as fluvial channels that formed during periods of lower sea level when the southern North Sea was free of ice. The remains of these terrestrial landscapes are frequently recovered by dredging and fishing activities in numerous areas around the southern North Sea, generally in the form of the remains of extinct megafauna (e.g. woolly mammoths, woolly rhinoceros, bison, horse, lion and hyena).
- 3.2.2 The discovery of actual human artefacts, such as stone tools and worked bone, and even remains is a rarer occurrence, but artefacts have been recovered (e.g. Hublin et al. 2009). Reported finds from offshore activity has, to date, produced a range of early prehistoric lithic artefacts indicating early prehistoric activity in submerged palaeolandscapes from Lower, Middle, and Upper Palaeolithic periods (Tizzard et al. 2015; WA 2011; 2013b), with notable collections of more recent Mesolithic artefacts from submerged palaeolandscape contexts (Momber et al. 2011; WA 2013a).
- 3.2.3 The earliest records of Lower Palaeolithic archaeology from northern Europe are associated with terrestrial deposits on the margins of the North Sea basin in East Anglia, most notably from Pakefield (Parfitt et al. 2005) and Happisburgh Site 3 (Parfitt et al. 2010). Whilst the

archaeology at Pakefield was created during a fully interglacial, more Mediterranean climate, at around MIS 17 (**Figure 2**), the remains at Happisburgh Site 3 are older (MIS 21 or MIS 25) and the environmental evidence is indicative of cool conditions at the edge the boreal zone (Candy et al. 2011) which implies that these early hominins were capable of surviving in northern Europe in periods not associated with fully interglacial environments (Parfitt et al. 2010). The importance of these sites is international, as they are currently unique at this latitude for this early date (WA 2013a).

- 3.2.4 Cohen et al. (2012) highlighted the North Sea basin as a key region for understanding Pleistocene hominins within a northerly, coastal environment. The east of England, particularly East Anglia, but also the southeast of England, are important regions for later Middle Pleistocene, Lower Palaeolithic archaeology (MIS 13-MIS 9). During this timeframe British archaeology reflects repeated episodes of hominin occupation during temperate interglacial and cool conditions, separated by phases of hominin absence during fully glacial periods.
- 3.2.5 Archaeological evidence is particularly abundant during MIS 13 and MIS 11 (**Figure 2**) (Wymer 1999; Pettitt and White 2012) when warmer climate conditions meant Britain was again available to be recolonised by hominin communities, after a period of absence during the preceding Anglian glaciation (MIS 12). Lower Palaeolithic archaeological assemblages of this date tend to be characterised by handaxes, although during the earlier part of MIS 11, collections lacking handaxes (termed Clactonian) have been recognised. The foreshore, cliffs and hinterland at Clacton-on Sea (Essex) comprise an important Lower Palaeolithic site which is a designated geological Site of Special Scientific Interest (SSSI). Channel sediments from the area are also an important site for the Lower Palaeolithic Clactonian flint industry and have yielded a rare wooden spear alongside lithic artefacts. This archaeology dates from the Hoxnian interglacial period (MIS 11, c. 423 – 380 ka, **Figure 2**) (Sumbler 1996; Bridgland et al. 1999), and the type site for the Hoxnian (the Hoxne Brick Pit) is located a relatively short distance inland outside of Diss, Suffolk (Ashton et al 2008).
- 3.2.6 During the MIS 10 glaciation (**Figure 2**) there appears to have been a hiatus in hominin activity in Britain (Pettitt and White 2012). The post MIS 10 occupation Britain is associated with the emergence of the Neanderthals and their associated archaeology and patterns of behaviour. From the later part of MIS 9 the archaeological record attests to the development of Levallois core working strategies (White and Ashton 2003). This is also seen to mark the end of the Lower Palaeolithic and the beginning of the Middle Palaeolithic. The Levallois technique comes to dominate the British archaeological record during the early Middle Palaeolithic (late MIS 8 and MIS 7), with handaxe production occurring infrequently (Scott and Ashton 2011).
- 3.2.7 The international importance of early Middle Palaeolithic archaeology in the southern North Sea is highlighted by the numerous sites preserved within the Thames river terraces (White 2006; Scott et al. 2011) and, in particular, by the submerged prehistoric Levallois lithic assemblage from marine aggregate licence Area 240 in the palaeo-Yare catchment. Over 120 artefacts have now been recovered from this locale, some of which are identifiable as Levallois, with many recovered from in situ or minimally disturbed contexts (Tizzard et al. 2014; 2015; WA 2013a; 2013b).
- 3.2.8 The substantial, mixed assemblage of handaxes also recovered from Area 240 may be of older Lower Palaeolithic origin (e.g. >MIS 9, **Figure 2**), or may date to the Later Middle Palaeolithic when handaxes re-emerge as one of the key components of the archaeological record (late MIS 4-MIS 3, **Figure 2**) (Boismier et al. 2012). However, based on

palaeoenvironmental and sedimentological evidence an early Middle Palaeolithic date is most likely (Tizzard et al. 2015).

- 3.2.9 Palaeogeographically, Area 240 is one of the most northerly Neanderthal sites in northwest Europe and of primary archaeological importance for defining Middle Palaeolithic potential and the contemporary palaeogeography across the southern North Sea basin (Tizzard et al. 2014). The site highlights the archaeological potential of preserved Pleistocene fluvial deposits within the southern North Sea.
- 3.2.10 Currently there is no definitive evidence of a hominin presence in Britain during the Ipswichian (MIS 5e) or the early Devensian (MIS 5d-a; Lewis et al. 2011). Within the context of early prehistory and submerged palaeogeography, however, substantial areas of the southern North Sea basin would have been dry land during the warming and cooling limbs of the various sub-stages (MIS 5d to 5a, **Figure 2**) and archaeological sites of this age are relatively abundant in northern France (Lewis et al. 2011; Pettitt and White 2012). Therefore, the potential exists for human activity to have occurred sporadically both within Britain and in any sub-aerially exposed parts of the southern North Sea basin, during the early Devensian.
- 3.2.11 From late MIS 4 to MIS 3 there is evidence in Britain for Neanderthal recolonization. This late Middle Palaeolithic archaeological record is associated with morphologically and technologically distinctive handaxes (White and Jacobi 2002). A key site belonging to this period is Lynford Quarry, Norfolk where a palaeochannel containing mammoth remains and associated late Middle Palaeolithic stone tools and debitage have been recovered (Boismier et al. 2012).
- 3.2.12 Climatically, MIS 3 was significantly colder than now but did not attain the glacial conditions of later or earlier glacial periods (e.g. MIS 6 or 2, **Figure 2**) (Pettitt and White 2012). For the Neanderthals that may have occupied the region at this time, surviving in the southern North Sea during this period may have been subject to a variety of technological and cultural adaptations (White 2006).
- 3.2.13 In the early Upper Palaeolithic, at the end of the Late Pleistocene, Neanderthals were replaced in northern Europe by modern humans who, occupying and moving through the southern North Sea, were present in Britain from around 34 ka (Jacobi and Higham 2011; Bicket and Tizzard 2015). Archaeological evidence for this period consists of blade point/leaf point assemblages, thought to be associated with the final Neanderthal occupation of Britain, and small number of findspots associated with Evolved Aurignacian and Gravettian lithic artefacts which were produced by modern humans (Jacobi and Higham 2011).
- 3.2.14 During the last glacial period, the offshore project area will have been close to the maximum Devensian ice margin (**Figure 4**). At the maximum of the last glacial period, the environment within the southern North Sea was relatively poor for human colonisation, with humans absent from Britain during these peak cold conditions. However, there was increasing human exploitation after ~15 ka. Humans at this time were hunting game, such as mammoth and deer, and evidence of these animals has been reported through marine aggregate dredging, and the associated reporting requirements (Bicket and Tizzard 2015).
- 3.2.15 The onshore archaeological record of later Upper Palaeolithic activity is marked by Creswellian/Final Magdalenian stone tool assemblages associated with the later Upper Palaeolithic recolonization of Britain (Higham and Jacobi 2011b), and offshore locations

may provide unique and important context for coastal and lowland human activity during this period (WA 2013b).

- 3.2.16 The Mesolithic period began in the early Holocene and at around 10 ka, sea levels were approximately 35 m below current levels (Shennan et al. 2018) sub-aerially exposing large parts of the southern North Sea and English Channel making them suitable for human occupation. Archaeological and palaeoenvironmental material from this period has been reported from North Sea contexts for over a century (Reid 1913; Godwin and Godwin 1933). For example, a Maglemosian harpoon artefact was trawled in the early 20th century and was later radiocarbon dated to around 12,000 years ago (Housely 1991).
- 3.2.17 Between 8 and 5 ka, much of the landscape was inundated by eustatically driven sea level change, and by 6 ka sea level was only approximately 7 m below the present level (Shennan et al. 2018). Around this time, Britain became an island again (Coles 1998). Settlements at the time were often transitory and seasonal, and therefore leave little trace in the archaeological record. It is possible that the now submerged environment within the Norfolk Boreas project area was occupied up until the final marine transgression thought to have occurred around 8,000 years ago.
- 3.2.18 It is clear from numerous research and development-led investigations that postglacial marine transgression has not destroyed Pleistocene and Holocene palaeogeography by default (WA 2013b). Areas of preserved palaeogeographic features do remain, and detailed reconstructions of palaeoenvironments and palaeogeography can be achieved for large parts of the North Sea basin (Tappin et al. 2011; Limpenny et al. 2011; Dix and Sturt, 2011).
- 3.2.19 Considerable attention has been paid to Mesolithic landscapes of the southern North Sea (Gaffney et al. 2007; Tappin et al. 2011) as the now-submerged palaeolandscapes provide key contextual evidence for recovered artefacts and a background landscape within which to place these human communities. Increasingly, a maritime perspective has developed for understanding the early prehistoric archaeological record, where coasts, estuaries and wetlands are key landscape elements (Ransley et al. 2013).

4 METHODS

4.1 Stage 4 analysis

- 4.1.1 Of the five vibrocores subject to Stage 3 assessment (WA 2018d) (**Figure 5**), four vibrocores (VC028, VC032, VC039 and VC016) were recommended for additional palaeoenvironmental analysis and dating as part of these Stage 4 works.
- 4.1.2 Recommended works included additional dating of Upper Brown Bank deposits in VC016 to test if dates are conformable. No additional foraminifera and ostracod assessment of Upper Brown Bank deposits was proposed.
- 4.1.3 Pollen analysis and additional radiocarbon dating on peat deposits preserved in VC028, VC032 and VC039 was recommended. Diatom analysis was also recommended on overlying intertidal deposits in VC032. Collectively, the results will be used to reconstruct palaeoenvironmental change at the Norfolk Boreas site from the Late Devensian through to the Early Holocene.
- 4.1.4 Full analytical methods for each palaeoenvironmental and dating technique are described below. All sub-sample depths are quoted as metres below sea floor (mbsf). In some cases, the elevation of sub-samples has been corrected to Lowest Astronomical Tide (LAT).



4.1.5 A full list of sub-samples is presented in **Appendix 1** and shown on **Figures 6-10**.

4.2 Diatom analysis

4.2.1 Five sub-samples from VC032 previously assessed as part of the Stage 3 works (WA 2018d) were selected for Diatom analysis. An additional five new sub-samples were taken for diatom analysis to increase the resolution of the palaeoenvironmental record.

4.2.2 Diatom preparation followed standard techniques (Battarbee et al. 2001). Two coverslips were made from each sample and fixed in Naphrax for diatom microscopy. A large area of the coverslips on each slide was scanned for diatoms at magnifications of x400 and x1000 under phase contrast illumination.

4.2.3 Diatom floras and taxonomic publications were consulted to assist with diatom identification; these include Hendey (1964), Werff & Huls (1957-1974), Hartley et al. (1996), Krammer & Lange-Bertalot (1986-1991) and Witkowski et al. (2000). Diatom species' salinity preferences are indicated using the halobian groups of Hustedt (1953, 1957), these salinity groups are summarised as follows:

1. Polyhalobian: marine $>30 \text{ g l}^{-1}$ salinity
2. Mesohalobian: brackish $0.2\text{-}30 \text{ g l}^{-1}$ salinity
3. Oligohalobian - Halophilous: optimum in slightly brackish water
4. Oligohalobian - Indifferent: optimum in freshwater but tolerant of slightly brackish water
5. Halophobous: exclusively freshwater
6. Unknown: taxa of unknown salinity preference.

4.2.4 Diatom analysis results are presented as percentages of the total number of diatoms counted. Full species percentage counts are presented in **Figure 11** and summarised according to salinity groups in **Figure 12**.

4.3 Pollen and charcoal analysis

4.3.1 Twelve sub-samples previously assessed as part of Stage 3 works were selected for pollen analysis. An additional forty-one sub-samples were taken to allow for a high-resolution reconstruction of past vegetation changes.

4.3.2 In total, fifty-three sub-samples of 1 ml volume were processed using standard pollen extraction methods (Moore et al. 1991), comprising 5 sub-samples from VC028, 35 sub-samples from VC032 and 13 sub-samples from VC039.

4.3.3 Pollen was identified and counted using a Nikon eclipse E400 biological research microscope. A total of 500 terrestrial pollen grains was counted for each sub-sample in addition to fern spores and aquatics. One Lycopodium tablet was added to enable calculation of pollen concentrations. Pollen counts were not possible from 3.83 mbsf (VC032) and 3.07 mbsf (VC039) due to poor preservation and concentration of palynomorphs.

- 4.3.4 Pollen and spores were identified to the lowest possible taxonomic level. Plant nomenclature followed Stace (1997) and Bennett et al. (1994). Pollen sums are based on total land pollen (TLP) excluding aquatics and fern spores which are calculated as a percentage of TLP plus the sum of the component taxa within the respective category. Identification of indeterminable grains was according to Cushing (1967).
- 4.3.5 Pollen diagrams were constructed using Tilia version 1.7.16 (Grimm 2011), with local pollen assemblage zones (LPAZ) determined by eye based on changes in principal pollen taxa (**Figures 13-15**). A composite conceptual model showing the relationship between LPAZs between cores is presented in **Figure 16**.
- 4.3.6 Pollen concentrations were calculated for each 1cm³ volume of sediment using the following sum; (total land pollen ÷ total number of *Lycopodium* spores counted) x (number of *Lycopodium* spores added to sample) x (*Lycopodium* spores in each tablet ÷ sample volume).
- 4.3.7 All pollen data are presented in **Appendix 2**.
- 4.3.8 Microscopic charcoal was quantified for each pollen sample using the point count method of Clark (1982). The point count method expresses the total charcoal count as an estimate of the area of charcoal on any given pollen slide for a standard 1cm³ volume of sediment.
- 4.3.9 Randomly spaced parallel transects were analysed to ensure that a representative portion of the slide was examined. This is important as pollen and microscopic charcoal are not distributed evenly across a microscope slide. Charcoal is identifiable as highly angular, usually opaque black fragments of varying size and shape, sometimes preserving cellular structure. Humified plant matter may appear very dark brown black under the microscope, but unlike charcoal, usually exhibits translucent and rounded edges.
- 4.3.10 Charcoal data are presented in **Appendix 2** and plotted alongside pollen results in **Figures 13-15**.
- 4.4 Plant macrofossils**
- 4.4.1 Four sub-samples were previously assessed for plant macrofossils during Stage 3 works (WA 2018d). An additional six sub-samples were obtained with the aim of obtaining suitable material for dating from the peat deposits in VC028, VC032 and VC039 (itemised in **Appendix 1**).
- 4.4.2 The sub-samples were processed by standard wet-sieving methods for the recovery of waterlogged plant remains; the organic fraction was retained on a 0.25 mm mesh. Flots were stored in sealed containers with water. The flots were scanned under a x10–x40 stereo-binocular microscope and the preservation and nature of the macro remains recorded. Nomenclature follows Stace (1997).
- 4.4.3 Additional sub-samples other than those to be submitted for radiocarbon dating were not assessed for plant macrofossils. This was due to the large volume of material that would be required to undertake the assessment given the highly compacted and decomposed nature of the peat deposits.



4.5 Radiocarbon dating and chronological modelling

- 4.5.1 Five sub-samples were taken for radiocarbon dating, comprising one from VC028, two from VC032 and two from VC039 (itemised in **Appendix 1**).
- 4.5.2 Suitable material was identified under a binocular microscope, stored in glass tubes, and sent to the 14CHRONO Centre at Queens University Belfast for dating. Reporting of the radiocarbon dating results (**Table 5**) follows international conventions (Bayliss and Marshall 2015; Millard 2014).
- 4.5.3 Macrofossils were treated with acid and bulk sediment samples with AAA, and the measurement was corrected using AMS $\delta^{13}\text{C}$ values. The calibrated age ranges were calculated with OxCal 4.2.3 (Bronk-Ramsey and Lee 2013) using the IntCal13 curve (Reimer et al. 2013). All radiocarbon dates are quoted as uncalibrated years before present (BP), followed by the lab code and the calibrated date-range (cal. BP) at the 2σ (95.4%) confidence, with the end points rounded out to the nearest 10 years. The age ranges have been calculated according to the maximum intercept method (Stuiver and Reimer 1986), modelled dates are given in italics (Bayliss and Marshall 2015).
- 4.5.4 The new dates were combined with existing dates acquired during the Stage 3 works (WA 2018d) resulting in a total of nine dates, from three separate peat sequences (VC028, VC032 and VC039) (**Table 3**).
- 4.5.5 Radiocarbon dates from VC032 and VC039 were modelled using Bayesian statistics implemented through the software OxCal 4.1 (Bronk-Ramsey and Lee 2013). This approach enables the integration of multiple dates to refine probability distributions for individual ages when the series is presented in relative order governed by the principle of superimposition or other prior knowledge (e.g. biostratigraphy, expert judgement).
- 4.5.6 The model generates a probability for each sub-sample, called a posterior density estimate, which is essentially a product of the prior information (e.g. relative order of dates in a sequence) and likelihood probabilities. The modelled posterior density estimates (italicised to differentiate them from the original dating information) (2 sigma) typically reduce uncertainty ranges by 40–50%. An agreement index for individual dates is calculated to assess the difference between the modelled posterior density distribution (dark grey; **Figure 17**) and the original age probability distributions (light grey; **Figure 17**). Thresholds for acceptable agreement are an index of >60% (Ramsey 2009).
- 4.5.7 Model outputs are presented in **Figure 17** and the modelled posterior density estimates are given in **Table 6** and **Table 7**.
- 4.5.8 Radiocarbon dating reports are presented in **Appendix 3**.

4.6 Optical dating

Core handling and storage

- 4.6.1 Vibrocores had been collected in transparent liners, and were split offshore into ~1 m sections, which were then sealed for onshore analysis. Vibrocores with geoarchaeological potential, identified during a Stage 1 review (WA 2018a), were transported to Wessex Archaeology for assessment.



- 4.6.2 At this stage, the ends of each core section and the outer surface of the core had already been exposed to light. Upon receipt, vibrocores were held in a dark core storage facility at Wessex Archaeology prior to geoarchaeological recording and sub-sampling.
- 4.6.3 When opened for geoarchaeological recording, plastic core liners were cut using a hand held vibrating multitool, cutting lengthways through the liner along either side of the core. Care was taken to minimise penetration into the sediment.
- 4.6.4 Depending on the nature of the sediment (cohesion, grain size etc.), the cores either naturally broke apart lengthways into two equal halves (2 x half round cores) or remained intact with minimal disturbance (whole round core).
- 4.6.5 During the geoarchaeological recording process, c.1-2 mm of sediment was removed from exposed core surfaces.
- 4.6.6 To avoid repeated disturbance of deposits, cores were opened and then immediately photographed and described. They were then sealed, wrapped in cling film and secured with Gorilla tape before being returned to the core storage facility. Unnecessary handling of cores was avoided.

Sample selection

- 4.6.7 Given the cohesive and compacted nature of Upper Brown Bank deposits recovered in cores, there was potential for these cores to be sub-sampled for OSL dating if a sample from the centre of the core could be extracted, avoiding the outer exposed surfaces.
- 4.6.8 Core photographs and geoarchaeological descriptions were used to identify potential core sections suitable for OSL dating, using the following criteria;
- Sediment must be undisturbed with no evidence of cracks, deformation slumping etc. as this could let light into the centre of the core or could allow reworked material to become incorporated into sample taken from the centre. By taking core photographs immediately after the core was opened, the opening/closing of any cracks could be monitored;
 - Sediment must be cohesive to avoid movement or disturbance of loose grains minimising the potential of exposed material becoming mixed with material from the centre of the core during sampling, and;
 - The core must not show evidence of drying out as this will affect water content calculations.
- 4.6.9 Four sub-samples from Upper Brown Bank deposits were submitted for OSL dating as part of Stage 3 works (WA 2018d), comprising two sub-samples from VC016 and two from VC047 (itemised in **Appendix 1**).
- 4.6.10 Diagnostics were used to estimate the influence of laboratory and environmental factors on the results as a means of testing the analytical validity of the OSL age (**Table 3**). Of the four sub-samples analysed, those from VC016 were considered accurate representations of the burial age. To test the reliability of these ages, the two sub-samples from VC016 were selected for K-feldspar Infrared Stimulated Luminescence (IRSL) dating to provide an independent chronological control through paired quartz and feldspar optical dating.

4.6.11 Feldspar has benefits over quartz for deposits that pre-date the Late Pleistocene as the feldspar luminescence signal saturates at a much higher level, thus potentially extending the age range. Feldspars also have higher sensitivity than quartz which may make them more suitable for dating heterogeneously bleached deposits (e.g. those deposited by water) (Colarossi et al. 2015). Historically, quartz was the preferred mineral for optical dating as the feldspar signal was considered less stable as it decreased over time (anomalous fading). However, methodological developments now allow a more stable component of the feldspar signal to be targeted for dating (Thomsen et al 2008).

Sample preparation and analysis

4.6.12 Once suitable deposits were identified for OSL dating, a sub-section of the entire core was removed for delivery to the OSL lab. This was achieved by cutting through both the core liner and the sediment to create a ~30 cm cylinder of sediment still sealed within the core liner. Care was taken to minimise the exposure of new surfaces to light by taking a section from the top or bottom of a core where possible. These sub-sections were sealed in cling film and black liners for transport to the OSL laboratory for sample preparation and analysis.

4.6.13 All sample preparation and analysis was undertaken by OSL specialists at the University of Gloucester. Sub-sections were opened and prepared under controlled laboratory illumination provided by Encapsulite RB-10 (red) filters. To isolate any material potentially exposed to light, i.e. the outer core surface, sediment located within 10 mm of each core face was carefully removed to target the centre of the core that had been shielded from light. Once the optical dating sample was isolated, the remaining core material was used to calculate Dose Rate (D_r) and moisture content.

4.6.14 The optical dating sample was dried and then sieved. The fine sand fraction was segregated and subjected to acid and alkaline digestion (10% HCl, 15% H_2O_2) to attain removal of carbonate and organic components respectively.

4.6.15 The sample was then divided in two. For one half, a further acid digestion in HF (40%, 60 mins) was used to etch the outer 10-15 μm layer affected by α radiation and degrade each samples' feldspar content. During HF treatment, continuous magnetic stirring was used to effect isotropic etching of grains. 10% HCl was then added to remove acid soluble fluorides. Each sample was dried, resieved and quartz isolated from the remaining heavy mineral fraction using a sodium polytungstate density separation at 2.68 g cm^{-3} . For the second half, density separations at 2.53 and 2.58 g cm^{-3} were undertaken to isolate the K-feldspar fraction.

4.6.16 Twelve 8 mm multi-grain aliquots (c. 3-6 mg) of quartz and K-feldspar were then mounted on aluminium discs for determination of D_e values.

4.6.17 All drying was conducted at 40°C to prevent thermal erosion of the signal. All acids and alkalis were Analar grade. All dilutions (removing toxic-corrosive and non-minerogenic luminescence-bearing substances) were conducted with distilled water to prevent signal contamination by extraneous particles.

4.6.18 Equivalent dose (D_e) was determined using the single-aliquot regenerative-dose (SAR) protocol (Murray and Wintle 2000, 2003 for quartz; Li et al., 2014 for K-feldspar). Lithogenic Dose Rate (D_r) values were defined through measurement of U, Th and K radionuclide concentration and conversion of these quantities into β and γ D_r values (Adamiec and Aitken, 1998), accounting for D_r modulation forced by grain size (Mejdahl, 1979) and present moisture content (Zimmerman, 1971) (**Table 6**). Cosmogenic D_r values were

calculated on the basis of sample depth, geographical position and matrix density (Prescott and Hutton, 1994). Note, no *in situ* γ spectrometry was undertaken due to these samples being collected offshore, therefore the level of U disequilibrium was estimated by laboratory-based Ge γ spectrometry.

- 4.6.19 Ages reported in **Table 6** provide an estimate of sediment burial period based on mean D_e and D_r values and their associated analytical uncertainties. OSL dating reports are presented in **Appendix 4**.

4.7 Palaeogeographic reconstructions

Introduction

- 4.7.1 A series of palaeogeographic reconstructions showing the geography of the Norfolk Boreas site at different time intervals in the past were produced (**Figure 18**).

- 4.7.2 To model palaeogeography, two key inputs are required;

- a digital elevation model (DEM) showing the topography of the area at a point in time (palaeoDEM), and;
- information on the approximate sea level (relative to the present day) during the same time period.

PalaeoDEM

- 4.7.3 PalaeoDEMs were created by Fugro for the base and top key deposits, as part of the site investigation process to inform the siting of individual wind turbines (Fugro 2018).

- 4.7.4 Ultra-high resolution (UHR) shallow seismic data was interpreted to identify boundaries between key stratigraphic units. These boundaries (horizons) were mapped along each seismic line, and the data interpolated to create a 3D isopach showing changes in the elevation of key horizons across the site. Corrections were applied to the mapped horizons to reduce them to meters below Lowest Astronomical Tide (mLAT). Full processing details are outlined in Fugro (2018). The horizons were provided in raster format for interrogation in ArcGIS.

- 4.7.5 At the Norfolk Boreas site, a horizon representing the boundary between Brown Bank Formation and the underlying Yarmouth Roads Formation, was mapped (H07; Fugro 2018). This horizon represents the topography of the Norfolk Boreas site prior to the deposition of Brown Bank Formation thus providing a palaeoDEM for the early Devensian (MIS 5d-5a).

- 4.7.6 Horizons representing the top of Brown Bank Formation (H05; Fugro 2018) and base of Holocene deposits (H01; Fugro 2018) were also mapped. Generating a site-wide PalaeoDEM for these horizons was problematic due to artefacts in data processing caused by attenuation of the seismic data by large sand banks or organic rich layers, and because deposits were not laterally continuous or had been eroded by modern seabed processes, making it difficult to map reflectors across seismic lines. Due to large gaps in data and processing artefacts (**Figure 19**), these horizons are considered unsuitable for palaeogeographic reconstructions.

Sea-level data

- 4.7.7 Early Devensian sea-level data was taken from a global stacked reconstruction based on ocean sediment core data and a wide variety of proxies and models (Spratt and Lisiecke

2016) (**Figure 20**). For each MIS stage, approximate sea level relative to the present day was extracted **Table 3**.

Palaeogeographic model

Two sea-level scenarios were selected for palaeogeographic modelling as outlined below in **Table 3**. The choice of scenarios was based on a review of sea-level data in comparison to the elevation range of the palaeoDEM (38-72 m below LAT).

Palaeogeographic reconstructions were undertaken in ArcGIS. The palaeoDEM was contoured and shaded to show areas above and below sea level at given time periods. An arbitrary tidal range of 2 m was applied to the data to show possible extents of an intertidal zone based on the topography. The palaeogeographic reconstructions are shown in **Figure 18**.

Palaeogeographic modelling was undertaken for two time periods during the Early Devensian when sea level was potentially low enough to expose the Norfolk Boreas site (**Figure 20**). Reconstructions were not undertaken for time periods of high sea level as the site would have been completely submerged, nor were they undertaken for MIS 4-3 when the site is expected to have become sub-aerially exposed as a PalaeoDEM for the top of the Brown Bank Formation (H05; Fugro 2018) was considered unsuitable for palaeogeographic modelling (**Figure 19**).

Table 3 Parameters used in Early Devensian palaeogeographic model

Scenario	Age (MIS)	¹ Sea level (relative to present day)	² Tidal range
B	~88 ka (MIS 5b)	-50 m (low)	2 m
A	~110 ka (MIS 5d)	-45 m (low)	2 m
¹ Spratt and Lisiecke (2016)			
² Tidal range inferred as no model data available for these time periods			

5 RESULTS

5.1 Deposit model

- 5.1.1 Earlier geological reviews of the Norfolk Boreas site defined the site stratigraphy (deposit model) using geophysical and geotechnical assessments undertaken for the East Anglia One Offshore Project Area, and Cameron et al. (1992). Recent site specific geophysical and geoarchaeological assessments within the Norfolk Boreas site (WA 2018a; 2018b; 2018c; 2018d) have allowed this stratigraphic model to be refined so it fully represents the deposits likely to be encountered in the shallow sub-surface (**Table 4**).
- 5.1.2 A comparison between the updated deposit model (**Table 4**) and previous iterations produced by Wessex Archaeology (WA 2018b and 2018c) and Fugro (Fugro 2018) is presented in **Appendix 5**. The deposit model is considered alongside the British Geological Survey lithostratigraphic framework for UK continental shelf deposits (Stoker et al. 2011). Where possible, the same Formation names have been adopted, but in some cases, they have been refined to reflect subtle changes in depositional environment and age within a Formation/Unit (e.g. Units 7a, 7b and 7c).
- 5.1.3 Note, the stratigraphic scheme presented here (**Table 4**) is based on interpretations of shallow geophysics and thus doesn't capture deeper, older deposits that are beyond the period of archaeological interest.



5.1.4 From herein, deposits are referred to according to the Unit Number and Unit Name presented in **Table 4**. A schematic 2D cross section showing the representative stratigraphy of the site is presented in **Figure 21**.

Table 4 Shallow-stratigraphy of the Norfolk Boreas site (deposit model)

WA Unit	WA Unit Name Age (MIS)	Geophysical characteristics ¹	Sediment type and depositional environment ²
8	Seabed sediments <i>Holocene post-transgression (MIS 1)</i>	Generally observed as a veneer or thickening into large sand wave and bank features up to 20 m in height. Boundary between surficial sediments and underlying units not always discernible.	Medium to coarse sand with frequent shell fragments – marine.
7c	Elbow Formation – intertidal <i>Early Holocene (MIS 1)</i>	Not identified within the geophysical data as deposit thickness is lower than geophysical data resolution.	Laminated sand, silt and clay – intertidal.
7b	Elbow Formation – organic <i>Late Devensian to Early Holocene (MIS 2-1)</i>	Extensive areas of intermittent, relatively flat, high amplitude reflectors. Often associated with shallow channelling.	Peat ranging from strongly to weakly decomposed with plant fragments (reeds) roots and wood preserved – terrestrial/coastal wetland.
7a	Elbow Formation – fluvial <i>Late Devensian to Early Holocene (MIS 2-1)</i>	Small, shallow, infilled channels. Fill characterised as acoustically chaotic or transparent, or by sub-parallel internal reflectors. Incises into the top of Upper Brown Bank.	Sand with silt and clay laminations, occasionally organic, may comprise plant/root or shell fragments – fluvial/alluvial, possible reworking of older deposits.
6	Twente Formation – <i>Late Devensian (MIS 2)</i>	Not identified in shallow geophysical data	Not identified in geotechnical core logs.
5	Upper Brown Bank <i>Early-Mid Devensian (MIS 5d-3)</i>	Observed as a blanket deposit across much of the area, either acoustically transparent or characterised by sub-horizontal layered reflectors. Contains numerous internal erosion surfaces, occasional fluid escape structures, and areas of acoustic blanking.	Silty clay and clayey silt with closely spaced fine laminations. May be sandy in places or comprise sand partings/laminations – restricted marine/open estuary.
4	Lower Brown Bank/Eem Formation <i>Ipswichian to Early Devensian (MIS 5e-5d)</i>	Observed within large topographically controlled depressions. Characterised by low relief basal reflector and either an acoustically transparent or well-layered fill.	Not identified in geotechnical data.
3	Swarte Bank <i>Anglian (MIS 12)</i>	Not identified in shallow geophysical data.	Not identified in geotechnical data.
2	Yarmouth Roads <i>Early to Mid-Pleistocene (>MIS 13)</i>	Thick unit either seismically chaotic or containing numerous areas of well-defined cross cutting channel complexes characterised by layered sub-parallel internal reflectors. Top of unit generally a well-defined regional erosion surface.	Not identified in geotechnical data.
1	Westkapelle Ground Formation <i>Late Pliocene to Early Pleistocene (MIS 63-103)</i>	No identified in shallow geophysical data	Not identified in geotechnical data

(¹) Based on geophysical data (WA 2018c)
(²) Based on Stage 1-3 geoarchaeological works (WA 2018a; 2018b; 2018d)



5.2 Diatom analysis

- 5.2.1 To supplement existing sub-samples from VC032, five new samples were prepared for diatom analysis. Of these, only four were suitable for analysis level percentage counts as the sample from 3.80 mbsf contained extremely low numbers of very poorly preserved, indeterminate diatom fragments.
- 5.2.2 A total of nine sub-samples from Unit 7c and Unit 8 in VC032 were analysed for diatoms (**Figure 11** and **Figure 12**).
- 5.2.3 Diatoms from the polyhalobous to mesohalobous (marine to brackish) group are dominant in both Unit 7c and Unit 8 in VC032. These taxa rise from 44% at the base of the sequence, to a maximum of 77% at 3.64 mbsf, declining to 44% at 3.50 mbsf and then increasing to 57% at 3.40 mbsf. The most important diatom in this group is *Cocconeis scutellum*, which comprises most of the polyhalobous to mesohalobous diatom assemblage. *Cocconeis scutellum* is a non-planktonic diatom that is found attached to submerged surfaces, such as macrophytes, rocks and sand grains, in shallow water.
- 5.2.4 *Hyalodiscus scoticus*, a polyhalobous to mesohalobous, semi-planktonic species, reaches maximum abundances in the top three samples; rising to a maximum of 7% at 3.50 mbsf. The polyhalobous to mesohalobous, non-planktonic species *Ardissonia crystalina* is present throughout the core. The planktonic polyhalobous to mesohalobous species *Actinoptychus undulatus* is present at above 1% abundance in the top three samples.
- 5.2.5 Polyhalobous (marine) diatoms are present throughout the sequence, decreasing from 6% at the base of the core to 3% at 3.64 mbsf, increasing to a maximum of 16% in the top sample. The marine planktonic diatom *Paralia sulcata* is present throughout, increases in the top part of the core reaching a maximum of 7% at 3.5 mbsf. Other marine diatoms present in the sequence, and more common at the top of the core, are *Podosira stelligera*, *Rhabdonema* sp., *Rhaphoneis surirella* and *Trachyneis aspera*. The benthic polyhalobous species *Nitzschia panduriformis* is most common in the bottom sample where it reaches a maximum of 4%. *Grammatophora* sp., represented mainly by girdle bands, are present in all nine samples.
- 5.2.6 Mesohalobous diatoms are present throughout the sequence with maxima of 14% at 3.75 mbsf and 20% at 3.53 mbsf. The mesohalobous diatoms are comprised almost entirely of shallow-water, benthic and attached species; an exception being the occurrence of the brackish water, planktonic diatom *Cyclotella striata*. The brackish water taxa include *Diploneis didyma*, *Rhopalodia musculus*, *Synedra tabulata*, *Nitzschia punctata*, *Nitzschia navicularis*, *Achnanthes brevipes*, *Achnanthes delicatula*, *Campylodiscus echeneis*, *Navicula digitoradiata*, *Diploneis aestuari* and *Nitzschia granulata*. The importance of non-planktonic, mesohalobous taxa indicates the presence of shallow water, tidal habitats.
- 5.2.7 At the base of the diatom sequence (3.77 mbsf) oligohalobous indifferent (optimum in freshwater but tolerant of slightly brackish water) diatoms reach a maximum of 30%. The freshwater epiphyte *Cocconeis placentula* comprises 27% of the total diatoms. *Fragilaria pinnata*, a freshwater diatom with wide environmental tolerance, reaches maximum abundance in the bottom 3 sub-samples of the sequence (maximum 4% at 3.75 mbsf). A number of other freshwater diatom taxa were recorded at the base of the diatom sequence. All of these are non-planktonic diatoms that grow in shallow water. Freshwater, oligohalobous indifferent diatoms are present in all nine samples decreasing to minima of

9% at 3.64 mbsf and 6% at 3.53 mbsf, rising to a maximum of 16% at 3.50 mbsf and falling to 7% in the top sample. Other freshwater diatom taxa recorded in the sub-samples include *Aulacoseira* sp., *Fragilaria brevistriata*, *Fragilaria construens* var. *venter*, *Fragilaria lapponica* and *Navicula scutelloides*.

- 5.2.8 The mixed halobian groups of the diatom assemblages in Unit 7c and Unit 8 in VC032, and the importance of marine and marine brackish taxa with large numbers of shallow water diatoms suggests that the samples represent intertidal deposits, or possibly shallow subtidal environments. The higher percentage of freshwater, and particularly epiphytic freshwater, diatoms towards the base of the sequence is consistent with a change in salinity from a freshwater environment, to the brackish and marine dominated habitats represented by the diatom assemblage. The further increases in the percentages of polyhalobous diatoms seen in the top samples may reflect increasing water depths.

5.3 Pollen and charcoal analysis

- 5.3.1 Pollen and charcoal analysis was undertaken on sub-samples from Unit 7b in VC028 and VC039, and Unit 7b and Unit 7c in VC032. The results allow the subdivision of the sequence into local pollen assemblage zones (LPAZ), as outlined in **Figures 13-15**, and described below.

VC028

LPAZ VC028-1; 2.60–2.56 mbsf

- 5.3.2 The zone is dominated by pollen of trees and shrubs (>80%), characterised by initially high but declining values for *Pinus sylvestris* (pine) (40–20%) and increasing values for *Corylus avellana* type (hazel) (23–34%) and *Salix* (willow) (8.7–16%). Non-arboreal pollen is dominated by Poaceae (grass family) increasing through the zone (8.7–16%), with small quantities of a restricted range of herbs, including Cyperaceae (sedge family), Rosaceae (rose family) and *Filipendula* (meadowsweets) (<1%). Fern spores and aquatics are present in consistent quantities (5% and 1.5% respectively). Total pollen concentrations in the two samples vary between 190 to 239x10³ grains/cm³. Microscopic charcoal area is low (≤ 0.1 cm²cm³).

LPAZ VC028-2; 2.56–2.50 mbsf

- 5.3.3 The zone remains dominated by pollen of trees and shrubs (~70%) although overall with decreasing values for *Pinus sylvestris* (27.5–13.5%) and *Salix* (16–1.5%) and increasing values for *Corylus avellana* type (21–45%). Herbaceous pollen values increase (max 35.8%) largely comprising Poaceae (26.5–33%) with a restricted range of other herb taxa similar to LPAZ VC028-1. Total pollen concentrations vary between 192x10³ grains/cm³ (2.52 mbsf) and 694 x10³ grains/cm³ (2.50 mbsf). There is an increase in microscopic charcoal area through the zone, with a peak at 2.50 mbsf (3.11 cm²cm³) mirroring an increase in total pollen concentrations.

VC032

LPAZ VC032-1; 4.13–4.05 mbsf

- 5.3.4 The zone is characterised by high values for herbaceous pollen (74–92%). Cyperaceae dominates within the base of the zone (max 76.7% at 4.1 mbsf), declining rapidly by 4.08 mbsf (8.3%) and giving way to increasing values for Poaceae (max. 61.7% at 4.08 mbsf) that themselves decline sharply from 4.06 mbsf. Several other herbaceous taxa are recorded in small quantities (<0.5%) including initially high values for Chenopodiaceae (goosefoot family) (7%).



- 5.3.5 Shrubs occur in very small quantities (1–3%), primarily comprising *Salix* and small quantities of *Corylus avellana* type and *Juniperus* (juniper). Trees occur in variable quantities; *Pinus sylvestris* initially decreases within the base of the zone (min. 4.3%), subsequently increasing towards the top of the zone (36%) accompanied by a peak in *Betula* (birch) (max. 12% at 4.08 mbsf).
- 5.3.6 Fern spores are present in low quantities, but with an increase in Pteropsida towards the top of the zone to ~8%). Aquatic pollen taxa occur in appreciable quantities, including a peak in *Potamogeton natans* type (pondweed) (27.8% at 4.08 mbsf) and *Typha* (bulrush) (6.5% at 4.10 mbsf).
- 5.3.7 Total pollen concentrations increase from 33 to 195x10³ grains/cm³ (4.13–4.10 mbsf), thereafter declining to 113 x10³ grains/cm³ at 4.06 mbsf.
- 5.3.8 Microscopic charcoal area is generally low but increases through the zone, with a peak at 4.06 mbsf (1.48 cm²cm³).

LPAZ VC032-2; 4.05–3.87 mbsf

- 5.3.9 The zone is characterised by increased values for pollen of trees (72–92%) and shrubs (max. 19% at 3.92 mbsf) with lower values for herbaceous taxa (13.7–5.7%). Trees are dominated by *Pinus sylvestris* (max. 89.5% at 4.03 mbsf) with lower but increasing values for *Corylus avellana* type (max. 17.4% at 3.92 mbsf) *Quercus* (oak) (1–9.3%) and *Ulmus* (elm) (<0.5–4.7%). A single grain of *Tilia* (lime) was recorded at 4.00 mbsf.
- 5.3.10 Herbs largely comprise Poaceae (13.4% declining to <5%) and Cyperaceae (max. 7% at 4.00 mbsf but mostly ≤2.5%), with several other herb taxa, including Rosaceae, *Filipendula* and Apiaceae (carrot family) recorded intermittently and in small quantities (<0.5 %).
- 5.3.11 Pteropsida spores (undifferentiated fern spores) peak within the base of the zone (39%) with values thereafter ranging between 3.4–11.5%. Other fern spores, including *Pteridium aquilinum* (bracken) and *Dryopteris filix mas* (male fern) occur in small quantities (<0.5 %).
- 5.3.12 Pollen of aquatics are present consistently through the zone, comprising *Potamogeton natans* type (up to 7.6%), *Typha* (<2.5%) and *Sparganium emersum* type (unbranched bur-reed) (<1%).
- 5.3.13 Total pollen concentrations vary significantly through the zone from a minimum of 14.3x10³ grains/cm³ (3.89 mbsf) to 196x10³ grains/cm³ (3.98 mbsf).
- 5.3.14 Microscopic charcoal area increases with a peak at 4.01 mbsf of 1.52 cm²cm³, declining thereafter.

LPAZ VC032-3; 3.87–3.81 mbsf

- 5.3.15 The zone is characterised by a significant decrease in trees and increasing values for shrubs, primarily reflecting the decline in *Pinus sylvestris* (63.3–29.8% from 3.88–3.87 mbsf) and increase in *Corylus avellana* type (16.5–41 % from 3.88–3.87 mbsf). *Betula* values increase (max. 6.8%) along with *Quercus* (max. 9.6%) with consistent values for *Ulmus* (3.6–4.2%). There is a small increase in herbs reflecting the increase in Poaceae.
- 5.3.16 Quantitates of fern spores increase significantly with peaks in *Thelypteris palustris* (marsh fern) (59% at 3.84 mbsf) and Pteropsida (43% at 3.82 mbsf). There are also peaks in aquatic



taxa, including *Potamogeton natans* type (31.7% at 3.87 mbsf), with a significant increase in *Typha* throughout the zone (12.7–20.4%).

- 5.3.17 Total pollen concentrations increase from a low of 14.6×10^3 grains/cm³ (3.84 mbsf) to 171×10^3 grains/cm³ (3.82 mbsf).
- 5.3.18 Microscopic charcoal area is generally low through the zone but increases to 1.24 cm²cm³ at 3.82 mbsf.

LPAZ VC032-4; 3.81–3.58 mbsf

- 5.3.19 Values for individual trees and shrubs remain consistent through this zone, characterised by large quantities of *Corylus avellana* type and lower quantities for *Pinus sylvestris*, *Betula*, *Quercus* and *Ulmus*. A single grain of *Tilia* was recorded at 3.71 mbsf.
- 5.3.20 Values for herbaceous taxa increase, ranging between 12.6% (3.63 mbsf) and 21.3% (3.73%), primarily through increases in Poaceae (max 15.6% at 3.73 mbsf) and Chenopodiaceae (max. 5.5% at 3.58 mbsf). There are consistent although small quantities (<1%) of pollen of Rosaceae and Aster type (daisies) with intermittent and small quantities of a range of other herbs, including *Anthemis* (chamomiles), *Artemisia* (mugworts), *Filipendula* and Brassicaceae (cabbage family).
- 5.3.21 Fern spores are represented primarily by Pteropsida (max. 12.4%), with occasional small quantities of *Pteridium aquilinum*, *Dryopteris filix mas* and *Thelypteris palustris*.
- 5.3.22 Aquatic pollen occurs in low quantities, largely represented by *Potamogeton natans* type (declining from 4% to <1%) and smaller quantities (<0.5%) of *Typha* with occasional *Sparganium emersum* type and *Myriophyllum alterniflorum* (alternate water-milfoil).
- 5.3.23 Total pollen concentrations are consistently high, ranging between 120×10^3 grains/cm³ (3.6 mbsf) to 298×10^3 grains/cm³ (3.64 mbsf).
- 5.3.24 Microscopic charcoal area increases with peaks of 1.25 cm²cm³ (3.71 mbsf) and 2.42 cm²cm³ (3.58 mbsf).

VC039

LPAZ VC039-1; 3.15–3.07 mbsf

- 5.3.25 The zone is dominated by herbaceous pollen taxa, principally Poaceae, though values decline steadily from 63.7% to 37.6%, and Cyperaceae which increases from 2.3% (3.11 mbsf) to 37.6% (3.08 mbsf). Other herb taxa include Rosaceae (1-3%), *Filipendula*, Apiaceae and *Artemisia* (<1.5%).
- 5.3.26 Shrubs form a minor component of the pollen assemblage (<3%), largely comprising *Salix* with smaller quantities of *Corylus avellana* type and occasional *Juniperus*. Values for trees peak at 39.3% (3.11 mbsf) represented mainly by *Betula* and smaller quantities of *Pinus sylvestris*; the former taxon increases to 32.7% (3.11 mbsf) before declining to 15.4% (3.08 mbsf), with *Pinus sylvestris* peaking at 6.6% (3.11 mbsf).
- 5.3.27 Aquatic plants taxa are represented by large quantities of *Typha* pollen, increasing to 16.8% (3.11 mbsf), *Potamogeton natans* type (2.3-4%), with smaller quantities of *Sparganium emersum* type (max. 1.9%), *Myriophyllum alterniflorum*, *Menyanthes trifoliata* (bogbean)

and *Nymphaea alba* (white water-lily). Values for aquatic plants decline sharply from 3.11 to 3.09 mbsf (21.5–1.9%).

- 5.3.28 Total pollen concentrations range between 27×10^3 to 67×10^3 grains/cm³. Microscopic charcoal was largely absent apart from very small quantities at 3.11 mbsf (0.01 cm²cm³).

LPAZ VC039-2: 3.07–2.95 mbsf

- 5.3.29 The zone is characterised by increasing values for trees and declining values for herbs, with a general trend for increasing quantities of *Pinus sylvestris* (max. 77.8% at 2.96 mbsf). Values for *Betula* fluctuate, peaking at 36–34.7% (3.04–3.02 mbsf) before declining sharply. The only other tree is represented by two pollen grains of *Quercus* at 2.98 mbsf. Values for shrubs increase marginally (max 14.1% at 2.98 mbsf), largely represented by *Corylus avellana* type which peaks at 12.8% (2.98 mbsf). Herb pollen values decline consistently through the zone, most apparent in the sharp decline in *Cyperaceae* from 36.6%–13.7% (3.06–3.04 mbsf) and *Poaceae* from 25.7–8.3% (3.04–3.2 mbsf).
- 5.3.30 Pteropsida spores increase significantly through the zone from 3.8% (3.08 mbsf) to 80.2% (2.96 mbsf), though declining sharply thereafter (16.9% at 2.95 mbsf). Aquatic pollen is represented by *Typha* and *Menyanthes trifoliata* (max. 3.1% at 3.06 mbsf).
- 5.3.31 Total pollen concentrations are lowest within the base of the zone, varying between as little as 9.8 to 95×10^3 grains/cm³, with a significant peak at 2.95 mbsf to 818×10^3 grains/cm³.
- 5.3.32 Microscopic charcoal is largely absent through the zone apart at 2.95 mbsf with a peak in values to 2.91 cm²cm³.

Vegetation history

- 5.3.33 The vegetation history of the Norfolk Boreas site can be broadly split into three phases as outlined below, and summarised in **Figure 16**.

Vegetation Phase 1

- 5.3.34 Vegetation Phase 1 correlates to LPAZ VC033-01 and LPAZ VC039-1 where the pollen suggests an open grassland landscape with sparse stands of birch (shrub rather than tree birch), and grasses likely growing within patches of wetland. In VC039, occasional hazel grains are present, but these are unlikely to indicate a local presence and instead most probably derive through long-distance transport. In VC032, there is a relative higher percentage of birch in comparison to VC039 which may suggest this core is slightly older in age than VC032. Wetland environments during this phase are initially dominated locally by herb fen comprising sedges, and later by reedswamp with aquatics of pondweed suggesting nearby slow or still moving water. The local presence of reedswamp is confirmed by frequent reed fragments noted Unit 7b in VC032. Towards the later end of this phase, reedswamp subsequently declines and this decline in grasses is followed by an increase in fern spores, although these have lost their outer coating (perisperm) making it difficult to determine whether they represent expansion of marsh fern.

Vegetation Phase 2

- 5.3.35 Vegetation Phase 2 correlates to LPAZ VC032-2, LPAZ VC039-2 and LPAZ VC028-1 and is characterised by a significant increase in pine woodland, visible in both VC032 and VC039, reflecting the immigration and spread of pine into the area. Pine may also have encroached into drier parts of the wetland, although the consistent presence of pondweed and bulrush suggest areas of shallow, still and/or slow-moving water. Pine was the

dominant woodland component before giving way to hazel. Hazel was likely initially a subordinate understorey component of the pine-dominated woodland but later became more dominant in the woodland, along with scattering of elm and oak.

Vegetation Phase 3

- 5.3.36 Vegetation Phase 3 correlates to LPAZ VC032-3, LAPZ VC032-4 and LPAZ VC028-2 and marks a shift to a saltmarsh to mudflat environment with an increase in vegetation tolerant to increased salinity. The wetland environment in LPAZ VC032-3 shows fluctuations in vegetation, with peak in pondweed, bulrush and marsh fern. These taxa suggest pondweed growing in slow-flowing habitats, with bulrushes growing near on in standing water no greater than 0.8m deep, with marsh ferns colonising fen and wetland edge environments. The expansion in aquatic and marsh taxa likely reflect the influence of a fluctuating but rising trend in sea-levels. Pollen of Chenopodiaceae and Aster type are characteristic of saltmarsh vegetation. Woodland on adjacent areas of dry ground remain dominated by hazel with elm and oak with a subordinate component of pine, birch and willow.

Evidence for fire

- 5.3.37 Microscopic charcoal particles were present in all three pollen sequences in variable quantities. In VC032 a defined concentration of microscopic charcoal occurs during the early rise of pine woodland and later towards the top of the peat and within the clays and laminated silts. Similar increases in microscopic charcoal are recorded at the top of the peats in VC039 and VC028. In these later three cases, increases in microscopic charcoal occur concurrent with increasing pollen concentrations, which could reflect slower sediment accumulation rates rather than an increase in fire incidence. However, the increase in microscopic charcoal in VC032 (zones VC032-1 and VC032-2) does not correspond to an increase in pollen concentration so more likely to reflect an increase in fire incidence.

5.4 Plant macrofossils

- 5.4.1 The plant macrofossil evidence from ten sub-samples from Unit 7b (VC028, VC032 and VC039) is dominated by the remains of wetland plants (see **Table 5**). These are mostly remains from vegetative parts but abundant fruiting parts are also present. Wood charcoal is noted in small quantities in one of the samples (VC028 2.50 mbsf). The plant macrofossil assemblages include a variety of mostly aquatic or wetland eutrophic plants, with some taxa that are quite precise palaeoecological indicators, such as *Sphagnum* mosses, stonewort algae (*Characeae*), reed (*Phragmites australis*), bulrush (*Typha* sp.) and bogbean (*Menyanthes trifoliata*). Other plants such as buttercups (*Ranunculus* sp.), sedges (*Cyperaceae*), birch (*Betula* sp.) and the mint family (*Lamiaceae*) were also present.
- 5.4.2 Remains of invertebrates, including foraminifera, crustaceans (ostracods and *Daphnia* sp.), aquatic molluscs and insects are also present in some of the samples.
- 5.4.3 The plant macrofossil assemblages recovered are generally consistent with a terrestrial wetland environment that becomes progressively submerged under rising sea levels. The reconstruction of vegetation patterns through the study of plant macrofossils from wetland environments is biased by the overrepresentation of plant parts that are more resistant to erosion, such as certain coated seeds, that may have been transported and accumulated as a result of alluvial processes, or winged seeds easily transported by wind (e.g. birch seeds). In addition, many aquatic plants reproduce vegetatively and therefore seed production is low, but non-woody vegetative plant parts are more rarely identifiable by binocular microscopy. Still, there are some vegetational landscape traits that can be gained



through the study of plant macrofossils, and this is complementary to the pollen evidence, which also has its own biases.

VC028

- 5.4.4 The presence of marine molluscs at the top of the sequence indicates some marine influence. Insects, water-flea egg cases and degraded plant parts were also present in the sample, with some seeds of birch and bulrush that may indicate some input from a freshwater wetland environment, possibly introduced by anemochory (wind dispersal).
- 5.4.5 A large volume of very degraded plant material (including wood) and a small number of insects were present in the sample from the bottom of this sequence. The fruits and potentially also bud scales of birch were identified.

VC032

- 5.4.6 No identifiable plant remains were observed in the sample from the base of the sequence. The two samples from middle parts of the sequence indicate a freshwater wetland environment, with bogbean, reeds, bulrush and sedges. There is also some input from terrestrial trees, namely birch which may be some distance away, although dwarf birch (*Betula nana*) can grow on waterlogged flat ground. The presence of marine molluscs at the top of the sequence, where no plant macro remains other than *Sphagnum* spp. moss leaves were identified, indicates some marine influence.

VC039

- 5.4.7 The bottom of this sequence is dominated by very degraded vegetative plant material but the presence of seeds of bogbean and bulrush and stonewort oospores indicate an open and shallow body of probably still and clear fresh water. The presence of birch seeds, easily dispersed by wind, may indicate some input from the surrounding terrestrial landscape, although dwarf birch also grows on waterlogged flat ground. There is a progressive disappearance of identifiable plant remains over time, until the increasing presence of foraminifera and marine molluscs at the top of the sequence indicates increasing marine influence.

Table 5 Plant macrofossils

Sample Code	Bulk volume (ml)	Vegetative plant parts	Other	Wood charcoal	Invertebrates
117122_VC028_2.5	20	A* - Degraded plant remains and woody fragments	A - <i>Betula</i> sp., <i>Typha</i> sp.	C	Moll-m, <i>Daphnia</i> sp. egg cases, insects (A)
117121_VC028_2.59-2.62	40	A*** inc. wood fragments	A - <i>Betula</i> sp. seeds, bud scales	-	Insects (C)
117122_VC032_3.61	20	A - Very degraded plant remains, inc. <i>Sphagnum</i> spp. leaves	-	-	Moll-m, <i>Daphnia</i> sp. egg cases, ostracods (C), insects (C)
117121_VC032_3.83	30	A*** inc. Bryophytae and <i>Phragmites australis</i> , leaves	A* - <i>Menyanthes trifoliata</i> , Cyperaceae, <i>Typha latifolia</i> , <i>Betula</i> sp., indets	-	-

Sample Code	Bulk volume (ml)	Vegetative plant parts	Other	Wood charcoal	Invertebrates
117122_VC032_3.95	20	A** - Degraded plant remains and woody fragments	C - Lamiaceae, <i>Ranunculus</i> sp., <i>Menyanthes trifoliata</i>	-	Insects (C)
117121_VC032_4.11	40	A* - Very degraded plant remains	-	-	-
117122_VC039_2.94	15	A* - Very degraded plant remains	-	-	Foraminifera (A*), Ostracods (C), moll-m
117122_VC039_2.96	15	A* - Very degraded plant remains	C - Fragments of <i>Menyanthes trifoliata</i>	-	Moll-m
117121_VC039_3.07	20	A** - Very degraded plant remains	A - <i>Menyanthes trifoliata</i> , Characeae, indets	-	-
117122_VC039_3.13	25	A - Very degraded plant remains and woody fragments	A - <i>Menyanthes trifoliata</i> , <i>Betula</i> sp., Characeae oospores, <i>Typha</i> sp.	-	Ostracods (A), insects (C)

Key: A*** = exceptional, A** = 100+, A* = 30-99, A = >10, B = 9-5, C = <5

5.5 Radiocarbon dating and chronological modelling

- 5.5.1 A total of nine sub-samples were submitted for radiocarbon dating from Unit 7 in vibrocores VC028, VC032 and VC039. Of these, one sub-sample from the top of Unit 7b in VC028 failed to return a date.
- 5.5.2 Four radiocarbon dates were acquired from VC032 spanning Unit 7b and Unit 7c (**Table 5**), and when all dates are considered together the sequence is unconformable as the date from 3.61 mbsf (UBA-39473) is older than UBA-38189 and UBA-39474 which are located at greater depth.
- 5.5.3 Bayesian chronological modelling of dates from VC032 confirm the sequence is unconformable showing a poor overall agreement index ($A_{model} < 60$). The model indicates that the date at 3.61 mbsf (UBA-39473) is out of sequence with the other dates. Subsequently, if the model is run with UBA-39473 defined as an outlier the model shows good agreement ($A_{model} = 100$) and the dates from Unit 7b are in sequence (**Figure 17a**).
- 5.5.4 The outlier date (UBA-39473) was taken from Unit 7c which is interpreted to represent deposition in an intertidal environment, while other dates from VC032 were from a peat deposit (Unit 7b). Plant macrofossils were highly degraded in the uppermost sample (**Table 5**) likely due to reworking in a dynamic intertidal environment. Therefore, there is potential for reworking of older plant material into the deposit which may explain why the radiocarbon date UBA-39473 is older than dates from lower in the sequence.
- 5.5.5 Radiocarbon dates from Unit 7b in VC032 place deposition between 9992 ± 51 BP (UBA-38190; 11710-11260 cal. BP) and 8697 ± 45 (UBA-38189; 9880-9540 cal. BP) suggesting the peat formed over a period of up to 2170 years during the Early Holocene, although it is not known if this was continuous or punctuated development.
- 5.5.6 A total of three radiocarbon dates were acquired from VC039, comprising one date (UBA-39472) from Unit 7a and two from Unit 7b (UBA-38191 and UBA-39472). When considered

collectively, the dates are out of sequence as the lowermost date (UBA-39472) is slightly younger than the overlying date (12550-12080).

- 5.5.7 Bayesian chronological modelling of all dates from VC039 show an overall poor agreement (Amodel: <60) and the model suggests the middle date (UBA-38191) is more likely to be an outlier when compared to the other dates (**Figure 17b**). The dating results suggest deposition of Unit 7a at 10435 ± 66 BP (UBA-39472; 12550-12080 cal. BP), with the peat forming sometime after, until at least 8510 ± 58 BP (UBA-39471; 9560-9430 cal. BP).
- 5.5.8 Due to one failed radiocarbon date from VC028 (UBA-39471), only one date is available suggesting the peat was forming at 8749 ± 40 BP (UBA-38188; 9900-9570 cal. BP), although there is no age information to constrain the initiation or termination of peat formation.

Table 6 AMS radiocarbon dates

Laboratory No	Material dated	Depth mbsf (mLAT)	Age BP	Modern F ¹⁴ C	Age range cal. BP (95.4%)	Modelled range cal. BP (posterior density estimates)
VC028						
UBA-39471	Betula sp., Typha sp.	2.50	Failed	-	-	-
UBA-38188 *	Bud scales	2.59-2.62	8749 ± 40	0.3365 ± 0.0016	9900-9570	-
VC032						
UBA-39473	Organic material with <i>Sphagnum</i> sp. leaves	3.61	9124 ± 77	0.3212 ± 0.0031	10500-10180	10510-10180
UBA-38189 *	<i>Menyanthes trifoliata</i> seeds	3.83	8697 ± 45	0.3387 ± 0.0019	9880-9540	9890-9540
UBA-39474	Lamiaceae, <i>Ranunculus</i> sp., <i>Menyanthes trifoliata</i> seeds	3.95	8894 ± 78	0.3305 ± 0.0032	10210-9710	10210-9740
UBA-38190 *	Bulk organic sediment	4.11	9992 ± 51	0.2882 ± 0.0018	11710-11260	11720-11250
VC039						
UBA-39471	<i>Menyanthes trifoliata</i> seed	2.96	8510 ± 58	0.3467 ± 0.0025	9560-9430	9560-9420
UBA-38191 *	<i>Menyanthes trifoliata</i> seed	3.07	10881 ± 60	0.2581 ± 0.0019	12890-12690	12740-12500
UBA-39472	<i>Menyanthes trifoliata</i> , <i>Betula</i> sp., Characeae oospores, <i>Typha</i> sp.	3.13	10435 ± 66	0.2728 ± 0.0022	12550-12080	12570-12070
* Indicates radiocarbon dates acquired during Stage 3						

- 5.5.9 The results from pollen analysis were used to sub-divide Unit 7 into three key vegetation phases as outlined in section 5.3 and **Figure 16**). The duration of each Vegetation Phase, and transitions between them were modelled (**Table 7**) (**Figure 17c**). Radiocarbon dates UBA-39473 and UBA-38191 were not included in the model as they were identified as outliers when considered alongside other dates within the same cores. Therefore, it was only possible to model the age range of vegetation phases 1 and 2.

5.5.10 The resulting model shows good agreement (Amodel: 98) (**Figure 17c**) and suggest Vegetation Phase 1 occurred between 12550-12060 cal. BP and 11710-11260 cal. BP for a duration of 460-1180 yrs (**Table 7**), which correlates to the later part of the Loch Lomond stadial during the Late Weichselian, to the very early parts of the Early Holocene. Vegetation Phase 2 occurred between 10200-9700 cal. BP and 9900-9560 cal. BP and was much shorter than Vegetation Phase 1, lasting 213-708 years during the Early Holocene. The transition between vegetation phases 1 and 2 occurred at 11490-9780 cal. BP according to the modelled posterior density estimate.

Table 7 Bayesian modelling of Vegetation Phases

Model Phase	Laboratory No	Age BP	Modelled range cal. BP (posterior density estimates)	Duration
Vegetation Phase 1	UBA-39472	10435 ± 66	12550-12060	460-1180 yrs
	UBA-38190	9992 ± 51	11710-11260	
Transition from 1 to 2	-	-	11490-9780	-
Vegetation Phase 2	UBA-39474	8894 ± 78	10200-9700	213-708 yrs
	UBA-39471	8510 ± 58	9560-9420	
	UBA-38188	8749 ± 40	9900-9560	

5.6 Optical dating

- 5.6.1 Two sub-samples from Unit 5 in VC016 were selected for K-feldspar IRSL dating to supplement quartz OSL dates from VC016 and VC047 acquired during Stage 3 assessment (WA 2018d) (**Table 6**).
- 5.6.2 Diagnostics were used to estimate the influence of laboratory and environmental factors on the results as a means of testing the analytical validity of the OSL age (**Table 6**).
- 5.6.3 When considered alongside the results of Stage 3 assessment (WA 2018d), a total of four quartz OSL and two K-feldspar IRSL dates, from Unit 5 were acquired. Of the Quartz OSL dates, two have been accepted without caveats (GL17154 and GL17153; VC016), and two have been accepted tentatively as they did not fully meet the criteria of the SAR protocol (GL17155 and GL17156; VC047). Both K-feldspar IRSL dates (GL17154 and GL17153; VC016) have been accepted as maximum age estimates as they failed dose recovery tests (**Table 6**). Full details on the limitations of optical dating are presented in **Appendix 4**.
- 5.6.4 In VC047, the lowermost sub-sample (GL17156) gave an age of 78.9 ± 8.3 ka (MIS 5a) and the overlying sub-sample (GL17155) returned an age of 60.5 ± 5.8 ka (MIS 4) indicating these ages are conformable (**Table 6**). However, both samples show overdispersion of the regenerated signal which implies the effectiveness of sensitivity correction, a key part of the laboratory protocol, may be problematic. This is a function of the individual sample's response to the SAR protocol and is not related to sample handling, storage or preparation.
- 5.6.5 In VC016, the lowermost sub-sample (GL17153) returned a quartz OSL age of 69.8 ± 7.7 ka and a K-feldspar IRSL age of 75.4 ± 8.2 ka. Both ages overlap within error margins and suggest deposition during the transition from MIS 5a to MIS 4. The overlying sub-sample in VC016 (GL17154), gave a quartz OSL age of 83.2 ± 9.5 ka (MIS 5a) and a K-feldspar IRSL age of 91.5 ± 8.1 ka (MIS 5b) and again, both ages overlap within error margins. Despite the K-feldspar IRSL dates being considered maximum age estimates due to possible effects of thermal transfer or sensitization of the natural signal (failed dose recovery test), they are

in broad agreement with quartz OSL. Of note, the difference in age between the lower and upper sample in VC016 is ~14 ka for the quartz OSL dates, and ~16 ka for the K-feldspar IRSL dates, suggesting there is a possible systematic offset between quartz and feldspar dates. When considering all dates from VC016, the ages are unconformable with the oldest dates coming from the uppermost sample and the youngest from the lower sub-sample. This could be a result of environmental and/or laboratory factors.

Table 8 Dose Rate (D_r) and Equivalent Dose (D_e) and resulting OSL age estimates. Age estimates expressed in ka relative to year of sampling. Uncertainties in age are quoted at 1σ confidence and include combined systematic and experimental variability.

Stage	Laboratory id (mineral)	Depth mbsf (mLAT)	Total D_r ($Gy.ka^{-1}$)	D_e (Gy)	Age (ka)	Considerations and analytical validity
VC016						
4	GL17154 (Quartz)	1.70-2.00 (-40.90 to -41.20)	2.19 ± 0.17	182.1 ± 15.0	83.2 ± 9.5	Accept
4	GL17154 K- (Feldspar)		2.71 ± 0.21	247.7 ± 11.1	91.5 ± 8.1	Failed dose recovery test, accept as maximum age
4	GL17153 (Quartz)	2.65-3.00 (-41.85 to -42.20)	2.14 ± 0.17	149.6 ± 11.1	69.8 ± 7.7	Accept
4	GL17153 K- (Feldspar)		2.75 ± 0.20	207.8 ± 16.7	75.4 ± 8.2	Failed dose recovery test, accept as maximum age
VC047						
3	GL17155 (Quartz)	2.55-3.00 (-37.05 to -37.50)	2.23 ± 0.18	135.1 ± 7.2	60.5 ± 5.8	Overdispersed interpolated to applied regenerative-dose ratio, accept tentatively
3	GL17156 (Quartz)	3.70-4.00 (-38.20 to -38.50)	2.38 ± 0.20	186.0 ± 11.6	78.9 ± 8.3	Overdispersed interpolated to applied regenerative-dose ratio, accept tentatively

- 5.6.6 The methodological approach to sub-sampling for OSL involved maximising the utility of vibrocores recovered in transparent liners where the outer surface had been exposed to light (see section 4.6). Measures were taken to reduce the risk of exposed grains from the outer surface of the cores becoming incorporated in the OSL sample that was taken from the centre of the core under controlled light conditions (see section 4.6). If recently exposed, fully or partially bleached grains were included in the aliquots measured, this would lead to an underestimation of the burial age.
- 5.6.7 There are a number of tests to detect for partial bleaching. Within this study, signal analysis of quartz OSL samples was used to quantify the change in D_e value with respect to optical stimulation time for multi-grain aliquots (**Figures 4 in Appendix 4**). A statistically significant increase in natural D_e with time is indicative of partial bleaching, but this assumes certain laboratory conditions are met (see **Appendix 4**). The results from signal analysis from each of the sub-samples do not show an increase in natural D_e with time suggesting there is no evidence of partial bleaching. However, it is noted that the utility of signal analysis is strongly dependent upon a sample's pre-burial experience of sunlight's spectrum and its residual to post-burial signal ratio, and that all laboratory conditions are met.
- 5.6.8 Inter-aliquot D_e distributions studies may be used to test for partial bleaching. At present, it is contended that asymmetric inter-grain D_e distributions are symptomatic of partial bleaching (Murray et al. 1995; Olley et al. 1999; 2004 and Bateman et al. 2003). Samples

GL17153 quartz and GL17156 exhibit asymmetric distributions which may be indicative of partial bleaching (**Figures 3** in **Appendix 4**). However, distinguishing between partial bleaching caused by the sampling process and that which occurred naturally during deposition is problematic, especially in water lain sediments (such as Upper Brown Bank) where partial bleaching is prolific (Murray et al. 1995). Single-grain analysis could be used to detect for statistical differences in D_e distribution but again, determining if this was caused by sample handling or depositional processes would remain problematic.

- 5.6.9 Based on accepted OSL ages (GL17153 and GL17154 quartz), deposition of Upper Brown Bank occurred between 69.8 ± 7.7 ka and 83.2 ± 9.5 ka, but the dates are unconformable introducing uncertainty. The K-feldspar IRSL dates from the same depths in VC016, suggest deposition occurred before 75.4 ± 8.2 ka to 91.5 ± 8.1 ka. Quartz OSL dates from VC047 (GL17155 and GL17156) are in broad agreement with the accepted ages from VC016 (78.9 ± 8.3 ka to 60.5 ± 5.8 ka). Collectively, optical dating results suggest Upper Brown Bank was deposited between 91.5 ± 8.1 ka (GL17154 feldspar) and 60.5 ± 5.8 ka (GL17155), from MIS 5b to MIS 4 during the Early Devensian.

5.7 Palaeogeographic reconstructions

- 5.7.1 Palaeogeographic reconstructions were compiled for two sea-level scenarios (see section **4.7** for selection criteria).
- 5.7.2 Scenario A corresponds to MIS 5d (115-105 ka) which is the earliest sub-stage (stadial) in the Early Devensian. During MIS 5d, sea level started to fall as climate cooled and ice sheets grew. According to global sea-level reconstructions (Spratt and Lisiecke 2016), sea level reached a maximum low of -46 m during MIS 5d, before it started to rise again. The palaeogeography of the Norfolk Boreas site at the lowest sea level (-46 m) during MIS 5d (~115 ka) is presented in (**Figure 18a**).
- 5.7.3 The results show a large proportion of the Norfolk Boreas site would have been sub-aerially exposed during sea-level scenario A with the exception of the south-eastern part of the project area where there is a large channel feature that would have remained flooded despite low sea level (**Figure 18a**). This channel may have formed an estuary, be part of a wider embayment or a restricted lagoon if a barrier existed to protect it. In the southwest of the project area, there are a series of localised isolated basins within the landscape that may have ponded water.
- 5.7.4 Scenario B corresponds to MIS 5b (92-84 ka) which is also a stadial (cool period) within the Early Devensian. At its lowest point, sea-level during this sub-stage reached -42 m (~80 ka) (Spratt and Lisiecke 2016). The palaeogeography of the Norfolk Boreas site under this sea-level scenario is presented in **Figure 18b**.
- 5.7.5 The results suggest the southern part of the Norfolk Boreas site would have been submerged during this time, but water depths are expected to have been shallow (<5 m) in the southeast and deeper in the southeast (up to 25 m). The northern part of the project area may have been sub-aerially exposed, but the area would have been low lying land, possible creating a series of small islands and a highly irregular coast.

6 DISCUSSION

6.1 Introduction

6.1.1 The palaeoenvironmental and dating results are considered collectively with reference to the aims and objectives outlined in **Section 2**, and to the regional research agenda (Medlycott 2011) and the national maritime research framework (Ransley et al. 2013).

6.1.2 The results are discussed according to key geological and archaeological periods as follows:

6.2 Middle to Upper Palaeolithic (Early-Mid Devensian) [MIS 5e – MIS 3]

Chronology

6.2.1 The age of Upper Brown Bank (Unit 5) is of archaeological interest as it has implications for our understanding of the palaeogeographic development of the southern North Sea during a period of hiatus in the British archaeological record (MIS 6-4) (Lewis et al. 2011).

6.2.2 Cameron et al. (1992) defined Brown Bank Formation (equivalent to Unit 5) as a shallow, restricted, brackish lagoon that resulted from sea-level fall during the Early Devensian. In the UK sector, Brown Bank Formation is characterised by a series of north-south trending channels in the west, and a broad basin in the east that extends into the Dutch sector (Hijma et al. 2012).

6.2.3 Brown Bank Formation has been previously dated using OSL (WA 2008; Limpenny et al. 2011; Tizzard et al. 2014; 2015) and ages fall into two broad ranges:

- 116.7 ± 11.2 ka to 96 ± 11 ka (MIS 5d-5c) (WA 2008; Tizzard et al. 2014; 2015), and;
- 53.4 ± 5.4 ka to 30.4 ± 6.9 ka (MIS 3) (Limpenny et al. 2011).

6.2.4 Based on previous evidence it was not clear if Unit 5 was deposited gradually over the duration of the Early Devensian, or periodically, possibly punctuated by periods of hiatus and subaerial exposure (Tizzard et al. 2015).

6.2.5 The accepted optical dating results from Unit 5 deposits in the Norfolk Boreas site suggest deposition occurred between 83.2 ± 9.5 and 69.8 ± 7.7 ka which extends from MIS 5a through to MIS 4 (**Figure 19**). When combined with dates tentatively accepted due to analytical considerations (**Table 8**), deposition of Unit 5 occurred over a longer time period, from 91.5 ± 8.1 ka (MIS 5b) to 60.5 ± 5.8 ka (MIS 4).

6.2.6 The optical dating results from the Norfolk Boreas site are broadly comparable to Unit 5 OSL dates from the adjacent Norfolk Vanguard site (WA 2019) which suggest Upper Brown Bank was deposited between 82.4 ± 8.5 and 57.2 ± 6.4 ka, from MIS 5b through to MIS 3. When combined with dates from previous studies (Limpenny et al. 2011; Tizzard et al. 2015), collectively the results suggest Brown Bank Formation was deposited gradually over the duration of the Early Devensian, a period of overall cooling and climatic instability characterised by stadial (cold) and interstadial (warm) sub-periods (**Figure 2**).

6.2.7 The optical dating results are supported by the biostratigraphical evidence from the ostracod assessment (WA 2018d). The ostracod *Roundstonia globulifera*, a species that has been extinct in Britain since MIS 3, was observed. This suggests Unit 5 was deposited before MIS 3.

Palaeoenvironmental and palaeogeographic evolution

- 6.2.8 The depositional history of Upper Brown Bank (Unit 5) is of archaeological interest. Early studies proposed that it was deposited within a shallow lagoon (Cameron et al. 1992), and assessments of geophysical data identified shallow gas, possibly indicating organic material, and internal surfaces that may represent hiatuses resulting from sub-aerial exposure (WA 2018c).
- 6.2.9 The results from foraminifera and ostracod assessment of sub-samples from VC016 and VC047 (WA 2018d) suggest Unit 5 was laid down in an outer estuarine to marine environment in a shallow embayment under cold/cool climate conditions. The diversity in VC047 is slightly lower than in VC016 possibly indicating a more restricted or protected location. VC047 is located in the northeast corner of the Norfolk Boreas site within a topographic depression according to palaeogeographic reconstructions (**Figure 17**). The wider geography of this topographic low beyond the project area boundary is unknown and it may form part of a channel system or isolated basin.
- 6.2.10 The foraminifera and ostracod assemblages from Unit 5 in the Norfolk Boreas site are comparable to the sequences from the Norfolk Vanguard East site (WA 2019) which is located directly to the south of the Norfolk Boreas site (**Figure 1**). The assemblages from Norfolk Vanguard West differ slightly in that they suggest a more open marine environment (WA 2019), but still within a shallow embayment. These observations imply Unit 5 becomes increasingly marine-marginal towards the east. If this is the case, Unit 5 may be a distal component of the Rhine-Meuse delta system prograding into the North Sea from the east (Hijma et al. 2012; Peeters et al. 2015).
- 6.2.11 Foraminifera and ostracod assemblages from Unit 5 at the Norfolk Boreas site are dominated by species indicative of a cool/cold environment (WA 2018e). However, in VC016 and VC047, the presence of large, ornate *Ammonia batavus* which are typical of warm interglacial climates, was noted in the uppermost sub-samples. The presence of both warm and cool/cold climate indicators within Unit 5 may reflect climatic instability during the Early Devensian, with the “warm” species flourishing during interstadials and “cold” species during stadials. The results from the microfossil assessment therefore support an Early Devensian age for Unit 5, as indicated by OSL dates.
- 6.2.12 By comparing the elevation of the Brown Bank deposits to past sea-level and climate data, the palaeogeographic evolution of the Norfolk Boreas site can be reconstructed. At a broad-scale, this provides information on when the site is likely to have been submerged and sub-aerially exposed (**Figure 19**), as summarised in **Table 9**.

Table 9 Palaeogeography of the Norfolk Boreas site during Early to Mid-Devensian

MIS ¹ (Age)	Sea-level ²	Climate	Palaeogeography
MIS 3 (~45 ka)	-70 m (low)	Pleniglacial (cold)	Entire site subaerially exposed
MIS 3 (~52 ka)	-60 m	Pleniglacial (cold)	Site largely sub-aerially exposed but may have been periodically submerged
MIS 4 (~65 ka)	-85 m (low)	Pleniglacial (cold)	Entire site subaerially exposed
MIS 5a (~80 ka)	-30 m (high)	Interstadial (warming)	Site submerged, water depths >10 m
MIS 5b (~88 ka)	-42 m (low)	Stadial (cooling)	Large are of the site potentially sub-aerially exposed with the exception of a large channel feature
MIS 5c (~100 ka)	-20 m (high)	Interstadial (warming)	Site submerged, water depths >20 m



MIS ¹ (Age)	Sea-level ²	Climate	Palaeogeography
MIS 5d (~110 ka)	-46 m (low)	Stadial (cooling)	Northern part of the site potentially sub-aerially exposed
MIS 5e (130-117 ka)	Highstand	Last Interglacial (warm)	Site submerged, 40-70 m water depth

¹MIS stratigraphy from Lisiecki and Raymo (2005)
²Sea level relative to today from Spratt and Lisiecki (2016)
Shaded rows = palaeogeographic models for these periods presented in Figure 17

- 6.2.13 The model suggests the Norfolk Boreas site was submerged for the majority of the Early Devensian until MIS 4 when globally sea-level fell to a low of -85 m (Spratt and Lisiecki 2016). Palaeogeographic reconstructions for these time periods show that even when sea-levels were at their lowest position during stadial periods (MIS 5d and MIS 5b), the Norfolk Boreas site was never fully exposed.
- 6.2.14 Globally, there is a period of relative sea-level rise at the transition between MIS 4 and MIS 3 which may have submerged the Norfolk Boreas site. However, this depends on how much Upper Brown Bank sediment was deposited during the preceding stadial and interstadial periods. During MIS 3 sea levels fell towards their low stand level of approximately -120 m and the entire Norfolk Boreas project area, and wider southern North Sea would have become subaerially exposed, but instead was a more marine-marginal environment.
- 6.2.15 There is a prominent channel feature in the southeast of the Norfolk Boreas site, which would have remained submerged throughout the Early Devensian. With fluctuating sea levels, water depths would have ranged between 20 m and 50 m. This channel will have been a prominent feature in the landscape during periods of low sea level, creating an estuary or restricted embayment/lagoon depending on the wider palaeogeographic configuration of the southern North Sea. The relatively shallow ground around the margins of the large channel would have formed a coastal plain which is of archaeological interest due to the potential to have been the focus of past human activity (Bailey and Parkington 1988).
- 6.2.16 The preservation of coastal deposits is typically poor due to reworking during sea-level rise. However, increasingly more examples of submerged and buried coastlines are being uncovered (Mellett and Plater 2017). In VC047 and VC016, iron minerals were observed in Unit 5. These iron precipitates may be associated with weathering or near-surface groundwaters (Ashton et al. 2005), possibly indicating periods of drying out and weathering (hiatus).
- 6.2.17 As part of the geophysical data assessment, a number of dune features were observed in seismic data directly below the boundary between Unit 4 and Unit 5. These dunes are similar to dune features observed in Norfolk Vanguard West (WA 2017), although more poorly developed. It is not known if these dunes may have formed in a terrestrial environment during sub-aerial exposure, or a sub-aqueous setting while submerged, but their preservation highlights the potential for preserving palaeolandscape features.
- 6.2.18 It is assumed periods of sub-aerial exposure of the Norfolk Boreas site would correspond to stadial periods when sea levels were relatively lower. Unfortunately, the chronological resolution of optical dating is not high enough to test this as the error margins on the dates (up to ± 8.5 ka) can be greater than the length of the stadial to interstadial sub-periods (~5-14 ka).

6.2.1 The palaeogeographic reconstructions can be tested with the palaeoenvironmental and dating results, which imply that Unit 5 was deposited in a near-marine embayment to open estuarine setting between 82.4 ± 8.5 ka and 57.6 ± 5.9 ka (MIS 5b to MIS 3). The results presented here suggest shallow marine conditions prevailed in the southern North Sea through MIS 4, which is an entire Marine Isotope Stage longer than predicted using global sea-level reconstructions. It also doesn't agree with terrestrial records that suggest MIS 4 in NW Europe was a period of intensive fluvial erosion and reworking driven by a fall in sea level (Busschers et al. 2007; Hijma et al. 2012). Furthermore, the palaeogeographic reconstructions do not account for past land-level (crustal) changes and assume the elevation of Unit 5 in the present-day is the same as in the past, which is unlikely given isostatic effects associated with the last glaciation (Shennan et al. 2013) and possible reactivation of older tectonic structures (Arfaï et al. 2018).

6.2.2

6.2.3 After MIS 4, sea levels continued to fall in MIS 3 reaching a low of ~120 m below present day during the Last Glacial Maximum (35-21 ka) (Chiverrell and Thomas 2010). During this time, the Norfolk Boreas site would have been subaerially exposed. However, no deposits from this period are preserved within the Norfolk Boreas site, possibly due to reworking by active channel belts and aeolian processes during the late glacial (Peeters et al. 2015).

Archaeological significance

6.2.4 The results indicate there was a shallow embayment fringed by more estuarine environments (the Brown Bank embayment) at the Norfolk Boreas site from the start of the Early Devensian (MIS 5b) through to MIS 4. The age of this embayment correlates to a period of hiatus in the British archaeological record (MIS 6-4) (Lewis et al. 2011). Therefore, it could be argued that the presence of the Brown Bank embayment created a significant geographic barrier to migration pathways through the southern North Sea during the Middle Palaeolithic.

6.2.5 The Brown Bank embayment appears to have been a persistent feature in the landscape, but there is potential for the Norfolk Boreas site to have been partially exposed during periods of lower sea level associated with cold stadial periods (MIS 5d and MIS 5b). The coastal configuration appears to have been dominated by a topographic low that may have formed an estuary within a wider embayment that was repeatedly flooded as sea levels fluctuated. This coastal setting would have been a challenging environment for hominin exploitation.

6.2.6 The earliest evidence of reoccupation after the MIS 6-4 hiatus occurred at ~60 ka (Boismier et al. 2012). At this time, the southern North Sea is expected to have emerged creating a terrestrial landscape that may have supported migration pathways from continental Europe into Britain. Within the Norfolk Boreas site, the Upper Palaeolithic is characterised by a hiatus in the geological record of ~40,000 thousand years. Our understanding of palaeolandscape development within the context of the already sparse Upper Palaeolithic record from Britain (Pettitt and White 2012) is therefore limited and the potential for preservation of archaeological material from this period is considered low (**Table 9**).

6.2.7 However, there is a need to understand the palaeogeographic evolution of the Brown Bank embayment within the context of the wider North Sea and English Channel, to fully explore its role in influencing migration pathways through the southern North Sea during the Middle to Upper Palaeolithic.



6.3 Late Upper Palaeolithic to Mesolithic (Late Devensian to Holocene) [MIS 2-1]

Chronology

- 6.3.1 Late Devensian to Early Holocene deposits are characterised by Unit 7 which has been subdivided into three sub-units (**Table 4**).
- 6.3.2 Peat deposits (Unit 7b) preserved in the Norfolk Boreas site are of archaeological interest as they contain palaeoenvironmental material that can be used to reconstruct landscape history. Overlying minerogenic deposits of Unit 7c are of interest as they mark the transition from a terrestrial to coastal, and later marine environment under the influence of rising sea levels. Establishing the age of these deposits is important to provide a chronological framework for environmental change, but also to constrain the timing of inundation of the now-submerged landscape.
- 6.3.3 Of the eight radiocarbon dates from Unit 7 (VC028, VC032 and VC039), UBA-38191 and UBA-39473 were identified as outliers raising questions about their reliability. The remaining six dates are considered reliable estimate of age based on chronological modelling (see section **5.5**).
- 6.3.4 When considered alongside the pollen results, there is possible uncertainty around one of the radiocarbon dates from VC039 (UBA-39471). In VC032 and VC028, the pollen assemblages record a shift from pine to hazel-dominated woodland which broadly correlates to the appearance of oak and elm. This change in vegetation is considered to have occurred in VC032 at c. 10,000-9500 cal. BP and before 9900-9570 cal. BP in VC028. The pine to hazel shift is also recorded in the peat sequence in VC074 at the adjacent Norfolk Vanguard project area, where it is expected to have occurred at c. 10,100 cal. BP (WA 2019). This vegetation trend is not observed in VC039 which suggests the peat sequence at this location predates the sequences in VC039 and VC028, despite the date from the top of VC039 (8510 ± 58 BP; UBA-39471; 9560-9430 cal. BP) being of a comparable to VC028 and VC039.
- 6.3.5 UBA-39471 was taken at the very top of Unit 7b in VC039. The contact between Unit 7b and overlying Unit 8 is erosional, likely due to reworking during transgression. There is therefore a possibility for removal of upper parts of the peat which would explain why the pine to hazel shift is not recorded in the pollen sequence. The same erosional processes may have incorporated younger, reworked material into the top of the peat.
- 6.3.6 The radiocarbon dates from Unit 7 span the Late Devensian, including the Loch Lomond stadial, through to the Early Holocene. A date from Unit 7a in VC039 suggests deposition at 10435 ± 66 BP (UBA-39472; 12550-12080 cal. BP). Peat formation (Unit 7b) commenced at the very start of the Holocene at 9992 ± 51 BP (UBA-38190; 11710-11260 cal. BP) in VC032 and continued for a period of up to ~700 yrs according to Bayesian chronological modelling. Inundation of the project area by rising sea-levels as represented by Unit 7c, occurred sometime after 8697 ± 45 BP (UBA-38189; 9880-9540 cal. BP).
- 6.3.7 The dates from the Norfolk Boreas site are broadly comparable with dates from peat and organic sequences recovered elsewhere in the southern North Sea (Hazell 2008; Brown et al. 2018; Geary et al. 2017).

Palaeoenvironmental and palaeogeographic evolution

- 6.3.8 The Late Devensian environments of the Norfolk Boreas site are represented by Unit 7a in VC028, VC032 and VC039. Microfauna is invariably preserved in Unit 7a. Diatoms are

absent from all three cores, likely due to taphonomic processes post-deposition. The lower parts of Unit 7a, comprise reworked Early Devensian marine foraminifera, suggesting erosion of the underlying Unit 5 deposits, although the exact process of erosion is unknown and could be related to river, wind or periglacial processes at any time during the Late Devensian. In VC032 and VC028, foraminifera and ostracods are absent from the upper parts of Unit 7a but plant fragments were noted (WA 2018d) indicating deposition in an active freshwater environment. This interpretation is corroborated by the occurrence of freshwater ostracods in Unit 7a in VC039.

- 6.3.9 Vibrocores VC028, VC032 and VC039 do not appear to be associated with palaeochannel features as mapped from geophysical data (WA 2018c; **Figures 7-9**). However, masking of the seismic signal by overlying peat deposits may have limited the interpretation. Elsewhere within the Norfolk Boreas site, a network of palaeochannels has been mapped indicating active river processes. At the adjacent Norfolk Vanguard site, Unit 7a is preserved in vibrocores located within, or along the margin of palaeochannel features (WA 2019). Therefore, while there is no direct association with palaeochannel features in the Norfolk Boreas site, Unit 7a is interpreted to represent deposition in active channels that cut into the underlying Upper Brown Bank deposits, during the Late Devensian.
- 6.3.10 BGS have mapped Twente Formation (Unit 6), a wind-blown sand, within the Norfolk Boreas site (Cameron et al. 1992). However, Unit 6 was not definitively identified during the geophysical assessment (WA 2018c). While Unit 7a shows similar characteristics to Twente Formation lithologically, the results presented here suggest Unit 7a is fluvial in origin, and therefore part of the Elbow Formation (**Table 4**). Unit 6 is considered absent from the project area.
- 6.3.11 Unit 7a is interpreted to represent a period of active fluvial processes during the Late Devensian. At its maximum southerly limit, the North Sea Lobe of the British Irish Ice Sheet (BIIS) would have been located ~20 km north of the Norfolk Boreas project area (**Figure 4**) and the site may have been influenced by ice-marginal glaciofluvial processes (e.g. Dove et al. 2017) resulting in deposition of Unit 7a. However, the geophysical data indicates palaeochannels within the Norfolk Boreas site are sinuous which are not characteristic of glaciofluvial processes, but instead are more typical of warmer climate fluvial processes. Deposits associated with these palaeochannels are therefore more likely to have formed in a fluvial setting, as appose to a highly erosive glaciofluvial environment.
- 6.3.12 Pollen results indicate the Late Devensian landscape was one of open grassland with scattered dwarf birch with areas of fen or reed wetland likely forming along the margins of river channels or in topographic depressions in slow moving or still water.
- 6.3.13 The morphology of the palaeochannel network preserved at the Norfolk Boreas site is visible in both multibeam bathymetry and seismic data (**Figure 3** and **Figure 19**). A sinuous channel is present at seabed and can be traced for ~6 km until it disappears under a sand bank (**Figure 19**). Of interest, this palaeochannel is a positive topographic feature, creating a ridge opposed to topographic depression. On seismic data, a bright reflector is observed at the location of the channel suggesting the presence of organic material, possibly peat, although no vibrocores penetrate the palaeochannel to test this. Peat deposits (Unit 7b) recovered in vibrocores are highly compacted and are therefore likely to be more resistant to erosion when compared with the sands, silts and clays of Unit 7a and Unit 5. This may explain why the palaeochannel has positive relief with peat that would have formed along the channel margins having higher preservation potential.



- 6.3.14 According to geophysical data, peat deposits (Unit 7b) are not restricted to palaeochannels but are also present in isolated patches, principally in the north of the Norfolk Boreas site, and collectively Unit 7b covers an area of up to ~45 km² (**Figure 3**).
- 6.3.15 Peat development commenced in the Early Holocene. The duration of peat formation in the Early Holocene is relatively short-lived, lasting 213-708 yrs according to chronological modelling (**Table 7**). When compared to Unit 7b at the adjacent Norfolk Vanguard project area, peat development appears to have commenced at a later date, although this may simply be a result of not recovering any earlier peat deposits in vibrocores.
- 6.3.16 The vegetation response to rapid climatic amelioration during the early Holocene is recorded in Unit 7b. A significant rise in the amount of tree pollen marks the return of woodland. Initially, pine was the dominant woodland component for at least c. 1500 years before giving way to hazel, dated in VC032 to sometime around c. 10,000-9500 cal. BP. Hazel was present prior to this date but as a subordinate understorey component of the pine-dominated woodland. Scattered elm and oak also appear at this time, probably around c. 10,500 cal. BP and increasing from 8894 ± 78 BP (UBA-39474, 10200-9700 cal. BP), becoming an important component of the hazel-dominated woodland.
- 6.3.17 Patterns of tree spreading for the British Isles typically show an expansion first of birch in the Early Holocene followed by pine (Birks 1989; Brewer et al. 2017). Only a small increase in birch (c. 10%) was recorded from VC032, with higher values (c. 30%) in VC039. The variable presence of birch could suggest local ecological constraints on expansion, for example, including competition with pine. However, there are also relatively low values of birch during the Early Holocene at the adjacent Norfolk Vanguard project area (WA 2019). At this location, higher values of birch are associated with the Windermere Interstadial during the Late Devensian (VC076).
- 6.3.18 The nearest comparable palynological sequence to both the Norfolk Boreas and Norfolk Vanguard sites is from the Dudgeon Offshore Wind Farm which is located c. 100 km west of the Norfolk Boreas site. The Dudgeon sequence differs in several respects to the abundance, timing and rate of expansion of key tree taxa (Brown et al. 2018). Birch values are higher during the late glacial and early Holocene; there is no significant increase in pine; hazel increases at around 11,250-11090 cal. BP, between 1000-1500 years earlier than at the Norfolk Boreas site, although there is a comparable increase in elm and oak from around 10,500 cal. BP. These differences are difficult to consider in relation to the pattern and timing of tree spreading into the North Sea basin given the paucity of pollen studies from the region compared to terrestrial landscapes of Britain and north-west Europe. Moreover, the most recent mapping of late glacial and Holocene European pollen data held in the EPD (European Pollen Database) (Brewer et al. 2017) omit data from offshore areas and lacks comparable data from the Netherlands, northwest Germany and eastern England.
- 6.3.19 The pollen sequences from the Norfolk Boreas site are broadly comparable with other pollen studies from palaeochannels in the southern North Sea, although Unit 7b is perhaps up to ~2000 years earlier than deposits studied by Gearey et al. (2017) and Tappin et al. (2011) in the Humber region.
- 6.3.20 Overlying Unit 7b in VC032, lies Unit 7c which is characterised initially by organic silty clay that is finely laminated with cross beds typical of deposition in a tidal environment (WA 2018b). Pollen results show an increase of species tolerant of increased salinity and the diatom assemblages are dominated by Polyhalobous (marine) to Mesohalobous (brackish) species. Collectively, the palaeoenvironmental data indicates a switch to a saltmarsh to

mudflat environment which marks inundation of the Norfolk Boreas site under rising sea-levels.

- 6.3.21 It is expected that as sea-levels rose, former river channels would have flooded and with increasing tidal influence, the landscape would have been dominated by a network of tidal creeks and flats. The fragmented extent of peat deposits (**Figure 3**) may be the result of erosion by a network of tidal channels as the landscape changed from freshwater wetlands with woodland, to saltmarsh and tidal flats.
- 6.3.22 Unit 7c is not present in VC028 or VC039. In these cores, the contact between Unit 7b and overlying Unit 8 is erosional which may indicate Unit 7a was removed during transgression. The upper parts of the peat in VC028 includes sandy intraclasts which provides evidence of reworking.
- 6.3.23 A date from the top of the peat in VC032, located directly below the contact between Unit 7b and Unit 7c gave an age of 8697 ± 45 (UB-38189; 9880-9540 cal. BP) and can be used to give an indication of past relative sea-level, i.e. a sea-level index point. In VC032, there is no evidence of erosion as the peat (Unit 7b) gradually transitions to intertidal deposits (Unit 7c) indicating a positive (rising) sea-level trend. The elevation of the radiocarbon sub-sample has been corrected to meters below LAT and the palaeoenvironmental data suggest deposition somewhere between Mean High Water and Mean Low Water which is estimated to represent a tidal range of 4 m based on the modern-day tidal range of the Norfolk coast. The resulting sea-level index point from VC032 is plotted against the modelled sea-level curve for offshore Norfolk (Shennan et al. 2018), in **Figure 20**. The sea-level index point suggests the Norfolk Boreas site flooded at c. 9700 cal. BP, which is slightly later than the model predicts. Rates of relative sea-level rise at this time were rapid (ca. 12-13 mm/yr; Smith et al. 2011), which may explain the sharp shift in depositional environment recorded in vibrocores.
- 6.3.24 At the time of inundation (~9700 cal. BP), reconstructions from paleogeographic modelling of the southern North Sea (Sturt et al. 2013) suggest sea-level flooded the Norfolk Boreas site from the south. If this is the case, the Dover Straits was open much earlier than previously predicted (Shennan et al. 2000; Gaffney et al. 2007). The timing of inundation at the Norfolk Boreas site lies within the range of dates recorded from other peat deposits preserved offshore (ca. 11.5-7.5 ka; WA 2013a). Of interest, the timing of inundation of the Norfolk Boreas site appears to have been slightly later (300 yrs) than at the Norfolk Vanguard site (~10,000 cal. BP) (WA 2019). However, this is based on only a few cores so does not account for any local topographic influences.

Archaeological significance

- 6.3.25 An extensive and rich submerged palaeolandscape record is preserved within the Norfolk Boreas site which documents palaeoenvironmental change from the late Upper Palaeolithic through to the early Mesolithic.
- 6.3.26 After initial recolonisation of Britain during MIS 3 (Boismier et al. 2012), there is evidence of sporadic incursions of various hominin groups into the southern North Sea from ~15 ka to the start of the Holocene (Jacobi and Highman 2011). This period is represented by Unit 7a at the Norfolk Boreas site, which was likely deposited in fluvial environment providing evidence for the presence of active rivers in the landscape which may have been exploited for resources, but also used as routeways to support migration. The potential for encountering in-situ or artefactual material within or along the margins of these channels is considered high (**Table 10**).

- 6.3.27 Extensive peat deposits (Unit 7b) (~45 km²) are preserved within the Norfolk Boreas site and they have high potential to contain palaeoenvironmental material which can be used to reconstruct landscape change. The discovery of submerged peat deposits is not novel and there are many examples of peats preserved locally within palaeochannels (WA 2008; Brown et al. 2018; Gaffney et al. 2007). However, uncovering a widespread “peatland”, along with peat-infilled and peat-fringed palaeochannels within a single site, is rare and unique within the context of submerged landscape studies undertaken to date. Furthermore, when combined with Norfolk Vanguard, a total of 85 km² of peat deposits have been discovered which could be considered one of the most significant finds in UK submerged landscape research in recent years.
- 6.3.28 The vegetation history of the Norfolk Boreas site is comparable to other records from the southern North Sea (Tappin et al. 2011; Gearey et al. 2017), but it has a role in bridging the gap between widely studied palaeoecological records from terrestrial settings on both sides of the North Sea.
- 6.3.29 The North Sea has been largely ignored in mapping of late glacial and Holocene pollen data (e.g. Birks 1989; Brewer et al 2017) due to a lack of data, and yet this area has a critical role to play in understanding the vegetation history of north-west Europe, including the migration history of key plant taxa (especially trees) into Britain. A greater spatial density in pollen studies would provide the basis for a more informed understanding of variability in vegetation habitats across the North Sea and their response to environmental factors. These data would in turn help to inform palaeogeographic models for the region and refine our understanding of the likely range of environmental contexts for human activity.
- 6.3.30 There is evidence in VC028, VC032 and VC039 of repeated fire-events during the early Holocene, although charcoal particles may have been transported long distances; therefore, it is not known if these fires are local or regional. Evidence for fire is widespread in Mesolithic Britain, in both upland and lowland environments (e.g. Simmons 1996; Mellars and Dark 1998; Bell 2007), although there is debate as to whether these fires are natural or anthropogenically induced events (Brown 1997; Moore 2000; Innes and Blackford 2003). At the Norfolk Boreas site, it is not possible to determine the cause of the fire-events, especially in the absence of known Mesolithic archaeology.
- 6.3.31 Peat development across the Norfolk Boreas site occurred from 9992 ± 51 BP (UB-38190; 11700-11260 cal. BP) to 8697 ± 45 BP (UB-9980-9540 cal. BP) which is broadly contemporaneous with key early Mesolithic sites located along the North Sea coast (e.g. Star Carr, Low Hauxley and Howick) (Waddington et al. 2015). The fluvial and wetland landscapes characteristic of the Norfolk Boreas site may have provided a pathway for Mesolithic hominin groups moving into Britain, driven by rising sea levels and landscape inundation. The potential for preservation of archaeological sites within this landscape is considered high (**Table 10**).
- 6.3.32 Inundation of the Norfolk Boreas site during the Mesolithic occurred sometime after ~9,700 cal. BP. The rate of landscape inundation is expected to have been rapid based on palaeogeographic modelling (Sturt et al. 2013) supported by evidence from vibrocores. The Norfolk Boreas site is located on the southern limb of what would have been the last land bridge between Britain and continental Europe (not including the Dogger Bank Island), before final inundation at ~8.5 ka (Sturt et al. 2013). The response of coastal communities to rapid rates of sea level rise is difficult to perceive without archaeological evidence. Given the relatively short life-expectancy of Mesolithic people (Burger et al 2012), it is unlikely coastal change would have been observable within a single generation.



- 6.3.33 It has been shown that the sediment sequences preserved in the Norfolk Boreas site can provide rare and necessary sea-level index points for the Early Holocene period (Hazell 2008; WA 2013a). This data can help refine understanding of the timing and nature of sea-level rise for a time period which is poorly represented in sediment sequences preserved onshore, it can also be used to constrain sea-level models.
- 6.3.34 The exceptional preservation of palaeolandscape features within the Norfolk Boreas site may in part be due to rapid inundation of the area during the early Holocene. When rates of sea-level rise outpace a coastlines ability to adjust, the landscape becomes submerged offshore and assuming limited reworking by waves, the former-landscapes have high preservation potential. Curiously, unlike at the adjacent Norfolk Vanguard site, the location of palaeolandscape features does not appear to be strongly related to the location of large sand banks. At the Norfolk Boreas site, modern seabed processes play a role in both preserving, through burial, and exposing palaeolandscape features making it difficult to predict where palaeolandscapes are most likely to be preserved.

Table 10 Archaeological potential of deposits studied within the Norfolk Boreas site

WA Unit	WA Unit Name Age (MIS)	Palaeoenvironment	Archaeological potential
8	Seabed sediments <i>Holocene post-transgression (MIS 1)</i>	Marine, active hydrodynamic processes.	Unlikely to comprise prehistoric archaeology. Has a role in protecting palaeolandscape features.
7c	Elbow Formation – intertidal <i>Early Holocene (MIS 1)</i>	Coastal, tidal creeks and flats deposited under influence of rapid rates of Early Holocene sea-level rise.	Potential to comprise Early Mesolithic artefactual archaeology.
7b	Elbow Formation – organic <i>Late Devensian to Early Holocene (MIS 2-1)</i>	Freshwater wetland forming within and along the margins of palaeochannels, or within topographic lows in the landscape, with woodland occupying dry ground. Possible hiatus in peat development associated with the Loch Lomond stadial.	High preservation of palaeoenvironmental material. Potential to comprise Upper Palaeolithic or Early Mesolithic artefactual archaeology.
7a	Elbow Formation – fluvial <i>Late Devensian to Early Holocene (MIS 2-1)</i>	Freshwater active fluvial channels. Palaeochannels can be highly sinuous indicating maturity of the river system.	Potential to comprise in-situ and reworked archaeology is high, both within channels and along their margins.
6	Twente Formation – <i>Late Devensian (MIS 2)</i>	Not present	
5	Upper Brown Bank - <i>Early-Mid Devensian (MIS 5d-3)</i>	A cold-climate, shallow near-marine embayment fringed by estuaries. Water depths shallowed during periods of lower sea-level, possibly creating an irregular, marine-marginal coastal landscape.	Potential for preservation of archaeological material low. However, the Brown Bank embayment may have created a significant geographic barrier to migration pathways through the southern North Sea during the Middle Palaeolithic, correlating to a period of absence in the British archaeological record.
4	Lower Brown Bank/Eem Formation - <i>Ipswichian to Early Devensian (MIS 5e-5d)</i>	Not identified in geotechnical data.	
3	Swarte Bank Formation - <i>Anglian (MIS 12)</i>	Not identified in geotechnical data.	



WA Unit	WA Unit Name Age (MIS)	Palaeoenvironment	Archaeological potential
2	Yarmouth Roads Formation - Early to Mid-Pleistocene (>MIS 13)		Not identified in geotechnical data.
1	Westkapelle Ground Formation – Late Pliocene to Early Pleistocene (MIS 63-103)		Not identified in geotechnical data

7 CONCLUSIONS

7.1.1 This report aims to assess the submerged palaeolandscape resource within the Norfolk Boreas site by addressing a series of research questions posed in **Section 2**. The key conclusions in relation to these research questions, are outlined below.

Middle to Upper Palaeolithic

- What is the age and depositional history of Brown Bank Formation?

7.1.2 Brown Bank Formation (Unit 5) was deposited between 83.2 ± 9.5 and 69.8 ± 7.7 ka (MIS 5a-4), in an outer estuarine environment within a shallow marine embayment during a period of climatic instability characterised by cool (stadial) and warm (interstadial) periods, in the Early Devensian.

- What is the palaeogeography of the area during deposition of Brown Bank Formation?

7.1.3 The paleogeography of the Norfolk Boreas site was part of a shallow near-marine embayment fringed by open estuaries. During periods of lower sea level associated with cool stadials, the Brown Bank embayment would have shallowed with some areas emerging creating a coastal plain along the margins of an estuary or restricted embayment/lagoon.

- How do the findings relate to the presence or absence of hominins in Britain during the Middle Palaeolithic?

7.1.4 The results suggest the Brown Bank embayment was a prominent feature in the southern North Sea during the Early Devensian, corresponding to a period of hiatus in the British archaeological record. The presence of this embayment would have created a significant geographic barrier to migration pathways through the southern North Sea during the Middle Palaeolithic and may in part explain the absence of hominins from Britain between MIS 6 and MIS 4.

Late Upper Palaeolithic to Mesolithic

- What is the age and formation history of the preserved peat deposits?

7.1.5 Peat formation commenced at the very start of the Holocene at 9992 ± 51 BP (UBA-38190; 11710-11260 cal. BP) in VC032 and continued for a period of up to ~700 yrs according to Bayesian chronological modelling, creating an extensive wetland environment in and around a network of fluvial channels.

- What is the landscape and vegetation history?



- 7.1.6 The Late Devensian landscape was characterised by active river systems with reed and fen wetlands forming along the margins, and open grassland scattered with dwarf birch. As climate warmed in the Early Holocene, woodland remained relatively open, but became dominated by pine, and later hazel with some oak and elm. Under rising sea levels, the coastline encroached, giving way to saltmarsh and tidal flats before final inundation.
- Is there evidence for hominin activity?
- 7.1.7 The presence of charcoal within peat deposits is evidence of repeated fire-events during the Early Holocene, although it is not possible to establish if these were caused by human activity. Despite the absence of known archaeological material, the potential for human activity within the extensive fluvial and wetland landscapes preserved at Norfolk Boreas is considered high.
- What is the timing and nature of landscape inundation?
- 7.1.8 A sea-level index point from VC032 indicates that the area now occupied by the Norfolk Boreas site became submerged shortly after c. 9700 cal. BP which agrees with sea-level and regional-palaeogeographic models. Rates of sea-level rise were rapid (12-12 mm/yr) leaving the landscape little time to adjust; the palaeolandscape features appear to have drowned in-situ, possibly leading to their exceptional preservation.

8 RECOMMENDATIONS

- 8.1.1 It is recommended the final results from geoarchaeological and geophysical works undertaken in support of the Norfolk Boreas project, are disseminated publicly through publication in a peer reviewed journal.
- 8.1.2 Typically, it is advised all results are published in a single manuscript. However, given similarities in the techniques employed and research objectives between the Norfolk Boreas site and the adjacent Norfolk Vanguard site, it is recommended the results are integrated for publication in two period specific manuscripts, as follows;
- Late Devensian to Early Holocene landscape development and inundation
 - A reappraisal of Brown Bank Formation - Implications for palaeogeography and hominin occupation
- 8.1.3 This approach will produce regional scale palaeolandscape reconstructions driven by period specific research questions, thus having a wider impact than more localised site-specific data driven reconstructions.
- 8.1.4 The results presented here, in combination with those from the adjacent Norfolk Vanguard project area, have the potential for significant impact beyond the academic community. A range of options are being discussed with the Client in order to maximise the public benefits arising from this work.



REFERENCES

- Adamiec, G and Aitken, M J 1998 Dose-rate conversion factors: new data, *Ancient TL* 16, 37-50
- Arfai, J, Franke, D, Lutz, R, Reinhardt, L, Kley, J and Gaedicke, C 2018 Rapid Quaternary subsidence in the northwestern German North Sea. *Scientific Reports* 8, 11524.
- Ashton, N, Lewis, S, Parfitt, S, Candy, I, Keen, D, Kemp, R, Penkman, K, Thomas, G, Whittaker, J & White, M 2005. Excavations at the Lower Palaeolithic site at Elveden, Suffolk, UK, *Proc Prehist Soc*, 71, 1-61
- Ashton, N, Lewis, S G, Parfitt, S A, Penkman, K E H and Coope, G R 2008. New evidence for complex climate change in MIS 11 from Hoxne, Suffolk, UK, *Quat Sci Rev* 27, 652–668
- Bailey, G and Parkington, J 1988 *The Archaeology of Prehistoric Coastlines* Cambridge, Cambridge University Press
- Bateman, M D, Frederick, C D, Jaiswal, M K and Singhvi, A K 2003 Investigations into the potential effects of pedoturbation on luminescence dating, *Quat Sci Rev* 22, 1169-1176
- Battarbee, R W, Jones, V J, Flower, R J, Cameron, N G, Bennion, H B, Carvalho, L and Juggins, S 2001. Diatoms, in J P Smol and H J B Birks (eds) *Tracking Environmental Change Using Lake Sediments Volume 3: Terrestrial, Algal, and Siliceous Indicators*, 155-202. Dordrecht, Kluwer Academic Publishers.
- Bell, M 2007 *Prehistoric coastal communities: the archaeology of western Britain 6000-3000 cal BC*. York, Council for British Archaeology Research Report 149
- Bennett, K D, Whittington, G and Edwards, K J 1994 Recent plant nomenclatural changes and pollen morphology in the British Isles, *Quat News* 73, 1–6.
- Bicket, A and Tizzard, L 2015 A review of the submerged prehistory and palaeolandscapes of the British Isles, *Proc Geol Assoc* 126, 6, 642-663
- Birks, H J B 1989 Pollen isochrone maps and patterns of tree-spreading in the British Isles, *J Biogeog* 16, 503-40.
- Boismier, W, Gamble, C, and Coward, F 2012 *Neanderthals among Mammoths: Excavations at Lynford Quarry, Norfolk, UK*. English Heritage
- Brewer, S, Giesecke, T, Davis, B A S, Finsinger, W, Wolters, S, Binney, H, de Beaulieu, J-L, Fyfe, R, Gil-Romera, G, Kuhl, N, Kunes, P, Leydet, M and Bradshaw, R H 2017 Late glacial and Holocene European pollen data, *J Maps* 13, 921–928
- Bridgland, D R, Field, M H, Holmes, J A, McNabb, J, Preece, R C, Selby, I, Wymer, J J, Boreham, S, Irving, B G, Parfitt, S A and Stuart, A J 1999 Middle Pleistocene interglacial Thames–Medway deposits at Clacton-on-Sea, England: Reconsideration of the biostratigraphical and environmental context of the type Clactonian Palaeolithic industry, *Quat Sci Rev* 18, 109–146
- Bronk-Ramsay, C 2009 *OxCal calibration programme version v4.10*. Radiocarbon accelerator Unit, University of Oxford.



- Bronk Ramsey, C and Lee, S 2013 Recent and planned development of the Program OxCal, *Radiocarbon* 55, (2-3), 720–730
- Brown, A G 1997 Clearances and clearings: deforestation in Mesolithic/Neolithic Britain, *Oxford J Archaeol* 16, 133-46
- Brown, A, Russel, J, Scaife, R, Tizzard, L, Whittaker, J and Wyles, S 2018 Lateglacial/early Holocene palaeoenvironments in the southern North Sea Basin: new data from the Dudgeon offshore wind farm, *J Quat Sci* 33 (6), 597-610
- Burger, O, Baudisch, A, and Vaupel, J W 2012 Human mortality improvement in evolutionary context, *Proc Nat Acad Sci USA* 109, 18210-18214
- Busschers, F S, Kasse, C, van Balen, R T, Vandenberghe, J, Cohen, K M, Weerts, H J T, Wallinga, J, Johns, C, Cleveringa, P, Bunnik, F P M 2007 Late Pleistocene evolution of the Rhine-Meuse system in the southern North Sea basin: imprints of climate change, sea-level oscillation and glacio-isostasy, *Quat Sci Rev* 26 (25-28), 3216-3248
- Cameron, T D J, Crosby, A, Balson, P S, Jeffery, D H, Lott, G K, Bulat, J and Harrison, D J 1992 *The Geology of the Southern North Sea*. London, British Geological Survey United Kingdom Offshore Regional Report HMSO
- Candy, I, Silva, B and Lee, J 2011 Climates of the Early Middle Pleistocene in Britain: Environments of the Earliest Humans in Northern Europe, in N Ashton, S G Lewis and C Stringer (eds) *The Ancient Human Occupation of Britain*. Amsterdam, Netherlands, Elsevier B.V.
- Clark, R L 1982 Point count estimate of charcoal in pollen preparations and thin sections of sediment, *Pollen et Spores* 24, 523-535.
- Cohen, K M, MacDonald, K, Joordens, J C A, Roebroeks, W and Gibbard, P L 2012 The Earliest Occupation of North-West Europe: a Coastal Perspective, *Quat Intl* 271, 70-83
- Colarossi, D, Duller, G A T, Roberts, H M, Tooth, S, Lyones, R 2015 Comparison of paired quartz OSL and feldspar post-IR IRSL dose distributions in poorly bleached fluvial sediments from South Africa. *Quat Geochron* 30, 233-238
- Coles, B 1998 Doggerland: a speculative survey. *Proc Prehist Soc* 64, 45-81
- Cushing, E J 1967 Evidence for differential pollen preservation in late Quaternary sediments in Minnesota. *Rev Palaeobot Palyn* 4, 87–101
- Dix, J and Sturt, F 2011 *The Relic Palaeo-landscapes of the Thames Estuary*. Southampton, University of Southampton for MALSF
- Dove, D, Evans, D J A, Lee, J R, Roberts, D H, Tappin, D R, Mellett, C L, Long, D, Callard, S L 2017 Phased occupation and retreat of the last British–Irish Ice Sheet in the southern North Sea: geomorphic and seismostratigraphic evidence of a dynamic ice lobe. *Quat Sci Rev* 163, 114-134.
- Emu Ltd. 2009 *Outer Thames Estuary Regional Environmental Characterisation*. MALSF
-



-
- Fugro 2018 Report 1 of 3: *Geophysical Investigation Report. Volume 2 of 2: Interpretive Site Investigation Report. Norfolk Boreas Offshore Wind Farm.* Unpubl rep GE059-R1-2.
- Gaffney, V, Thomson, K and Fitch, S 2007 *Mapping Doggerland: The Mesolithic Landscapes of the Southern North Sea.* Oxford, Archaeopress
- Gearey, B, Hopla, E, Griffiths, S, Boomer, I, Smith, D, Marshall, P, Fitch, S and Tappin, D 2017 Integrating multi-proxy palaeoecological and archaeological approaches to submerged landscapes: a case study from the southern North Sea in H Williams, H Hill, I Boomer and I Wilkinson (eds) *The Archaeological and Forensic Applications of Microfossils: A Deeper Understanding of Human History.* Geological Society Special Publication
- Godwin, H and Godwin, M E 1933 British Maglemose Harpoon Sites. *Antiquity* 7, 36–48
- Grimm, E C 2011. Tilia 1.7.16 Software. Illinois State Museum, Research and Collection Center, Springfield.
- Hartley, B, Barber, H G, Carter, J R and Sims, P A 1996 *An Atlas of British Diatoms.* Bristol, Biopress Limited
- Hazell, Z 2008 Offshore and intertidal peat deposits, England – a resource assessment and development of a database, *Env Arch* 13 (2) 101-110
- Hendey, N I 1964 *An Introductory Account of the Smaller Algae of British Coastal Waters. Part V. Bacillariophyceae (Diatoms).* Ministry of Agriculture Fisheries and Food, Series IV
- Hijma, M P, Cohen, K M, Roebroeks, W, Westerhoff, W E and Busschers, F S 2012 Pleistocene Rhine-Thames landscapes: Geological background for hominin occupation of the southern North Sea region, *J Quat Sci* 27, 17-39.
- Housley, R A 1991 AMS Dates from the Late Glacial and Early Postglacial in North-West Europe: a Review in N Barton, A J Roberts, and D A Roe (eds) *The Late Glacial in North-West Europe: Human Adaptation and Environmental Change at the End of the Pleistocene.* 25-36. London, Council for British Archaeology
- Hublin J-J, Weston D and Gunz P 2009 Out of the North Sea: the Zeeland Ridges Neandertal, *J Hum Evol* 57, 777– 785
- Hustedt, F 1953 Die Systematik der Diatomeen in ihren Beziehungen zur Geologie und Ökologie nebst einer Revision des Halobien-systems, *Sv Bot Tidskr* 47, 509-519
- Hustedt, F 1957 Die Diatomeenflora des Fluss-systems der Weser im Gebiet der Hansestadt Bremen, *Ab naturw Ver Bremen* 34, 181-440
- Innes, J B and Blackford, J J 2003 The ecology of Late Mesolithic woodland disturbances: model testing with fungal spore assemblage data, *J Archaeol Sci* 30, 185-94
- Jacobi, R, and Higham, T 2011 The Later Upper Palaeolithic Recolonisation of Britain: New Results from AMS Radiocarbon Dating, in N Ashton, S G Lewis and C Stringer (eds) *The Ancient Human Occupation of Britain.* Vol. 14, 223–247. Amsterdam, Netherlands, Elsevier B.V.
- Krammer, K and Lange-Bertalot, H 1986-1991 *Bacillariophyceae.* Stuttgart, Gustav Fisher Verlag.
-



- Lewis S G, Ashton N and Jacobi, R 2011 Testing Human Presence during the Last Interglacial (MIS 5e): A Review of the British Evidence, in N Ashton, S G Lewis and C Stringer (eds) *The Ancient Human Occupation of Britain*. Vol.14, 125-247. Amsterdam, Netherlands, Elsevier
- Limpenny, S E, Barrio Froján, C, Cotterill, C, Foster-Smith, R L, Pearce, B, Tizzard, L, Limpenny, D L, Long, D, Walmsley, S, Kirby, S, Baker, K, Meadows, W J, Rees, J, Hill, J, Wilson, C, Leivers, M, Churchley, S, Russell, J, Birchenough, A C, Green, S L and Law, R J 2011 *The East Coast Regional Environmental Characterisation*. MEPF
- Lisiecki, L E and M E Raymo 2005 A Pliocene-Pleistocene stack of 57 globally distributed benthic $\delta^{18}O$ records, *Paleoceanography*, 20, PA1003
- Medlycott, M 2011 Research and archaeology revisited: a revised framework for the East of England. *East Anglian Archaeology* 24
- Mejdahl, V 1979 Thermoluminescence dating: beta-dose attenuation in quartz grains. *Archaeometry*, 21, 61-72
- Mellars, P A and Dark, S P 1998 *Star Carr in context*. Cambridge, MacDonald Institute for Archaeological Research.
- Mellett, C L and Plater, A J 2017 Drowned barriers as archives of coastal-response to rapid sea-level rise in L Moore and B Murray (eds) *Barrier dynamics and response to changing climate*. Springer
- Millard, A R 2014 Conventions for Reporting Radiocarbon Determinations. *Radiocarbon* 56(2), 555–559
- Momber, G, Tomalin, D, Scaife, R, Satchell, J and Gillespie, J 2011 *Mesolithic Occupation at Bouldner Cliff and the Submerged Prehistory Landscapes of the Solent*. Council for British Archaeology CBA Report 164
- Moore, P D, Webb, J A and Collinson, M E 1991 *Pollen analysis*. Oxford, Blackwell
- Moore, J 2000 Forest fire and human interaction in the early Holocene woodlands of Britain. *Palaeogeog, Palaeoclim, Palaeoecol* 164, 125-37
- Murray, A S and Wintle, A G 2000 Luminescence dating of quartz using an improved single-aliquot regenerative-dose protocol, *Rad Meas* 32, 57-73
- Murray, A S and Wintle, A G 2003 The single aliquot regenerative dose protocol: potential for improvements in reliability, *Rad Meas* 37, 377-381
- Murray, A S, Olley, J M and Caitcheon, G G 1995 Measurement of equivalent doses in quartz from contemporary water-lain sediments using optically stimulated luminescence. *Quat Sci Rev* 14, 365-371
- Olley, J M, Caitcheon, G G and Roberts R G 1999 The origin of dose distributions in fluvial sediments, and the prospect of dating single grains from fluvial deposits using -optically stimulated luminescence. *Rad Meas* 30, 207-217



- Olley, J M, Pietsch, T and Roberts, R G 2004 Optical dating of Holocene sediments from a variety of geomorphic settings using single grains of quartz, *Geomorp* 60, 337-358
- Parfitt, S A, Barendregt, R W, Breda, M, Candy, I, Collins, M J, Coope, G R, Durbidge, P, Field, M H, Lee, J R, Lister, A M, Mutch, R, Penkman, K E H, Preece, R C, Rose, J, Stringer, C B, Symmons, R, Whittaker, J E, Wymer J, and Stuart, A J 2005 The earliest record of human activity in northern Europe, *Nature* 438, 1008–1012
- Parfitt, S A, Ashton, N M, Lewis, S G, Abel, R L, Coope, G R., Field, M H, Gale, R, Hoare, P G, Larkin, N R, Lewis, M D, Karloukovski, V, Maher, B A, Peglar, S M, Preece, R C, Whittaker, J E, and Stringer, C B, 2010 Early Pleistocene human occupation at the edge of the boreal zone in northwest Europe, *Nature* 466 (7303), 229–33
- Peeters, J, Busschers, F S and Stouthamer, E 2015 Fluvial evolution of the Rhine during the last interglacial-glacial cycle in the southern North Sea basin: A review and look forward. *Quat Int* 357, 176-188
- Pettitt, P, and White, M J 2012 *The British Palaeolithic: Human Societies at the Edge of the Pleistocene World*. Abingdon, Routledge
- Prescott, J R and Hutton, J T 1994 Cosmic ray contributions to dose rates for luminescence and ESR dating: large depths and long-term time variations. *Rad Meas* 23, 497-500
- Ramsey, C B 2009 Dealing with Outliers and Offsets in Radiocarbon Dating. *Radiocarbon* 51, 1023-1045
- Ransley, J, Sturt, F, Dix, J, Adams, J and Blue, L, 2013 *People and the sea: a maritime archaeological research agenda for England*. York, Council for British Archaeology Research Report 171
- Reid, C 1913 *Submerged Forests*. London, Cambridge University Press
- Reimer, P J, Bard, E, Bayliss, A, Beck, J W, Blackwell, P G, Bronk Ramsey, C, Grootes, P M, Guilderson, T P, Haflidason, H, Hajdas, I, HattŽ, C, Heaton, T J, Hoffmann, D L, Hogg, A G, Hughen, K A, Kaiser, K F, Kromer, B, Manning, S W, Niu, M, Reimer, R W, Richards, D A, Scott, E M, Southon, J R, Staff, R A, Turney, C S M and van der Plicht, J 2013. IntCal13 and Marine13 Radiocarbon Age Calibration Curves 0-50,000 Years cal BP, *Radiocarbon*, 55(4), 1869–1887.
- Simmons, I G 1996 *The Environmental impact of later Mesolithic Cultures*. Edinburgh, Edinburgh University Press
- Scott, B, and Ashton, N 2011 The Early Middle Palaeolithic: The European Context, in N Ashton, S G Lewis and C Stringer (eds) *The Ancient Human Occupation of Britain*. Volume 14, 91–112. Amsterdam, Netherlands, Elsevier B.V.
- Scott, B, Ashton, N, Lewis, S G, Parfitt, S, and White, M, 2011 Technology and Landscape Use in the Early Middle Palaeolithic of the Thames Valley, in N Ashton, S G Lewis and C Stringer (eds) *The Ancient Human Occupation of Britain*. Volume 14, 67-89, Amsterdam, Netherlands, Elsevier B.V.



- Shennan, I, Lambeck, K, Flather, R, Horton, B, McArthur, J, Innes, J, Lloyd, J, Rutherford, M, Wingfield, R 2000 Modelling western North Sea palaeogeographies and tidal changes during the Holocene, in I Shennan and J E Andrews (eds) *Holocene Land-ocean Interaction and Environmental Change Around the Western North Sea*. Vol. 166. Geological Society Special Publication
- Shennan I, Bradley, S, and Edwards, R 2018 Relative sea-level changes and crustal movements in Britain and Ireland since the Last Glacial Maximum, *Quat Sci Rev* 188, 143-159
- Smith, D E, Harrison, S, Firth, C R and Jordan, J T 2011 The early Holocene sea level rise. *Quat Sci Rev* 30, 1846-1860
- Spratt, R M and Lisiecke, L E 2016 A Late Pleistocene sea level stack. *Clim. Past* 12, 1079-1092
- Stace, C 1997 *New flora of the British Isles* (2nd edition), Cambridge, Cambridge University Press.
- Stoker, M S, Balson, P S, Long, D, Tappin, D R 2011 *An overview of the lithostratigraphical framework for the Quaternary deposits on the United Kingdom continental shelf*. Keyworth, British Geological Survey Research Report RR/11/03
- Stuiver, M and Reimer, P J 1986 A computer program for radiocarbon age calculation. *Radiocarbon* 28, 1022–30
- Sturt, F, Garrow, D and Bradley, S 2013 New models of North West European Holocene palaeogeography and inundation. *J Arch Sci* 40, 3963-3976
- Sumbler, M G 1996 *British Regional Geology; London and the Thames Valley*. London, HMSO
- Tappin, D R, Pearce, B, Fitch, S, Dove, D, Gearey, B, Hill, J M, Chambers, C, Bates, R, Pinnion, J, Diaz Doce, D, Green, M, Gallyot, J, Georgiou, L, Brutto, D, Marzioletti, S, Hopla, E, Ramsay, E, and Fielding, H 2011 *The Humber Regional Environmental Characterisation*. British Geological Survey Open Report OR/10/54
- Thomsen, K J, Murray, A S, Jain, M and Botter-Jensen, L 2008 Laboratory fading rates of various luminescence signals from feldspar-rich sediment extracts, *Rad Meas* 43, 1474-1486
- Tizzard, L, Bicket, A R, Benjamin, J, and De Loecker, D 2014 A Middle Palaeolithic Site in the Southern North Sea: Investigating the Archaeology and Palaeogeography of Area 240. *J Quat Sci* 29, 698–710
- Tizzard, L, Bicket, A R, Benjamin, J and De Loecker, D 2015 *A Middle Palaeolithic Site in the Southern North Sea: Investigating the Archaeology and Palaeogeography of Area 240*. Salisbury, Wessex Archaeology Monograph no 35
- Waddington C 2015 Mesolithic re-colonisation of Britain following on the drowning of North Sea landscapes in N Ashton and C Harris (eds) *No Stone Unturned. Papers in Honour of Roger Jacobi*. 221-232. London, Lithic Studies Society
- Werff, A Van Der and Huls, H 1957-1974 *Diatomeenflora van Nederland*, 10 volumes
- Wessex Archaeology 2008 *Seabed Prehistory: Gauging the Effects of Marine Aggregate Dredging. Round 2 Final Report, Volume II: Arun*. Salisbury, unpubl rep 57422.32
-



- Wessex Archaeology 2011 Seabed Prehistory: Site Evaluation Techniques (Area 240). Salisbury, unpubl report, ref: 70754.04
- Wessex Archaeology 2013a *Audit of Current State of Knowledge of Submerged Palaeolandscapes and Sites*. Salisbury, unpubl report, ref: 84570.01
- Wessex Archaeology 2013b *Palaeo-Yare Catchment Assessment*. Salisbury, unpubl rep 83740.04
- Wessex Archaeology 2017a. *Norfolk Vanguard Offshore Wind Farm, marine archaeological technical report*. Salisbury, unpubl rep 112380.02.
- Wessex Archaeology 2017b *Vanguard Offshore Wind Farm, Stage 1 geoarchaeological review*. Salisbury, unpubl rep 114840.01.
- Wessex Archaeology 2018a *Norfolk Boreas Offshore Wind Farm: Stage 1 Geoarchaeological Report*, Salisbury, unpublished report ref 117120.01
- Wessex Archaeology 2018b *Norfolk Boreas Offshore Wind Farm: Stage 2 Geoarchaeological Review*. Salisbury, unpubl rep 117120.02
- Wessex Archaeology 2018c *Norfolk Boreas Offshore Wind Farm: Archaeological assessment of geophysical data*. Salisbury, unpubl rep 114843.03
- Wessex Archaeology 2018d *Norfolk Boreas Offshore Wind Farm: Stage 3 Palaeoenvironmental Assessment*. Salisbury, unpubl rep 117122.02
- Wessex Archaeology 2018e. *Norfolk Vanguard Offshore Windfarm: Stage 2 Geoarchaeological Recording*. Salisbury, unpubl rep 112380.03.
- Wessex Archaeology 2018f. *Norfolk Vanguard Offshore Windfarm: Stage 3 Palaeoenvironmental Assessment*. Salisbury, unpubl rep 114843.01.
- Wessex Archaeology 2019 *Norfolk Vanguard Offshore Wind Farm: Stage 4 Palaeoenvironmental Analysis*. Salisbury, unpubl rep 114844.01
- White, M 2006 Things to Do in Doggerland when you're Dead: Surviving OIS3 at the Northwestern-Most Fringe of Middle Palaeolithic Europe, *World Archaeology* 44, 0–28
- White, M J and Ashton, N 2003 Lower Paleolithic Core Technology and the Origins of the Levallois Method in North-Western Europe. *Current Anthropology* 44 (4), 598-609.
- White, M I and Jacobi, R 2002 Two sides to every story: bout coupe handaxes revisited, *Oxford J Arch* 21, 109-133
- Witkowski, A, Lange-Bertalot, H and Metzeltin, D 2000 Diatom Flora of Marine Coasts I. Iconographia Diatomologica in H Lange-Bertalot (ed) Annotated Diatom Micrographs. Königstein, Germany, A.R.G. Gantner Verlag. Koeltz Scientific Books
- Wymer, J J 1999 *The Lower Palaeolithic Occupation of Britain*. Wessex Archaeology and English Heritage
-



Zimmerman, D W 1971 Thermoluminescent dating using fine grains from pottery, *Archaeometry*, 13, 29-52



APPENDICES

Appendix 1 – list of sub-samples

VC028				
Depth (m down core)		Depth (m LAT)		Technique
From	To	From	To	
Stage 3				
2.50		-33.70		Pollen assessment
2.55		-33.75		Pollen assessment
2.60		-33.80		Pollen assessment
2.59	2.62	-33.79	-33.82	Radiocarbon and plant macrofossils
2.75		-33.95		Foraminifera and ostracod
2.75		-33.95		Diatom assessment
2.90		-34.10		Foraminifera and ostracod
2.90		-34.10		Diatom assessment
3.05		-34.25		Foraminifera and ostracod
3.05		-34.25		Diatom assessment
Stage 4				
2.50		-33.70		Radiocarbon and plant macrofossils
2.50		-33.70		Pollen analysis
2.52		-33.72		Pollen analysis
2.55		-33.75		Pollen analysis
2.57		-33.77		Pollen analysis



VC032				
Depth (m down core)		Depth (m LAT)		Technique
From	To	From	To	
Stage 3				
3.30		-35.20		Foraminifera and ostracod
3.30		-35.20		Diatom assessment
3.40		-35.30		Foraminifera and ostracod
3.40		-35.30		Diatom assessment
3.50		-35.40		Foraminifera and ostracod
3.50		-35.40		Diatom assessment
3.58		-35.48		Foraminifera and ostracod
3.58		-35.48		Diatom assessment
3.58		-35.48		Pollen assessment
3.69		-35.59		Foraminifera and ostracod
3.69		-35.59		Diatom assessment
3.61		-35.51		Pollen assessment
3.77		-35.67		Foraminifera and ostracod
3.77		-35.67		Diatom assessment
3.63		-35.53		Pollen assessment
3.65		-35.55		Pollen assessment
3.83		-35.73		Radiocarbon and plant macrofossils
3.67		-35.57		Pollen assessment
3.69		-35.59		Pollen assessment
3.71		-35.61		Pollen assessment
4.11		-36.01		Radiocarbon and plant macrofossils
3.73		-35.63		Pollen assessment
4.17		-36.07		Diatom assessment
4.17		-36.07		Foraminifera and ostracod
4.32		-36.22		Diatom assessment
4.32		-36.22		Foraminifera and ostracod
4.44		-36.34		Diatom assessment
4.44		-36.34		Foraminifera and ostracod
4.56		-36.46		Diatom assessment
4.56		-36.46		Foraminifera and ostracod
Stage 4				
3.58		-35.48		Pollen analysis
3.61		-35.51		Pollen analysis
3.61		-35.51		Radiocarbon and plant macrofossils
3.63		-35.53		Pollen analysis
3.67		-35.57		Pollen analysis
3.69		-35.59		Pollen analysis
3.71		-35.61		Pollen analysis



VC032				
Depth (m down core)		Depth (m LAT)		Technique
From	To	From	To	
3.73		-35.63		Pollen assessment
3.75		-35.65		Pollen analysis
3.77		-35.67		Pollen analysis
3.80		-35.70		Pollen analysis
3.82		-35.72		Pollen analysis
3.84		-35.74		Pollen analysis
3.85		-35.75		Pollen analysis
3.86		-35.76		Pollen analysis
3.87		-35.77		Pollen analysis
3.88		-35.78		Pollen analysis
3.89		-35.79		Pollen analysis
3.90		-35.80		Pollen analysis
3.92		-35.82		Pollen analysis
3.94		-35.84		Pollen analysis
3.95		-35.85		Radiocarbon and plant macrofossils
3.96		-35.86		Pollen analysis
3.98		-35.88		Pollen analysis
3.99		-35.89		Pollen analysis
4.00		-35.90		Pollen analysis
4.01		-35.91		Pollen analysis
4.02		-35.92		Pollen analysis
4.03		-35.93		Pollen analysis
4.04		-35.94		Pollen analysis
4.05		-35.95		Pollen analysis
4.06		-35.96		Pollen analysis
4.08		-35.98		Pollen analysis
4.10		-36.00		Pollen analysis
4.13		-36.03		Pollen analysis
3.40		-35.30		Diatom analysis
3.50		-35.40		Diatom analysis
3.58		-35.48		Diatom analysis
3.69		-35.59		Diatom analysis
3.77		-35.67		Diatom analysis
3.53		-35.43		Diatom analysis
3.64		-35.54		Diatom analysis
3.72		-35.62		Diatom analysis
3.75		-35.65		Diatom analysis
3.80		-35.70		Diatom assessment



VC039				
Depth (m down core)		Depth (m LAT)		Technique
From	To	From	To	
Stage 3				
2.75		-35.45		Diatom assessment
2.75		-35.45		Foraminifera and ostracod
2.90		-35.60		Diatom assessment
2.90		-35.60		Foraminifera and ostracod
2.94		-35.64		Pollen assessment
2.96		-35.66		Pollen assessment
3.07		-35.77		Radiocarbon and plant macrofossils
3.15		-35.85		Foraminifera and ostracod
3.15		-35.85		Diatom assessment
2.98		-35.68		Pollen assessment
3.31		-36.01		Diatom assessment
3.31		-36.01		Foraminifera and ostracod
3.51		-36.21		Diatom assessment
3.51		-36.21		Foraminifera and ostracod
Stage 4				
2.94		-35.64		Pollen analysis
2.96		-35.66		Pollen analysis
2.98		-35.68		Pollen analysis
3.00		-35.70		Pollen analysis
3.02		-35.72		Pollen analysis
3.04		-35.74		Pollen analysis
3.06		-35.76		Pollen analysis
3.08		-35.78		Pollen analysis
3.09		-35.79		Pollen analysis
3.11		-35.81		Pollen analysis
3.13		-35.83		Pollen analysis
3.15		-35.85		Pollen analysis
3.07		-35.77		Radiocarbon and plant macrofossils
3.13		-35.83		Radiocarbon and plant macrofossils



VC039				
Depth (m down core)		Depth (m LAT)		Technique
From	To	From	To	
Stage 3				
2.75		-35.45		Diatom assessment
2.75		-35.45		Foraminifera and ostracod
2.90		-35.60		Diatom assessment
2.90		-35.60		Foraminifera and ostracod
2.94		-35.64		Pollen assessment
2.96		-35.66		Pollen assessment
3.07		-35.77		Radiocarbon and plant macrofossils
3.15		-35.85		Foraminifera and ostracod
3.15		-35.85		Diatom assessment
2.98		-35.68		Pollen assessment
3.31		-36.01		Diatom assessment
3.31		-36.01		Foraminifera and ostracod
3.51		-36.21		Diatom assessment
3.51		-36.21		Foraminifera and ostracod
Stage 4				
2.94		-35.64		Pollen analysis
2.96		-35.66		Pollen analysis
2.98		-35.68		Pollen analysis
3.00		-35.70		Pollen analysis
3.02		-35.72		Pollen analysis
3.04		-35.74		Pollen analysis
3.06		-35.76		Pollen analysis
3.08		-35.78		Pollen analysis
3.09		-35.79		Pollen analysis
3.11		-35.81		Pollen analysis
3.13		-35.83		Pollen analysis
3.15		-35.85		Pollen analysis
2.96		-35.66		Radiocarbon and plant macrofossils
3.13		-35.83		Radiocarbon and plant macrofossils



VC016				
Depth (m down core)		Depth (m LAT)		Technique
From	To	From	To	
Stage 3				
0.20		-39.40		Diatom assessment
0.22		-39.42		Foraminifera and ostracod
0.45		-39.65		Diatom assessment
0.47		-39.67		Foraminifera and ostracod
0.70		-39.90		Diatom assessment
0.72		-39.92		Foraminifera and ostracod
0.95		-40.15		Diatom assessment
0.97		-40.17		Foraminifera and ostracod
1.15		-40.35		Diatom assessment
1.17		-40.37		Foraminifera and ostracod
1.40		-40.60		Diatom assessment
1.42		-40.62		Foraminifera and ostracod
1.65		-40.85		Diatom assessment
1.67		-40.87		Foraminifera and ostracod
1.70	2.00	-40.90	-41.20	OSL
2.18		-41.38		Diatom assessment
2.20		-41.40		Foraminifera and ostracod
2.38		-41.58		Diatom assessment
2.40		-41.60		Foraminifera and ostracod
2.58		-41.78		Diatom assessment
2.60		-41.80		Foraminifera and ostracod
2.65	3.00	-41.85	-42.20	OSL
3.35		-42.55		Diatom assessment
3.37		-42.57		Foraminifera and ostracod
3.85		-43.05		Diatom assessment
3.87		-43.07		Foraminifera and ostracod
4.38		-43.58		Foraminifera and ostracod
4.40		-43.60		Diatom assessment
4.85		-44.05		Foraminifera and ostracod
4.87		-44.07		Diatom assessment
Stage 4				
1.70	2.00	-40.90	-41.20	K-feldspar IRSL
2.65	3.00	-41.85	-42.20	K-feldspar IRSL



VC047				
Depth (m down core)		Depth (m LAT)		Technique
From	To	From	To	
Stage 3				
1.70		-36.20		Foraminifera and ostracod
1.70		-36.20		Diatom assessment
1.90		-36.40		Foraminifera and ostracod
1.90		-36.40		Diatom assessment
2.10		-36.60		Diatom assessment
2.15		-36.65		Foraminifera and ostracod
2.35		-36.85		Diatom assessment
2.40		-36.90		Foraminifera and ostracod
2.55	3.00	-37.05	-37.50	OSL
2.60		-37.10		Diatom assessment
2.65		-37.15		Foraminifera and ostracod
2.80		-37.30		Diatom assessment
2.85		-37.35		Foraminifera and ostracod
3.35		-37.85		Diatom assessment
3.40		-37.90		Foraminifera and ostracod
3.70	4.00	-38.20	-38.50	OSL
3.80		-38.30		Diatom assessment
3.85		-38.35		Foraminifera and ostracod
4.35		-38.85		Diatom assessment
4.40		-38.90		Foraminifera and ostracod
4.80		-39.30		Diatom assessment
4.85		-39.35		Foraminifera and ostracod



Appendix 2 – raw pollen data

VC028

Depth (mbsf)	2.50	2.52	2.55	2.57	2.60
Sample volume	1	1	1	1	1
Lycopodium tablets	1	1	1	1	1
Lycopodium in tablets	20848	20848	20848	20848	20848
Exotic	15	55	31	56	45
<i>Betula</i>	15	30	33	42	26
<i>Pinus sylvestris</i>	80	68	139	84	212
<i>Corylus avellana</i> type	184	229	107	175	119
<i>Ulmus</i>	19	13	14	12	15
<i>Quercus</i>	22	26	25	20	33
<i>Salix</i>	5	2	7	83	45
<i>Frangula alnus</i>	0	0	0	1	0
<i>Viburnum lantana</i>	0	0	0	1	1
<i>Ilex aquifolium</i>	1	0	0	0	0
Ericaceae	0	0	0	2	0
Poaceae	164	135	156	82	45
Cyperaceae	2	1	24	3	8
Ranunculaceae	1	1	0	0	0
Brassicaceae	0	0	1	0	0
Chenopodiaceae	3	0	0	0	0
<i>Rumex acetosa</i>	0	0	0	0	1
Rosaceae	2	2	0	2	3
<i>Filipendula</i>	0	0	0	1	5
Apiaceae	0	0	0	3	0
Rubiaceae	0	0	0	0	1
Lactuceae	0	0	0	0	1
<i>Artemisia</i> type	0	1	0	0	0
<i>Aster</i> type	2	0	0	0	2
Pteropsida undiff.	29	30	15	12	27
<i>Pteridium aquilinum</i>	3	0	3	0	4
<i>Thelypteris palustris</i>	5	0	1	2	1
<i>Potamogeton natans</i> type	16	7	19	4	4
<i>Sparganium emersum</i> type	0	0	4	0	2
<i>Typha latifolia</i>	7	4	4	1	2
Indeterminables	0	4	6	2	11
TLP	500	508	506	511	517
Charcoal	634	90	57	15	22



Depth (mbsf)	2.50	2.52	2.55	2.57	2.60
Points	202	202	202	202	202
Charcoal/points	3.14	0.45	0.28	0.07	0.11
Field of view	0.00238	0.00238	0.00238	0.00238	0.00238
No lycopodium spores	20848	20848	20848	20848	20848
Lycopodium spores counted	50	50	50	50	50
Total spores/total counted	416.96	416.96	416.96	416.96	416.96
Total	3.11	0.44	0.28	0.07	0.11
Total pollen concentration	694933	192560	340293	190238	239520



VC032

Depth (mbsf)	3.58	3.60	3.63	3.65	3.67	3.69	3.71	3.73
Sample volume	1	1	1	1	1	1	1	1
Lycopodium tablets	1	1	1	1	1	1	1	1
Lycopodium in tablets	20848	20848	20848	20848	20848	20848	20848	20848
Exotic	45	87	35	61	73	66	64	58
<i>Betula</i>	35	28	46	33	21	31	22	14
<i>Pinus sylvestris</i>	67	95	60	73	95	69	96	72
<i>Corylus avellana</i> type	258	265	271	255	249	258	269	257
<i>Ulmus</i>	16	14	9	17	18	19	15	19
<i>Quercus</i>	37	20	46	39	34	29	29	47
<i>Tilia</i>	0	0	0	0	0	0	1	0
<i>Juniperus communis</i>	0	0	0	0	0	0	0	0
<i>Salix</i>	3	2	5	4	3	3	2	3
<i>Rosa</i>	0	0	0	0	0	0	0	0
<i>Viburnum</i>	0	0	0	0	0	0	0	0
<i>Ilex aquifolium</i>	0	0	0	0	0	1	0	0
<i>Hedera helix</i>	0	0	1	0	1	1	0	0
Ericaceae	0	0	0	0	0	0	1	0
Poaceae	55	45	42	49	58	67	43	79
Cyperaceae	1	4	0	3	4	5	5	4
Ranunculaceae	0	0	0	0	0	0	0	1
Caryophyllaceae	0	0	0	0	0	1	0	0
<i>Silene</i> type	0	0	0	0	0	0	0	0
Brassicaceae	0	1	0	0	0	0	0	0
<i>Persicaria bistorta</i>	0	0	0	0	0	1	0	0
Chenopodiaceae	28	19	19	23	20	18	21	5
<i>Drosera rotundifolia</i>	0	0	0	0	0	0	0	0
Rosaceae	0	4	1	2	2	0	1	1
<i>Filipendula</i>	1	0	0	1	0	0	2	2
<i>Potentilla</i>	0	0	0	0	0	0	0	0
<i>Trifolium</i> type	1	0	0	0	0	1	0	0
Apiaceae	0	0	1	1	0	0	0	0
<i>Apium nodiflorum</i>	0	0	0	0	0	0	0	0
Lamiaceae	0	0	0	0	0	0	0	0
<i>Plantago media-major</i>	0	0	0	0	0	0	0	0
<i>Rhinanthus</i> type	0	0	0	0	0	0	0	0
Rubiaceae	0	0	0	0	0	0	1	0
<i>Cirsium</i>	0	0	0	0	0	0	0	0
Lactuceae	0	1	0	0	1	0	0	0



Depth (mbsf)	3.58	3.60	3.63	3.65	3.67	3.69	3.71	3.73
<i>Artemisia</i> type	0	1	0	0	0	1	0	0
<i>Aster</i> type	4	2	0	2	2	2	1	2
<i>Anthemis</i>	0	0	0	0	1	0	0	0
Pteropsida undiff.	26	0	45	47	73	67	38	34
<i>Pteridium aquilinum</i>	3	0	0	2	1	0	0	0
<i>Dryopteris filix-mas</i>	0	0	0	0	2	0	0	0
<i>Thelypteris palustris</i>	2	0	1	2	3	0	0	0
<i>Polypodium vulgare</i>	1	0	0	0	0	0	0	0
<i>Myriophyllum alterniflorum</i>	0	0	0	0	0	0	1	0
<i>Potamogeton natans</i> type (pondweed)	10	6	2	4	8	8	19	22
<i>Sparganium emersum</i> type	1	0	0	0	0	1	0	0
<i>Typha</i>	1	2	0	3	3	4	5	1
<i>Menyanthes trifoliata</i>	1	0	0	0	0	0	0	0
<i>Sphagnum</i>	1	0	0	2	0	1	0	1
Indeterminables	0	3	4	7	9	2	3	0
TLP	506	501	501	502	509	507	509	506
Charcoal	493	185	87	115	155	245	255	27
Points	202	202	202	202	202	202	202	202
Charcoal/points	2.44	0.92	0.43	0.57	0.77	1.21	1.26	0.13
Field of view	0.00238	0.00238	0.00238	0.00238	0.00238	0.00238	0.00238	0.00238
No lycopodium spores	20848	20848	20848	20848	20848	20848	20848	20848
Lycopodium spores counted	50	50	50	50	50	50	50	50
Total spores/total counted	417	417	417	417	417	417	417	417
Total	2.42	0.91	0.43	0.56	0.76	1.20	1.25	0.13
Total pollen concentration	234424	120056	298424	171569	145365	160151	165807	181881
<i>Betula</i>	16215	6710	27400	11278	5997	9792	7167	5032
<i>Pinus sylvestris</i>	31040	22765	35739	24949	27131	21796	31272	25880
<i>Corylus avellana</i> type	119529	63503	161423	87151	71112	81497	87627	92378
<i>Ulmus</i>	7413	3355	5361	5810	5141	6002	4886	6830
<i>Quercus</i>	17142	4793	27400	13329	9710	9160	9447	16894
<i>Tilia</i>	0	0	0	0	0	0	326	0
<i>Juniperus communis</i>	0	0	0	0	0	0	0	0
<i>Salix</i>	1390	479	2978	1367	857	948	652	1078
<i>Rosa</i>	0	0	0	0	0	0	0	0
<i>Viburnum</i>	0	0	0	0	0	0	0	0
<i>Ilex aquifolium</i>	0	0	0	0	0	316	0	0



Depth (mbsf)	3.58	3.60	3.63	3.65	3.67	3.69	3.71	3.73
<i>Hedera helix</i>	0	0	596	0	286	316	0	0
Ericaceae	0	0	0	0	0	0	326	0
Poaceae	25481	10783	25018	16747	16564	21164	14007	28396
Cyperaceae	463	959	0	1025	1142	1579	1629	1438
Ranunculaceae	0	0	0	0	0	0	0	359
Caryophyllaceae	0	0	0	0	0	316	0	0
<i>Silene</i> type	0	0	0	0	0	0	0	0
Brassicaceae	0	240	0	0	0	0	0	0
<i>Persicaria bistorta</i>	0	240	0	0	0	0	0	0
Chenopodiaceae	12972	4553	11317	7861	5712	5686	6841	1797
<i>Drosera rotundifolia</i>	0	0	0	0	0	0	0	0
Rosaceae	0	959	596	684	571	0	326	359
<i>Filipendula</i>	463	0	0	342	0	0	652	719
<i>Potentilla</i>	0	0	0	0	0	0	0	0
<i>Trifolium</i> type	463	0	0	0	0	316	0	0
Apiaceae	0	0	596	342	0	0	0	0
<i>Apium nodiflorum</i>	0	0	0	0	0	0	0	0
Lamiaceae	0	0	0	0	0	0	0	0
<i>Plantago media-major</i>	0	0	0	0	0	0	0	0
<i>Rhinanthus</i> type	0	0	0	0	0	0	0	0
Rubiaceae	0	0	0	0	0	0	326	0
<i>Cirsium</i>	0	0	0	0	0	0	0	0
Lactuceae	0	240	0	0	286	0	0	0
<i>Artemisia</i> type	0	240	0	0	0	316	0	0
<i>Aster</i> type	1853	479	0	684	571	632	326	719
<i>Anthemis</i>	0	0	0	0	286	0	0	0
Pteropsida undiff.	12046	0	26805	16063	20848	21164	12379	12221
<i>Pteridium aquilinum</i>	1390	0	0	684	286	0	0	0
<i>Dryopteris filix-mas</i>	0	0	0	0	571	0	0	0
<i>Thelypteris palustris</i>	927	0	596	684	857	0	0	0
<i>Polypodium vulgare</i>	463	0	0	0	0	0	0	0
<i>Myriophyllum alterniflorum</i>	0	0	0	0	0	0	326	0
<i>Potamogeton natans</i> type (pondweed)	4633	1438	1191	1367	2285	2527	6189	7908
<i>Sparganium emersum</i> type	463	0	0	0	0	316	0	0
<i>Typha</i>	463	479	0	1025	857	1264	1629	359
<i>Menyanthes trifoliata</i>	463	0	0	0	0	0	0	0
<i>Sphagnum</i>	463	0	0	684	0	316	0	359



VC032 (continued)

Depth (mbsf)	3.75	3.77	3.80	3.82	3.84	3.85	3.86	3.87
Sample volume	1	1	1	1	1	1	1	1
Lycopodium tablets	1	1	1	1	1	1	1	1
Lycopodium in tablets	20848	20848	20848	20848	20848	20848	20848	20848
Exotic	55	67	71	60	533	404	456	303
<i>Betula</i>	21	27	24	33	34	32	35	30
<i>Pinus sylvestris</i>	64	67	74	86	101	117	157	151
<i>Corylus avellana</i> type	243	220	265	293	233	207	189	207
<i>Ulmus</i>	21	20	18	20	21	19	21	24
<i>Quercus</i>	46	32	28	23	42	40	49	47
<i>Tilia</i>	0	0	0	0	0	0	0	0
<i>Juniperus communis</i>	0	0	0	0	0	0	0	0
<i>Salix</i>	4	0	6	3	4	5	5	6
<i>Rosa</i>	0	0	0	0	0	1	0	0
<i>Viburnum</i>	0	0	0	0	0	0	0	0
<i>Ilex aquifolium</i>	0	0	0	0	0	0	0	0
<i>Hedera helix</i>	0	0	0	0	0	1	1	0
Ericaceae	0	0	0	1	0	0	0	0
Poaceae	77	94	57	26	46	56	39	23
Cyperaceae	6	10	13	7	11	14	3	8
Ranunculaceae	0	0	0	0	1	0	1	0
Caryophyllaceae	1	0	0	0	0	0	0	0
<i>Silene</i> type	0	0	0	0	0	0	0	0
Brassicaceae	1	1	0	4	0	0	0	0
<i>Persicaria bistorta</i>	0	0	0	0	0	0	0	0
Chenopodiaceae	19	21	7	0	1	0	0	1
<i>Drosera rotundifolia</i>	0	0	0	0	0	0	0	0
Rosaceae	3	2	4	1	5	3	3	1
<i>Filipendula</i>	1	0	1	2	3	1	0	1
<i>Potentilla</i>	0	0	1	0	0	1	1	0
<i>Trifolium</i> type	0	0	0	0	0	0	0	1
Apiaceae	0	0	0	0	0	0	0	2
<i>Apium nodiflorum</i>	0	0	0	0	0	0	3	4
Lamiaceae	0	0	0	0	0	0	1	0
<i>Plantago media-major</i>	0	0	0	0	0	0	0	0
<i>Rhinanthus</i> type	0	0	0	0	0	0	1	0
Rubiaceae	0	0	0	0	0	1	0	0
<i>Cirsium</i>	0	0	0	0	0	1	0	0
Lactuceae	0	1	1	0	0	0	0	0



Depth (mbsf)	3.75	3.77	3.80	3.82	3.84	3.85	3.86	3.87
<i>Artemisia</i> type	0	1	0	0	0	0	0	0
<i>Aster</i> type	0	6	2	1	1	1	4	0
<i>Anthemis</i>	0	2	0	0	0	0	0	0
Pteropsida undiff.	41	53	48	936	444	211	11	4
<i>Pteridium aquilinum</i>	2	1	3	2	3	0	2	1
<i>Dryopteris filix-mas</i>	0	0	0	2	1	1	2	0
<i>Thelypteris palustris</i>	1	6	5	740	1371	395	22	8
<i>Polypodium vulgare</i>	0	0	0	0	0	0	0	0
<i>Myriophyllum alterniflorum</i>	0	1	0	0	0	0	1	0
<i>Potamogeton natans</i> type (pondweed)	11	7	23	58	4	10	236	291
<i>Sparganium emersum</i> type	1	1	0	6	0	0	17	13
<i>Typha</i>	2	0	7	134	74	131	116	107
<i>Menyanthes trifoliata</i>	0	0	0	0	0	0	0	0
<i>Sphagnum</i>	1	1	0	0	0	0	0	0
Indeterminables	3	0	2	6	2	0	19	17
TLP	507	504	501	500	503	500	513	506
Charcoal	110	53	45	252	0	20	5	0
Points	202	202	202	202	202	202	202	202
Charcoal/points	0.54	0.26	0.22	1.25	0.00	0.10	0.02	0.00
Field of view	0.00238	0.00238	0.00238	0.00238	0.00238	0.00238	0.00238	0.00238
No lycopodium spores	20848	20848	20848	20848	20848	20848	20848	20848
Lycopodium spores counted	50	50	50	50	50	50	50	50
Total spores/total counted	417	417	417	417	417	417	417	417
Total	0.54	0.26	0.22	1.24	0.00	0.10	0.02	0.00
Total pollen concentration	192181	156827	147111	173733	19675	25802	23454	34815
<i>Betula</i>	7960	8401	7047	11466	1330	1651	1600	2064
<i>Pinus sylvestris</i>	24259	20848	21729	29882	3951	6038	7178	10390
<i>Corylus avellana</i> type	92110	68456	77813	101808	9114	10682	8641	14243
<i>Ulmus</i>	7960	6223	5285	6949	821	980	960	1651
<i>Quercus</i>	17437	9957	8222	7992	1643	2064	2240	3234
<i>Tilia</i>	0	0	0	0	0	0	0	0
<i>Juniperus communis</i>	0	0	0	0	0	0	0	0
<i>Salix</i>	1516	0	1762	1042	156	258	229	413
<i>Rosa</i>	0	0	0	0	0	52	0	0
<i>Viburnum</i>	0	0	0	0	0	0	0	0
<i>Ilex aquifolium</i>	0	0	0	0	0	0	0	0



Depth (mbsf)	3.75	3.77	3.80	3.82	3.84	3.85	3.86	3.87
<i>Hedera helix</i>	0	0	0	0	0	52	46	0
Ericaceae	0	0	0	347	0	0	0	0
Poaceae	29187	29249	16737	9034	1799	2890	1783	1583
Cyperaceae	2274	3112	3817	2432	430	722	137	550
Ranunculaceae	0	0	0	0	39	0	46	0
Caryophyllaceae	379	0	0	0	0	0	0	0
<i>Silene</i> type	0	0	0	0	0	0	0	0
Brassicaceae	379	311	0	1390	0	0	0	0
<i>Persicaria bistorta</i>	379	311	0	1390	0	0	0	0
Chenopodiaceae	7202	6534	2055	0	39	0	0	69
<i>Drosera rotundifolia</i>	0	0	0	0	0	0	0	0
Rosaceae	1137	622	1175	347	196	155	137	69
<i>Filipendula</i>	379	0	294	695	117	52	0	69
<i>Potentilla</i>	0	0	294	0	0	52	46	0
<i>Trifolium</i> type	0	0	0	0	0	0	0	69
Apiaceae	0	0	0	0	0	0	0	138
<i>Apium nodiflorum</i>	0	0	0	0	0	0	137	275
Lamiaceae	0	0	0	0	0	0	46	0
<i>Plantago media-major</i>	0	0	0	0	0	0	0	0
<i>Rhinanthus</i> type	0	0	0	0	0	0	46	0
Rubiaceae	0	0	0	0	0	52	0	0
<i>Cirsium</i>	0	0	0	0	0	52	0	0
Lactuceae	0	311	294	0	0	0	0	0
<i>Artemisia</i> type	0	311	0	0	0	0	0	0
<i>Aster</i> type	0	1867	587	347	39	52	183	0
<i>Anthemis</i>	0	622	0	0	0	0	0	0
Pteropsida undiff.	15541	16492	14094	325229	17367	10888	503	275
<i>Pteridium aquilinum</i>	758	311	881	695	117	0	91	69
<i>Dryopteris filix-mas</i>	0	0	0	695	39	52	91	0
<i>Thelypteris palustris</i>	379	1867	1468	257125	53626	20384	1006	550
<i>Polypodium vulgare</i>	0	0	0	0	0	0	0	0
<i>Myriophyllum alterniflorum</i>	0	311	0	0	0	0	46	0
<i>Potamogeton natans</i> type (pondweed)	4170	2178	6754	20153	156	516	10790	20022
<i>Sparganium emersum</i> type	379	311	0	2085	0	0	777	894
<i>Typha</i>	758	0	2055	46561	2894	6760	5303	7362
<i>Menyanthes trifoliata</i>	0	0	0	0	0	0	0	0
<i>Sphagnum</i>	379	311	0	0	0	0	0	0



VC032 (continued)

Depth (mbsf)	3.88	3.89	3.90	3.92	3.94	3.96	3.98	3.99
Sample volume	1	1	1	1	1	1	1	1
Lycopodium tablets	1	1	1	1	1	1	1	1
Lycopodium in tablets	20848	20848	20848	20848	20848	20848	20848	20848
Exotic	465	438	83	249	580	151	54	156
<i>Betula</i>	13	4	8	8	7	9	12	4
<i>Pinus sylvestris</i>	318	220	230	349	344	392	385	420
<i>Corylus avellana</i> type	83	29	27	88	73	56	63	15
<i>Ulmus</i>	12	2	2	2	8	4	0	1
<i>Quercus</i>	27	9	13	12	29	8	6	5
<i>Tilia</i>	0	0	0	0	0	0	0	0
<i>Juniperus communis</i>	0	0	0	0	0	0	0	0
<i>Salix</i>	3	3	1	9	3	3	1	3
<i>Rosa</i>	0	0	0	0	0	0	0	0
<i>Viburnum</i>	0	1	0	0	0	0	0	0
<i>Ilex aquifolium</i>	0	0	1	0	0	0	0	0
<i>Hedera helix</i>	0	0	1	0	1	0	0	0
Ericaceae	0	0	0	0	0	0	0	0
Poaceae	33	13	10	23	29	20	27	15
Cyperaceae	9	18	3	12	12	13	13	36
Ranunculaceae	1	0	0	0	1	0	0	0
Caryophyllaceae	0	0	0	0	0	0	0	0
<i>Silene</i> type	0	0	0	0	0	0	0	0
Brassicaceae	0	0	0	0	0	0	0	0
<i>Persicaria bistorta</i>	0	0	0	0	0	0	0	0
Chenopodiaceae	0	0	1	1	0	0	0	0
<i>Drosera rotundifolia</i>	0	0	0	0	0	0	0	0
Rosaceae	2	0	2	0	2	0	0	2
<i>Filipendula</i>	0	0	1	1	0	0	0	3
<i>Potentilla</i>	0	0	0	0	0	0	0	0
<i>Trifolium</i> type	0	1	0	0	0	0	0	0
Apiaceae	1	0	0	0	1	2	1	0
<i>Apium nodiflorum</i>	0	0	0	0	0	1	0	0
Lamiaceae	0	0	0	0	0	0	0	1
<i>Plantago media-major</i>	0	0	0	0	0	0	0	0
<i>Rhinanthus</i> type	0	1	0	0	0	0	0	0
Rubiaceae	0	0	0	0	0	0	2	0
<i>Cirsium</i>	0	0	0	0	0	0	0	0
Lactuceae	0	0	0	0	0	0	0	0



Depth (mbsf)	3.88	3.89	3.90	3.92	3.94	3.96	3.98	3.99
<i>Artemisia</i> type	0	0	0	0	1	1	0	0
<i>Aster</i> type	0	0	0	0	0	0	0	1
<i>Anthemis</i>	0	0	0	0	0	0	0	0
Pteropsida undiff.	28	39	17	27	20	40	18	33
<i>Pteridium aquilinum</i>	0	0	1	5	0	4	1	2
<i>Dryopteris filix-mas</i>	0	0	0	0	0	0	0	0
<i>Thelypteris palustris</i>	9	0	2	0	11	0	0	0
<i>Polypodium vulgare</i>	0	0	0	0	0	0	0	0
<i>Myriophyllum alterniflorum</i>	0	0	0	0	0	0	0	0
<i>Potamogeton natans</i> type (pondweed)	30	11	7	8	43	15	22	13
<i>Sparganium emersum</i> type	4	0	3	0	4	0	2	1
<i>Typha</i>	12	2	3	1	10	7	13	8
<i>Menyanthes trifoliata</i>	1	0	0	0	0	0	0	0
<i>Sphagnum</i>	0	0	0	0	1	1	2	1
Indeterminables	4	6	14	7	11	4	4	3
TLP	502	301	300	505	511	509	510	506
Charcoal	0	0	0	0	0	0	15	35
Points	202	202	202	202	202	202	202	202
Charcoal/points	0.00	0.00	0.00	0.00	0.00	0.00	0.07	0.17
Field of view	0.00238	0.00238	0.00238	0.00238	0.00238	0.00238	0.00238	0.00238
No lycopodium spores	20848	20848	20848	20848	20848	20848	20848	20848
Lycopodium spores counted	50	50	50	50	50	50	50	50
Total spores/total counted	417	417	417	417	417	417	417	417
Total	0.00	0.00	0.00	0.00	0.00	0.00	0.07	0.17
Total pollen concentration	22507	14327	75354	42282	18368	70276	196898	67622
<i>Betula</i>	583	190	2009	670	252	1243	4633	535
<i>Pinus sylvestris</i>	14257	10472	57772	29221	12365	54122	148639	56129
<i>Corylus avellana</i> type	3721	1380	6782	7368	2624	7732	24323	2005
<i>Ulmus</i>	538	95	502	167	288	552	0	134
<i>Quercus</i>	1211	428	3265	1005	1042	1105	2316	668
<i>Tilia</i>	0	0	0	0	0	0	0	0
<i>Juniperus communis</i>	0	0	0	0	0	0	0	0
<i>Salix</i>	135	143	251	754	108	414	386	401
<i>Rosa</i>	0	0	0	0	0	0	0	0
<i>Viburnum</i>	0	48	0	0	0	0	0	0
<i>Ilex aquifolium</i>	0	0	251	0	0	0	0	0



Depth (mbsf)	3.88	3.89	3.90	3.92	3.94	3.96	3.98	3.99
<i>Hedera helix</i>	0	0	251	0	36	0	0	0
Ericaceae	0	0	0	0	0	0	0	0
Poaceae	1480	619	2512	1926	1042	2761	10424	2005
Cyperaceae	404	857	754	1005	431	1795	5019	4811
Ranunculaceae	45	0	0	0	36	0	0	0
Caryophyllaceae	0	0	0	0	0	0	0	0
<i>Silene</i> type	0	0	0	0	0	0	0	0
Brassicaceae	0	0	0	0	0	0	0	0
<i>Persicaria bistorta</i>	0	0	0	0	0	0	0	0
Chenopodiaceae	0	0	251	84	0	0	0	0
<i>Drosera rotundifolia</i>	0	0	0	0	0	0	0	0
Rosaceae	90	0	502	0	72	0	0	267
<i>Filipendula</i>	0	0	251	84	0	0	0	401
<i>Potentilla</i>	0	0	0	0	0	0	0	0
<i>Trifolium</i> type	0	48	0	0	0	0	0	0
Apiaceae	45	0	0	0	36	276	386	0
<i>Apium nodiflorum</i>	0	0	0	0	0	138	0	0
Lamiaceae	0	0	0	0	0	0	0	134
<i>Plantago media-major</i>	0	0	0	0	0	0	0	0
<i>Rhinanthus</i> type	0	48	0	0	0	0	0	0
Rubiaceae	0	0	0	0	0	0	772	0
<i>Cirsium</i>	0	0	0	0	0	0	0	0
Lactuceae	0	0	0	0	0	0	0	0
<i>Artemisia</i> type	0	0	0	0	36	138	0	0
<i>Aster</i> type	0	0	0	0	0	0	0	134
<i>Anthemis</i>	0	0	0	0	0	0	0	0
Pteropsida undiff.	1255	1856	4270	2261	719	5523	6949	4410
<i>Pteridium aquilinum</i>	0	0	251	419	0	552	386	267
<i>Dryopteris filix-mas</i>	0	0	0	0	0	0	0	0
<i>Thelypteris palustris</i>	404	0	502	0	395	0	0	0
<i>Polypodium vulgare</i>	0	0	0	0	0	0	0	0
<i>Myriophyllum alterniflorum</i>	0	0	0	0	0	0	0	0
<i>Potamogeton natans</i> type (pondweed)	1345	524	1758	670	1546	2071	8494	1737
<i>Sparganium emersum</i> type	179	0	754	0	144	0	772	134
<i>Typha</i>	538	95	754	84	359	966	5019	1069
<i>Menyanthes trifoliata</i>	45	0	0	0	0	0	0	0
<i>Sphagnum</i>	0	0	0	0	36	138	772	134



VC032 (continued)

Depth (mbsf)	4.00	4.01	4.02	4.03	4.04	4.05	4.06	4.08
Sample volume	1	1	1	1	1	1	1	1
Lycopodium tablets	1	1	1	1	1	1	1	1
Lycopodium in tablets	20848	20848	20848	20848	20848	20848	20848	20848
Exotic	222	87	181	190	261	367	92	80
<i>Betula</i>	1	7	9	10	8	18	22	61
<i>Pinus sylvestris</i>	405	421	434	452	438	349	185	55
<i>Corylus avellana</i> type	19	29	18	15	6	4	2	5
<i>Ulmus</i>	1	3	3	1	0	0	0	0
<i>Quercus</i>	6	0	2	3	0	2	3	1
<i>Tilia</i>	1	0	0	0	0	0	0	0
<i>Juniperus communis</i>	0	0	0	0	0	0	0	1
<i>Salix</i>	7	1	2	1	4	18	7	10
<i>Rosa</i>	0	0	0	0	0	0	0	0
<i>Viburnum</i>	0	0	0	0	0	0	0	0
<i>Ilex aquifolium</i>	0	0	0	0	0	0	0	0
<i>Hedera helix</i>	0	0	0	0	0	0	0	0
Ericaceae	0	0	0	0	0	0	0	0
Poaceae	32	29	20	12	33	69	239	314
Cyperaceae	36	13	14	9	8	40	40	42
Ranunculaceae	0	0	0	0	3	2	1	3
Caryophyllaceae	0	0	0	0	0	0	0	0
<i>Silene</i> type	0	0	0	0	0	0	0	0
Brassicaceae	0	0	0	0	0	0	0	0
<i>Persicaria bistorta</i>	0	0	0	0	0	0	0	0
Chenopodiaceae	0	0	0	0	1	0	6	3
<i>Drosera rotundifolia</i>	0	0	0	0	0	0	0	0
Rosaceae	1	1	1	0	1	4	2	2
<i>Filipendula</i>	0	0	1	1	0	3	0	6
<i>Potentilla</i>	0	0	0	0	0	0	0	0
<i>Trifolium</i> type	1	0	0	0	2	0	0	0
Apiaceae	0	0	1	0	1	1	0	4
<i>Apium nodiflorum</i>	0	0	0	0	1	0	2	0
Lamiaceae	0	0	0	0	0	1	0	1
<i>Plantago media-major</i>	0	0	0	0	0	1	0	0
<i>Rhinanthus</i> type	0	0	0	0	0	0	0	0
Rubiaceae	0	0	0	0	0	0	0	0
<i>Cirsium</i>	0	0	0	0	0	0	0	1
Lactuceae	0	0	0	0	0	0	0	0



Depth (mbsf)	4.00	4.01	4.02	4.03	4.04	4.05	4.06	4.08
<i>Artemisia</i> type	0	0	0	0	0	1	0	0
<i>Aster</i> type	0	0	0	1	0	1	0	0
<i>Anthemis</i>	0	0	0	0	0	0	0	0
Pteropsida undiff.	25	23	69	326	138	119	47	15
<i>Pteridium aquilinum</i>	0	0	0	0	0	1	1	0
<i>Dryopteris filix-mas</i>	0	0	0	0	0	0	0	0
<i>Thelypteris palustris</i>	0	0	0	0	0	0	0	0
<i>Polypodium vulgare</i>	0	0	0	0	0	0	0	0
<i>Myriophyllum alterniflorum</i>	0	0	0	0	0	0	0	0
<i>Potamogeton natans</i> type (pondweed)	22	24	7	7	3	26	24	209
<i>Sparganium emersum</i> type	2	4	1	0	1	0	8	7
<i>Typha</i>	6	13	3	8	5	2	2	28
<i>Menyanthes trifoliata</i>	0	0	0	0	0	0	0	0
<i>Sphagnum</i>	2	0	0	0	1	1	1	0
Indeterminables	5	17	2	0	1	4	3	14
TLP	510	504	505	505	506	514	509	509
Charcoal	58	310	231	120	111	85	302	60
Points	202	202	202	202	202	202	202	202
Charcoal/points	0.29	1.53	1.14	0.59	0.55	0.42	1.50	0.30
Field of view	0.00238	0.00238	0.00238	0.00238	0.00238	0.00238	0.00238	0.00238
No lycopodium spores	20848	20848	20848	20848	20848	20848	20848	20848
Lycopodium spores counted	50	50	50	50	50	50	50	50
Total spores/total counted	417	417	417	417	417	417	417	417
Total	0.28	1.52	1.13	0.59	0.54	0.42	1.48	0.29
Total pollen concentration	47894	120775	58167	55412	40418	29199	115344	132645
<i>Betula</i>	94	1677	1037	1097	639	1023	4985	15897
<i>Pinus sylvestris</i>	38034	100885	49989	49596	34986	19825	41923	14333
<i>Corylus avellana</i> type	1784	6949	2073	1646	479	227	453	1303
<i>Ulmus</i>	94	719	346	110	0	0	0	0
<i>Quercus</i>	563	0	230	329	0	114	680	261
<i>Tilia</i>	94	0	0	0	0	0	0	0
<i>Juniperus communis</i>	0	0	0	0	0	0	0	261
<i>Salix</i>	657	240	230	110	320	1023	1586	2606
<i>Rosa</i>	0	0	0	0	0	0	0	0
<i>Viburnum</i>	0	0	0	0	0	0	0	0
<i>Ilex aquifolium</i>	0	0	0	0	0	0	0	0



Depth (mbsf)	4.00	4.01	4.02	4.03	4.04	4.05	4.06	4.08
<i>Hedera helix</i>	0	0	0	0	0	0	0	0
Ericaceae	0	0	0	0	0	0	0	0
Poaceae	3005	6949	2304	1317	2636	3920	54159	81828
Cyperaceae	3381	3115	1613	988	639	2272	9064	10945
Ranunculaceae	0	0	0	0	240	114	227	782
Caryophyllaceae	0	0	0	0	0	0	0	0
<i>Silene</i> type	0	0	0	0	0	0	0	0
Brassicaceae	0	0	0	0	0	0	0	0
<i>Persicaria bistorta</i>	0	0	0	0	0	0	0	0
Chenopodiaceae	0	0	0	0	80	0	1360	782
<i>Drosera rotundifolia</i>	0	0	0	0	0	0	0	0
Rosaceae	94	240	115	0	80	227	453	521
<i>Filipendula</i>	0	0	115	110	0	170	0	1564
<i>Potentilla</i>	0	0	0	0	0	0	0	0
<i>Trifolium</i> type	94	0	0	0	160	0	0	0
Apiaceae	0	0	115	0	80	57	0	1042
<i>Apium nodiflorum</i>	0	0	0	0	80	0	453	0
Lamiaceae	0	0	0	0	0	57	0	261
<i>Plantago media-major</i>	0	0	0	0	0	57	0	0
<i>Rhinanthus</i> type	0	0	0	0	0	0	0	0
Rubiaceae	0	0	0	0	0	0	0	0
<i>Cirsium</i>	0	0	0	0	0	0	0	261
Lactuceae	0	0	0	0	0	0	0	0
<i>Artemisia</i> type	0	0	0	0	0	57	0	0
<i>Aster</i> type	0	0	0	110	0	57	0	0
<i>Anthemis</i>	0	0	0	0	0	0	0	0
Pteropsida undiff.	2348	5512	7948	35771	11023	6760	10651	3909
<i>Pteridium aquilinum</i>	0	0	0	0	0	57	227	0
<i>Dryopteris filix-mas</i>	0	0	0	0	0	0	0	0
<i>Thelypteris palustris</i>	0	0	0	0	0	0	0	0
<i>Polypodium vulgare</i>	0	0	0	0	0	0	0	0
<i>Myriophyllum alterniflorum</i>	0	0	0	0	0	0	0	0
<i>Potamogeton natans</i> type (pondweed)	2066	5751	806	768	240	1477	5439	54465
<i>Sparganium emersum</i> type	188	959	115	0	80	0	1813	1824
<i>Typha</i>	563	3115	346	878	399	114	453	7297
<i>Menyanthes trifoliata</i>	0	0	0	0	0	0	0	0
<i>Sphagnum</i>	188	0	0	0	80	57	227	0



VC032 (continued)

Depth (mbsf)	4.10	4.13
Sample volume	1	1
Lycopodium tablets	1	1
Lycopodium in tablets	20848	20848
Exotic	55	189
<i>Betula</i>	15	7
<i>Pinus sylvestris</i>	22	57
<i>Corylus avellana</i> type	0	2
<i>Ulmus</i>	0	0
<i>Quercus</i>	0	1
<i>Tilia</i>	0	0
<i>Juniperus communis</i>	1	0
<i>Salix</i>	4	2
<i>Rosa</i>	0	0
<i>Viburnum</i>	0	0
<i>Ilex aquifolium</i>	0	0
<i>Hedera helix</i>	0	0
Ericaceae	0	1
Poaceae	38	22
Cyperaceae	395	175
Ranunculaceae	1	0
Caryophyllaceae	0	1
<i>Silene</i> type	1	0
Brassicaceae	0	0
<i>Persicaria bistorta</i>	0	0
Chenopodiaceae	20	22
<i>Drosera rotundifolia</i>	1	0
Rosaceae	5	4
<i>Filipendula</i>	2	0
<i>Potentilla</i>	2	1
<i>Trifolium</i> type	0	0
Apiaceae	4	0
<i>Apium nodiflorum</i>	0	0
Lamiaceae	0	0
<i>Plantago media-major</i>	0	0
<i>Rhinanthus</i> type	0	0
Rubiaceae	3	0
<i>Cirsium</i>	0	0
Lactuceae	0	7



Depth (mbsf)	4.10	4.13
<i>Artemisia</i> type	1	0
<i>Aster</i> type	0	0
<i>Anthemis</i>	0	0
Pteropsida undiff.	1	7
<i>Pteridium aquilinum</i>	0	0
<i>Dryopteris filix-mas</i>	0	0
<i>Thelypteris palustris</i>	0	0
<i>Polypodium vulgare</i>	0	0
<i>Myriophyllum alterniflorum</i>	0	0
<i>Potamogeton natans</i> type (pondweed)	0	0
<i>Sparganium emersum</i> type	0	1
<i>Typha</i>	36	6
<i>Menyanthes trifoliata</i>	0	0
<i>Sphagnum</i>	0	0
Indeterminables	0	4
TLP	515	302
Charcoal	44	5
Points	202	202
Charcoal/points	0.22	0.02
Field of view	0.00238	0.00238
No lycopodium spores	20848	20848
Lycopodium spores counted	50	50
Total spores/total counted	417	417
Total	0.22	0.02
Total pollen concentration	195213	33313
<i>Betula</i>	5686	772
<i>Pinus sylvestris</i>	8339	6287
<i>Corylus avellana</i> type	0	221
<i>Ulmus</i>	0	0
<i>Quercus</i>	0	110
<i>Tilia</i>	0	0
<i>Juniperus communis</i>	379	0
<i>Salix</i>	1516	221
<i>Rosa</i>	0	0
<i>Viburnum</i>	0	0
<i>Ilex aquifolium</i>	0	0
<i>Hedera helix</i>	0	0
Ericaceae	0	110



Depth (mbsf)	4.10	4.13
Poaceae	14404	2427
Cyperaceae	149727	19304
Ranunculaceae	379	0
Caryophyllaceae	0	110
<i>Silene</i> type	379	0
Brassicaceae	0	0
<i>Persicaria bistorta</i>	0	0
Chenopodiaceae	7581	2427
<i>Drosera rotundifolia</i>	379	0
Rosaceae	1895	441
<i>Filipendula</i>	758	0
<i>Potentilla</i>	758	110
<i>Trifolium</i> type	0	0
Apiaceae	1516	0
<i>Apium nodiflorum</i>	0	0
Lamiaceae	0	0
<i>Plantago media-major</i>	0	0
<i>Rhinanthus</i> type	0	0
Rubiaceae	1137	0
<i>Cirsium</i>	0	0
Lactuceae	0	772
<i>Artemisia</i> type	379	0
<i>Aster</i> type	0	0
<i>Anthemis</i>	0	0
Pteropsida undiff.	379	772
<i>Pteridium aquilinum</i>	0	0
<i>Dryopteris filix-mas</i>	0	0
<i>Thelypteris palustris</i>	0	0
<i>Polypodium vulgare</i>	0	0
<i>Myriophyllum alterniflorum</i>	0	0
<i>Potamogeton natans</i> type (pondweed)	0	0
<i>Sparganium emersum</i> type	0	110
<i>Typha</i>	13646	662
<i>Menyanthes trifoliata</i>	0	0
<i>Sphagnum</i>	0	0



VC039

Depth (mbsf)	2.95	2.96	2.98	3.00	3.02	3.04
Sample volume	1	1	1	1	1	1
Lycopodium tablets	1	1	1	1	1	1
Lycopodium in tablets	20848	20848	20848	20848	20848	20848
Exotic	8	69	121	574	908	141
Betula	7	15	36	12	105	108
Pinus sylvestris	221	245	152	213	107	41
Corylus avellana type	5	8	39	15	10	10
Ulmus	0	0	0	0	0	0
Quercus	0	0	2	0	0	0
Tilia	0	0	0	0	0	0
Juniperus communis	0	0	0	0	0	0
Salix	1	3	4	5	0	7
Rosa	0	0	0	0	0	0
Viburnum	0	0	0	0	0	0
Ilex aquifolium	0	0	0	0	0	0
Hedera helix	0	0	0	0	0	0
Ericaceae	0	0	0	0	0	0
Poaceae	14	12	11	8	25	77
Cyperaceae	60	30	58	48	49	41
Ranunculaceae	0	0	0	0	1	2
Caryophyllaceae	0	0	0	0	0	0
Silene type	0	0	0	0	0	0
Brassicaceae	0	0	0	0	0	2
Persicaria bistorta	0	0	0	0	0	0
Chenopodiaceae	0	0	2	0	0	0
Rumex acetosa	0	0	0	0	0	0
Rosaceae	4	1	0	3	3	4
Filipendula	1	0	0	0	2	3
Potentilla	0	0	0	0	0	0
Trifolium type	0	0	0	0	0	0
Apiaceae	0	0	0	0	0	1
Apium nodiflorum	0	0	0	0	0	3
Lamiaceae	0	0	0	0	1	0
Plantago media-major	0	0	0	0	0	0
Rhinanthus type	0	0	0	0	0	0
Rubiaceae	0	0	0	0	0	0
Cirsium	0	0	0	0	0	0
Lactuceae	0	0	0	0	0	0



Depth (mbsf)	2.95	2.96	2.98	3.00	3.02	3.04
Artemisia type	1	0	0	0	0	0
Aster type	0	1	1	1	0	1
Anthemis	0	0	0	0	0	0
Pteropsida undiff.	64	1276	712	791	364	190
Pteridium aquilinum	0	0	0	0	0	0
Dryopteris filix-mas	0	0	2	0	0	0
Thelypteris palustris	0	0	0	0	0	0
Polypodium vulgare	0	0	0	0	0	0
Myriophyllum alterniflorum	0	0	0	0	0	0
Potamogeton natans type (pondweed)	0	0	1	0	1	3
Sparganium emersum type	0	0	0	0	0	0
Typha	0	1	0	0	5	11
Menyanthes trifoliata	0	0	0	0	0	7
Nymphaea alba	0	0	0	0	0	0
Sphagnum	0	2	0	3	0	2
Indeterminables	17	5	0	3	16	7
TLP	314	315	305	305	303	300
Charcoal	593	1	5	0	0	15
Points	202	202	202	202	202	202
Charcoal/points	2.94	0.00	0.02	0.00	0.00	0.07
Field of view	0.00238	0.00238	0.00238	0.00238	0.00238	0.00238
No lycopodium spores	20848	20848	20848	20848	20848	20848
Lycopodium spores counted	50	50	50	50	50	50
Total spores/total counted	416.96	416.96	416.96	416.96	416.96	416.96
Total	2.91	0.00	0.02	0.00	0.00	0.07
Total pollen concentration	818284	95176	52551	11078	6957	44357



VC039 (continued)

Depth (mbsf)	3.06	3.08	3.09	3.11	3.13	3.15
Sample volume	1	1	1	1	1	1
Lycopodium tablets	1	1	1	1	1	1
Lycopodium in tablets	20848	20848	20848	20848	20848	20848
Exotic	633	117	148	250	230	93
Betula	50	47	70	99	84	69
Pinus sylvestris	78	10	4	20	13	17
Corylus avellana type	4	2	0	1	0	2
Ulmus	0	0	0	0	0	0
Quercus	0	0	0	0	0	0
Tilia	0	0	0	0	0	0
Juniperus communis	0	0	0	1	0	1
Salix	7	7	8	5	6	2
Rosa	0	0	0	0	0	0
Viburnum	0	0	0	0	0	0
Ilex aquifolium	0	0	0	0	0	0
Hedera helix	0	0	0	0	0	0
Ericaceae	0	0	0	0	0	0
Poaceae	44	115	125	155	181	191
Cyperaceae	109	115	88	7	6	5
Ranunculaceae	1	2	3	0	0	0
Caryophyllaceae	0	0	0	0	0	0
Silene type	0	0	0	0	0	0
Brassicaceae	1	0	0	0	0	0
Persicaria bistorta	0	0	0	0	0	0
Chenopodiaceae	0	0	0	0	0	0
Rumex acetosa	0	0	0	0	0	1
Rosaceae	3	3	3	9	3	3
Filipendula	1	4	3	2	3	4
Potentilla	0	0	0	0	0	0
Trifolium type	0	0	0	0	0	0
Apiaceae	1	0	0	3	1	2
Apium nodiflorum	0	0	0	0	0	0
Lamiaceae	0	0	0	0	0	1
Plantago media-major	0	0	0	0	0	0
Rhinanthus type	0	0	0	0	0	0
Rubiaceae	0	0	0	0	1	0
Cirsium	0	0	0	0	0	0
Lactuceae	0	0	0	0	0	0



Depth (mbsf)	3.06	3.08	3.09	3.11	3.13	3.15
Artemisia type	0	1	1	1	2	2
Aster type	1	0	0	0	0	0
Anthemis	0	0	0	0	0	0
Pteropsida undiff.	100	12	8	0	1	3
Pteridium aquilinum	0	0	0	0	0	1
Dryopteris filix-mas	1	1	1	0	0	0
Thelypteris palustris	0	1	0	0	0	0
Polypodium vulgare	0	0	0	0	0	0
Myriophyllum alterniflorum	0	0	1	3	1	1
Potamogeton natans type (pondweed)	1	0	0	9	14	13
Sparganium emersum type	0	0	0	1	1	7
Typha	10	8	4	65	37	37
Menyanthes trifoliata	10	2	0	1	0	5
Nymphaea alba	0	1	1	4	0	0
Sphagnum	2	0	0	0		0
Indeterminables	9	2	2	2	3	2
TLP	300	306	305	303	300	300
Charcoal	0	0	0	2	0	0
Points	202	202	202	202	202	202
Charcoal/points	0.00	0.00	0.00	0.01	0.00	0.00
Field of view	0.00238	0.00238	0.00238	0.00238	0.00238	0.00238
No lycopodium spores	20848	20848	20848	20848	20848	20848
Lycopodium spores counted	50	50	50	50	50	50
Total spores/total counted	416.96	416.96	416.96	416.96	416.96	416.96
Total	0.00	0.00	0.00	0.01	0.00	0.00
Total pollen concentration	9881	54526	42964	25268	27193	67252



Appendix 3 – radiocarbon dating reports



Appendix 4 – OSL dating report



Appendix 5 – Norfolk Boreas site stratigraphy (deposit model)

WA Deposit Model (Stage 2) ¹		Fugro Soil Stratigraphy ²		BGS Lithostratigraphy ³	WA Deposit Model (Stage 4)		
Unit No	Unit Name	Soil Unit	Soil Unit Name	Formation	Unit No	Unit Name	Age
5	Holocene seabed sediments	A1	Bligh Bank	Southern Bight Formation	8	Seabed sediments	Holocene post-transgression (MIS 1)
4	Holocene sediments	A2	Elbow	Elbow Formation	7c	Elbow Formation – intertidal	Early Holocene (MIS 1)
					7b	Elbow Formation – organic	Late Devensian to Early Holocene (MIS 2-1)
					7a	Elbow Formation – fluvial	Late Devensian to Early Holocene (MIS 2-1)
-	Twente Formation	B	Twente	Twente Formation	6	Twente Formation	Late Devensian (MIS 2)
3	Upper Brown Bank Formation	C	Brown Bank	Brown Bank Formation	5	Upper Brown Bank	Early Devensian (MIS 5d-3)
2	Lower Brown Bank Formation/Eem Formation	C	Brown Bank	Brown Bank Formation and Eem Formation	4	Lower Brown Bank/Eem Formation	Ipswichian or Early Devensian (MIS 5e - 5d)
-	Swarte Bank Formation	D	Swarte Bank	Swarte Bank Formation	3	Swarte Bank Formation	Anglian (MIS 12)
1	Yarmouth Roads Formation	E	Yarmouth Roads	Yarmouth Road Formation	2	Yarmouth Roads Formation	Early to Middle Pleistocene (MIS >13)
-	-	I	Winterton Shoal/Smith's Knoll	Winterton Shoal Formation or Smith's Knoll Formation	1	Westkapelle Ground Formation	Late Pliocene to Early Pleistocene (MIS 63-103)

¹ Wessex Archaeology (2018b)

² Fugro (2018)

³ Stoker et al. (2011)



APPENDICES

Appendix 1 – list of sub-samples

VC028				
Depth (m down core)		Depth (m LAT)		Technique
From	To	From	To	
Stage 3				
2.50		-33.70		Pollen assessment
2.55		-33.75		Pollen assessment
2.60		-33.80		Pollen assessment
2.59	2.62	-33.79	-33.82	Radiocarbon and plant macrofossils
2.75		-33.95		Foraminifera and ostracod
2.75		-33.95		Diatom assessment
2.90		-34.10		Foraminifera and ostracod
2.90		-34.10		Diatom assessment
3.05		-34.25		Foraminifera and ostracod
3.05		-34.25		Diatom assessment
Stage 4				
2.50		-33.70		Radiocarbon and plant macrofossils
2.50		-33.70		Pollen analysis
2.52		-33.72		Pollen analysis
2.55		-33.75		Pollen analysis
2.57		-33.77		Pollen analysis



VC032				
Depth (m down core)		Depth (m LAT)		Technique
From	To	From	To	
Stage 3				
3.30		-35.20		Foraminifera and ostracod
3.30		-35.20		Diatom assessment
3.40		-35.30		Foraminifera and ostracod
3.40		-35.30		Diatom assessment
3.50		-35.40		Foraminifera and ostracod
3.50		-35.40		Diatom assessment
3.58		-35.48		Foraminifera and ostracod
3.58		-35.48		Diatom assessment
3.58		-35.48		Pollen assessment
3.69		-35.59		Foraminifera and ostracod
3.69		-35.59		Diatom assessment
3.61		-35.51		Pollen assessment
3.77		-35.67		Foraminifera and ostracod
3.77		-35.67		Diatom assessment
3.63		-35.53		Pollen assessment
3.65		-35.55		Pollen assessment
3.83		-35.73		Radiocarbon and plant macrofossils
3.67		-35.57		Pollen assessment
3.69		-35.59		Pollen assessment
3.71		-35.61		Pollen assessment
4.11		-36.01		Radiocarbon and plant macrofossils
3.73		-35.63		Pollen assessment
4.17		-36.07		Diatom assessment
4.17		-36.07		Foraminifera and ostracod
4.32		-36.22		Diatom assessment
4.32		-36.22		Foraminifera and ostracod
4.44		-36.34		Diatom assessment
4.44		-36.34		Foraminifera and ostracod
4.56		-36.46		Diatom assessment
4.56		-36.46		Foraminifera and ostracod
Stage 4				
3.58		-35.48		Pollen analysis
3.61		-35.51		Pollen analysis
3.61		-35.51		Radiocarbon and plant macrofossils
3.63		-35.53		Pollen analysis
3.67		-35.57		Pollen analysis
3.69		-35.59		Pollen analysis
3.71		-35.61		Pollen analysis



VC032				
Depth (m down core)		Depth (m LAT)		Technique
From	To	From	To	
3.73		-35.63		Pollen assessment
3.75		-35.65		Pollen analysis
3.77		-35.67		Pollen analysis
3.80		-35.70		Pollen analysis
3.82		-35.72		Pollen analysis
3.84		-35.74		Pollen analysis
3.85		-35.75		Pollen analysis
3.86		-35.76		Pollen analysis
3.87		-35.77		Pollen analysis
3.88		-35.78		Pollen analysis
3.89		-35.79		Pollen analysis
3.90		-35.80		Pollen analysis
3.92		-35.82		Pollen analysis
3.94		-35.84		Pollen analysis
3.95		-35.85		Radiocarbon and plant macrofossils
3.96		-35.86		Pollen analysis
3.98		-35.88		Pollen analysis
3.99		-35.89		Pollen analysis
4.00		-35.90		Pollen analysis
4.01		-35.91		Pollen analysis
4.02		-35.92		Pollen analysis
4.03		-35.93		Pollen analysis
4.04		-35.94		Pollen analysis
4.05		-35.95		Pollen analysis
4.06		-35.96		Pollen analysis
4.08		-35.98		Pollen analysis
4.10		-36.00		Pollen analysis
4.13		-36.03		Pollen analysis
3.40		-35.30		Diatom analysis
3.50		-35.40		Diatom analysis
3.58		-35.48		Diatom analysis
3.69		-35.59		Diatom analysis
3.77		-35.67		Diatom analysis
3.53		-35.43		Diatom analysis
3.64		-35.54		Diatom analysis
3.72		-35.62		Diatom analysis
3.75		-35.65		Diatom analysis
3.80		-35.70		Diatom assessment



VC039				
Depth (m down core)		Depth (m LAT)		Technique
From	To	From	To	
Stage 3				
2.75		-35.45		Diatom assessment
2.75		-35.45		Foraminifera and ostracod
2.90		-35.60		Diatom assessment
2.90		-35.60		Foraminifera and ostracod
2.94		-35.64		Pollen assessment
2.96		-35.66		Pollen assessment
3.07		-35.77		Radiocarbon and plant macrofossils
3.15		-35.85		Foraminifera and ostracod
3.15		-35.85		Diatom assessment
2.98		-35.68		Pollen assessment
3.31		-36.01		Diatom assessment
3.31		-36.01		Foraminifera and ostracod
3.51		-36.21		Diatom assessment
3.51		-36.21		Foraminifera and ostracod
Stage 4				
2.94		-35.64		Pollen analysis
2.96		-35.66		Pollen analysis
2.98		-35.68		Pollen analysis
3.00		-35.70		Pollen analysis
3.02		-35.72		Pollen analysis
3.04		-35.74		Pollen analysis
3.06		-35.76		Pollen analysis
3.08		-35.78		Pollen analysis
3.09		-35.79		Pollen analysis
3.11		-35.81		Pollen analysis
3.13		-35.83		Pollen analysis
3.15		-35.85		Pollen analysis
3.07		-35.77		Radiocarbon and plant macrofossils
3.13		-35.83		Radiocarbon and plant macrofossils



VC039				
Depth (m down core)		Depth (m LAT)		Technique
From	To	From	To	
Stage 3				
2.75		-35.45		Diatom assessment
2.75		-35.45		Foraminifera and ostracod
2.90		-35.60		Diatom assessment
2.90		-35.60		Foraminifera and ostracod
2.94		-35.64		Pollen assessment
2.96		-35.66		Pollen assessment
3.07		-35.77		Radiocarbon and plant macrofossils
3.15		-35.85		Foraminifera and ostracod
3.15		-35.85		Diatom assessment
2.98		-35.68		Pollen assessment
3.31		-36.01		Diatom assessment
3.31		-36.01		Foraminifera and ostracod
3.51		-36.21		Diatom assessment
3.51		-36.21		Foraminifera and ostracod
Stage 4				
2.94		-35.64		Pollen analysis
2.96		-35.66		Pollen analysis
2.98		-35.68		Pollen analysis
3.00		-35.70		Pollen analysis
3.02		-35.72		Pollen analysis
3.04		-35.74		Pollen analysis
3.06		-35.76		Pollen analysis
3.08		-35.78		Pollen analysis
3.09		-35.79		Pollen analysis
3.11		-35.81		Pollen analysis
3.13		-35.83		Pollen analysis
3.15		-35.85		Pollen analysis
2.96		-35.66		Radiocarbon and plant macrofossils
3.13		-35.83		Radiocarbon and plant macrofossils



VC016				
Depth (m down core)		Depth (m LAT)		Technique
From	To	From	To	
Stage 3				
0.20		-39.40		Diatom assessment
0.22		-39.42		Foraminifera and ostracod
0.45		-39.65		Diatom assessment
0.47		-39.67		Foraminifera and ostracod
0.70		-39.90		Diatom assessment
0.72		-39.92		Foraminifera and ostracod
0.95		-40.15		Diatom assessment
0.97		-40.17		Foraminifera and ostracod
1.15		-40.35		Diatom assessment
1.17		-40.37		Foraminifera and ostracod
1.40		-40.60		Diatom assessment
1.42		-40.62		Foraminifera and ostracod
1.65		-40.85		Diatom assessment
1.67		-40.87		Foraminifera and ostracod
1.70	2.00	-40.90	-41.20	OSL
2.18		-41.38		Diatom assessment
2.20		-41.40		Foraminifera and ostracod
2.38		-41.58		Diatom assessment
2.40		-41.60		Foraminifera and ostracod
2.58		-41.78		Diatom assessment
2.60		-41.80		Foraminifera and ostracod
2.65	3.00	-41.85	-42.20	OSL
3.35		-42.55		Diatom assessment
3.37		-42.57		Foraminifera and ostracod
3.85		-43.05		Diatom assessment
3.87		-43.07		Foraminifera and ostracod
4.38		-43.58		Foraminifera and ostracod
4.40		-43.60		Diatom assessment
4.85		-44.05		Foraminifera and ostracod
4.87		-44.07		Diatom assessment
Stage 4				
1.70	2.00	-40.90	-41.20	K-feldspar IRSL
2.65	3.00	-41.85	-42.20	K-feldspar IRSL



VC047				
Depth (m down core)		Depth (m LAT)		Technique
From	To	From	To	
Stage 3				
1.70		-36.20		Foraminifera and ostracod
1.70		-36.20		Diatom assessment
1.90		-36.40		Foraminifera and ostracod
1.90		-36.40		Diatom assessment
2.10		-36.60		Diatom assessment
2.15		-36.65		Foraminifera and ostracod
2.35		-36.85		Diatom assessment
2.40		-36.90		Foraminifera and ostracod
2.55	3.00	-37.05	-37.50	OSL
2.60		-37.10		Diatom assessment
2.65		-37.15		Foraminifera and ostracod
2.80		-37.30		Diatom assessment
2.85		-37.35		Foraminifera and ostracod
3.35		-37.85		Diatom assessment
3.40		-37.90		Foraminifera and ostracod
3.70	4.00	-38.20	-38.50	OSL
3.80		-38.30		Diatom assessment
3.85		-38.35		Foraminifera and ostracod
4.35		-38.85		Diatom assessment
4.40		-38.90		Foraminifera and ostracod
4.80		-39.30		Diatom assessment
4.85		-39.35		Foraminifera and ostracod



Appendix 2 – raw pollen data

VC028

Depth (mbsf)	2.50	2.52	2.55	2.57	2.60
Sample volume	1	1	1	1	1
Lycopodium tablets	1	1	1	1	1
Lycopodium in tablets	20848	20848	20848	20848	20848
Exotic	15	55	31	56	45
<i>Betula</i>	15	30	33	42	26
<i>Pinus sylvestris</i>	80	68	139	84	212
<i>Corylus avellana</i> type	184	229	107	175	119
<i>Ulmus</i>	19	13	14	12	15
<i>Quercus</i>	22	26	25	20	33
<i>Salix</i>	5	2	7	83	45
<i>Frangula alnus</i>	0	0	0	1	0
<i>Viburnum lantana</i>	0	0	0	1	1
<i>Ilex aquifolium</i>	1	0	0	0	0
Ericaceae	0	0	0	2	0
Poaceae	164	135	156	82	45
Cyperaceae	2	1	24	3	8
Ranunculaceae	1	1	0	0	0
Brassicaceae	0	0	1	0	0
Chenopodiaceae	3	0	0	0	0
<i>Rumex acetosa</i>	0	0	0	0	1
Rosaceae	2	2	0	2	3
<i>Filipendula</i>	0	0	0	1	5
Apiaceae	0	0	0	3	0
Rubiaceae	0	0	0	0	1
Lactuceae	0	0	0	0	1
<i>Artemisia</i> type	0	1	0	0	0
<i>Aster</i> type	2	0	0	0	2
Pteropsida undiff.	29	30	15	12	27
<i>Pteridium aquilinum</i>	3	0	3	0	4
<i>Thelypteris palustris</i>	5	0	1	2	1
<i>Potamogeton natans</i> type	16	7	19	4	4
<i>Sparganium emersum</i> type	0	0	4	0	2
<i>Typha latifolia</i>	7	4	4	1	2
Indeterminables	0	4	6	2	11
TLP	500	508	506	511	517
Charcoal	634	90	57	15	22



Depth (mbsf)	2.50	2.52	2.55	2.57	2.60
Points	202	202	202	202	202
Charcoal/points	3.14	0.45	0.28	0.07	0.11
Field of view	0.00238	0.00238	0.00238	0.00238	0.00238
No lycopodium spores	20848	20848	20848	20848	20848
Lycopodium spores counted	50	50	50	50	50
Total spores/total counted	416.96	416.96	416.96	416.96	416.96
Total	3.11	0.44	0.28	0.07	0.11
Total pollen concentration	694933	192560	340293	190238	239520



VC032

Depth (mbsf)	3.58	3.60	3.63	3.65	3.67	3.69	3.71	3.73
Sample volume	1	1	1	1	1	1	1	1
Lycopodium tablets	1	1	1	1	1	1	1	1
Lycopodium in tablets	20848	20848	20848	20848	20848	20848	20848	20848
Exotic	45	87	35	61	73	66	64	58
<i>Betula</i>	35	28	46	33	21	31	22	14
<i>Pinus sylvestris</i>	67	95	60	73	95	69	96	72
<i>Corylus avellana</i> type	258	265	271	255	249	258	269	257
<i>Ulmus</i>	16	14	9	17	18	19	15	19
<i>Quercus</i>	37	20	46	39	34	29	29	47
<i>Tilia</i>	0	0	0	0	0	0	1	0
<i>Juniperus communis</i>	0	0	0	0	0	0	0	0
<i>Salix</i>	3	2	5	4	3	3	2	3
<i>Rosa</i>	0	0	0	0	0	0	0	0
<i>Viburnum</i>	0	0	0	0	0	0	0	0
<i>Ilex aquifolium</i>	0	0	0	0	0	1	0	0
<i>Hedera helix</i>	0	0	1	0	1	1	0	0
Ericaceae	0	0	0	0	0	0	1	0
Poaceae	55	45	42	49	58	67	43	79
Cyperaceae	1	4	0	3	4	5	5	4
Ranunculaceae	0	0	0	0	0	0	0	1
Caryophyllaceae	0	0	0	0	0	1	0	0
<i>Silene</i> type	0	0	0	0	0	0	0	0
Brassicaceae	0	1	0	0	0	0	0	0
<i>Persicaria bistorta</i>	0	0	0	0	0	1	0	0
Chenopodiaceae	28	19	19	23	20	18	21	5
<i>Drosera rotundifolia</i>	0	0	0	0	0	0	0	0
Rosaceae	0	4	1	2	2	0	1	1
<i>Filipendula</i>	1	0	0	1	0	0	2	2
<i>Potentilla</i>	0	0	0	0	0	0	0	0
<i>Trifolium</i> type	1	0	0	0	0	1	0	0
Apiaceae	0	0	1	1	0	0	0	0
<i>Apium nodiflorum</i>	0	0	0	0	0	0	0	0
Lamiaceae	0	0	0	0	0	0	0	0
<i>Plantago media-major</i>	0	0	0	0	0	0	0	0
<i>Rhinanthus</i> type	0	0	0	0	0	0	0	0
Rubiaceae	0	0	0	0	0	0	1	0
<i>Cirsium</i>	0	0	0	0	0	0	0	0
Lactuceae	0	1	0	0	1	0	0	0



Depth (mbsf)	3.58	3.60	3.63	3.65	3.67	3.69	3.71	3.73
<i>Artemisia</i> type	0	1	0	0	0	1	0	0
<i>Aster</i> type	4	2	0	2	2	2	1	2
<i>Anthemis</i>	0	0	0	0	1	0	0	0
Pteropsida undiff.	26	0	45	47	73	67	38	34
<i>Pteridium aquilinum</i>	3	0	0	2	1	0	0	0
<i>Dryopteris filix-mas</i>	0	0	0	0	2	0	0	0
<i>Thelypteris palustris</i>	2	0	1	2	3	0	0	0
<i>Polypodium vulgare</i>	1	0	0	0	0	0	0	0
<i>Myriophyllum alterniflorum</i>	0	0	0	0	0	0	1	0
<i>Potamogeton natans</i> type (pondweed)	10	6	2	4	8	8	19	22
<i>Sparganium emersum</i> type	1	0	0	0	0	1	0	0
<i>Typha</i>	1	2	0	3	3	4	5	1
<i>Menyanthes trifoliata</i>	1	0	0	0	0	0	0	0
<i>Sphagnum</i>	1	0	0	2	0	1	0	1
Indeterminables	0	3	4	7	9	2	3	0
TLP	506	501	501	502	509	507	509	506
Charcoal	493	185	87	115	155	245	255	27
Points	202	202	202	202	202	202	202	202
Charcoal/points	2.44	0.92	0.43	0.57	0.77	1.21	1.26	0.13
Field of view	0.00238	0.00238	0.00238	0.00238	0.00238	0.00238	0.00238	0.00238
No lycopodium spores	20848	20848	20848	20848	20848	20848	20848	20848
Lycopodium spores counted	50	50	50	50	50	50	50	50
Total spores/total counted	417	417	417	417	417	417	417	417
Total	2.42	0.91	0.43	0.56	0.76	1.20	1.25	0.13
Total pollen concentration	234424	120056	298424	171569	145365	160151	165807	181881
<i>Betula</i>	16215	6710	27400	11278	5997	9792	7167	5032
<i>Pinus sylvestris</i>	31040	22765	35739	24949	27131	21796	31272	25880
<i>Corylus avellana</i> type	119529	63503	161423	87151	71112	81497	87627	92378
<i>Ulmus</i>	7413	3355	5361	5810	5141	6002	4886	6830
<i>Quercus</i>	17142	4793	27400	13329	9710	9160	9447	16894
<i>Tilia</i>	0	0	0	0	0	0	326	0
<i>Juniperus communis</i>	0	0	0	0	0	0	0	0
<i>Salix</i>	1390	479	2978	1367	857	948	652	1078
<i>Rosa</i>	0	0	0	0	0	0	0	0
<i>Viburnum</i>	0	0	0	0	0	0	0	0
<i>Ilex aquifolium</i>	0	0	0	0	0	316	0	0



Depth (mbsf)	3.58	3.60	3.63	3.65	3.67	3.69	3.71	3.73
<i>Hedera helix</i>	0	0	596	0	286	316	0	0
Ericaceae	0	0	0	0	0	0	326	0
Poaceae	25481	10783	25018	16747	16564	21164	14007	28396
Cyperaceae	463	959	0	1025	1142	1579	1629	1438
Ranunculaceae	0	0	0	0	0	0	0	359
Caryophyllaceae	0	0	0	0	0	316	0	0
<i>Silene</i> type	0	0	0	0	0	0	0	0
Brassicaceae	0	240	0	0	0	0	0	0
<i>Persicaria bistorta</i>	0	240	0	0	0	0	0	0
Chenopodiaceae	12972	4553	11317	7861	5712	5686	6841	1797
<i>Drosera rotundifolia</i>	0	0	0	0	0	0	0	0
Rosaceae	0	959	596	684	571	0	326	359
<i>Filipendula</i>	463	0	0	342	0	0	652	719
<i>Potentilla</i>	0	0	0	0	0	0	0	0
<i>Trifolium</i> type	463	0	0	0	0	316	0	0
Apiaceae	0	0	596	342	0	0	0	0
<i>Apium nodiflorum</i>	0	0	0	0	0	0	0	0
Lamiaceae	0	0	0	0	0	0	0	0
<i>Plantago media-major</i>	0	0	0	0	0	0	0	0
<i>Rhinanthus</i> type	0	0	0	0	0	0	0	0
Rubiaceae	0	0	0	0	0	0	326	0
<i>Cirsium</i>	0	0	0	0	0	0	0	0
Lactuceae	0	240	0	0	286	0	0	0
<i>Artemisia</i> type	0	240	0	0	0	316	0	0
<i>Aster</i> type	1853	479	0	684	571	632	326	719
<i>Anthemis</i>	0	0	0	0	286	0	0	0
Pteropsida undiff.	12046	0	26805	16063	20848	21164	12379	12221
<i>Pteridium aquilinum</i>	1390	0	0	684	286	0	0	0
<i>Dryopteris filix-mas</i>	0	0	0	0	571	0	0	0
<i>Thelypteris palustris</i>	927	0	596	684	857	0	0	0
<i>Polypodium vulgare</i>	463	0	0	0	0	0	0	0
<i>Myriophyllum alterniflorum</i>	0	0	0	0	0	0	326	0
<i>Potamogeton natans</i> type (pondweed)	4633	1438	1191	1367	2285	2527	6189	7908
<i>Sparganium emersum</i> type	463	0	0	0	0	316	0	0
<i>Typha</i>	463	479	0	1025	857	1264	1629	359
<i>Menyanthes trifoliata</i>	463	0	0	0	0	0	0	0
<i>Sphagnum</i>	463	0	0	684	0	316	0	359



VC032 (continued)

Depth (mbsf)	3.75	3.77	3.80	3.82	3.84	3.85	3.86	3.87
Sample volume	1	1	1	1	1	1	1	1
Lycopodium tablets	1	1	1	1	1	1	1	1
Lycopodium in tablets	20848	20848	20848	20848	20848	20848	20848	20848
Exotic	55	67	71	60	533	404	456	303
<i>Betula</i>	21	27	24	33	34	32	35	30
<i>Pinus sylvestris</i>	64	67	74	86	101	117	157	151
<i>Corylus avellana</i> type	243	220	265	293	233	207	189	207
<i>Ulmus</i>	21	20	18	20	21	19	21	24
<i>Quercus</i>	46	32	28	23	42	40	49	47
<i>Tilia</i>	0	0	0	0	0	0	0	0
<i>Juniperus communis</i>	0	0	0	0	0	0	0	0
<i>Salix</i>	4	0	6	3	4	5	5	6
<i>Rosa</i>	0	0	0	0	0	1	0	0
<i>Viburnum</i>	0	0	0	0	0	0	0	0
<i>Ilex aquifolium</i>	0	0	0	0	0	0	0	0
<i>Hedera helix</i>	0	0	0	0	0	1	1	0
Ericaceae	0	0	0	1	0	0	0	0
Poaceae	77	94	57	26	46	56	39	23
Cyperaceae	6	10	13	7	11	14	3	8
Ranunculaceae	0	0	0	0	1	0	1	0
Caryophyllaceae	1	0	0	0	0	0	0	0
<i>Silene</i> type	0	0	0	0	0	0	0	0
Brassicaceae	1	1	0	4	0	0	0	0
<i>Persicaria bistorta</i>	0	0	0	0	0	0	0	0
Chenopodiaceae	19	21	7	0	1	0	0	1
<i>Drosera rotundifolia</i>	0	0	0	0	0	0	0	0
Rosaceae	3	2	4	1	5	3	3	1
<i>Filipendula</i>	1	0	1	2	3	1	0	1
<i>Potentilla</i>	0	0	1	0	0	1	1	0
<i>Trifolium</i> type	0	0	0	0	0	0	0	1
Apiaceae	0	0	0	0	0	0	0	2
<i>Apium nodiflorum</i>	0	0	0	0	0	0	3	4
Lamiaceae	0	0	0	0	0	0	1	0
<i>Plantago media-major</i>	0	0	0	0	0	0	0	0
<i>Rhinanthus</i> type	0	0	0	0	0	0	1	0
Rubiaceae	0	0	0	0	0	1	0	0
<i>Cirsium</i>	0	0	0	0	0	1	0	0
Lactuceae	0	1	1	0	0	0	0	0



Depth (mbsf)	3.75	3.77	3.80	3.82	3.84	3.85	3.86	3.87
<i>Artemisia</i> type	0	1	0	0	0	0	0	0
<i>Aster</i> type	0	6	2	1	1	1	4	0
<i>Anthemis</i>	0	2	0	0	0	0	0	0
Pteropsida undiff.	41	53	48	936	444	211	11	4
<i>Pteridium aquilinum</i>	2	1	3	2	3	0	2	1
<i>Dryopteris filix-mas</i>	0	0	0	2	1	1	2	0
<i>Thelypteris palustris</i>	1	6	5	740	1371	395	22	8
<i>Polypodium vulgare</i>	0	0	0	0	0	0	0	0
<i>Myriophyllum alterniflorum</i>	0	1	0	0	0	0	1	0
<i>Potamogeton natans</i> type (pondweed)	11	7	23	58	4	10	236	291
<i>Sparganium emersum</i> type	1	1	0	6	0	0	17	13
<i>Typha</i>	2	0	7	134	74	131	116	107
<i>Menyanthes trifoliata</i>	0	0	0	0	0	0	0	0
<i>Sphagnum</i>	1	1	0	0	0	0	0	0
Indeterminables	3	0	2	6	2	0	19	17
TLP	507	504	501	500	503	500	513	506
Charcoal	110	53	45	252	0	20	5	0
Points	202	202	202	202	202	202	202	202
Charcoal/points	0.54	0.26	0.22	1.25	0.00	0.10	0.02	0.00
Field of view	0.00238	0.00238	0.00238	0.00238	0.00238	0.00238	0.00238	0.00238
No lycopodium spores	20848	20848	20848	20848	20848	20848	20848	20848
Lycopodium spores counted	50	50	50	50	50	50	50	50
Total spores/total counted	417	417	417	417	417	417	417	417
Total	0.54	0.26	0.22	1.24	0.00	0.10	0.02	0.00
Total pollen concentration	192181	156827	147111	173733	19675	25802	23454	34815
<i>Betula</i>	7960	8401	7047	11466	1330	1651	1600	2064
<i>Pinus sylvestris</i>	24259	20848	21729	29882	3951	6038	7178	10390
<i>Corylus avellana</i> type	92110	68456	77813	101808	9114	10682	8641	14243
<i>Ulmus</i>	7960	6223	5285	6949	821	980	960	1651
<i>Quercus</i>	17437	9957	8222	7992	1643	2064	2240	3234
<i>Tilia</i>	0	0	0	0	0	0	0	0
<i>Juniperus communis</i>	0	0	0	0	0	0	0	0
<i>Salix</i>	1516	0	1762	1042	156	258	229	413
<i>Rosa</i>	0	0	0	0	0	52	0	0
<i>Viburnum</i>	0	0	0	0	0	0	0	0
<i>Ilex aquifolium</i>	0	0	0	0	0	0	0	0



Depth (mbsf)	3.75	3.77	3.80	3.82	3.84	3.85	3.86	3.87
<i>Hedera helix</i>	0	0	0	0	0	52	46	0
Ericaceae	0	0	0	347	0	0	0	0
Poaceae	29187	29249	16737	9034	1799	2890	1783	1583
Cyperaceae	2274	3112	3817	2432	430	722	137	550
Ranunculaceae	0	0	0	0	39	0	46	0
Caryophyllaceae	379	0	0	0	0	0	0	0
<i>Silene</i> type	0	0	0	0	0	0	0	0
Brassicaceae	379	311	0	1390	0	0	0	0
<i>Persicaria bistorta</i>	379	311	0	1390	0	0	0	0
Chenopodiaceae	7202	6534	2055	0	39	0	0	69
<i>Drosera rotundifolia</i>	0	0	0	0	0	0	0	0
Rosaceae	1137	622	1175	347	196	155	137	69
<i>Filipendula</i>	379	0	294	695	117	52	0	69
<i>Potentilla</i>	0	0	294	0	0	52	46	0
<i>Trifolium</i> type	0	0	0	0	0	0	0	69
Apiaceae	0	0	0	0	0	0	0	138
<i>Apium nodiflorum</i>	0	0	0	0	0	0	137	275
Lamiaceae	0	0	0	0	0	0	46	0
<i>Plantago media-major</i>	0	0	0	0	0	0	0	0
<i>Rhinanthus</i> type	0	0	0	0	0	0	46	0
Rubiaceae	0	0	0	0	0	52	0	0
<i>Cirsium</i>	0	0	0	0	0	52	0	0
Lactuceae	0	311	294	0	0	0	0	0
<i>Artemisia</i> type	0	311	0	0	0	0	0	0
<i>Aster</i> type	0	1867	587	347	39	52	183	0
<i>Anthemis</i>	0	622	0	0	0	0	0	0
Pteropsida undiff.	15541	16492	14094	325229	17367	10888	503	275
<i>Pteridium aquilinum</i>	758	311	881	695	117	0	91	69
<i>Dryopteris filix-mas</i>	0	0	0	695	39	52	91	0
<i>Thelypteris palustris</i>	379	1867	1468	257125	53626	20384	1006	550
<i>Polypodium vulgare</i>	0	0	0	0	0	0	0	0
<i>Myriophyllum alterniflorum</i>	0	311	0	0	0	0	46	0
<i>Potamogeton natans</i> type (pondweed)	4170	2178	6754	20153	156	516	10790	20022
<i>Sparganium emersum</i> type	379	311	0	2085	0	0	777	894
<i>Typha</i>	758	0	2055	46561	2894	6760	5303	7362
<i>Menyanthes trifoliata</i>	0	0	0	0	0	0	0	0
<i>Sphagnum</i>	379	311	0	0	0	0	0	0



VC032 (continued)

Depth (mbsf)	3.88	3.89	3.90	3.92	3.94	3.96	3.98	3.99
Sample volume	1	1	1	1	1	1	1	1
Lycopodium tablets	1	1	1	1	1	1	1	1
Lycopodium in tablets	20848	20848	20848	20848	20848	20848	20848	20848
Exotic	465	438	83	249	580	151	54	156
<i>Betula</i>	13	4	8	8	7	9	12	4
<i>Pinus sylvestris</i>	318	220	230	349	344	392	385	420
<i>Corylus avellana</i> type	83	29	27	88	73	56	63	15
<i>Ulmus</i>	12	2	2	2	8	4	0	1
<i>Quercus</i>	27	9	13	12	29	8	6	5
<i>Tilia</i>	0	0	0	0	0	0	0	0
<i>Juniperus communis</i>	0	0	0	0	0	0	0	0
<i>Salix</i>	3	3	1	9	3	3	1	3
<i>Rosa</i>	0	0	0	0	0	0	0	0
<i>Viburnum</i>	0	1	0	0	0	0	0	0
<i>Ilex aquifolium</i>	0	0	1	0	0	0	0	0
<i>Hedera helix</i>	0	0	1	0	1	0	0	0
Ericaceae	0	0	0	0	0	0	0	0
Poaceae	33	13	10	23	29	20	27	15
Cyperaceae	9	18	3	12	12	13	13	36
Ranunculaceae	1	0	0	0	1	0	0	0
Caryophyllaceae	0	0	0	0	0	0	0	0
<i>Silene</i> type	0	0	0	0	0	0	0	0
Brassicaceae	0	0	0	0	0	0	0	0
<i>Persicaria bistorta</i>	0	0	0	0	0	0	0	0
Chenopodiaceae	0	0	1	1	0	0	0	0
<i>Drosera rotundifolia</i>	0	0	0	0	0	0	0	0
Rosaceae	2	0	2	0	2	0	0	2
<i>Filipendula</i>	0	0	1	1	0	0	0	3
<i>Potentilla</i>	0	0	0	0	0	0	0	0
<i>Trifolium</i> type	0	1	0	0	0	0	0	0
Apiaceae	1	0	0	0	1	2	1	0
<i>Apium nodiflorum</i>	0	0	0	0	0	1	0	0
Lamiaceae	0	0	0	0	0	0	0	1
<i>Plantago media-major</i>	0	0	0	0	0	0	0	0
<i>Rhinanthus</i> type	0	1	0	0	0	0	0	0
Rubiaceae	0	0	0	0	0	0	2	0
<i>Cirsium</i>	0	0	0	0	0	0	0	0
Lactuceae	0	0	0	0	0	0	0	0



Depth (mbsf)	3.88	3.89	3.90	3.92	3.94	3.96	3.98	3.99
<i>Artemisia</i> type	0	0	0	0	1	1	0	0
<i>Aster</i> type	0	0	0	0	0	0	0	1
<i>Anthemis</i>	0	0	0	0	0	0	0	0
Pteropsida undiff.	28	39	17	27	20	40	18	33
<i>Pteridium aquilinum</i>	0	0	1	5	0	4	1	2
<i>Dryopteris filix-mas</i>	0	0	0	0	0	0	0	0
<i>Thelypteris palustris</i>	9	0	2	0	11	0	0	0
<i>Polypodium vulgare</i>	0	0	0	0	0	0	0	0
<i>Myriophyllum alterniflorum</i>	0	0	0	0	0	0	0	0
<i>Potamogeton natans</i> type (pondweed)	30	11	7	8	43	15	22	13
<i>Sparganium emersum</i> type	4	0	3	0	4	0	2	1
<i>Typha</i>	12	2	3	1	10	7	13	8
<i>Menyanthes trifoliata</i>	1	0	0	0	0	0	0	0
<i>Sphagnum</i>	0	0	0	0	1	1	2	1
Indeterminables	4	6	14	7	11	4	4	3
TLP	502	301	300	505	511	509	510	506
Charcoal	0	0	0	0	0	0	15	35
Points	202	202	202	202	202	202	202	202
Charcoal/points	0.00	0.00	0.00	0.00	0.00	0.00	0.07	0.17
Field of view	0.00238	0.00238	0.00238	0.00238	0.00238	0.00238	0.00238	0.00238
No lycopodium spores	20848	20848	20848	20848	20848	20848	20848	20848
Lycopodium spores counted	50	50	50	50	50	50	50	50
Total spores/total counted	417	417	417	417	417	417	417	417
Total	0.00	0.00	0.00	0.00	0.00	0.00	0.07	0.17
Total pollen concentration	22507	14327	75354	42282	18368	70276	196898	67622
<i>Betula</i>	583	190	2009	670	252	1243	4633	535
<i>Pinus sylvestris</i>	14257	10472	57772	29221	12365	54122	148639	56129
<i>Corylus avellana</i> type	3721	1380	6782	7368	2624	7732	24323	2005
<i>Ulmus</i>	538	95	502	167	288	552	0	134
<i>Quercus</i>	1211	428	3265	1005	1042	1105	2316	668
<i>Tilia</i>	0	0	0	0	0	0	0	0
<i>Juniperus communis</i>	0	0	0	0	0	0	0	0
<i>Salix</i>	135	143	251	754	108	414	386	401
<i>Rosa</i>	0	0	0	0	0	0	0	0
<i>Viburnum</i>	0	48	0	0	0	0	0	0
<i>Ilex aquifolium</i>	0	0	251	0	0	0	0	0



Depth (mbsf)	3.88	3.89	3.90	3.92	3.94	3.96	3.98	3.99
<i>Hedera helix</i>	0	0	251	0	36	0	0	0
Ericaceae	0	0	0	0	0	0	0	0
Poaceae	1480	619	2512	1926	1042	2761	10424	2005
Cyperaceae	404	857	754	1005	431	1795	5019	4811
Ranunculaceae	45	0	0	0	36	0	0	0
Caryophyllaceae	0	0	0	0	0	0	0	0
<i>Silene</i> type	0	0	0	0	0	0	0	0
Brassicaceae	0	0	0	0	0	0	0	0
<i>Persicaria bistorta</i>	0	0	0	0	0	0	0	0
Chenopodiaceae	0	0	251	84	0	0	0	0
<i>Drosera rotundifolia</i>	0	0	0	0	0	0	0	0
Rosaceae	90	0	502	0	72	0	0	267
<i>Filipendula</i>	0	0	251	84	0	0	0	401
<i>Potentilla</i>	0	0	0	0	0	0	0	0
<i>Trifolium</i> type	0	48	0	0	0	0	0	0
Apiaceae	45	0	0	0	36	276	386	0
<i>Apium nodiflorum</i>	0	0	0	0	0	138	0	0
Lamiaceae	0	0	0	0	0	0	0	134
<i>Plantago media-major</i>	0	0	0	0	0	0	0	0
<i>Rhinanthus</i> type	0	48	0	0	0	0	0	0
Rubiaceae	0	0	0	0	0	0	772	0
<i>Cirsium</i>	0	0	0	0	0	0	0	0
Lactuceae	0	0	0	0	0	0	0	0
<i>Artemisia</i> type	0	0	0	0	36	138	0	0
<i>Aster</i> type	0	0	0	0	0	0	0	134
<i>Anthemis</i>	0	0	0	0	0	0	0	0
Pteropsida undiff.	1255	1856	4270	2261	719	5523	6949	4410
<i>Pteridium aquilinum</i>	0	0	251	419	0	552	386	267
<i>Dryopteris filix-mas</i>	0	0	0	0	0	0	0	0
<i>Thelypteris palustris</i>	404	0	502	0	395	0	0	0
<i>Polypodium vulgare</i>	0	0	0	0	0	0	0	0
<i>Myriophyllum alterniflorum</i>	0	0	0	0	0	0	0	0
<i>Potamogeton natans</i> type (pondweed)	1345	524	1758	670	1546	2071	8494	1737
<i>Sparganium emersum</i> type	179	0	754	0	144	0	772	134
<i>Typha</i>	538	95	754	84	359	966	5019	1069
<i>Menyanthes trifoliata</i>	45	0	0	0	0	0	0	0
<i>Sphagnum</i>	0	0	0	0	36	138	772	134



VC032 (continued)

Depth (mbsf)	4.00	4.01	4.02	4.03	4.04	4.05	4.06	4.08
Sample volume	1	1	1	1	1	1	1	1
Lycopodium tablets	1	1	1	1	1	1	1	1
Lycopodium in tablets	20848	20848	20848	20848	20848	20848	20848	20848
Exotic	222	87	181	190	261	367	92	80
<i>Betula</i>	1	7	9	10	8	18	22	61
<i>Pinus sylvestris</i>	405	421	434	452	438	349	185	55
<i>Corylus avellana</i> type	19	29	18	15	6	4	2	5
<i>Ulmus</i>	1	3	3	1	0	0	0	0
<i>Quercus</i>	6	0	2	3	0	2	3	1
<i>Tilia</i>	1	0	0	0	0	0	0	0
<i>Juniperus communis</i>	0	0	0	0	0	0	0	1
<i>Salix</i>	7	1	2	1	4	18	7	10
<i>Rosa</i>	0	0	0	0	0	0	0	0
<i>Viburnum</i>	0	0	0	0	0	0	0	0
<i>Ilex aquifolium</i>	0	0	0	0	0	0	0	0
<i>Hedera helix</i>	0	0	0	0	0	0	0	0
Ericaceae	0	0	0	0	0	0	0	0
Poaceae	32	29	20	12	33	69	239	314
Cyperaceae	36	13	14	9	8	40	40	42
Ranunculaceae	0	0	0	0	3	2	1	3
Caryophyllaceae	0	0	0	0	0	0	0	0
<i>Silene</i> type	0	0	0	0	0	0	0	0
Brassicaceae	0	0	0	0	0	0	0	0
<i>Persicaria bistorta</i>	0	0	0	0	0	0	0	0
Chenopodiaceae	0	0	0	0	1	0	6	3
<i>Drosera rotundifolia</i>	0	0	0	0	0	0	0	0
Rosaceae	1	1	1	0	1	4	2	2
<i>Filipendula</i>	0	0	1	1	0	3	0	6
<i>Potentilla</i>	0	0	0	0	0	0	0	0
<i>Trifolium</i> type	1	0	0	0	2	0	0	0
Apiaceae	0	0	1	0	1	1	0	4
<i>Apium nodiflorum</i>	0	0	0	0	1	0	2	0
Lamiaceae	0	0	0	0	0	1	0	1
<i>Plantago media-major</i>	0	0	0	0	0	1	0	0
<i>Rhinanthus</i> type	0	0	0	0	0	0	0	0
Rubiaceae	0	0	0	0	0	0	0	0
<i>Cirsium</i>	0	0	0	0	0	0	0	1
Lactuceae	0	0	0	0	0	0	0	0



Depth (mbsf)	4.00	4.01	4.02	4.03	4.04	4.05	4.06	4.08
<i>Artemisia</i> type	0	0	0	0	0	1	0	0
<i>Aster</i> type	0	0	0	1	0	1	0	0
<i>Anthemis</i>	0	0	0	0	0	0	0	0
Pteropsida undiff.	25	23	69	326	138	119	47	15
<i>Pteridium aquilinum</i>	0	0	0	0	0	1	1	0
<i>Dryopteris filix-mas</i>	0	0	0	0	0	0	0	0
<i>Thelypteris palustris</i>	0	0	0	0	0	0	0	0
<i>Polypodium vulgare</i>	0	0	0	0	0	0	0	0
<i>Myriophyllum alterniflorum</i>	0	0	0	0	0	0	0	0
<i>Potamogeton natans</i> type (pondweed)	22	24	7	7	3	26	24	209
<i>Sparganium emersum</i> type	2	4	1	0	1	0	8	7
<i>Typha</i>	6	13	3	8	5	2	2	28
<i>Menyanthes trifoliata</i>	0	0	0	0	0	0	0	0
<i>Sphagnum</i>	2	0	0	0	1	1	1	0
Indeterminables	5	17	2	0	1	4	3	14
TLP	510	504	505	505	506	514	509	509
Charcoal	58	310	231	120	111	85	302	60
Points	202	202	202	202	202	202	202	202
Charcoal/points	0.29	1.53	1.14	0.59	0.55	0.42	1.50	0.30
Field of view	0.00238	0.00238	0.00238	0.00238	0.00238	0.00238	0.00238	0.00238
No lycopodium spores	20848	20848	20848	20848	20848	20848	20848	20848
Lycopodium spores counted	50	50	50	50	50	50	50	50
Total spores/total counted	417	417	417	417	417	417	417	417
Total	0.28	1.52	1.13	0.59	0.54	0.42	1.48	0.29
Total pollen concentration	47894	120775	58167	55412	40418	29199	115344	132645
<i>Betula</i>	94	1677	1037	1097	639	1023	4985	15897
<i>Pinus sylvestris</i>	38034	100885	49989	49596	34986	19825	41923	14333
<i>Corylus avellana</i> type	1784	6949	2073	1646	479	227	453	1303
<i>Ulmus</i>	94	719	346	110	0	0	0	0
<i>Quercus</i>	563	0	230	329	0	114	680	261
<i>Tilia</i>	94	0	0	0	0	0	0	0
<i>Juniperus communis</i>	0	0	0	0	0	0	0	261
<i>Salix</i>	657	240	230	110	320	1023	1586	2606
<i>Rosa</i>	0	0	0	0	0	0	0	0
<i>Viburnum</i>	0	0	0	0	0	0	0	0
<i>Ilex aquifolium</i>	0	0	0	0	0	0	0	0



Depth (mbsf)	4.00	4.01	4.02	4.03	4.04	4.05	4.06	4.08
<i>Hedera helix</i>	0	0	0	0	0	0	0	0
Ericaceae	0	0	0	0	0	0	0	0
Poaceae	3005	6949	2304	1317	2636	3920	54159	81828
Cyperaceae	3381	3115	1613	988	639	2272	9064	10945
Ranunculaceae	0	0	0	0	240	114	227	782
Caryophyllaceae	0	0	0	0	0	0	0	0
<i>Silene</i> type	0	0	0	0	0	0	0	0
Brassicaceae	0	0	0	0	0	0	0	0
<i>Persicaria bistorta</i>	0	0	0	0	0	0	0	0
Chenopodiaceae	0	0	0	0	80	0	1360	782
<i>Drosera rotundifolia</i>	0	0	0	0	0	0	0	0
Rosaceae	94	240	115	0	80	227	453	521
<i>Filipendula</i>	0	0	115	110	0	170	0	1564
<i>Potentilla</i>	0	0	0	0	0	0	0	0
<i>Trifolium</i> type	94	0	0	0	160	0	0	0
Apiaceae	0	0	115	0	80	57	0	1042
<i>Apium nodiflorum</i>	0	0	0	0	80	0	453	0
Lamiaceae	0	0	0	0	0	57	0	261
<i>Plantago media-major</i>	0	0	0	0	0	57	0	0
<i>Rhinanthus</i> type	0	0	0	0	0	0	0	0
Rubiaceae	0	0	0	0	0	0	0	0
<i>Cirsium</i>	0	0	0	0	0	0	0	261
Lactuceae	0	0	0	0	0	0	0	0
<i>Artemisia</i> type	0	0	0	0	0	57	0	0
<i>Aster</i> type	0	0	0	110	0	57	0	0
<i>Anthemis</i>	0	0	0	0	0	0	0	0
Pteropsida undiff.	2348	5512	7948	35771	11023	6760	10651	3909
<i>Pteridium aquilinum</i>	0	0	0	0	0	57	227	0
<i>Dryopteris filix-mas</i>	0	0	0	0	0	0	0	0
<i>Thelypteris palustris</i>	0	0	0	0	0	0	0	0
<i>Polypodium vulgare</i>	0	0	0	0	0	0	0	0
<i>Myriophyllum alterniflorum</i>	0	0	0	0	0	0	0	0
<i>Potamogeton natans</i> type (pondweed)	2066	5751	806	768	240	1477	5439	54465
<i>Sparganium emersum</i> type	188	959	115	0	80	0	1813	1824
<i>Typha</i>	563	3115	346	878	399	114	453	7297
<i>Menyanthes trifoliata</i>	0	0	0	0	0	0	0	0
<i>Sphagnum</i>	188	0	0	0	80	57	227	0



VC032 (continued)

Depth (mbsf)	4.10	4.13
Sample volume	1	1
Lycopodium tablets	1	1
Lycopodium in tablets	20848	20848
Exotic	55	189
<i>Betula</i>	15	7
<i>Pinus sylvestris</i>	22	57
<i>Corylus avellana</i> type	0	2
<i>Ulmus</i>	0	0
<i>Quercus</i>	0	1
<i>Tilia</i>	0	0
<i>Juniperus communis</i>	1	0
<i>Salix</i>	4	2
<i>Rosa</i>	0	0
<i>Viburnum</i>	0	0
<i>Ilex aquifolium</i>	0	0
<i>Hedera helix</i>	0	0
Ericaceae	0	1
Poaceae	38	22
Cyperaceae	395	175
Ranunculaceae	1	0
Caryophyllaceae	0	1
<i>Silene</i> type	1	0
Brassicaceae	0	0
<i>Persicaria bistorta</i>	0	0
Chenopodiaceae	20	22
<i>Drosera rotundifolia</i>	1	0
Rosaceae	5	4
<i>Filipendula</i>	2	0
<i>Potentilla</i>	2	1
<i>Trifolium</i> type	0	0
Apiaceae	4	0
<i>Apium nodiflorum</i>	0	0
Lamiaceae	0	0
<i>Plantago media-major</i>	0	0
<i>Rhinanthus</i> type	0	0
Rubiaceae	3	0
<i>Cirsium</i>	0	0
Lactuceae	0	7



Depth (mbsf)	4.10	4.13
<i>Artemisia</i> type	1	0
<i>Aster</i> type	0	0
<i>Anthemis</i>	0	0
Pteropsida undiff.	1	7
<i>Pteridium aquilinum</i>	0	0
<i>Dryopteris filix-mas</i>	0	0
<i>Thelypteris palustris</i>	0	0
<i>Polypodium vulgare</i>	0	0
<i>Myriophyllum alterniflorum</i>	0	0
<i>Potamogeton natans</i> type (pondweed)	0	0
<i>Sparganium emersum</i> type	0	1
<i>Typha</i>	36	6
<i>Menyanthes trifoliata</i>	0	0
<i>Sphagnum</i>	0	0
Indeterminables	0	4
TLP	515	302
Charcoal	44	5
Points	202	202
Charcoal/points	0.22	0.02
Field of view	0.00238	0.00238
No lycopodium spores	20848	20848
Lycopodium spores counted	50	50
Total spores/total counted	417	417
Total	0.22	0.02
Total pollen concentration	195213	33313
<i>Betula</i>	5686	772
<i>Pinus sylvestris</i>	8339	6287
<i>Corylus avellana</i> type	0	221
<i>Ulmus</i>	0	0
<i>Quercus</i>	0	110
<i>Tilia</i>	0	0
<i>Juniperus communis</i>	379	0
<i>Salix</i>	1516	221
<i>Rosa</i>	0	0
<i>Viburnum</i>	0	0
<i>Ilex aquifolium</i>	0	0
<i>Hedera helix</i>	0	0
Ericaceae	0	110



Depth (mbsf)	4.10	4.13
Poaceae	14404	2427
Cyperaceae	149727	19304
Ranunculaceae	379	0
Caryophyllaceae	0	110
<i>Silene</i> type	379	0
Brassicaceae	0	0
<i>Persicaria bistorta</i>	0	0
Chenopodiaceae	7581	2427
<i>Drosera rotundifolia</i>	379	0
Rosaceae	1895	441
<i>Filipendula</i>	758	0
<i>Potentilla</i>	758	110
<i>Trifolium</i> type	0	0
Apiaceae	1516	0
<i>Apium nodiflorum</i>	0	0
Lamiaceae	0	0
<i>Plantago media-major</i>	0	0
<i>Rhinanthus</i> type	0	0
Rubiaceae	1137	0
<i>Cirsium</i>	0	0
Lactuceae	0	772
<i>Artemisia</i> type	379	0
<i>Aster</i> type	0	0
<i>Anthemis</i>	0	0
Pteropsida undiff.	379	772
<i>Pteridium aquilinum</i>	0	0
<i>Dryopteris filix-mas</i>	0	0
<i>Thelypteris palustris</i>	0	0
<i>Polypodium vulgare</i>	0	0
<i>Myriophyllum alterniflorum</i>	0	0
<i>Potamogeton natans</i> type (pondweed)	0	0
<i>Sparganium emersum</i> type	0	110
<i>Typha</i>	13646	662
<i>Menyanthes trifoliata</i>	0	0
<i>Sphagnum</i>	0	0



VC039

Depth (mbsf)	2.95	2.96	2.98	3.00	3.02	3.04
Sample volume	1	1	1	1	1	1
Lycopodium tablets	1	1	1	1	1	1
Lycopodium in tablets	20848	20848	20848	20848	20848	20848
Exotic	8	69	121	574	908	141
Betula	7	15	36	12	105	108
Pinus sylvestris	221	245	152	213	107	41
Corylus avellana type	5	8	39	15	10	10
Ulmus	0	0	0	0	0	0
Quercus	0	0	2	0	0	0
Tilia	0	0	0	0	0	0
Juniperus communis	0	0	0	0	0	0
Salix	1	3	4	5	0	7
Rosa	0	0	0	0	0	0
Viburnum	0	0	0	0	0	0
Ilex aquifolium	0	0	0	0	0	0
Hedera helix	0	0	0	0	0	0
Ericaceae	0	0	0	0	0	0
Poaceae	14	12	11	8	25	77
Cyperaceae	60	30	58	48	49	41
Ranunculaceae	0	0	0	0	1	2
Caryophyllaceae	0	0	0	0	0	0
Silene type	0	0	0	0	0	0
Brassicaceae	0	0	0	0	0	2
Persicaria bistorta	0	0	0	0	0	0
Chenopodiaceae	0	0	2	0	0	0
Rumex acetosa	0	0	0	0	0	0
Rosaceae	4	1	0	3	3	4
Filipendula	1	0	0	0	2	3
Potentilla	0	0	0	0	0	0
Trifolium type	0	0	0	0	0	0
Apiaceae	0	0	0	0	0	1
Apium nodiflorum	0	0	0	0	0	3
Lamiaceae	0	0	0	0	1	0
Plantago media-major	0	0	0	0	0	0
Rhinanthus type	0	0	0	0	0	0
Rubiaceae	0	0	0	0	0	0
Cirsium	0	0	0	0	0	0
Lactuceae	0	0	0	0	0	0



Depth (mbsf)	2.95	2.96	2.98	3.00	3.02	3.04
Artemisia type	1	0	0	0	0	0
Aster type	0	1	1	1	0	1
Anthemis	0	0	0	0	0	0
Pteropsida undiff.	64	1276	712	791	364	190
Pteridium aquilinum	0	0	0	0	0	0
Dryopteris filix-mas	0	0	2	0	0	0
Thelypteris palustris	0	0	0	0	0	0
Polypodium vulgare	0	0	0	0	0	0
Myriophyllum alterniflorum	0	0	0	0	0	0
Potamogeton natans type (pondweed)	0	0	1	0	1	3
Sparganium emersum type	0	0	0	0	0	0
Typha	0	1	0	0	5	11
Menyanthes trifoliata	0	0	0	0	0	7
Nymphaea alba	0	0	0	0	0	0
Sphagnum	0	2	0	3	0	2
Indeterminables	17	5	0	3	16	7
TLP	314	315	305	305	303	300
Charcoal	593	1	5	0	0	15
Points	202	202	202	202	202	202
Charcoal/points	2.94	0.00	0.02	0.00	0.00	0.07
Field of view	0.00238	0.00238	0.00238	0.00238	0.00238	0.00238
No lycopodium spores	20848	20848	20848	20848	20848	20848
Lycopodium spores counted	50	50	50	50	50	50
Total spores/total counted	416.96	416.96	416.96	416.96	416.96	416.96
Total	2.91	0.00	0.02	0.00	0.00	0.07
Total pollen concentration	818284	95176	52551	11078	6957	44357



VC039 (continued)

Depth (mbsf)	3.06	3.08	3.09	3.11	3.13	3.15
Sample volume	1	1	1	1	1	1
Lycopodium tablets	1	1	1	1	1	1
Lycopodium in tablets	20848	20848	20848	20848	20848	20848
Exotic	633	117	148	250	230	93
Betula	50	47	70	99	84	69
Pinus sylvestris	78	10	4	20	13	17
Corylus avellana type	4	2	0	1	0	2
Ulmus	0	0	0	0	0	0
Quercus	0	0	0	0	0	0
Tilia	0	0	0	0	0	0
Juniperus communis	0	0	0	1	0	1
Salix	7	7	8	5	6	2
Rosa	0	0	0	0	0	0
Viburnum	0	0	0	0	0	0
Ilex aquifolium	0	0	0	0	0	0
Hedera helix	0	0	0	0	0	0
Ericaceae	0	0	0	0	0	0
Poaceae	44	115	125	155	181	191
Cyperaceae	109	115	88	7	6	5
Ranunculaceae	1	2	3	0	0	0
Caryophyllaceae	0	0	0	0	0	0
Silene type	0	0	0	0	0	0
Brassicaceae	1	0	0	0	0	0
Persicaria bistorta	0	0	0	0	0	0
Chenopodiaceae	0	0	0	0	0	0
Rumex acetosa	0	0	0	0	0	1
Rosaceae	3	3	3	9	3	3
Filipendula	1	4	3	2	3	4
Potentilla	0	0	0	0	0	0
Trifolium type	0	0	0	0	0	0
Apiaceae	1	0	0	3	1	2
Apium nodiflorum	0	0	0	0	0	0
Lamiaceae	0	0	0	0	0	1
Plantago media-major	0	0	0	0	0	0
Rhinanthus type	0	0	0	0	0	0
Rubiaceae	0	0	0	0	1	0
Cirsium	0	0	0	0	0	0
Lactuceae	0	0	0	0	0	0



Depth (mbsf)	3.06	3.08	3.09	3.11	3.13	3.15
Artemisia type	0	1	1	1	2	2
Aster type	1	0	0	0	0	0
Anthemis	0	0	0	0	0	0
Pteropsida undiff.	100	12	8	0	1	3
Pteridium aquilinum	0	0	0	0	0	1
Dryopteris filix-mas	1	1	1	0	0	0
Thelypteris palustris	0	1	0	0	0	0
Polypodium vulgare	0	0	0	0	0	0
Myriophyllum alterniflorum	0	0	1	3	1	1
Potamogeton natans type (pondweed)	1	0	0	9	14	13
Sparganium emersum type	0	0	0	1	1	7
Typha	10	8	4	65	37	37
Menyanthes trifoliata	10	2	0	1	0	5
Nymphaea alba	0	1	1	4	0	0
Sphagnum	2	0	0	0		0
Indeterminables	9	2	2	2	3	2
TLP	300	306	305	303	300	300
Charcoal	0	0	0	2	0	0
Points	202	202	202	202	202	202
Charcoal/points	0.00	0.00	0.00	0.01	0.00	0.00
Field of view	0.00238	0.00238	0.00238	0.00238	0.00238	0.00238
No lycopodium spores	20848	20848	20848	20848	20848	20848
Lycopodium spores counted	50	50	50	50	50	50
Total spores/total counted	416.96	416.96	416.96	416.96	416.96	416.96
Total	0.00	0.00	0.00	0.01	0.00	0.00
Total pollen concentration	9881	54526	42964	25268	27193	67252



Appendix 3 – radiocarbon dating reports

UBANo	Sample ID	Material Type	¹⁴ C Age	±	F14C	±
UBA-38188	117121_VC028_2.59-2.62	Bud scales	8749	40	0.3365	0.0016
UBA-38189	117121_VC032_3.83	Menyanthes trifoliata seeds	8697	45	0.3387	0.0019
UBA-38190	117121_VC032_4.11	Bulk sediment	9992	51	0.2882	0.0018
UBA-38191	117121_VC039_3.07	Menyanthes trifoliata seeds	10881	60	0.2581	0.0019

Inez Lopez-Doriga
Wessex Archaeology
Portway House
Old Sarum Park
Salisbury, Wiltshire SP4
6EB
England
Customer No. 2144166



¹⁴CHRONO Centre
Queens University
Belfast
42 Fitzwilliam Street
Belfast BT9 6AX
Northern Ireland

Radiocarbon Date Certificate

Laboratory Identification: UBA-38188
Date of Measurement: 2018-06-22
Site: Boreas
Sample ID: 117121_VC028_2.59-2.62
Material Dated: plant macrofossil
Pretreatment: Acid Only
Submitted by: Ines Lopez Doriga

Conventional ¹⁴ C	
Age:	8749±40 BP
	using AMS
Fraction corrected δ ¹³ C	

Inez Lopez-Doriga
Wessex Archaeology
Portway House
Old Sarum Park
Salisbury, Wiltshire SP4
6EB
England
Customer No. 2144166



¹⁴CHRONO Centre
Queens University
Belfast
42 Fitzwilliam Street
Belfast BT9 6AX
Northern Ireland

Radiocarbon Date Certificate

Laboratory Identification: UBA-38189
Date of Measurement: 2018-06-22
Site: Boreas
Sample ID: 117121_VC032_3.83
Material Dated: plant macrofossil
Pretreatment: Acid Only
Submitted by: Ines Lopez Doriga

Conventional ¹⁴ C
Age: 8697±45 BP
using AMS
Fraction corrected δ ¹³ C

Inez Lopez-Doriga
Wessex Archaeology
Portway House
Old Sarum Park
Salisbury, Wiltshire SP4
6EB
England
Customer No. 2144166



¹⁴CHRONO Centre
Queens University
Belfast
42 Fitzwilliam Street
Belfast BT9 6AX
Northern Ireland

Radiocarbon Date Certificate

Laboratory Identification: UBA-38190
Date of Measurement: 2018-06-19
Site: Boreas
Sample ID: 117121_VC032_4.11
Material Dated: peat,soil,sediment (bulk)
Pretreatment: AAA
Submitted by: Ines Lopez Doriga

Conventional ¹⁴ C
Age: 9992±51 BP
using AMS
Fraction corrected δ ¹³ C

Inez Lopez-Doriga
Wessex Archaeology
Portway House
Old Sarum Park
Salisbury, Wiltshire SP4
6EB
England
Customer No. 2144166



¹⁴CHRONO Centre
Queens University
Belfast
42 Fitzwilliam Street
Belfast BT9 6AX
Northern Ireland

Radiocarbon Date Certificate

Laboratory Identification: UBA-38191
Date of Measurement: 2018-06-29
Site: Boreas
Sample ID: 117121_VC039_3.07
Material Dated: plant macrofossil
Pretreatment: Acid Only
Submitted by: Ines Lopez Doriga

Conventional ¹⁴ C	10881±60
Age:	BP
Fraction	using AMS
corrected	δ ¹³ C

Information about radiocarbon calibration

RADIOCARBON CALIBRATION PROGRAM*

CALIB REV7.0.0

Copyright 1986–2013 M Stuiver and PJ Reimer

*To be used in conjunction with:

Stuiver, M., and Reimer, P.J., 1993, Radiocarbon, 35, 215–230.

Annotated results (text) - -

Export file - c14res.csv

38188

UBA-38188

Radiocarbon Age BP 8749 +/- 40

Calibration data set: intcal13.14c

% area enclosed cal AD age ranges

68.3 (1 sigma) cal BC 7936– 7927

7916– 7899

7843– 7703

7699– 7680

95.4 (2 sigma) cal BC 7951– 7635

7622– 7615

Reimer et al. 2013

relative area under
probability distribution

0.036

0.073

0.813

0.079

0.989

0.011

38189

UBA-38189

Radiocarbon Age BP 8697 +/- 45

Calibration data set: intcal13.14c

% area enclosed cal AD age ranges

68.3 (1 sigma) cal BC 7735– 7610

95.4 (2 sigma) cal BC 7934– 7929

7913– 7900

7866– 7861

7843– 7594

Reimer et al. 2013

relative area under
probability distribution

1.000

0.004

0.009

0.004

0.983

38190

UBA-38190

Radiocarbon Age BP 9992 +/- 51

Calibration data set: intcal13.14c

% area enclosed cal AD age ranges

68.3 (1 sigma) cal BC 9654– 9578

9551– 9473

9467– 9375

95.4 (2 sigma) cal BC 9758– 9714

9700– 9314

Reimer et al. 2013

relative area under
probability distribution

0.311

0.306

0.383

0.047

0.953

38191

UBA-38191

Radiocarbon Age BP 10881 +/- 60

Calibration data set: intcal13.14c

% area enclosed cal AD age ranges

68.3 (1 sigma) cal BC 10842– 10762

95.4 (2 sigma) cal BC 10939– 10736

Reimer et al. 2013

relative area under
probability distribution

1.000

1.000

References for calibration datasets:

Reimer PJ, Bard E, Bayliss A, Beck JW, Blackwell PG, Bronk Ramsey C, Buck CE, Cheng H, Edwards RL, Friedrich M, Grootes PM, Guilderson TP, Hafliðason H, Hajdas I, Hattä C, Heaton TJ, Hogg AG, Hughen KA, Kaiser KF, Kromer B,

Manning SW, Niu M, Reimer RW, Richards DA, Scott EM, Southon JR, Turney CSM,
van der Plicht J.

IntCal13 and MARINE13 radiocarbon age calibration curves 0-50000 years calBP
Radiocarbon 55(4). DOI: 10.2458/azu_js_rc.55.16947

Comments:

* This standard deviation (error) includes a lab error multiplier.

** 1 sigma = square root of (sample std. dev.^2 + curve std. dev.^2)

** 2 sigma = 2 x square root of (sample std. dev.^2 + curve std. dev.^2)

where ^2 = quantity squared.

[] = calibrated range impinges on end of calibration data set

0* represents a "negative" age BP

1955* or 1960* denote influence of nuclear testing C-14

NOTE: Cal ages and ranges are rounded to the nearest year which
may be too precise in many instances. Users are advised to
round results to the nearest 10 yr for samples with standard
deviation in the radiocarbon age greater than 50 yr.

<>

UBANo	Sample ID	Material Type	¹⁴ C Age	±	F14C	±
UBA-39469	114844_VC074_1.18m	Cyperaceae, Solanum sp. and Alisma sp. seeds, Poaceae husks	9696	44	0.2991	0.0016
UBA-39470	114844_VC075_1.45m	Juncus sp., Betula sp., Caryophyllaceae, Alisma sp., Chenopodiaceae and Carex sp. seeds	9613	39	0.3022	0.0015
UBA-39471	117122_VC039_2.96m	Menyanthes trifoliata seed	8510	58	0.3467	0.0025
UBA-39472	117122_VC039_3.13m	Menyanthes trifoliata, Betula sp., Characeae oospores, Typha sp.	10435	66	0.2728	0.0022
UBA-39473	117122_VC032_3.61m	Organic material with Sphagnum sp. leaves	9124	77	0.3212	0.0031
UBA-39474	117122_VC032_3.95m	Lamiaceae, Ranunculus sp., Menyanthes trifoliata seeds	8894	78	0.3305	0.0032
UBA-39475	117122_VC028_2.5m	Failed	Failed	Failed	Failed	Failed

Inez Lopez-Doriga
Wessex Archaeology
Portway House
Old Sarum Park
Salisbury, Wiltshire
SP4 6EB
England
Customer No.
2144166



¹⁴CHRONO Centre
Queens University
Belfast
42 Fitzwilliam
Street
Belfast BT9 6AX
Northern Ireland

Radiocarbon Date Certificate

Laboratory Identification: UBA-39469
Date of Measurement: 2018-12-12
Site: Vanguard
Sample ID: 114844_VC074_1.18m
Material Dated: plant macrofossil
Pretreatment: Acid Only
Submitted by: Ines Lopez Doriga

Conventional	9696±44
¹⁴ C Age:	BP
	using
Fraction	AMS
corrected	δ ¹³ C

Inez Lopez-Doriga
Wessex Archaeology
Portway House
Old Sarum Park
Salisbury, Wiltshire
SP4 6EB
England
Customer No.
2144166



¹⁴CHRONO Centre
Queens University
Belfast
42 Fitzwilliam
Street
Belfast BT9 6AX
Northern Ireland

Radiocarbon Date Certificate

Laboratory Identification: UBA-39470
Date of Measurement: 2018-12-12
Site: Vanguard
Sample ID: 114844_VC075_1.45m
Material Dated: plant macrofossil
Pretreatment: Acid Only
Submitted by: Ines Lopez Doriga

Conventional	9613±39
¹⁴ C Age:	BP
	using
Fraction	AMS
corrected	δ ¹³ C

Inez Lopez-Doriga
Wessex Archaeology
Portway House
Old Sarum Park
Salisbury, Wiltshire
SP4 6EB
England
Customer No.
2144166



¹⁴CHRONO Centre
Queens University
Belfast
42 Fitzwilliam
Street
Belfast BT9 6AX
Northern Ireland

Radiocarbon Date Certificate

Laboratory Identification: UBA-39471
Date of Measurement: 2018-12-12
Site: Boreas
Sample ID: 117122_VC039_2.96m
Material Dated: plant macrofossil
Pretreatment: Acid Only
Submitted by: Ines Lopez Doriga

Conventional	8510±58
¹⁴ C Age:	BP
	using
Fraction	AMS
corrected	δ ¹³ C

Inez Lopez-Doriga
Wessex Archaeology
Portway House
Old Sarum Park
Salisbury, Wiltshire
SP4 6EB
England
Customer No.
2144166



¹⁴CHRONO Centre
Queens University
Belfast
42 Fitzwilliam
Street
Belfast BT9 6AX
Northern Ireland

Radiocarbon Date Certificate

Laboratory Identification: UBA-39472
Date of Measurement: 2018-12-12
Site: Boreas
Sample ID: 117122_VC039_3.13m
Material Dated: plant macrofossil
Pretreatment: Acid Only
Submitted by: Ines Lopez Doriga

Conventional	10435±66
¹⁴ C Age:	BP
	using
Fraction	AMS
corrected	δ ¹³ C

Inez Lopez-Doriga
Wessex Archaeology
Portway House
Old Sarum Park
Salisbury, Wiltshire
SP4 6EB
England
Customer No.
2144166



¹⁴CHRONO Centre
Queens University
Belfast
42 Fitzwilliam
Street
Belfast BT9 6AX
Northern Ireland

Radiocarbon Date Certificate

Laboratory Identification: UBA-39473
Date of Measurement: 2018-12-12
Site: Boreas
Sample ID: 117122_VC032_3.61m
Material Dated: plant macrofossil
Pretreatment: Acid Only
Submitted by: Ines Lopez Doriga

Conventional	9124±77
¹⁴ C Age:	BP
	using
Fraction	AMS
corrected	δ ¹³ C

Inez Lopez-Doriga
Wessex Archaeology
Portway House
Old Sarum Park
Salisbury, Wiltshire
SP4 6EB
England
Customer No.
2144166



¹⁴CHRONO Centre
Queens University
Belfast
42 Fitzwilliam
Street
Belfast BT9 6AX
Northern Ireland

Radiocarbon Date Certificate

Laboratory Identification: UBA-39474
Date of Measurement: 2018-12-12
Site: Boreas
Sample ID: 117122_VC032_3.95m
Material Dated: plant macrofossil
Pretreatment: Acid Only
Submitted by: Ines Lopez Doriga

Conventional	8894±78
¹⁴ C Age:	BP
	using
Fraction	AMS
corrected	δ ¹³ C

Information about radiocarbon calibration

RADIOCARBON CALIBRATION PROGRAM*

CALIB REV7.0.0

Copyright 1986-2013 M Stuiver and PJ Reimer

*To be used in conjunction with:

Stuiver, M., and Reimer, P.J., 1993, Radiocarbon, 35, 215-230.

Annotated results (text) - -

Export file - c14res.csv

39469

UBA-39469

Radiocarbon Age BP 9696 +/- 44

Calibration data set: intcal13.14c

% area enclosed cal AD age ranges

68.3 (1 sigma) cal BC 9252- 9151

95.4 (2 sigma) cal BC 9276- 9121

9002- 8918

8890- 8864

Reimer et al. 2013
relative area under
probability distribution

1.000

0.819

0.164

0.016

39470

UBA-39470

Radiocarbon Age BP 9613 +/- 39

Calibration data set: intcal13.14c

% area enclosed cal AD age ranges

68.3 (1 sigma) cal BC 9174- 9118

9068- 9060

9009- 8913

8902- 8848

95.4 (2 sigma) cal BC 9215- 9101

9089- 8827

Reimer et al. 2013
relative area under
probability distribution

0.249

0.033

0.488

0.230

0.278

0.722

39471

UBA-39471

Radiocarbon Age BP 8510 +/- 58

Calibration data set: intcal13.14c

% area enclosed cal AD age ranges

68.3 (1 sigma) cal BC 7587- 7533

95.4 (2 sigma) cal BC 7606- 7479

Reimer et al. 2013
relative area under
probability distribution

1.000

1.000

39472

UBA-39472

Radiocarbon Age BP 10435 +/- 66

Calibration data set: intcal13.14c

% area enclosed cal AD age ranges

68.3 (1 sigma) cal BC 10572- 10526

10479- 10418

10407- 10280

10261- 10213

95.4 (2 sigma) cal BC 10601- 10131

Reimer et al. 2013
relative area under
probability distribution

0.150

0.234

0.459

0.156

1.000

39473

UBA-39473

Radiocarbon Age BP 9124 +/- 77

Calibration data set: intcal13.14c

% area enclosed cal AD age ranges

68.3 (1 sigma) cal BC 8446- 8362

Reimer et al. 2013
relative area under
probability distribution

0.428

	8356- 8271	0.572
95.4 (2 sigma)	cal BC 8554- 8230	1.000
39474		
UBA-39474		
Radiocarbon Age BP	8894 +/- 78	
Calibration data set: intcal13.14c		# Reimer et al. 2013
% area enclosed	cal AD age ranges	relative area under probability distribution
68.3 (1 sigma)	cal BC 8227- 7957	1.000
95.4 (2 sigma)	cal BC 8263- 7784	0.992
	7769- 7758	0.008

References for calibration datasets:

Reimer PJ, Bard E, Bayliss A, Beck JW, Blackwell PG, Bronk Ramsey C, Buck CE, Cheng H, Edwards RL, Friedrich M, Grootes PM, Guilderson TP, Hafliðason H, Hajdas I, Hattala C, Heaton TJ, Hogg AG, Hughen KA, Kaiser KF, Kromer B, Manning SW, Niu M, Reimer RW, Richards DA, Scott EM, Southon JR, Turney CSM, van der Plicht J.

IntCal13 and MARINE13 radiocarbon age calibration curves 0-50000 years calBP Radiocarbon 55(4). DOI: 10.2458/azu_js_rc.55.16947

Comments:

* This standard deviation (error) includes a lab error multiplier.
 ** 1 sigma = square root of (sample std. dev.^2 + curve std. dev.^2)
 ** 2 sigma = 2 x square root of (sample std. dev.^2 + curve std. dev.^2)
 where ^2 = quantity squared.
 [] = calibrated range impinges on end of calibration data set
 0* represents a "negative" age BP
 1955* or 1960* denote influence of nuclear testing C-14

NOTE: Cal ages and ranges are rounded to the nearest year which may be too precise in many instances. Users are advised to round results to the nearest 10 yr for samples with standard deviation in the radiocarbon age greater than 50 yr.

<>

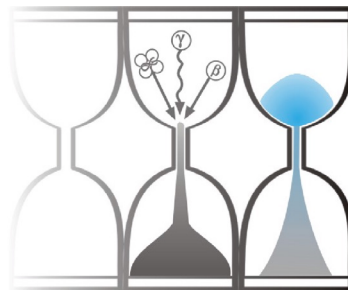


Appendix 4 – OSL dating report



University of Gloucestershire

Luminescence dating laboratory



Optical dating of sediments: Boreas Offshore Windfarm

to

Dr C. Mellett

Wessex Archaeology

**Analysis & Reporting, Dr P.S. Toms
Sample Preparation & Measurement, Mr J.C. Wood
14 August 2018**

Contents

Section		Page
	Table 1 D_r , D_e and Age data of submitted samples	3
	Table 2 Analytical validity of sample suite ages	4
1.0	Mechanisms and Principles	5
2.0	Sample Preparation	5
3.0	Acquisition and accuracy of D_e value	6
	3.1 Laboratory Factors	6
	3.1.1 Feldspar Contamination	6
	3.1.2 Preheating	6
	3.1.3 Irradiation	7
	3.1.4 Internal Consistency	7
	3.2 Environmental Factors	7
	3.2.1 Incomplete Zeroing	7
	3.2.2 Turbation	8
4.0	Acquisition and accuracy of D_r value	8
5.0	Estimation of age	9
6.0	Analytical Uncertainty	9
	Sample diagnostics, luminescence and age data	12
	References	16

Scope of Report

This is a standard report of the Luminescence dating laboratory, University of Gloucestershire. In large part, the document summarises the processes, diagnostics and data drawn upon to deliver Table 1. A conclusion on the analytical validity of each sample's optical age estimate is expressed in Table 2; where there are caveats, the reader is directed to the relevant section of the report that explains the issue further in general terms.

Copyright Notice

Permission must be sought from Dr P.S. Toms of the University of Gloucestershire Luminescence dating laboratory in using the content of this report, in part or whole, for the purpose of publication.

Field Code	Lab Code	Overburden (m)	Grain size (μm)	Moisture content (%)	NaI γ -spectrometry (<i>in situ</i>) γD_r ($\text{Gy.k}\text{a}^{-1}$)	Ge γ -spectrometry (<i>ex situ</i>)			βD_r ($\text{Gy.k}\text{a}^{-1}$)	γD_r ($\text{Gy.k}\text{a}^{-1}$)	Cosmic D_r ($\text{Gy.k}\text{a}^{-1}$)	Preheat ($^{\circ}\text{C}$ for 10s)	Low Dose Repeat Ratio	Interpolated:Applied Low Regenerative-dose D_e	High Dose Repeat Ratio	Interpolated:Applied High Regenerative-dose D_e	Post-IR OSL Ratio
						K (%)	Th (ppm)	U (ppm)									
						NBOWF_VC016: 2.65-3.00 m	GL17153	2.83									
NBOWF_VC016: 1.70-2.00 m	GL17154	1.85	125-180	15 \pm 4	-	1.50 \pm 0.10	7.81 \pm 0.53	1.93 \pm 0.14	1.25 \pm 0.14	0.79 \pm 0.10	0.15 \pm 0.01	220	1.04 \pm 0.01	1.07 \pm 0.02	1.01 \pm 0.01	1.05 \pm 0.03	1.01 \pm 0.01
NBOWF_VC047: 2.55-3.00 m	GL17155	2.78	125-180	16 \pm 4	-	1.55 \pm 0.10	8.25 \pm 0.53	1.92 \pm 0.14	1.29 \pm 0.14	0.82 \pm 0.11	0.13 \pm 0.01	240	1.04 \pm 0.02	1.08 \pm 0.03	1.02 \pm 0.02	1.11 \pm 0.05	1.04 \pm 0.02
NBOWF_VC047: 3.70-4.00 m	GL17156	3.85	125-180	17 \pm 4	-	1.73 \pm 0.11	8.95 \pm 0.57	1.97 \pm 0.14	1.38 \pm 0.16	0.87 \pm 0.11	0.11 \pm 0.01	240	1.06 \pm 0.03	1.12 \pm 0.04	1.04 \pm 0.02	1.21 \pm 0.09	1.05 \pm 0.02

Field Code	Lab Code	Total D_r ($\text{Gy.k}\text{a}^{-1}$)	D_e (Gy)	Age (ka)
NBOWF_VC016: 2.65-3.00 m	GL17153	2.14 \pm 0.17	149.6 \pm 11.1	69.8 \pm 7.7 (6.9)
NBOWF_VC016: 1.70-2.00 m	GL17154	2.19 \pm 0.17	182.1 \pm 15.0	83.2 \pm 9.5 (8.7)
NBOWF_VC047: 2.55-3.00 m	GL17155	2.23 \pm 0.18	135.1 \pm 7.2	60.5 \pm 5.8 (5.0)
NBOWF_VC047: 3.70-4.00 m	GL17156	2.38 \pm 0.20	186.0 \pm 11.6	78.9 \pm 8.3 (7.4)

Table 1 D_r , D_e and Age data of submitted samples located at c. 53°N, 3°E, 0m. Age estimates expressed relative to year of sampling. Uncertainties in age are quoted at 1 σ confidence, are based on analytical errors and reflect combined systematic and experimental variability and (in parenthesis) experimental variability alone (see 6.0). **Blue** indicates samples with accepted age estimates, **red**, age estimates with caveats (see Table 2).

Generic considerations	Field Code	Lab Code	Sample specific considerations
Absence of <i>in situ</i> γ spectrometry data (see section 4.0)	NBOWF_VC016: 2.65-3.00 m	GL17153	None
	NBOWF_VC016: 1.70-2.00 m	GL17154	None
	NBOWF_VC047: 2.55-3.00 m	GL17155	Overdispersed interpolated to applied regenerative-dose ratio (see section 3.1.4 and Table 1) Accept tentatively
	NBOWF_VC047: 3.70-4.00 m	GL17156	Overdispersed interpolated to applied regenerative-dose ratio (see section 3.1.4 and Table 1) Accept tentatively

Table 2 Analytical validity of sample suite age estimates and caveats for consideration

1.0 Mechanisms and principles

Upon exposure to ionising radiation, electrons within the crystal lattice of insulating minerals are displaced from their atomic orbits. Whilst this dislocation is momentary for most electrons, a portion of charge is redistributed to meta-stable sites (traps) within the crystal lattice. In the absence of significant optical and thermal stimuli, this charge can be stored for extensive periods. The quantity of charge relocation and storage relates to the magnitude and period of irradiation. When the lattice is optically or thermally stimulated, charge is evicted from traps and may return to a vacant orbit position (hole). Upon recombination with a hole, an electron's energy can be dissipated in the form of light generating crystal luminescence providing a measure of dose absorption.

Herein, quartz is segregated for dating. The utility of this minerogenic dosimeter lies in the stability of its datable signal over the mid to late Quaternary period, predicted through isothermal decay studies (e.g. Smith *et al.*, 1990; retention lifetime 630 Ma at 20°C) and evidenced by optical age estimates concordant with independent chronological controls (e.g. Murray and Olley, 2002). This stability is in contrast to the anomalous fading of comparable signals commonly observed for other ubiquitous sedimentary minerals such as feldspar and zircon (Wintle, 1973; Templer, 1985; Spooner, 1993)

Optical age estimates of sedimentation (Huntley *et al.*, 1985) are premised upon reduction of the minerogenic time dependent signal (Optically Stimulated Luminescence, OSL) to zero through exposure to sunlight and, once buried, signal reformulation by absorption of litho- and cosmogenic radiation. The signal accumulated post burial acts as a dosimeter recording total dose absorption, converting to a chronometer by estimating the rate of dose absorption quantified through the assay of radioactivity in the surrounding lithology and streaming from the cosmos.

$$\text{Age} = \frac{\text{Mean Equivalent Dose (D}_e\text{, Gy)}}{\text{Mean Dose Rate (D}_r\text{, Gy.ka}^{-1}\text{)}}$$

Aitken (1998) and Bøtter-Jensen *et al.* (2003) offer a detailed review of optical dating.

2.0 Sample Preparation

Four sediment samples were submitted within cores for Optical dating. To preclude optical erosion of the datable signal prior to measurement, all samples were opened and prepared under controlled laboratory illumination provided by Encapsulite RB-10 (red) filters. To isolate that material potentially exposed to daylight during sampling, sediment located within 10 mm of each core face was removed.

The remaining sample was dried and then sieved. The fine sand fraction was segregated and subjected to acid and alkaline digestion (10% HCl, 15% H₂O₂) to attain removal of carbonate and organic components respectively. A further acid digestion in HF (40%, 60 mins) was used to etch the outer 10-15 µm layer affected by α radiation and degrade each samples' feldspar content. During HF treatment, continuous magnetic stirring was used to effect isotropic etching of grains. 10% HCl was then added to remove acid soluble fluorides. Each sample was dried, resieved and quartz isolated from the remaining heavy mineral fraction using a sodium polytungstate density separation at 2.68g.cm⁻³. Twelve 8 mm multi-grain aliquots (c. 3-6 mg) of quartz from each sample were then mounted on aluminium discs for determination of D_e values.

All drying was conducted at 40°C to prevent thermal erosion of the signal. All acids and alkalis were Analar grade. All dilutions (removing toxic-corrosive and non-minerogenic luminescence-bearing substances) were conducted with distilled water to prevent signal contamination by extraneous particles.

3.0 Acquisition and accuracy of D_e value

All minerals naturally exhibit marked inter-sample variability in luminescence per unit dose (sensitivity). Therefore, the estimation of D_e acquired since burial requires calibration of the natural signal using known amounts of laboratory dose. D_e values were quantified using a single-aliquot regenerative-dose (SAR) protocol (Murray and Wintle 2000; 2003) facilitated by a Risø TL-DA-15 irradiation-stimulation-detection system (Markey *et al.*, 1997; Bøtter-Jensen *et al.*, 1999). Within this apparatus, optical signal stimulation is provided by an assembly of blue diodes (5 packs of 6 Nichia NSPB500S), filtered to 470 ± 80 nm conveying $15 \text{ mW}\cdot\text{cm}^{-2}$ using a 3 mm Schott GG420 positioned in front of each diode pack. Infrared (IR) stimulation, provided by 6 IR diodes (Telefunken TSHA 6203) stimulating at 875 ± 80 nm delivering $\sim 5 \text{ mW}\cdot\text{cm}^{-2}$, was used to indicate the presence of contaminant feldspars (Hütt *et al.*, 1988). Stimulated photon emissions from quartz aliquots are in the ultraviolet (UV) range and were filtered from stimulating photons by 7.5 mm HOYA U-340 glass and detected by an EMI 9235QA photomultiplier fitted with a blue-green sensitive bialkali photocathode. Aliquot irradiation was conducted using a $1.48 \text{ GBq } ^{90}\text{Sr}/^{90}\text{Y } \beta$ source calibrated for multi-grain aliquots of 125-180 μm quartz against the 'Hotspot 800' $^{60}\text{Co } \gamma$ source located at the National Physical Laboratory (NPL), UK.

SAR by definition evaluates D_e through measuring the natural signal (Fig. 1) of a single aliquot and then regenerating that aliquot's signal by using known laboratory doses to enable calibration. For each aliquot, five different regenerative-doses were administered so as to image dose response. D_e values for each aliquot were then interpolated, and associated counting and fitting errors calculated, by way of exponential plus linear regression (Fig. 1). Weighted (geometric) mean D_e values were calculated from 12 aliquots using the central age model outlined by Galbraith *et al.* (1999) and are quoted at 1σ confidence (Table 1). The accuracy with which D_e equates to total absorbed dose and that dose absorbed since burial was assessed. The former can be considered a function of laboratory factors, the latter, one of environmental issues. Diagnostics were deployed to estimate the influence of these factors and criteria instituted to optimise the accuracy of D_e values.

3.1 Laboratory Factors

3.1.1 Feldspar contamination

The propensity of feldspar signals to fade and underestimate age, coupled with their higher sensitivity relative to quartz makes it imperative to quantify feldspar contamination. At room temperature, feldspars generate a signal (IRSL; Fig. 1) upon exposure to IR whereas quartz does not. The signal from feldspars contributing to OSL can be depleted by prior exposure to IR. For all aliquots the contribution of any remaining feldspars was estimated from the OSL IR depletion ratio (Duller, 2003). The influence of IR depletion on the OSL signal can be illustrated by comparing the regenerated post-IR OSL D_e with the applied regenerative-dose. If the addition to OSL by feldspars is insignificant, then the repeat dose ratio of OSL to post-IR OSL should be statistically consistent with unity (Table 1). If any aliquots do not fulfil this criterion, then the sample age estimate should be accepted tentatively. The source of feldspar contamination is rarely rooted in sample preparation; it predominantly results from the occurrence of feldspars as inclusions within quartz.

3.1.2 Preheating

Preheating aliquots between irradiation and optical stimulation is necessary to ensure comparability between natural and laboratory-induced signals. However, the multiple irradiation and preheating steps that are required to define single-aliquot regenerative-dose response leads to signal sensitisation, rendering calibration of the natural signal inaccurate. The SAR protocol (Murray and Wintle, 2000; 2003) enables this sensitisation to be monitored and corrected using a test dose, here set at 5 Gy preheated to 220°C for 10s, to track signal sensitivity between irradiation-preheat steps. However, the accuracy of sensitisation correction for both natural and laboratory signals can be preheat dependent.

The Dose Recovery test was used to assess the optimal preheat temperature for accurate correction and calibration of the time dependent signal. Dose Recovery (Fig. 2) attempts to quantify the combined effects of thermal transfer and

sensitisation on the natural signal, using a precise lab dose to simulate natural dose. The ratio between the applied dose and recovered D_e value should be statistically concordant with unity. For this diagnostic, 6 aliquots were each assigned a 10 s preheat between 180°C and 280°C.

That preheat treatment fulfilling the criterion of accuracy within the Dose Recovery test was selected to generate the final D_e value from a further 12 aliquots. Further thermal treatments, prescribed by Murray and Wintle (2000; 2003), were applied to optimise accuracy and precision. Optical stimulation occurred at 125°C in order to minimise effects associated with photo-transferred thermoluminescence and maximise signal to noise ratios. Inter-cycle optical stimulation was conducted at 280°C to minimise recuperation.

3.1.3 Irradiation

For all samples having D_e values in excess of 100 Gy, matters of signal saturation and laboratory irradiation effects are of concern. With regards the former, the rate of signal accumulation generally adheres to a saturating exponential form and it is this that limits the precision and accuracy of D_e values for samples having absorbed large doses. For such samples, the functional range of D_e interpolation by SAR has been verified up to 600 Gy by Pawley *et al.* (2010). Age estimates based on D_e values exceeding this value should be accepted tentatively.

3.1.4 Internal consistency

Abanico plots (Dietze *et al.*, 2016) are used to illustrate inter-aliquot D_e variability (Fig. 3). D_e values are standardised relative to the central D_e value for natural signals and are described as overdispersed when >5% lie beyond $\pm 2\sigma$ of the standardising value; resulting from a heterogeneous absorption of burial dose and/or response to the SAR protocol. For multi-grain aliquots, overdispersion of natural signals does not necessarily imply inaccuracy. However where overdispersion is observed for regenerated signals, the efficacy of sensitivity correction may be problematic. Murray and Wintle (2000; 2003) suggest repeat dose ratios (Table 1) offer a measure of SAR protocol success, whereby ratios ranging across 0.9-1.1 are acceptable. However, this variation of repeat dose ratios in the high-dose region can have a significant impact on D_e interpolation. The influence of this effect can be outlined by quantifying the ratio of interpolated to applied regenerative-dose ratio (Table 1). In this study, where both the repeat dose ratios and interpolated to applied regenerative-dose ratios range across 0.9-1.1, sensitivity-correction is considered effective.

3.2 Environmental factors

3.2.1 Incomplete zeroing

Post-burial OSL signals residual of pre-burial dose absorption can result where pre-burial sunlight exposure is limited in spectrum, intensity and/or period, leading to age overestimation. This effect is particularly acute for material eroded and redeposited sub-aqueously (Olley *et al.*, 1998, 1999; Wallinga, 2002) and exposed to a burial dose of <20 Gy (e.g. Olley *et al.*, 2004), has some influence in sub-aerial contexts but is rarely of consequence where aerial transport has occurred. Within single-aliquot regenerative-dose optical dating there are two diagnostics of partial resetting (or bleaching); signal analysis (Agersnap-Larsen *et al.*, 2000; Bailey *et al.*, 2003) and inter-aliquot D_e distribution studies (Murray *et al.*, 1995).

Within this study, signal analysis was used to quantify the change in D_e value with respect to optical stimulation time for multi-grain aliquots. This exploits the existence of traps within minerogenic dosimeters that bleach with different efficiency for a given wavelength of light to verify partial bleaching. $D_e(t)$ plots (Fig. 4; Bailey *et al.*, 2003) are constructed from separate integrals of signal decay as laboratory optical stimulation progresses. A statistically significant increase in natural $D_e(t)$ is indicative of partial bleaching assuming three conditions are fulfilled. Firstly, that a statistically significant increase in $D_e(t)$ is observed when partial bleaching is simulated within the laboratory. Secondly, that there is no significant rise in $D_e(t)$ when full bleaching is simulated. Finally, there should be no significant augmentation in $D_e(t)$ when zero dose is simulated. Where partial bleaching is detected, the age derived from the sample should be considered a maximum estimate only. However, the utility of signal analysis is strongly dependent upon a samples pre-burial

experience of sunlight's spectrum and its residual to post-burial signal ratio. Given in the majority of cases, the spectral exposure history of a deposit is uncertain, the absence of an increase in natural D_e (t) does not necessarily testify to the absence of partial bleaching.

Where requested and feasible, the insensitivities of multi-grain single-aliquot signal analysis may be circumvented by inter-aliquot D_e distribution studies. This analysis uses aliquots of single sand grains to quantify inter-grain D_e distribution. At present, it is contended that asymmetric inter-grain D_e distributions are symptomatic of partial bleaching and/or pedoturbation (Murray *et al.*, 1995; Olley *et al.*, 1999; Olley *et al.*, 2004; Bateman *et al.*, 2003). For partial bleaching at least, it is further contended that the D_e acquired during burial is located in the minimum region of such ranges. The mean and breadth of this minimum region is the subject of current debate, as it is additionally influenced by heterogeneity in microdosimetry, variable inter-grain response to SAR and residual to post-burial signal ratios.

3.2.2 Turbation

As noted in section 3.1.1, the accuracy of sedimentation ages can further be controlled by post-burial trans-strata grain movements forced by pedo- or cryoturbation. Berger (2003) contends pedogenesis prompts a reduction in the apparent sedimentation age of parent material through bioturbation and illuviation of younger material from above and/or by biological recycling and resetting of the datable signal of surface material. Berger (2003) proposes that the chronological products of this remobilisation are A-horizon age estimates reflecting the cessation of pedogenic activity, Bc/C-horizon ages delimiting the maximum age for the initiation of pedogenesis with estimates obtained from Bt-horizons providing an intermediate age 'close to the age of cessation of soil development'. Singhvi *et al.* (2001), in contrast, suggest that B and C-horizons closely approximate the age of the parent material, the A-horizon, that of the 'soil forming episode'. Recent analyses of inter-aliquot D_e distributions have reinforced this complexity of interpreting burial age from pedoturbated deposits (Lombard *et al.*, 2011; Gliganic *et al.*, 2015; Jacobs *et al.*, 2008; Bateman *et al.*, 2007; Gliganic *et al.*, 2016). At present there is no definitive post-sampling mechanism for the direct detection of and correction for post-burial sediment remobilisation. However, intervals of palaeosol evolution can be delimited by a maximum age derived from parent material and a minimum age obtained from a unit overlying the palaeosol. Inaccuracy forced by cryoturbation may be bidirectional, heaving older material upwards or drawing younger material downwards into the level to be dated. Cryogenic deformation of matrix-supported material is, typically, visible; sampling of such cryogenically-disturbed sediments can be avoided.

4.0 Acquisition and accuracy of D_r value

Lithogenic D_r values were defined through measurement of U, Th and K radionuclide concentration and conversion of these quantities into β and γ D_r values (Table 1). β contributions were estimated from sub-samples by laboratory-based γ spectrometry using an Ortec GEM-S high purity Ge coaxial detector system, calibrated using certified reference materials supplied by CANMET. γ dose rates can be estimated from *in situ* NaI gamma spectrometry or, where direct measurements are unavailable as in the present case, from laboratory-based Ge γ spectrometry. *In situ* measurements reduce uncertainty relating to potential heterogeneity in the γ dose field surrounding each sample. The level of U disequilibrium was estimated by laboratory-based Ge γ spectrometry. Estimates of radionuclide concentration were converted into D_r values (Adamiec and Aitken, 1998), accounting for D_r modulation forced by grain size (Mejdahl, 1979) and present moisture content (Zimmerman, 1971). Cosmogenic D_r values were calculated on the basis of sample depth, geographical position and matrix density (Prescott and Hutton, 1994).

The spatiotemporal validity of D_r values can be considered a function of five variables. Firstly, age estimates devoid of *in situ* γ spectrometry data should be accepted tentatively if the sampled unit is heterogeneous in texture or if the sample is located within 300 mm of strata consisting of differing texture and/or mineralogy. However, where samples are obtained

throughout a vertical profile, consistent values of γD_r based solely on laboratory measurements may evidence the homogeneity of the γ field and hence accuracy of γD_r values. Secondly, disequilibrium can force temporal instability in U and Th emissions. The impact of this infrequent phenomenon (Olley *et al.*, 1996) upon age estimates is usually insignificant given their associated margins of error. However, for samples where this effect is pronounced (>50% disequilibrium between ^{238}U and ^{226}Ra ; Fig. 5), the resulting age estimates should be accepted tentatively. Thirdly, pedogenically-induced variations in matrix composition of B and C-horizons, such as radionuclide and/or mineral remobilisation, may alter the rate of energy emission and/or absorption. If D_r is invariant through a dated profile and samples encompass primary parent material, then element mobility is likely limited in effect. Fourthly, spatiotemporal detractions from present moisture content are difficult to assess directly, requiring knowledge of the magnitude and timing of differing contents. However, the maximum influence of moisture content variations can be delimited by recalculating D_r for minimum (zero) and maximum (saturation) content. Finally, temporal alteration in the thickness of overburden alters cosmic D_r values. Cosmic D_r often forms a negligible portion of total D_r . It is possible to quantify the maximum influence of overburden flux by recalculating D_r for minimum (zero) and maximum (surface sample) cosmic D_r .

5.0 Estimation of Age

Ages reported in Table 1 provide an estimate of sediment burial period based on mean D_e and D_r values and their associated analytical uncertainties. Uncertainty in age estimates is reported as a product of systematic and experimental errors, with the magnitude of experimental errors alone shown in parenthesis (Table 1). Cumulative frequency plots indicate the inter-aliquot variability in age (Fig. 6). The maximum influence of temporal variations in D_r forced by minima-maxima in moisture content and overburden thickness is also illustrated in Fig. 6. Where uncertainty in these parameters exists this age range may prove instructive, however the combined extremes represented should not be construed as preferred age estimates. The analytical validity of each sample is presented in Table 2.

6.0 Analytical uncertainty

All errors are based upon analytical uncertainty and quoted at 1σ confidence. Error calculations account for the propagation of systematic and/or experimental (random) errors associated with D_e and D_r values.

For D_e values, systematic errors are confined to laboratory β source calibration. Uncertainty in this respect is that combined from the delivery of the calibrating γ dose (1.2%; NPL, pers. comm.), the conversion of this dose for SiO_2 using the respective mass energy-absorption coefficient (2%; Hubbell, 1982) and experimental error, totalling 3.5%. Mass attenuation and bremsstrahlung losses during γ dose delivery are considered negligible. Experimental errors relate to D_e interpolation using sensitisation corrected dose responses. Natural and regenerated sensitisation corrected dose points (S_i) were quantified by,

$$S_i = (D_i - x.L_i) / (d_i - x.L_i) \quad \text{Eq.1}$$

where D_i = Natural or regenerated OSL, initial 0.2 s
 L_i = Background natural or regenerated OSL, final 5 s
 d_i = Test dose OSL, initial 0.2 s
 x = Scaling factor, 0.08

The error on each signal parameter is based on counting statistics, reflected by the square-root of measured values. The propagation of these errors within Eq. 1 generating σS_i follows the general formula given in Eq. 2. σS_i were then used to define fitting and interpolation errors within exponential plus linear regressions.

For D_r values, systematic errors accommodate uncertainty in radionuclide conversion factors (5%), β attenuation coefficients (5%), a -value (4%; derived from a systematic α source uncertainty of 3.5% and experimental error), matrix density (0.20 g.cm^{-3}), vertical thickness of sampled section (specific to sample collection device), saturation moisture content (3%), moisture content attenuation (2%), and burial moisture content (25% relative, unless direct evidence exists of the magnitude and period of differing content) and Ge gamma spectrometer calibration (3%). Experimental errors are associated with radionuclide quantification for each sample by Ge gamma spectrometry.

The propagation of these errors through to age calculation was quantified using the expression,

$$\sigma_y (\delta y / \delta x) = (\sum ((\delta y / \delta x_n) \cdot \sigma_{x_n})^2)^{1/2} \quad \text{Eq. 2}$$

where y is a value equivalent to that function comprising terms x_n and where σ_y and σ_{x_n} are associated uncertainties.

Errors on age estimates are presented as combined systematic and experimental errors and experimental errors alone. The former (combined) error should be considered when comparing luminescence ages herein with independent chronometric controls. The latter assumes systematic errors are common to luminescence age estimates generated by means identical to those detailed herein and enable direct comparison with those estimates.

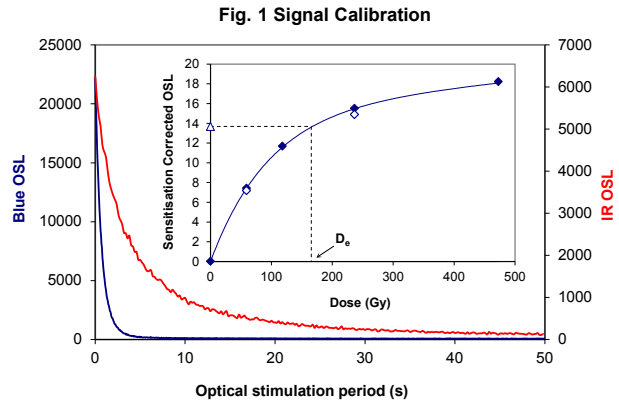


Fig. 1 Signal Calibration

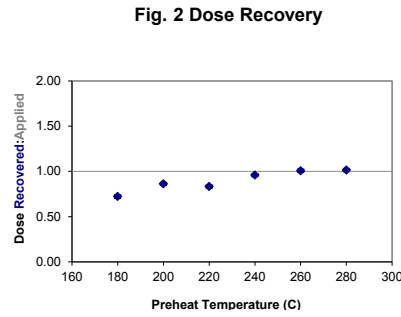


Fig. 2 Dose Recovery

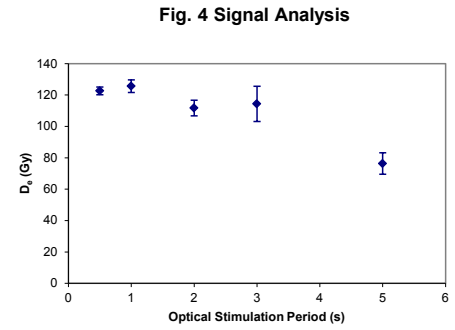


Fig. 4 Signal Analysis

Fig. 3 Inter-aliquot D_e distribution

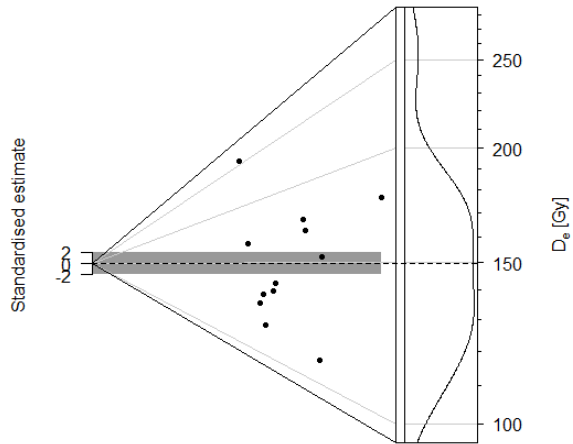


Fig. 1 Signal Calibration Natural blue and laboratory-induced infrared (IR) OSL signals. Detectable IR signal decays are diagnostic of feldspar contamination. Inset, the natural blue OSL signal (open triangle) of each aliquot is calibrated against known laboratory doses to yield equivalent dose (D_e) values. Repeats of low and high doses (open diamonds) illustrate the success of sensitivity correction.

Fig. 2 Dose Recovery The acquisition of D_e values is necessarily predicated upon thermal treatment of aliquots succeeding environmental and laboratory irradiation. The Dose Recovery test quantifies the combined effects of thermal transfer and sensitisation on the natural signal using a precise lab dose to simulate natural dose. Based on this an appropriate thermal treatment is selected to generate the final D_e value.

Fig. 3 Inter-aliquot D_e distribution Abanico plot of inter-aliquot statistical concordance in D_e values derived from natural irradiation. Discordant data (those points lying beyond ± 2 standardised $\ln D_e$) reflect heterogeneous dose absorption and/or inaccuracies in calibration.

Fig. 4 Signal Analysis Statistically significant increase in natural D_e value with signal stimulation period is indicative of a partially-bleached signal, provided a significant increase in D_e results from simulated partial bleaching followed by insignificant adjustment in D_e for simulated zero and full bleach conditions. Ages from such samples are considered maximum estimates. In the absence of a significant rise in D_e with stimulation time, simulated partial bleaching and zero/full bleach tests are not assessed.

Fig. 5 U Activity Statistical concordance (equilibrium) in the activities of the daughter radioisotope ^{226}Ra with its parent ^{238}U may signify the temporal stability of D_e emissions from these chains. Significant differences (disequilibrium; $>50\%$) in activity indicate addition or removal of isotopes creating a time-dependent shift in D_e values and increased uncertainty in the accuracy of age estimates. A 20% disequilibrium marker is also shown.

Fig. 6 Age Range The Cumulative frequency plot indicates the inter-aliquot variability in age. It also shows the mean age range: an estimate of sediment burial period based on mean D_e and D_e values with associated analytical uncertainties. The maximum influence of temporal variations in D_e forced by minima-maxima variation in moisture content and overburden thickness is outlined and may prove instructive where there is uncertainty in these parameters. However the combined extremes represented should not be construed as preferred age estimates.

Fig. 5 U Decay Activity

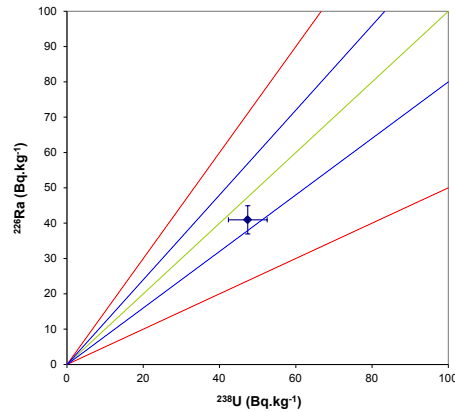
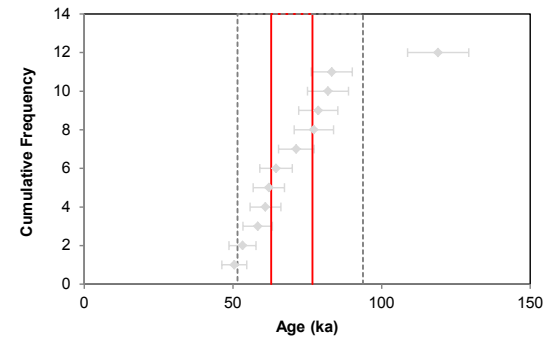
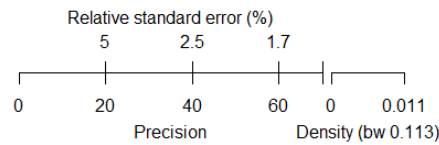


Fig. 6 Age Range



Sample: GL17153

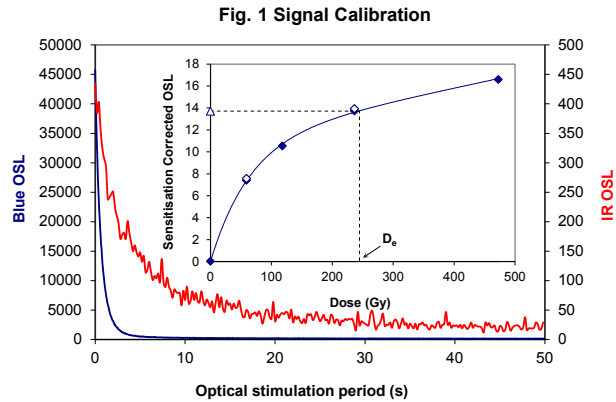


Fig. 1 Signal Calibration Natural blue and laboratory-induced infrared (IR) OSL signals. Detectable IR signal decays are diagnostic of feldspar contamination. Inset, the natural blue OSL signal (open triangle) of each aliquot is calibrated against known laboratory doses to yield equivalent dose (D_e) values. Repeats of low and high doses (open diamonds) illustrate the success of sensitivity correction.

Fig. 2 Dose Recovery The acquisition of D_e values is necessarily predicated upon thermal treatment of aliquots succeeding environmental and laboratory irradiation. The Dose Recovery test quantifies the combined effects of thermal transfer and sensitisation on the natural signal using a precise lab dose to simulate natural dose. Based on this an appropriate thermal treatment is selected to generate the final D_e value.

Fig. 3 Inter-aliquot D_e distribution Abanico plot of inter-aliquot statistical concordance in D_e values derived from natural irradiation. Discordant data (those points lying beyond ± 2 standardised ln D_e) reflect heterogeneous dose absorption and/or inaccuracies in calibration.

Fig. 4 Signal Analysis Statistically significant increase in natural D_e value with signal stimulation period is indicative of a partially-bleached signal, provided a significant increase in D_e results from simulated partial bleaching followed by insignificant adjustment in D_e for simulated zero and full bleach conditions. Ages from such samples are considered maximum estimates. In the absence of a significant rise in D_e with stimulation time, simulated partial bleaching and zero/full bleach tests are not assessed.

Fig. 5 U Activity Statistical concordance (equilibrium) in the activities of the daughter radioisotope ^{226}Ra with its parent ^{238}U may signify the temporal stability of D_e emissions from these chains. Significant differences (disequilibrium; $>50\%$) in activity indicate addition or removal of isotopes creating a time-dependent shift in D_e values and increased uncertainty in the accuracy of age estimates. A 20% disequilibrium marker is also shown.

Fig. 6 Age Range The Cumulative frequency plot indicates the inter-aliquot variability in age. It also shows the mean age range: an estimate of sediment burial period based on mean D_e and D_e values with associated analytical uncertainties. The maximum influence of temporal variations in D_e forced by minima-maxima variation in moisture content and overburden thickness is outlined and may prove instructive where there is uncertainty in these parameters. However the combined extremes represented should not be construed as preferred age estimates.

Fig. 2 Dose Recovery

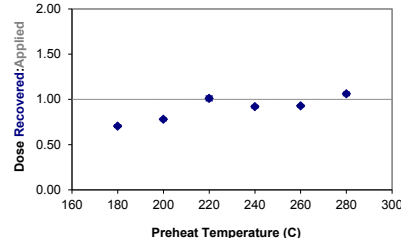
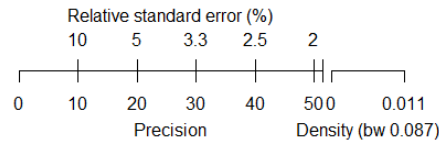
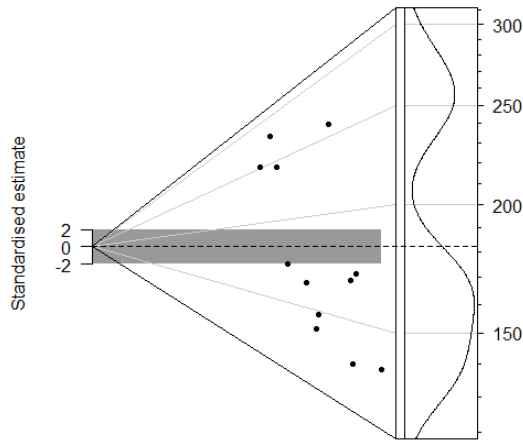


Fig. 3 Inter-aliquot D_e distribution



Sample: GL17154

Fig. 4 Signal Analysis

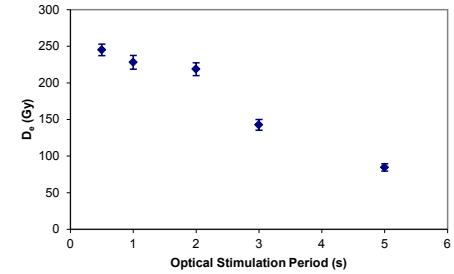


Fig. 5 U Decay Activity

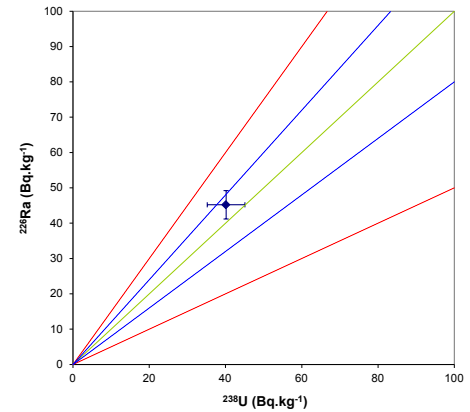
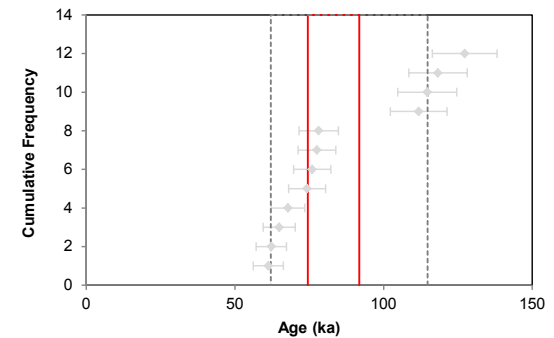


Fig. 6 Age Range



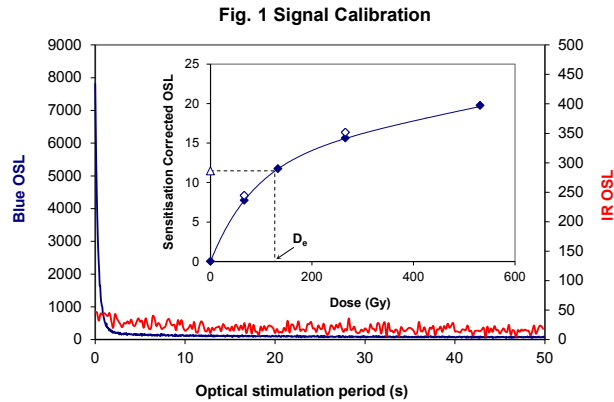


Fig. 1 Signal Calibration

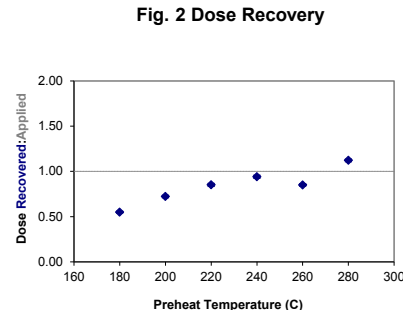


Fig. 2 Dose Recovery

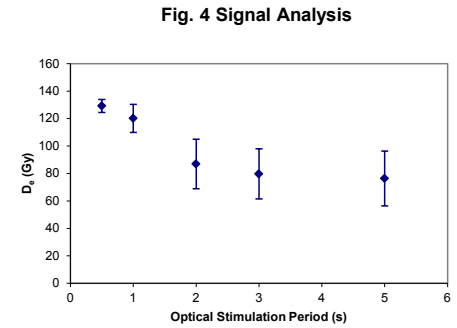


Fig. 4 Signal Analysis

Fig. 3 Inter-aliquot D_e distribution

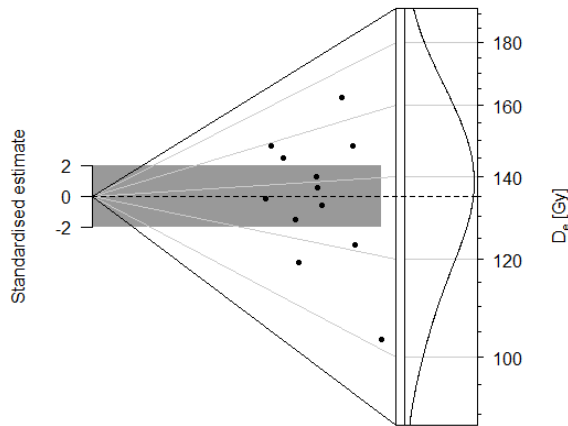


Fig. 1 Signal Calibration Natural blue and laboratory-induced infrared (IR) OSL signals. Detectable IR signal decays are diagnostic of feldspar contamination. Inset, the natural blue OSL signal (open triangle) of each aliquot is calibrated against known laboratory doses to yield equivalent dose (D_e) values. Repeats of low and high doses (open diamonds) illustrate the success of sensitivity correction.

Fig. 2 Dose Recovery The acquisition of D_e values is necessarily predicated upon thermal treatment of aliquots succeeding environmental and laboratory irradiation. The Dose Recovery test quantifies the combined effects of thermal transfer and sensitisation on the natural signal using a precise lab dose to simulate natural dose. Based on this an appropriate thermal treatment is selected to generate the final D_e value.

Fig. 3 Inter-aliquot D_e distribution Abanico plot of inter-aliquot statistical concordance in D_e values derived from natural irradiation. Discordant data (those points lying beyond ± 2 standardised $\ln D_e$) reflect heterogeneous dose absorption and/or inaccuracies in calibration.

Fig. 4 Signal Analysis Statistically significant increase in natural D_e value with signal stimulation period is indicative of a partially-bleached signal, provided a significant increase in D_e results from simulated partial bleaching followed by insignificant adjustment in D_e for simulated zero and full bleach conditions. Ages from such samples are considered maximum estimates. In the absence of a significant rise in D_e with stimulation time, simulated partial bleaching and zero/full bleach tests are not assessed.

Fig. 5 U Activity Statistical concordance (equilibrium) in the activities of the daughter radioisotope ^{226}Ra with its parent ^{238}U may signify the temporal stability of D_e emissions from these chains. Significant differences (disequilibrium; $>50\%$) in activity indicate addition or removal of isotopes creating a time-dependent shift in D_e values and increased uncertainty in the accuracy of age estimates. A 20% disequilibrium marker is also shown.

Fig. 6 Age Range The Cumulative frequency plot indicates the inter-aliquot variability in age. It also shows the mean age range: an estimate of sediment burial period based on mean D_e and D_e values with associated analytical uncertainties. The maximum influence of temporal variations in D_e forced by minima-maxima variation in moisture content and overburden thickness is outlined and may prove instructive where there is uncertainty in these parameters. However the combined extremes represented should not be construed as preferred age estimates.

Fig. 5 U Decay Activity

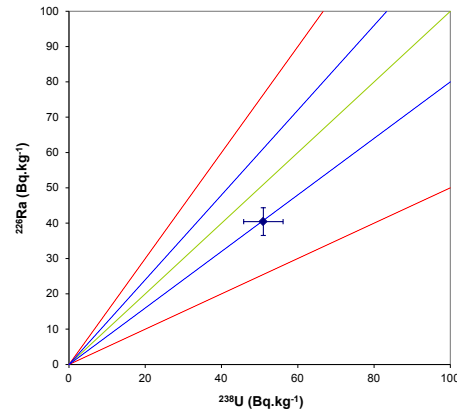
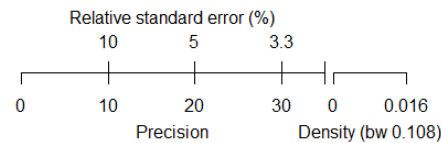
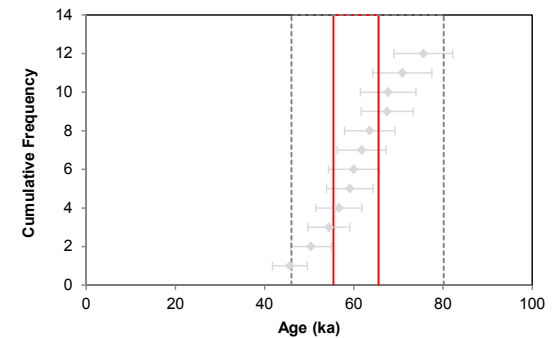


Fig. 6 Age Range



Sample: GL17155



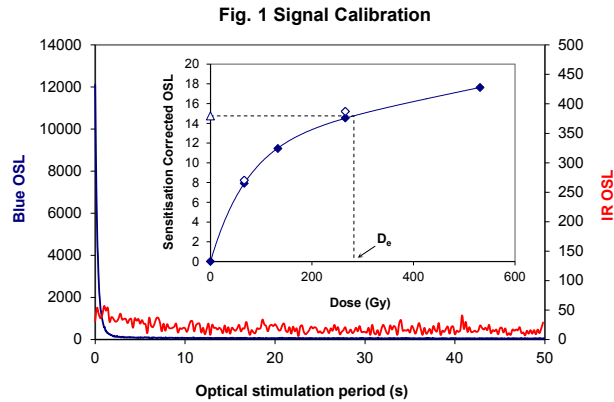


Fig. 1 Signal Calibration

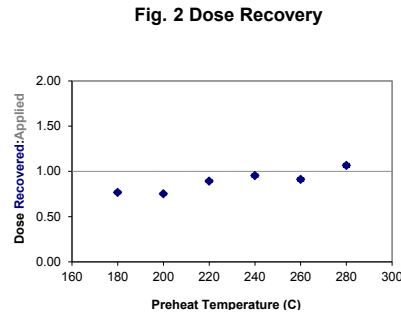


Fig. 2 Dose Recovery

Fig. 3 Inter-aliquot D0 distribution

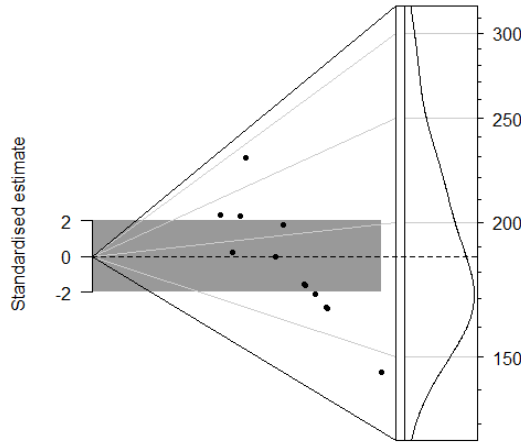


Fig. 1 Signal Calibration Natural blue and laboratory-induced infrared (IR) OSL signals. Detectable IR signal decays are diagnostic of feldspar contamination. Inset, the natural blue OSL signal (open triangle) of each aliquot is calibrated against known laboratory doses to yield equivalent dose (D_0) values. Repeats of low and high doses (open diamonds) illustrate the success of sensitivity correction.

Fig. 2 Dose Recovery The acquisition of D_0 values is necessarily predicated upon thermal treatment of aliquots succeeding environmental and laboratory irradiation. The Dose Recovery test quantifies the combined effects of thermal transfer and sensitisation on the natural signal using a precise lab dose to simulate natural dose. Based on this an appropriate thermal treatment is selected to generate the final D_0 value.

Fig. 3 Inter-aliquot D_0 distribution Abanico plot of inter-aliquot statistical concordance in D_0 values derived from natural irradiation. Discordant data (those points lying beyond ± 2 standardised $\ln D_0$) reflect heterogeneous dose absorption and/or inaccuracies in calibration.

Fig. 4 Signal Analysis Statistically significant increase in natural D_0 value with signal stimulation period is indicative of a partially-bleached signal, provided a significant increase in D_0 results from simulated partial bleaching followed by insignificant adjustment in D_0 for simulated zero and full bleach conditions. Ages from such samples are considered maximum estimates. In the absence of a significant rise in D_0 with stimulation time, simulated partial bleaching and zero/full bleach tests are not assessed.

Fig. 5 U Activity Statistical concordance (equilibrium) in the activities of the daughter radioisotope ^{226}Ra with its parent ^{238}U may signify the temporal stability of D_0 emissions from these chains. Significant differences (disequilibrium; $>50\%$) in activity indicate addition or removal of isotopes creating a time-dependent shift in D_0 values and increased uncertainty in the accuracy of age estimates. A 20% disequilibrium marker is also shown.

Fig. 6 Age Range The Cumulative frequency plot indicates the inter-aliquot variability in age. It also shows the mean age range: an estimate of sediment burial period based on mean D_0 and D_0 values with associated analytical uncertainties. The maximum influence of temporal variations in D_0 forced by minima-maxima variation in moisture content and overburden thickness is outlined and may prove instructive where there is uncertainty in these parameters. However the combined extremes represented should not be construed as preferred age estimates.

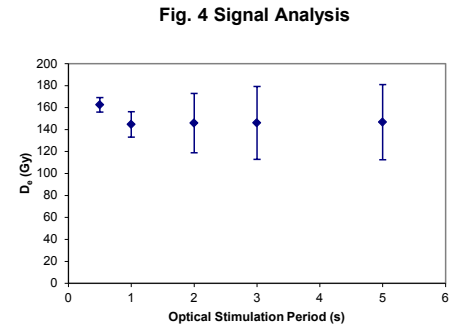


Fig. 4 Signal Analysis

Fig. 5 U Decay Activity

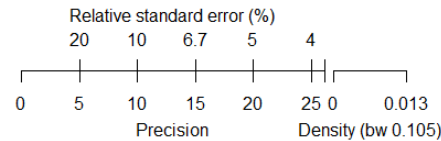
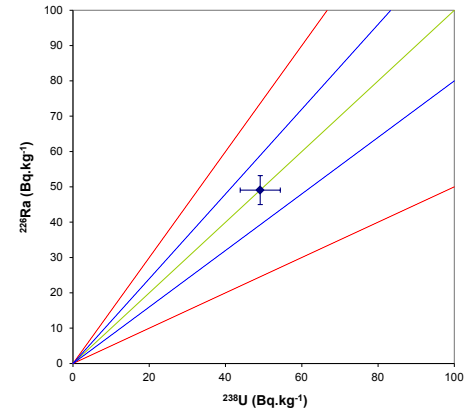
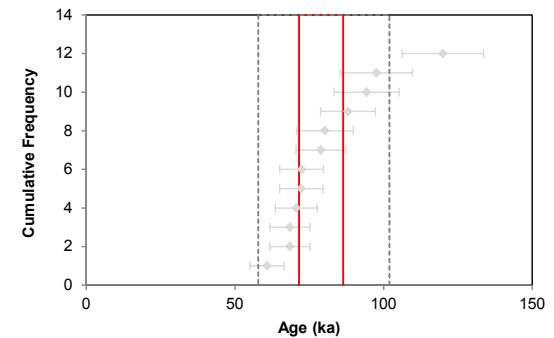


Fig. 6 Age Range



Sample: GL17156

References

- Adamiec, G. and Aitken, M.J. (1998) Dose-rate conversion factors: new data. *Ancient TL*, 16, 37-50.
- Agersnap-Larsen, N., Bulur, E., Bøtter-Jensen, L. and McKeever, S.W.S. (2000) Use of the LM-OSL technique for the detection of partial bleaching in quartz. *Radiation Measurements*, 32, 419-425.
- Aitken, M. J. (1998) An introduction to optical dating: the dating of Quaternary sediments by the use of photon-stimulated luminescence. Oxford University Press.
- Bailey, R.M., Singarayer, J.S. , Ward, S. and Stokes, S. (2003) Identification of partial resetting using D_e as a function of illumination time. *Radiation Measurements*, 37, 511-518.
- Bateman, M.D., Frederick, C.D., Jaiswal, M.K., Singhvi, A.K. (2003) Investigations into the potential effects of pedoturbation on luminescence dating. *Quaternary Science Reviews*, 22, 1169-1176.
- Bateman, M.D., Boulter, C.H., Carr, A.S., Frederick, C.D., Peter, D. and Wilder, M. (2007) Detecting post-depositional sediment disturbance in sandy deposits using optical luminescence. *Quaternary Geochronology*, 2, 57-64.
- Berger, G.W. (2003). Luminescence chronology of late Pleistocene loess-paleosol and tephra sequences near Fairbanks, Alaska. *Quaternary Research*, 60, 70-83.
- Bøtter-Jensen, L., Mejdahl, V. and Murray, A.S. (1999) New light on OSL. *Quaternary Science Reviews*, 18, 303-310.
- Bøtter-Jensen, L., McKeever, S.W.S. and Wintle, A.G. (2003) *Optically Stimulated Luminescence Dosimetry*. Elsevier, Amsterdam.
- Dietze, M., Kreutzer, S., Burow, C., Fuchs, M.C., Fischer, M., Schmidt, C. (2016) The abanico plot: visualising chronometric data with individual standard errors. *Quaternary Geochronology*, 31, 1-7.
- Duller, G.A.T (2003) Distinguishing quartz and feldspar in single grain luminescence measurements. *Radiation Measurements*, 37, 161-165.
- Galbraith, R. F., Roberts, R. G., Laslett, G. M., Yoshida, H. and Olley, J. M. (1999) Optical dating of single and multiple grains of quartz from Jinmium rock shelter (northern Australia): Part I, Experimental design and statistical models. *Archaeometry*, 41, 339-364.
- Glignani, L.A., May, J.-H. and Cohen, T.J. (2015). All mixed up: using single-grain equivalent dose distributions to identify phases of pedogenic mixing on a dryland alluvial fan. *Quaternary International*, 362, 23-33.
- Glignani, L.A., Cohen, T.J., Slack, M. and Feathers, J.K. (2016) Sediment mixing in Aeolian sandsheets identified and quantified using single-grain optically stimulated luminescence. *Quaternary Geochronology*, 32, 53-66.
- Huntley, D.J., Godfrey-Smith, D.I. and Thewalt, M.L.W. (1985) Optical dating of sediments. *Nature*, 313, 105-107.
- Hubbell, J.H. (1982) Photon mass attenuation and energy-absorption coefficients from 1keV to 20MeV. *International Journal of Applied Radioisotopes*, 33, 1269-1290.

- Hütt, G., Jaek, I. and Tchonka, J. (1988) Optical dating: K-feldspars optical response stimulation spectra. *Quaternary Science Reviews*, 7, 381-386.
- Jacobs, A., Wintle, A.G., Duller, G.A.T, Roberts, R.G. and Wadley, L. (2008) New ages for the post-Howiesons Poort, late and finale middle stone age at Sibdu, South Africa. *Journal of Archaeological Science*, 35, 1790-1807.
- Lombard, M., Wadley, L., Jacobs, Z., Mohapi, M. and Roberts, R.G. (2011) Still Bay and serrated points from the Umhlatuzana rock shelter, Kwazulu-Natal, South Africa. *Journal of Archaeological Science*, 37, 1773-1784.
- Markey, B.G., Bøtter-Jensen, L., and Duller, G.A.T. (1997) A new flexible system for measuring thermally and optically stimulated luminescence. *Radiation Measurements*, 27, 83-89.
- Mejdahl, V. (1979) Thermoluminescence dating: beta-dose attenuation in quartz grains. *Archaeometry*, 21, 61-72.
- Murray, A.S. and Olley, J.M. (2002) Precision and accuracy in the Optically Stimulated Luminescence dating of sedimentary quartz: a status review. *Geochronometria*, 21, 1-16.
- Murray, A.S. and Wintle, A.G. (2000) Luminescence dating of quartz using an improved single-aliquot regenerative-dose protocol. *Radiation Measurements*, 32, 57-73.
- Murray, A.S. and Wintle, A.G. (2003) The single aliquot regenerative dose protocol: potential for improvements in reliability. *Radiation Measurements*, 37, 377-381.
- Murray, A.S., Olley, J.M. and Caitcheon, G.G. (1995) Measurement of equivalent doses in quartz from contemporary water-lain sediments using optically stimulated luminescence. *Quaternary Science Reviews*, 14, 365-371.
- Olley, J.M., Murray, A.S. and Roberts, R.G. (1996) The effects of disequilibria in the Uranium and Thorium decay chains on burial dose rates in fluvial sediments. *Quaternary Science Reviews*, 15, 751-760.
- Olley, J.M., Caitcheon, G.G. and Murray, A.S. (1998) The distribution of apparent dose as determined by optically stimulated luminescence in small aliquots of fluvial quartz: implications for dating young sediments. *Quaternary Science Reviews*, 17, 1033-1040.
- Olley, J.M., Caitcheon, G.G. and Roberts R.G. (1999) The origin of dose distributions in fluvial sediments, and the prospect of dating single grains from fluvial deposits using -optically stimulated luminescence. *Radiation Measurements*, 30, 207-217.
- Olley, J.M., Pietsch, T. and Roberts, R.G. (2004) Optical dating of Holocene sediments from a variety of geomorphic settings using single grains of quartz. *Geomorphology*, 60, 337-358.
- Pawley, S.M., Toms, P.S., Armitage, S.J., Rose, J. (2010) Quartz luminescence dating of Anglian Stage fluvial sediments: Comparison of SAR age estimates to the terrace chronology of the Middle Thames valley, UK. *Quaternary Geochronology*, 5, 569-582.
- Prescott, J.R. and Hutton, J.T. (1994) Cosmic ray contributions to dose rates for luminescence and ESR dating: large depths and long-term time variations. *Radiation Measurements*, 23, 497-500.

Singhvi, A.K., Bluszcz, A., Bateman, M.D., Someshwar Rao, M. (2001). Luminescence dating of loess-palaeosol sequences and coversands: methodological aspects and palaeoclimatic implications. *Earth Science Reviews*, 54, 193-211.

Smith, B.W., Rhodes, E.J., Stokes, S., Spooner, N.A. (1990) The optical dating of sediments using quartz. *Radiation Protection Dosimetry*, 34, 75-78.

Spooner, N.A. (1993) The validity of optical dating based on feldspar. Unpublished D.Phil. thesis, Oxford University.

Templer, R.H. (1985) The removal of anomalous fading in zircons. *Nuclear Tracks and Radiation Measurements*, 10, 531-537.

Wallinga, J. (2002) Optically stimulated luminescence dating of fluvial deposits: a review. *Boreas* 31, 303-322.

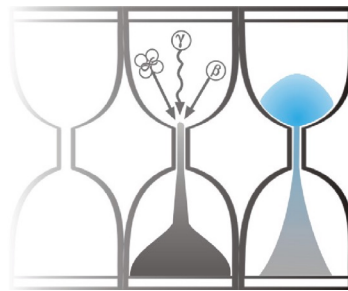
Wintle, A.G. (1973) Anomalous fading of thermoluminescence in mineral samples. *Nature*, 245, 143-144.

Zimmerman, D. W. (1971) Thermoluminescent dating using fine grains from pottery. *Archaeometry*, 13, 29-52.



University of Gloucestershire

Luminescence dating laboratory



**Paired Quartz & K-Feldspar Optical dating of sediments:
Boreas Offshore Windfarm**

to

**Dr C. Mellett
Wessex Archaeology**

**Analysis & Reporting, Prof. P.S. Toms
Sample Preparation & Measurement, Mr J.C. Wood
29 January 2019**

Contents

Section		Page
	Table 1 D_r , D_e and Age data of submitted samples	3
	Table 2 Analytical validity of sample suite ages	4
1.0	Mechanisms and Principles	5
2.0	Sample Preparation	5
3.0	Acquisition and accuracy of D_e value	6
	3.1 Laboratory Factors	6
	3.1.1 Feldspar Contamination of Quartz	6
	3.1.2 Preheating	6
	3.1.3 Internal Consistency	7
	3.2 Environmental Factors	7
	3.2.1 Incomplete Zeroing	7
	3.2.2 Turbation	8
4.0	Acquisition and accuracy of D_r value	8
5.0	Estimation of age	9
6.0	Analytical Uncertainty	9
	Sample diagnostics, luminescence and age data	12
	References	16

Scope of Report

This is a standard report of the Luminescence dating laboratory, University of Gloucestershire. In large part, the document summarises the processes, diagnostics and data drawn upon to deliver Table 1. A conclusion on the analytical validity of each sample's optical age estimate is expressed in Table 2; where there are caveats, the reader is directed to the relevant section of the report that explains the issue further in general terms.

Copyright Notice

Permission must be sought from Prof. P.S. Toms of the University of Gloucestershire Luminescence dating laboratory in using the content of this report, in part or whole, for the purpose of publication.

Field Code	Lab Code	Overburden (m)	Grain size (μm)	Moisture content (%)	Nal γ -spectrometry (<i>in situ</i>) γ D, (Gy.ka ⁻¹)	Ge γ -spectrometry (<i>ex situ</i>)			Internal β D, (Gy.ka ⁻¹)	External β D, (Gy.ka ⁻¹)	External γ D, (Gy.ka ⁻¹)	Cosmic D, (Gy.ka ⁻¹)	Preheat (°C for 10s)	Low Dose Repeat Ratio	High Dose Repeat Ratio	Post-IR OSL Ratio
						K (%)	Th (ppm)	U (ppm)								
						NBOWF_VC016: 2.65-3.00 m	GL17153 Quartz GL17153 K-Feldspar	2.83								
NBOWF_VC016: 1.70-2.00 m	GL17154 Quartz GL17154 K-Feldspar	1.85	125-180	15 ± 4	-	1.50 ± 0.10	7.81 ± 0.53	1.93 ± 0.14	- 0.57 ± 0.11	1.25 ± 0.14	0.79 ± 0.10	0.15 ± 0.01	220 -	1.04 ± 0.01 0.98 ± 0.02	1.01 ± 0.01 0.95 ± 0.01	1.01 ± 0.01 -

Field Code	Lab Code	Total D, (Gy.ka ⁻¹)	D _e (Gy)	Age (ka)
NBOWF_VC016: 2.65-3.00 m	GL17153 Quartz	2.14 ± 0.17	149.6 ± 11.1	69.8 ± 7.7 (6.9)
	GL17153 K-Feldspar	2.71 ± 0.21	247.7 ± 11.1	91.5 ± 8.1 (7.0)
NBOWF_VC016: 1.70-2.00 m	GL17154 Quartz	2.19 ± 0.17	182.1 ± 15.0	83.2 ± 9.5 (8.7)
	GL17154 K-Feldspar	2.75 ± 0.20	207.8 ± 16.7	75.4 ± 8.2 (7.6)

Table 1 D_r, D_e and Age data of submitted samples located at c. 53°N, 3°E, 0m. Age estimates expressed relative to year of sampling. Uncertainties in age are quoted at 1 σ confidence, are based on analytical errors and reflect combined systematic and experimental variability and (in parenthesis) experimental variability alone (see 6.0). **Blue** indicates samples with accepted age estimates, **red**, age estimates with caveats (see Table 2).

Generic considerations	Field Code	Lab Code	Sample specific considerations
Absence of <i>in situ</i> γ spectrometry data (see section 4.0)	NBOWF_VC016: 2.65-3.00 m	GL17153 Quartz	None
		GL17153 K-Feldspar	Failed Dose Recovery Test (see section 3.2.1 and Fig. 3) Accept as maximum age estimate
	NBOWF_VC016: 1.70-2.00 m	GL17154 Quartz	None
		GL17154 K-Feldspar	Failed Dose Recovery Test (see section 3.2.1 and Fig. 3) Accept as maximum age estimate

Table 2 Analytical validity of sample suite age estimates and caveats for consideration

1.0 Mechanisms and principles

Upon exposure to ionising radiation, electrons within the crystal lattice of insulating minerals are displaced from their atomic orbits. Whilst this dislocation is momentary for most electrons, a portion of charge is redistributed to meta-stable sites (traps) within the crystal lattice. In the absence of significant optical and thermal stimuli, this charge can be stored for extensive periods. The quantity of charge relocation and storage relates to the magnitude and period of irradiation. When the lattice is optically or thermally stimulated, charge is evicted from traps and may return to a vacant orbit position (hole). Upon recombination with a hole, an electron's energy can be dissipated in the form of light generating crystal luminescence providing a measure of dose absorption.

In this report, both quartz and K-feldspar were segregated for dating. The utility of quartz as a minerogenic dosimeter lies in the stability of its datable signal over the mid to late Quaternary period, predicted through isothermal decay studies (e.g. Smith *et al.*, 1990; retention lifetime 630 Ma at 20°C) and evidenced by optical age estimates concordant with independent chronological controls (e.g. Murray and Olley, 2002). This stability is in contrast to the anomalous fading of comparable signals commonly observed for other ubiquitous sedimentary minerals such as feldspar and zircon (Wintle, 1973; Templer, 1985; Spooner, 1993). However, recent studies of K-feldspar have identified a non-fading signal (Thomsen *et al.*, 2008). And with the ability of feldspar to accumulate signal over periods longer than that of quartz, paired quartz and K-feldspar dating is a pragmatic approach for samples that may date earlier than the Late Pleistocene.

Optical age estimates of sedimentation (Huntley *et al.*, 1985) are premised upon reduction of the minerogenic time dependent signal (Optically Stimulated Luminescence, OSL) to zero through exposure to sunlight and, once buried, signal reformulation by absorption of litho- and cosmogenic radiation. The signal accumulated post burial acts as a dosimeter recording total dose absorption, converting to a chronometer by estimating the rate of dose absorption quantified through the assay of radioactivity in the surrounding lithology and streaming from the cosmos.

$$\text{Age} = \frac{\text{Mean Equivalent Dose (D}_e\text{, Gy)}}{\text{Mean Dose Rate (D}_r\text{, Gy.ka}^{-1}\text{)}}$$

Aitken (1998) and Bøtter-Jensen *et al.* (2003) offer a detailed review of optical dating.

2.0 Sample Preparation

Two sediment cores were collected within opaque tubing and submitted for Optical dating. To preclude optical erosion of the datable signal prior to measurement, the samples were opened and prepared under controlled laboratory illumination provided by Encapsulite RB-10 (red) filters. To isolate that material potentially exposed to daylight during sampling, sediment located within 10 mm of each core face was removed.

The remaining sample was dried and then sieved. The fine sand fraction was segregated and subjected to acid and alkaline digestion (10% HCl, 15% H₂O₂) to attain removal of carbonate and organic components respectively. The sample was then divided in two. For one half, a further acid digestion in HF (40%, 60 mins) was used to etch the outer 10-15 µm layer affected by α radiation and degrade each samples' feldspar content. During HF treatment, continuous magnetic stirring was used to effect isotropic etching of grains. 10% HCl was then added to remove acid soluble fluorides. Each sample was dried, resieved and quartz isolated from the remaining heavy mineral fraction using a sodium polytungstate density separation at 2.68g.cm⁻³. For the second half, density separations at 2.53 and 2.58 g cm⁻³ were undertaken to isolate the K-feldspar fraction. Twelve 8 mm multi-grain aliquots (c. 3-6 mg) of quartz and K-feldspar were then mounted on aluminium discs for determination of D_e values.

All drying was conducted at 40°C to prevent thermal erosion of the signal. All acids and alkalis were Analar grade. All dilutions (removing toxic-corrosive and non-minerogenic luminescence-bearing substances) were conducted with distilled water to prevent signal contamination by extraneous particles.

3.0 Acquisition and accuracy of D_e value

All minerals naturally exhibit marked inter-sample variability in luminescence per unit dose (sensitivity). Therefore, the estimation of D_e acquired since burial requires calibration of the natural signal using known amounts of laboratory dose. D_e values were quantified using a single-aliquot regenerative-dose (SAR) protocol (Murray and Wintle 2000, 2003 for quartz; Li et al., 2014 for K-feldspar) facilitated by a Risø TL-DA-15 irradiation-stimulation-detection system (Markey *et al.*, 1997; Bøtter-Jensen *et al.*, 1999). Within this apparatus, optical signal stimulation of quartz is provided by an assembly of blue diodes (5 packs of 6 Nichia NSPB500S), filtered to 470 ± 80 nm conveying $15 \text{ mW}\cdot\text{cm}^{-2}$ using a 3 mm Schott GG420 positioned in front of each diode pack. Infrared (IR) stimulation for K-feldspars is provided by 6 IR diodes (Telefunken TSHA 6203) stimulating at 875 ± 80 nm delivering $\sim 5 \text{ mW}\cdot\text{cm}^{-2}$. Stimulated photon emissions from quartz aliquots are in the ultraviolet (UV) range and were filtered from stimulating photons by 7.5 mm HOYA U-340 glass and detected by an EMI 9235QA photomultiplier fitted with a blue-green sensitive alkali photocathode. K-feldspar emissions were filtered by 2 mm Schott BG-39 and 3mm Schott BG-3 glass. Aliquot irradiation was conducted using a 1.48 GBq $^{90}\text{Sr}/^{90}\text{Y}$ β source calibrated for multi-grain aliquots of 125-180 μm quartz and feldspar against the 'Hotspot 800' ^{60}Co γ source located at the National Physical Laboratory (NPL), UK.

SAR by definition evaluates D_e through measuring the natural signal (Fig. 1) of a single aliquot and then regenerating that aliquot's signal by using known laboratory doses to enable calibration. For each aliquot, five different regenerative-doses were administered so as to image dose response. D_e values for each aliquot were then interpolated, and associated counting and fitting errors calculated, by way of exponential plus linear regression (Fig. 1). Weighted (geometric) mean D_e values were calculated from 12 aliquots using the central age model outlined by Galbraith *et al.* (1999) and are quoted at 1σ confidence (Table 1). The accuracy with which D_e equates to total absorbed dose and that dose absorbed since burial was assessed. The former can be considered a function of laboratory factors, the latter, one of environmental issues. Diagnostics were deployed to estimate the influence of these factors and criteria instituted to optimise the accuracy of D_e values.

3.1 Laboratory Factors

3.1.1 Feldspar contamination of quartz

The propensity of feldspar signals to fade and underestimate age, coupled with their higher sensitivity relative to quartz makes it imperative to quantify feldspar contamination. At room temperature, feldspars generate a signal (IRSL; Fig. 1) upon exposure to IR whereas quartz does not. The signal from feldspars contributing to OSL can be depleted by prior exposure to IR. For all aliquots the contribution of any remaining feldspars was estimated from the OSL IR depletion ratio (Duller, 2003). The influence of IR depletion on the OSL signal can be illustrated by comparing the regenerated post-IR OSL D_e with the applied regenerative-dose. If the addition to OSL by feldspars is insignificant, then the repeat dose ratio of OSL to post-IR OSL should be statistically consistent with unity (Table 1). If any aliquots do not fulfil this criterion, then the sample age estimate should be accepted tentatively. The source of feldspar contamination is rarely rooted in sample preparation; it predominantly results from the occurrence of feldspars as inclusions within quartz.

3.1.2 Preheating

Preheating aliquots between irradiation and optical stimulation is necessary to ensure comparability between natural and laboratory-induced signals. However, the multiple irradiation and preheating steps that are required to define single-aliquot regenerative-dose response leads to signal sensitisation, rendering calibration of the natural signal inaccurate.

The SAR protocol (Murray and Wintle, 2000; 2003) enables this sensitisation to be monitored and corrected using a test dose to track signal sensitivity between irradiation-preheat steps. In the case of quartz a 5 Gy test dose preheated to 220°C for 10s was used. For K-feldspar a 30 Gy test dose and 300°C preheat for 60s was applied (Li et al. 2014), However, the accuracy of sensitisation correction for both natural and laboratory signals can be preheat dependent.

The Dose Recovery test was used to assess the optimal preheat temperature for accurate correction and calibration of the time dependent signal. Dose Recovery (Fig. 2) attempts to quantify the combined effects of thermal transfer and sensitisation on the natural signal, using a precise lab dose to simulate natural dose. The ratio between the applied dose and recovered D_e value should be statistically concordant with unity. For this diagnostic, in the case of quartz, 6 aliquots were each assigned a 10 s preheat between 180°C and 280°C. For the K-feldspar fraction, the efficacy of the 300°C, 60s preheat in Dose Recovery was assessed from the average of three aliquots.

That preheat treatment fulfilling the criterion of accuracy within the Dose Recovery test was selected to generate the final D_e value from a further 12 aliquots. Further thermal treatments, prescribed by Murray and Wintle (2000; 2003), were applied to optimise accuracy and precision. Optical stimulation of quartz occurred at 125°C in order to minimise effects associated with photo-transferred thermoluminescence and maximise signal to noise ratios (Murray and Wintle, 2000; 2003). For K-feldspar, optical stimulation was performed at 50°C then 200°C to remove the fading signal, with the non-fading signal then measured at 250°C (Li et al., 2014). Inter-cycle optical stimulation was conducted at 280°C for quartz and 320°C for K-feldspar to minimise recuperation.

3.1.3 Internal consistency

Abanico plots (Dietze *et al.*, 2016) are used to illustrate inter-aliquot D_e variability (Fig. 3). D_e values are standardised relative to the central D_e value for natural signals and are described as overdispersed when >5% lie beyond $\pm 2\sigma$ of the standardising value; resulting from a heterogeneous absorption of burial dose and/or response to the SAR protocol. For multi-grain aliquots, overdispersion of natural signals does not necessarily imply inaccuracy. However where overdispersion is observed for regenerated signals, the efficacy of sensitivity correction may be problematic. Murray and Wintle (2000; 2003) suggest repeat dose ratios (Table 1) offer a measure of SAR protocol success, whereby ratios ranging across 0.9-1.1 represent effective sensitivity correction. However, this variation of repeat dose ratios in the high-dose region can have a significant impact on D_e interpolation.

3.2 Environmental factors

3.2.1 Incomplete zeroing

Post-burial OSL signals residual of pre-burial dose absorption can result where pre-burial sunlight exposure is limited in spectrum, intensity and/or period, leading to age overestimation. In the case of quartz, this effect is particularly acute for material eroded and redeposited sub-aqueously (Olley *et al.*, 1998, 1999; Wallinga, 2002) and exposed to a burial dose of <20 Gy (e.g. Olley *et al.*, 2004), has some influence in sub-aerial contexts but is rarely of consequence where aerial transport has occurred. The signal used herein for K-feldspar dating, whilst non-fading, requires extensive sunlight exposure; it is therefore more susceptible to partial bleaching than quartz. Within single-aliquot regenerative-dose optical dating there are two diagnostics of partial resetting (or bleaching); signal analysis (Agersnap-Larsen *et al.*, 2000; Bailey *et al.*, 2003) and inter-aliquot D_e distribution studies (Murray *et al.*, 1995).

Within this study signal analysis, which is only applicable to quartz, was used to quantify the change in D_e value with respect to optical stimulation time for multi-grain aliquots. This exploits the existence of traps within minerogenic dosimeters that bleach with different efficiency for a given wavelength of light to verify partial bleaching. $D_e(t)$ plots (Fig. 4; Bailey *et al.*, 2003) are constructed from separate integrals of signal decay as laboratory optical stimulation progresses. A statistically significant increase in natural $D_e(t)$ is indicative of partial bleaching assuming three conditions

are fulfilled. Firstly, that a statistically significant increase in $D_e(t)$ is observed when partial bleaching is simulated within the laboratory. Secondly, that there is no significant rise in $D_e(t)$ when full bleaching is simulated. Finally, there should be no significant augmentation in $D_e(t)$ when zero dose is simulated. Where partial bleaching is detected, the age derived from the sample should be considered a maximum estimate only. However, the utility of signal analysis is strongly dependent upon a samples pre-burial experience of sunlight's spectrum and its residual to post-burial signal ratio. Given in the majority of cases, the spectral exposure history of a deposit is uncertain, the absence of an increase in natural $D_e(t)$ does not necessarily testify to the absence of partial bleaching.

Where requested and feasible, the insensitivities of multi-grain single-aliquot signal analysis may be circumvented by inter-aliquot D_e distribution studies, which can be attempted on both quartz and K-feldspars. This analysis uses aliquots of single sand grains to quantify inter-grain D_e distribution. At present, it is contended that asymmetric inter-grain D_e distributions are symptomatic of partial bleaching and/or pedoturbation (Murray *et al.*, 1995; Olley *et al.*, 1999; Olley *et al.*, 2004; Bateman *et al.*, 2003). For partial bleaching at least, it is further contended that the D_e acquired during burial is located in the minimum region of such ranges. The mean and breadth of this minimum region is the subject of current debate, as it is additionally influenced by heterogeneity in microdosimetry, variable inter-grain response to SAR, residual to post-burial signal ratios and, in the case of K-feldspar, inter-grain variations in K content.

3.2.2 Turbation

As noted in section 3.1.1, the accuracy of sedimentation ages can further be controlled by post-burial trans-strata grain movements forced by pedo- or cryoturbation. Berger (2003) contends pedogenesis prompts a reduction in the apparent sedimentation age of parent material through bioturbation and illuviation of younger material from above and/or by biological recycling and resetting of the datable signal of surface material. Berger (2003) proposes that the chronological products of this remobilisation are A-horizon age estimates reflecting the cessation of pedogenic activity, Bc/C-horizon ages delimiting the maximum age for the initiation of pedogenesis with estimates obtained from Bt-horizons providing an intermediate age 'close to the age of cessation of soil development'. Singhvi *et al.* (2001), in contrast, suggest that B and C-horizons closely approximate the age of the parent material, the A-horizon, that of the 'soil forming episode'. Recent analyses of inter-aliquot D_e distributions have reinforced this complexity of interpreting burial age from pedoturbated deposits (Lombard *et al.*, 2011; Gliganic *et al.*, 2015; Jacobs *et al.*, 2008; Bateman *et al.*, 2007; Gliganic *et al.*, 2016). At present there is no definitive post-sampling mechanism for the direct detection of and correction for post-burial sediment remobilisation. However, intervals of palaeosol evolution can be delimited by a maximum age derived from parent material and a minimum age obtained from a unit overlying the palaeosol. Inaccuracy forced by cryoturbation may be bidirectional, heaving older material upwards or drawing younger material downwards into the level to be dated. Cryogenic deformation of matrix-supported material is, typically, visible; sampling of such cryogenically-disturbed sediments can be avoided.

4.0 Acquisition and accuracy of D_r value

For lithogenic radiation external to the grains of quartz and K-feldspar, D_r values were defined through measurement of U, Th and K radionuclide concentration and conversion of these quantities into β and γ D_r values (Table 1). β contributions were estimated from sub-samples by laboratory-based γ spectrometry using an Ortec GEM-S high purity Ge coaxial detector system, calibrated using certified reference materials supplied by CANMET. γ dose rates can be estimated from *in situ* NaI gamma spectrometry or, where direct measurements are unavailable as in the present case, from laboratory-based Ge γ spectrometry. *In situ* measurements reduce uncertainty relating to potential heterogeneity in the γ dose field surrounding each sample. The level of U disequilibrium was estimated by laboratory-based Ge γ spectrometry. Estimates of radionuclide concentration were converted into D_r values (Adamiec and Aitken, 1998), accounting for D_r modulation forced by grain size (Mejdahl, 1979) and present moisture content (Zimmerman, 1971).

Lithogenic radiation internal to K-feldspar grains was assumed to be derived from a K content of 12.5%. Cosmogenic D_r values were calculated on the basis of sample depth, geographical position and matrix density (Prescott and Hutton, 1994).

The spatiotemporal validity of D_r values can be considered a function of five variables. Firstly, age estimates devoid of *in situ* γ spectrometry data should be accepted tentatively if the sampled unit is heterogeneous in texture or if the sample is located within 300 mm of strata consisting of differing texture and/or mineralogy. However, where samples are obtained throughout a vertical profile, consistent values of γ D_r based solely on laboratory measurements may evidence the homogeneity of the γ field and hence accuracy of γ D_r values. Secondly, disequilibrium can force temporal instability in U and Th emissions. The impact of this infrequent phenomenon (Olley *et al.*, 1996) upon age estimates is usually insignificant given their associated margins of error. However, for samples where this effect is pronounced (>50% disequilibrium between ^{238}U and ^{226}Ra ; Fig. 5), the resulting age estimates should be accepted tentatively. Thirdly, pedogenically-induced variations in matrix composition of B and C-horizons, such as radionuclide and/or mineral remobilisation, may alter the rate of energy emission and/or absorption. If D_r is invariant through a dated profile and samples encompass primary parent material, then element mobility is likely limited in effect. Fourthly, spatiotemporal detractors from present moisture content are difficult to assess directly, requiring knowledge of the magnitude and timing of differing contents. However, the maximum influence of moisture content variations can be delimited by recalculating D_r for minimum (zero) and maximum (saturation) content. Finally, temporal alteration in the thickness of overburden alters cosmic D_r values. Cosmic D_r often forms a negligible portion of total D_r . It is possible to quantify the maximum influence of overburden flux by recalculating D_r for minimum (zero) and maximum (surface sample) cosmic D_r .

5.0 Estimation of Age

Ages reported in Table 1 provide an estimate of sediment burial period based on mean D_e and D_r values and their associated analytical uncertainties. Uncertainty in age estimates is reported as a product of systematic and experimental errors, with the magnitude of experimental errors alone shown in parenthesis (Table 1). Cumulative frequency plots indicate the inter-aliquot variability in age (Fig. 6). The maximum influence of temporal variations in D_r forced by minima-maxima in moisture content and overburden thickness is also illustrated in Fig. 6. Where uncertainty in these parameters exists this age range may prove instructive, however the combined extremes represented should not be construed as preferred age estimates. The analytical validity of each sample is presented in Table 2.

6.0 Analytical uncertainty

All errors are based upon analytical uncertainty and quoted at 1σ confidence. Error calculations account for the propagation of systematic and/or experimental (random) errors associated with D_e and D_r values.

For D_e values, systematic errors are confined to laboratory β source calibration. Uncertainty in this respect is that combined from the delivery of the calibrating γ dose (1.2%; NPL, pers. comm.), the conversion of this dose for SiO_2 using the respective mass energy-absorption coefficient (2%; Hubbell, 1982) and experimental error, totalling 3.5%. Mass attenuation and bremsstrahlung losses during γ dose delivery are considered negligible. Experimental errors relate to D_e interpolation using sensitisation corrected dose responses. Natural and regenerated sensitisation corrected dose points (S_i) were quantified by,

$$S_i = (D_i - x.L_i) / (d_i - x.L_i) \quad \text{Eq.1}$$

where D_i = Natural or regenerated OSL, initial 0.2 s
 L_i = Background natural or regenerated OSL, final 5 s
 d_i = Test dose OSL, initial 0.2 s
 x = Scaling factor, 0.08

The error on each signal parameter is based on counting statistics, reflected by the square-root of measured values. The propagation of these errors within Eq. 1 generating σS_i follows the general formula given in Eq. 2. σS_i were then used to define fitting and interpolation errors within exponential plus linear regressions.

For D_r values, systematic errors accommodate uncertainty in radionuclide conversion factors (5%), β attenuation coefficients (5%), matrix density (0.20 g.cm^{-3}), vertical thickness of sampled section (specific to sample collection device), saturation moisture content (3%), moisture content attenuation (2%) and burial moisture content (25% relative, unless direct evidence exists of the magnitude and period of differing content). Experimental errors are associated with radionuclide quantification for each sample by Ge gamma spectrometry.

The propagation of these errors through to age calculation was quantified using the expression,

$$\sigma_y (\delta y / \delta x) = (\sum ((\delta y / \delta x_n) \cdot \sigma_{x_n})^2)^{1/2} \quad \text{Eq. 2}$$

where y is a value equivalent to that function comprising terms x_n and where σ_y and σ_{x_n} are associated uncertainties.

Errors on age estimates are presented as combined systematic and experimental errors and experimental errors alone. The former (combined) error should be considered when comparing luminescence ages herein with independent chronometric controls. The latter assumes systematic errors are common to luminescence age estimates generated by means identical to those detailed herein and enable direct comparison with those estimates.

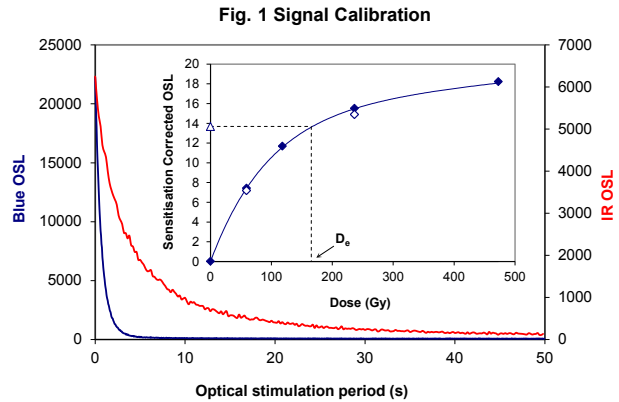


Fig. 1 Signal Calibration

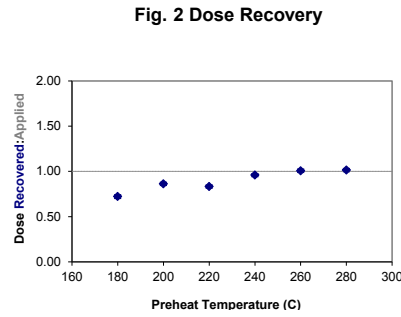


Fig. 2 Dose Recovery

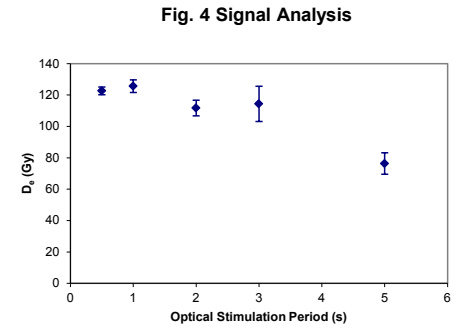


Fig. 4 Signal Analysis

Fig. 3 Inter-aliquot D0 distribution

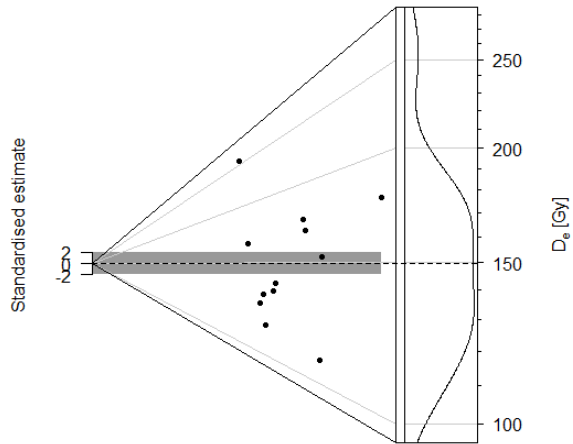


Fig. 1 Signal Calibration Natural blue and laboratory-induced infrared (IR) OSL signals. Detectable IR signal decays are diagnostic of feldspar contamination. Inset, the natural blue OSL signal (open triangle) of each aliquot is calibrated against known laboratory doses to yield equivalent dose (D_0) values. Repeats of low and high doses (open diamonds) illustrate the success of sensitivity correction.

Fig. 2 Dose Recovery The acquisition of D_0 values is necessarily predicated upon thermal treatment of aliquots succeeding environmental and laboratory irradiation. The Dose Recovery test quantifies the combined effects of thermal transfer and sensitisation on the natural signal using a precise lab dose to simulate natural dose. Based on this an appropriate thermal treatment is selected to generate the final D_0 value.

Fig. 3 Inter-aliquot D_0 distribution Abanico plot of inter-aliquot statistical concordance in D_0 values derived from natural irradiation. Discordant data (those points lying beyond ± 2 standardised $\ln D_0$) reflect heterogeneous dose absorption and/or inaccuracies in calibration.

Fig. 4 Signal Analysis Statistically significant increase in natural D_0 value with signal stimulation period is indicative of a partially-bleached signal, provided a significant increase in D_0 results from simulated partial bleaching followed by insignificant adjustment in D_0 for simulated zero and full bleach conditions. Ages from such samples are considered maximum estimates. In the absence of a significant rise in D_0 with stimulation time, simulated partial bleaching and zero/full bleach tests are not assessed.

Fig. 5 U Activity Statistical concordance (equilibrium) in the activities of the daughter radioisotope ^{226}Ra with its parent ^{238}U may signify the temporal stability of D_0 emissions from these chains. Significant differences (disequilibrium; $>50\%$) in activity indicate addition or removal of isotopes creating a time-dependent shift in D_0 values and increased uncertainty in the accuracy of age estimates. A 20% disequilibrium marker is also shown.

Fig. 6 Age Range The Cumulative frequency plot indicates the inter-aliquot variability in age. It also shows the mean age range: an estimate of sediment burial period based on mean D_0 and D_0 values with associated analytical uncertainties. The maximum influence of temporal variations in D_0 forced by minima-maxima variation in moisture content and overburden thickness is outlined and may prove instructive where there is uncertainty in these parameters. However the combined extremes represented should not be construed as preferred age estimates.

Fig. 5 U Decay Activity

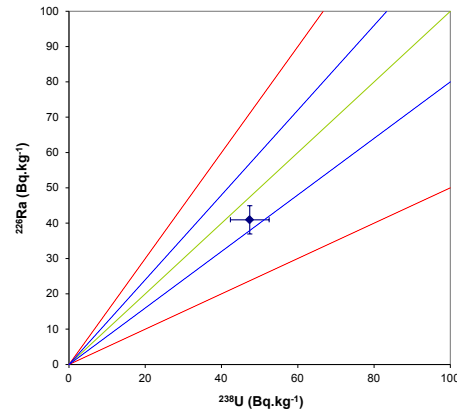
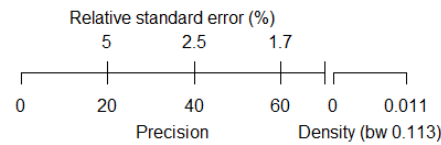
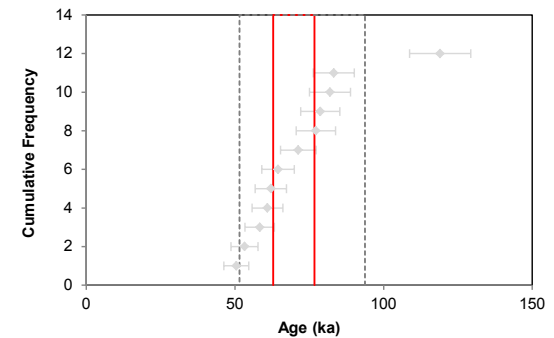


Fig. 6 Age Range



Sample: GL17153 Quartz



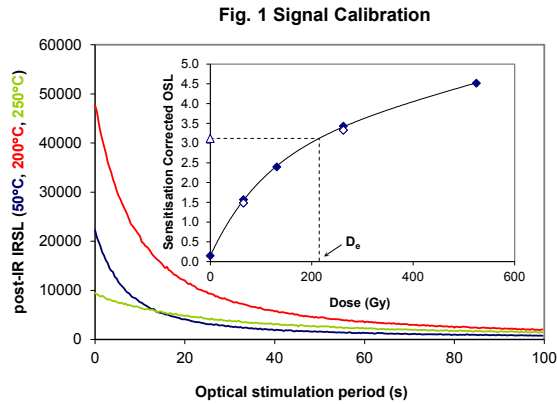


Fig. 1 Signal Calibration

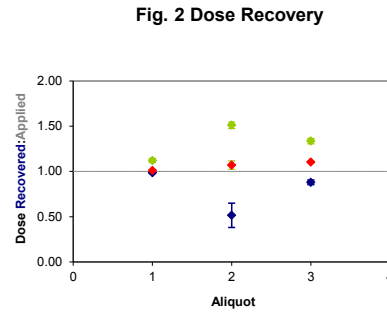


Fig. 2 Dose Recovery

Fig. 3 Inter-aliquot D_e distribution

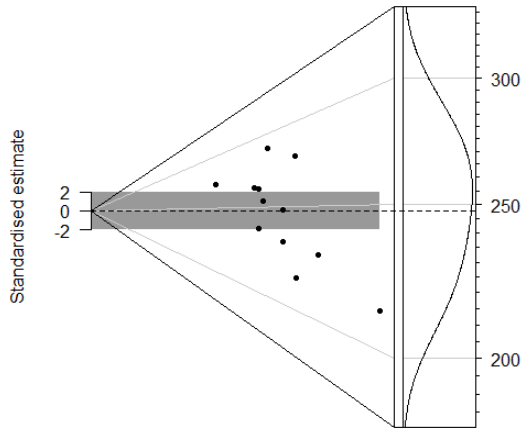


Fig. 1 Signal Calibration Natural post-IR IRSL signal stimulated at 50°C, 200°C and 250°C. The non-fading signal at 250°C is used to estimate the burial dose. Inset, the natural post-IR IRSL signal (open triangle) of each aliquot is calibrated against known laboratory doses to yield equivalent dose (D_e) values. Repeats of low and high doses (open diamonds) illustrate the success of sensitivity correction.

Fig. 2 Dose Recovery The acquisition of D_e values is necessarily predicated upon thermal treatment of aliquots succeeding environmental and laboratory irradiation. The Dose Recovery test quantifies the combined effects of thermal transfer and sensitisation on the natural signal using a precise lab dose to simulate natural dose. Based on this the likely accuracy of D_e produced by a SAR protocol that uses a 300°C, 60s preheat can be assessed. Outcomes for this test are shown for post-IR IRSL signals stimulated at 50°C, 200°C and 250°C.

Fig. 3 Inter-aliquot D_e distribution Abanico plot of inter-aliquot statistical concordance in D_e values derived from natural irradiation. Discordant data (those points lying beyond ± 2 standardised $\ln D_e$) reflect heterogeneous dose absorption and/or inaccuracies in calibration.

Fig. 4 Signal Analysis applies only to OSL dating of quartz.

Fig. 5 U Activity Statistical concordance (equilibrium) in the activities of the daughter radioisotope ^{226}Ra with its parent ^{238}U may signify the temporal stability of D_e emissions from these chains. Significant differences (disequilibrium; $>50\%$) in activity indicate addition or removal of isotopes creating a time-dependent shift in D_e values and increased uncertainty in the accuracy of age estimates. A 20% disequilibrium marker is also shown.

Fig. 6 Age Range The Cumulative frequency plot indicates the inter-aliquot variability in age. It also shows the mean age range: an estimate of sediment burial period based on mean D_e and D_e values with associated analytical uncertainties. The maximum influence of temporal variations in D_e forced by minima-maxima variation in moisture content and overburden thickness is outlined and may prove instructive where there is uncertainty in these parameters. However the combined extremes represented should not be construed as preferred age estimates.

Fig. 4 Signal Analysis

Applies only to OSL dating of quartz

Fig. 5 U Decay Activity

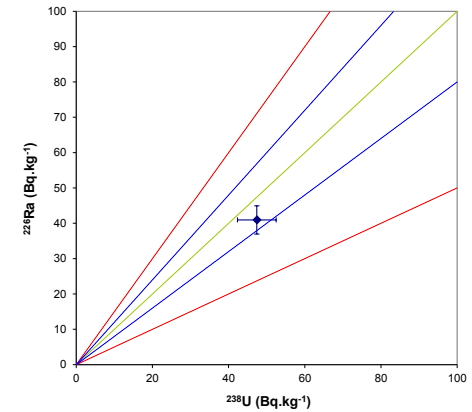
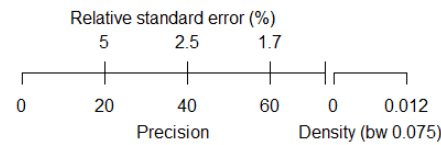
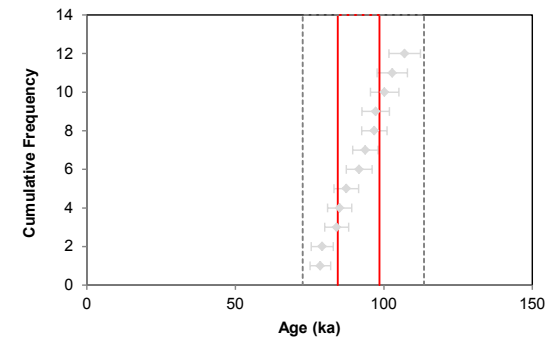


Fig. 6 Age Range



Sample: GL17153 K-feldspar

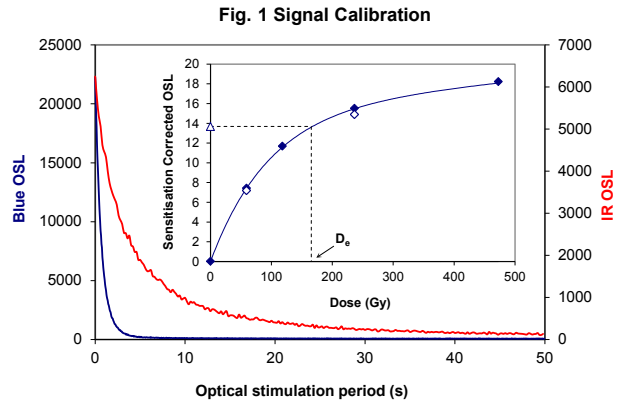


Fig. 1 Signal Calibration Natural blue and laboratory-induced infrared (IR) OSL signals. Detectable IR signal decays are diagnostic of feldspar contamination. Inset, the natural blue OSL signal (open triangle) of each aliquot is calibrated against known laboratory doses to yield equivalent dose (D_e) values. Repeats of low and high doses (open diamonds) illustrate the success of sensitivity correction.

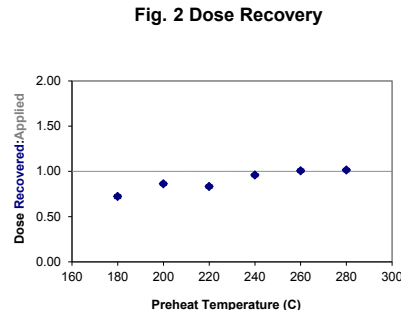


Fig. 2 Dose Recovery

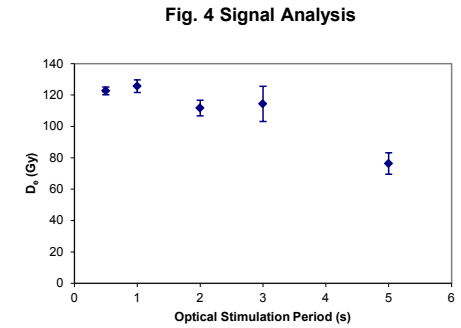


Fig. 4 Signal Analysis

Fig. 2 Dose Recovery The acquisition of D_e values is necessarily predicated upon thermal treatment of aliquots succeeding environmental and laboratory irradiation. The Dose Recovery test quantifies the combined effects of thermal transfer and sensitisation on the natural signal using a precise lab dose to simulate natural dose. Based on this an appropriate thermal treatment is selected to generate the final D_e value.

Fig. 3 Inter-aliquot D_e distribution Abanico plot of inter-aliquot statistical concordance in D_e values derived from natural irradiation. Discordant data (those points lying beyond ± 2 standardised $\ln D_e$) reflect heterogeneous dose absorption and/or inaccuracies in calibration.

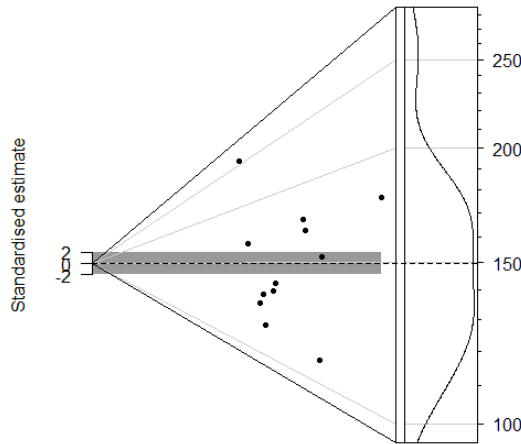


Fig. 4 Signal Analysis Statistically significant increase in natural D_e value with signal stimulation period is indicative of a partially-bleached signal, provided a significant increase in D_e results from simulated partial bleaching followed by insignificant adjustment in D_e for simulated zero and full bleach conditions. Ages from such samples are considered maximum estimates. In the absence of a significant rise in D_e with stimulation time, simulated partial bleaching and zero/full bleach tests are not assessed.

Fig. 5 U Activity Statistical concordance (equilibrium) in the activities of the daughter radioisotope ^{226}Ra with its parent ^{238}U may signify the temporal stability of D_e emissions from these chains. Significant differences (disequilibrium; $>50\%$) in activity indicate addition or removal of isotopes creating a time-dependent shift in D_e values and increased uncertainty in the accuracy of age estimates. A 20% disequilibrium marker is also shown.

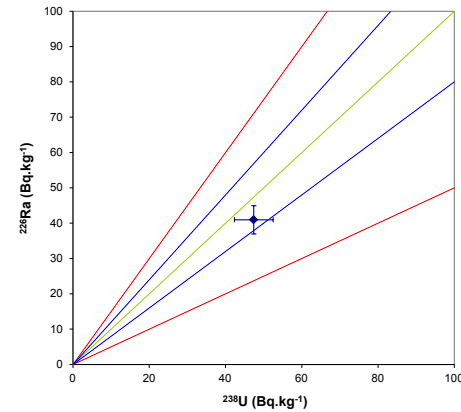
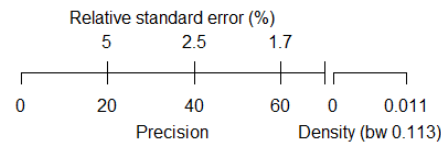


Fig. 5 U Decay Activity

Fig. 6 Age Range The Cumulative frequency plot indicates the inter-aliquot variability in age. It also shows the mean age range: an estimate of sediment burial period based on mean D_e and D_e values with associated analytical uncertainties. The maximum influence of temporal variations in D_e forced by minima-maxima variation in moisture content and overburden thickness is outlined and may prove instructive where there is uncertainty in these parameters. However the combined extremes represented should not be construed as preferred age estimates.



Sample: GL17154 Quartz

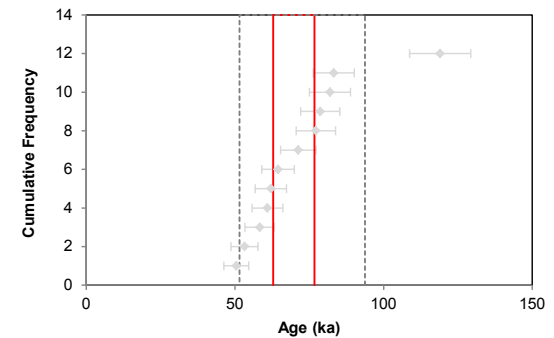


Fig. 1 Signal Calibration

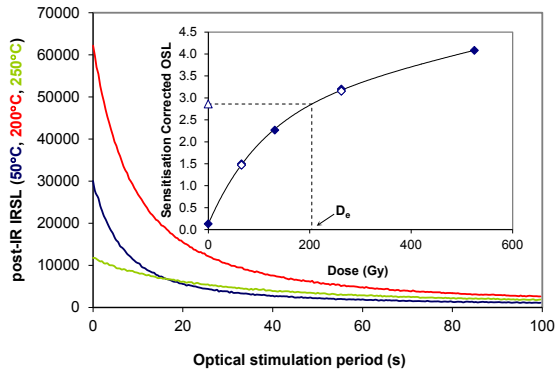


Fig. 1 Signal Calibration Natural post-IR IRSL signal stimulated at 50°C, 200°C and 250°C. The non-fading signal at 250°C is used to estimate the burial dose. Inset, the natural post-IR IRSL signal (open triangle) of each aliquot is calibrated against known laboratory doses to yield equivalent dose (D_0) values. Repeats of low and high doses (open diamonds) illustrate the success of sensitivity correction.

Fig. 2 Dose Recovery The acquisition of D_0 values is necessarily predicated upon thermal treatment of aliquots succeeding environmental and laboratory irradiation. The Dose Recovery test quantifies the combined effects of thermal transfer and sensitisation on the natural signal using a precise lab dose to simulate natural dose. Based on this the likely accuracy of D_0 produced by a SAR protocol that uses a 300°C, 60s preheat can be assessed. Outcomes for this test are shown for post-IR IRSL signals stimulated at 50°C, 200°C and 250°C.

Fig. 3 Inter-aliquot D_0 distribution Abanico plot of inter-aliquot statistical concordance in D_0 values derived from natural irradiation. Discordant data (those points lying beyond ± 2 standardised $\ln D_0$) reflect heterogeneous dose absorption and/or inaccuracies in calibration.

Fig. 4 Signal Analysis applies only to OSL dating of quartz.

Fig. 5 U Activity Statistical concordance (equilibrium) in the activities of the daughter radioisotope ^{226}Ra with its parent ^{238}U may signify the temporal stability of D_0 emissions from these chains. Significant differences (disequilibrium; $>50\%$) in activity indicate addition or removal of isotopes creating a time-dependent shift in D_0 values and increased uncertainty in the accuracy of age estimates. A 20% disequilibrium marker is also shown.

Fig. 6 Age Range The Cumulative frequency plot indicates the inter-aliquot variability in age. It also shows the mean age range; an estimate of sediment burial period based on mean D_0 and D_0 values with associated analytical uncertainties. The maximum influence of temporal variations in D_0 forced by minima-maxima variation in moisture content and overburden thickness is outlined and may prove instructive where there is uncertainty in these parameters. However the combined extremes represented should not be construed as preferred age estimates.

Fig. 2 Dose Recovery

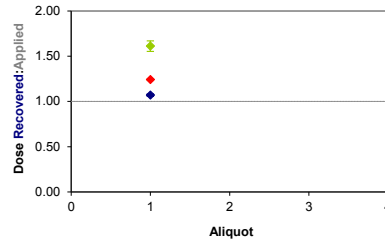


Fig. 3 Inter-aliquot D_0 distribution

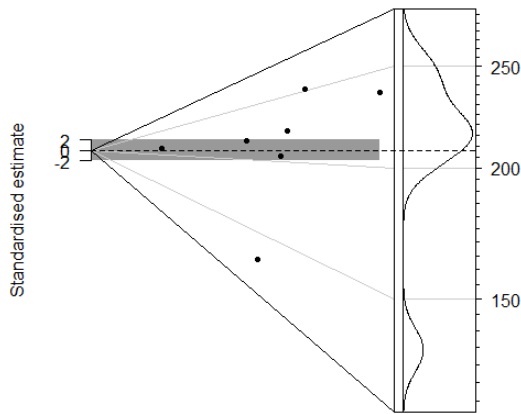


Fig. 4 Signal Analysis

Applies only to OSL dating of quartz

Fig. 5 U Decay Activity

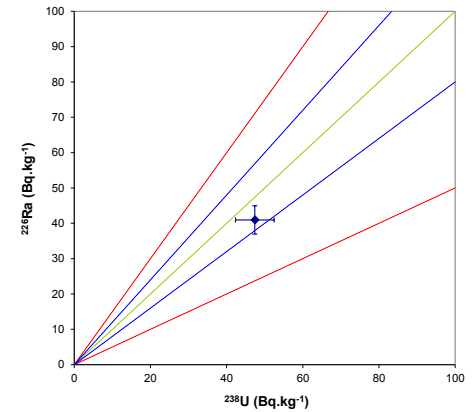
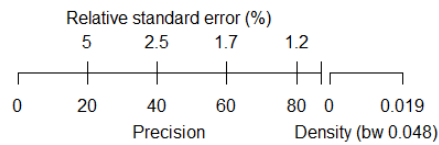
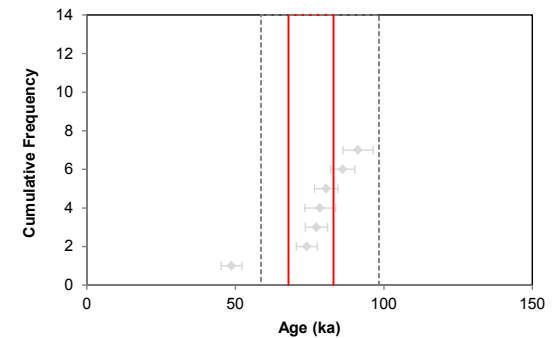


Fig. 6 Age Range



Sample: GL17154 K-feldspar

References

- Adamiec, G. and Aitken, M.J. (1998) Dose-rate conversion factors: new data. *Ancient TL*, 16, 37-50.
- Agersnap-Larsen, N., Bulur, E., Bøtter-Jensen, L. and McKeever, S.W.S. (2000) Use of the LM-OSL technique for the detection of partial bleaching in quartz. *Radiation Measurements*, 32, 419-425.
- Aitken, M. J. (1998) An introduction to optical dating: the dating of Quaternary sediments by the use of photon-stimulated luminescence. Oxford University Press.
- Bailey, R.M., Singarayer, J.S. , Ward, S. and Stokes, S. (2003) Identification of partial resetting using D_e as a function of illumination time. *Radiation Measurements*, 37, 511-518.
- Bateman, M.D., Frederick, C.D., Jaiswal, M.K., Singhvi, A.K. (2003) Investigations into the potential effects of pedoturbation on luminescence dating. *Quaternary Science Reviews*, 22, 1169-1176.
- Bateman, M.D., Boulter, C.H., Carr, A.S., Frederick, C.D., Peter, D. and Wilder, M. (2007) Detecting post-depositional sediment disturbance in sandy deposits using optical luminescence. *Quaternary Geochronology*, 2, 57-64.
- Berger, G.W. (2003). Luminescence chronology of late Pleistocene loess-paleosol and tephra sequences near Fairbanks, Alaska. *Quaternary Research*, 60, 70-83.
- Bøtter-Jensen, L., Mejdahl, V. and Murray, A.S. (1999) New light on OSL. *Quaternary Science Reviews*, 18, 303-310.
- Bøtter-Jensen, L., McKeever, S.W.S. and Wintle, A.G. (2003) *Optically Stimulated Luminescence Dosimetry*. Elsevier, Amsterdam.
- Dietze, M., Kreutzer, S., Burow, C., Fuchs, M.C., Fischer, M., Schmidt, C. (2016) The abanico plot: visualising chronometric data with individual standard errors. *Quaternary Geochronology*, 31, 1-7.
- Duller, G.A.T (2003) Distinguishing quartz and feldspar in single grain luminescence measurements. *Radiation Measurements*, 37, 161-165.
- Galbraith, R. F., Roberts, R. G., Laslett, G. M., Yoshida, H. and Olley, J. M. (1999) Optical dating of single and multiple grains of quartz from Jinmium rock shelter (northern Australia): Part I, Experimental design and statistical models. *Archaeometry*, 41, 339-364.
- Glignic, L.A., May, J.-H. and Cohen, T.J. (2015). All mixed up: using single-grain equivalent dose distributions to identify phases of pedogenic mixing on a dryland alluvial fan. *Quaternary International*, 362, 23-33.
- Glignic, L.A., Cohen, T.J., Slack, M. and Feathers, J.K. (2016) Sediment mixing in Aeolian sandsheets identified and quantified using single-grain optically stimulated luminescence. *Quaternary Geochronology*, 32, 53-66.
- Huntley, D.J., Godfrey-Smith, D.I. and Thewalt, M.L.W. (1985) Optical dating of sediments. *Nature*, 313, 105-107.
- Hubbell, J.H. (1982) Photon mass attenuation and energy-absorption coefficients from 1keV to 20MeV. *International Journal of Applied Radioisotopes*, 33, 1269-1290.

- Jacobs, A., Wintle, A.G., Duller, G.A.T, Roberts, R.G. and Wadley, L. (2008) New ages for the post-Howiesons Poort, late and finale middle stone age at Sibdu, South Africa. *Journal of Archaeological Science*, 35, 1790-1807.
- Li, B., Roberts, R.G., Jacobs, Z. and Li, S-H (2014) A single-aliquot luminescence dating procedure for K-feldspar based on the dose-dependent MET-pIRIR signal sensitivity. *Quaternary Geochronology*, 20, 51-64.
- Lombard, M., Wadley, L., Jacobs, Z., Mohapi, M. and Roberts, R.G. (2011) Still Bay and serrated points from the Umhlatuzana rock shelter, Kwazulu-Natal, South Africa. *Journal of Archaeological Science*, 37, 1773-1784.
- Markey, B.G., Bøtter-Jensen, L., and Duller, G.A.T. (1997) A new flexible system for measuring thermally and optically stimulated luminescence. *Radiation Measurements*, 27, 83-89.
- Mejdahl, V. (1979) Thermoluminescence dating: beta-dose attenuation in quartz grains. *Archaeometry*, 21, 61-72.
- Murray, A.S. and Olley, J.M. (2002) Precision and accuracy in the Optically Stimulated Luminescence dating of sedimentary quartz: a status review. *Geochronometria*, 21, 1-16.
- Murray, A.S. and Wintle, A.G. (2000) Luminescence dating of quartz using an improved single-aliquot regenerative-dose protocol. *Radiation Measurements*, 32, 57-73.
- Murray, A.S. and Wintle, A.G. (2003) The single aliquot regenerative dose protocol: potential for improvements in reliability. *Radiation Measurements*, 37, 377-381.
- Murray, A.S., Olley, J.M. and Caitcheon, G.G. (1995) Measurement of equivalent doses in quartz from contemporary water-lain sediments using optically stimulated luminescence. *Quaternary Science Reviews*, 14, 365-371.
- Olley, J.M., Murray, A.S. and Roberts, R.G. (1996) The effects of disequilibria in the Uranium and Thorium decay chains on burial dose rates in fluvial sediments. *Quaternary Science Reviews*, 15, 751-760.
- Olley, J.M., Caitcheon, G.G. and Murray, A.S. (1998) The distribution of apparent dose as determined by optically stimulated luminescence in small aliquots of fluvial quartz: implications for dating young sediments. *Quaternary Science Reviews*, 17, 1033-1040.
- Olley, J.M., Caitcheon, G.G. and Roberts R.G. (1999) The origin of dose distributions in fluvial sediments, and the prospect of dating single grains from fluvial deposits using -optically stimulated luminescence. *Radiation Measurements*, 30, 207-217.
- Olley, J.M., Pietsch, T. and Roberts, R.G. (2004) Optical dating of Holocene sediments from a variety of geomorphic settings using single grains of quartz. *Geomorphology*, 60, 337-358.
- Pawley, S.M., Toms, P.S., Armitage, S.J., Rose, J. (2010) Quartz luminescence dating of Anglian Stage fluvial sediments: Comparison of SAR age estimates to the terrace chronology of the Middle Thames valley, UK. *Quaternary Geochronology*, 5, 569-582.
- Prescott, J.R. and Hutton, J.T. (1994) Cosmic ray contributions to dose rates for luminescence and ESR dating: large depths and long-term time variations. *Radiation Measurements*, 23, 497-500.

- Singhvi, A.K., Bluszcz, A., Bateman, M.D., Someshwar Rao, M. (2001). Luminescence dating of loess-palaeosol sequences and coversands: methodological aspects and palaeoclimatic implications. *Earth Science Reviews*, 54, 193-211.
- Smith, B.W., Rhodes, E.J., Stokes, S., Spooner, N.A. (1990) The optical dating of sediments using quartz. *Radiation Protection Dosimetry*, 34, 75-78.
- Spooner, N.A. (1993) The validity of optical dating based on feldspar. Unpublished D.Phil. thesis, Oxford University.
- Templer, R.H. (1985) The removal of anomalous fading in zircons. *Nuclear Tracks and Radiation Measurements*, 10, 531-537.
- Thomsen, K.J., Murray, A.S., Jain, M. and Botter-Jensen, L. (2008) Laboratory fading rates of various luminescence signals from feldspar-rich sediment extracts. *Radiation Measurements*, 43, 1474-1486.
- Wallinga, J. (2002) Optically stimulated luminescence dating of fluvial deposits: a review. *Boreas* 31, 303-322.
- Wintle, A.G. (1973) Anomalous fading of thermoluminescence in mineral samples. *Nature*, 245, 143-144.
- Zimmerman, D. W. (1971) Thermoluminescent dating using fine grains from pottery. *Archaeometry*, 13, 29-52.



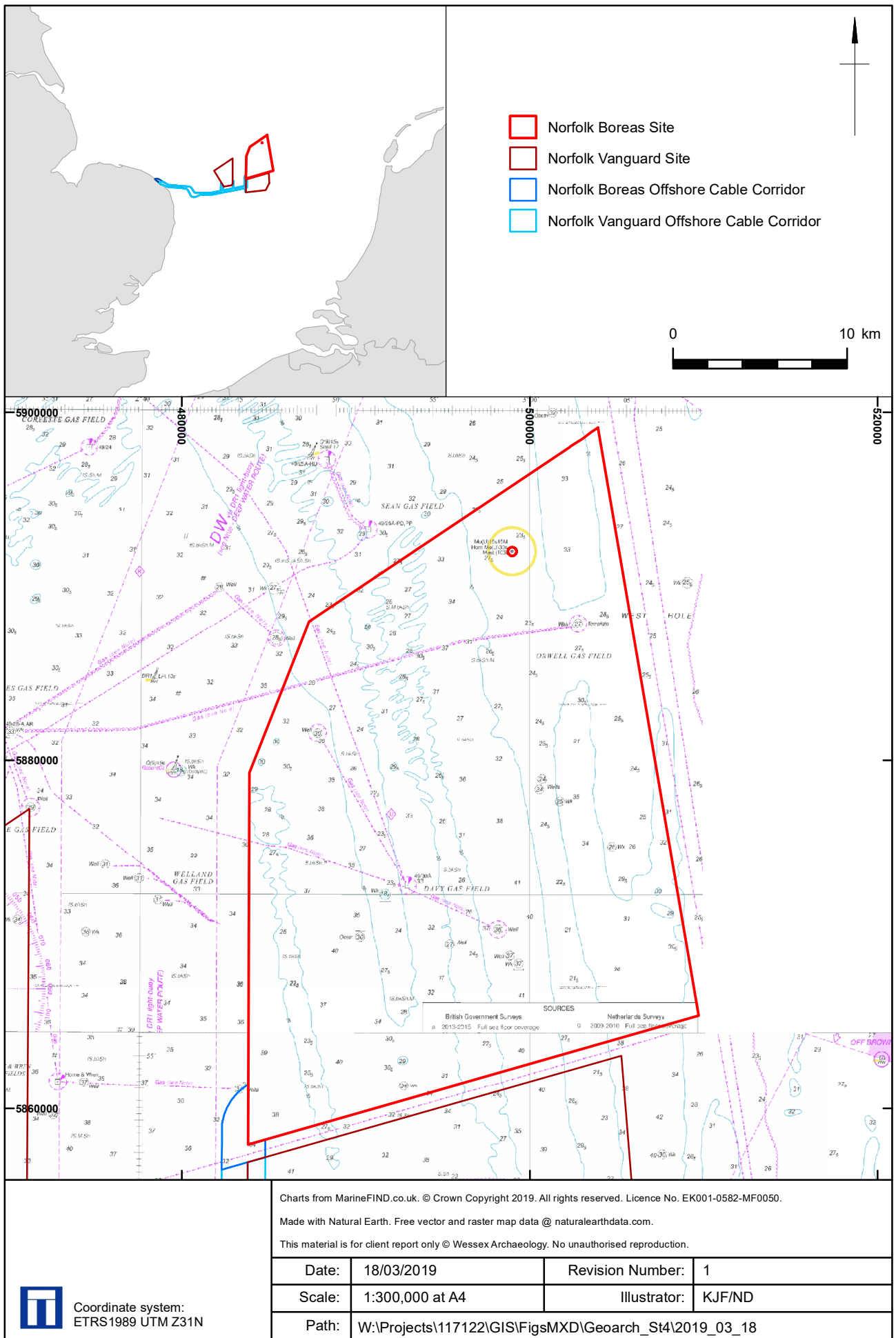
Appendix 5 – Norfolk Boreas site stratigraphy (deposit model)

WA Deposit Model (Stage 2) ¹		Fugro Soil Stratigraphy ²		BGS Lithostratigraphy ³	WA Deposit Model (Stage 4)		
Unit No	Unit Name	Soil Unit	Soil Unit Name	Formation	Unit No	Unit Name	Age
5	Holocene seabed sediments	A1	Bligh Bank	Southern Bight Formation	8	Seabed sediments	Holocene post-transgression (MIS 1)
4	Holocene sediments	A2	Elbow	Elbow Formation	7c	Elbow Formation – intertidal	Early Holocene (MIS 1)
					7b	Elbow Formation – organic	Late Devensian to Early Holocene (MIS 2-1)
					7a	Elbow Formation – fluvial	Late Devensian to Early Holocene (MIS 2-1)
-	Twente Formation	B	Twente	Twente Formation	6	Twente Formation	Late Devensian (MIS 2)
3	Upper Brown Bank Formation	C	Brown Bank	Brown Bank Formation	5	Upper Brown Bank	Early Devensian (MIS 5d-3)
2	Lower Brown Bank Formation/Eem Formation	C	Brown Bank	Brown Bank Formation and Eem Formation	4	Lower Brown Bank/Eem Formation	Ipswichian or Early Devensian (MIS 5e - 5d)
-	Swarte Bank Formation	D	Swarte Bank	Swarte Bank Formation	3	Swarte Bank Formation	Anglian (MIS 12)
1	Yarmouth Roads Formation	E	Yarmouth Roads	Yarmouth Road Formation	2	Yarmouth Roads Formation	Early to Middle Pleistocene (MIS >13)
-	-	I	Winterton Shoal/Smith's Knoll	Winterton Shoal Formation or Smith's Knoll Formation	1	Westkapelle Ground Formation	Late Pliocene to Early Pleistocene (MIS 63-103)

¹ Wessex Archaeology (2018b)

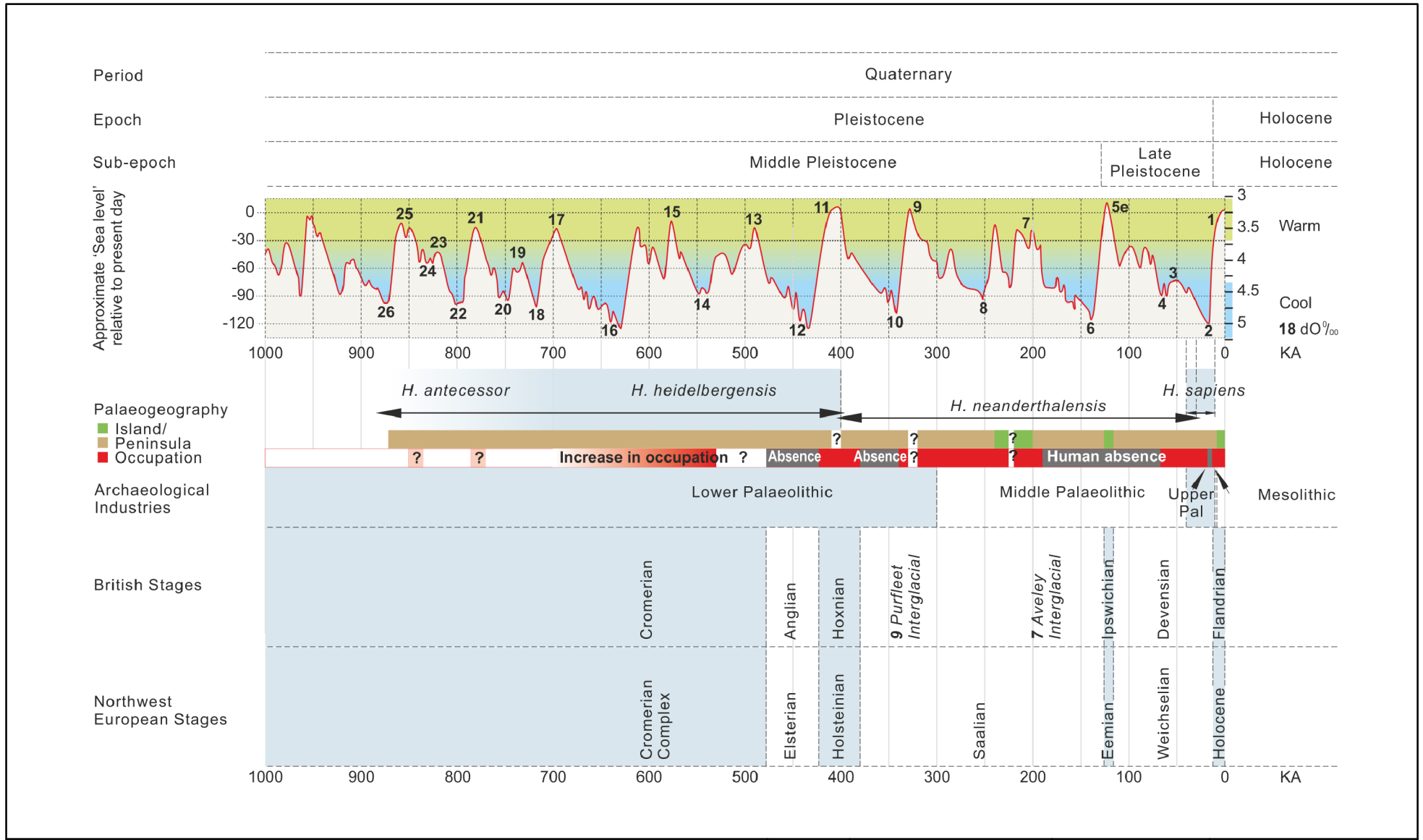
² Fugro (2018)

³ Stoker et al. (2011)



Location of Norfolk Boreas Site

Figure 1



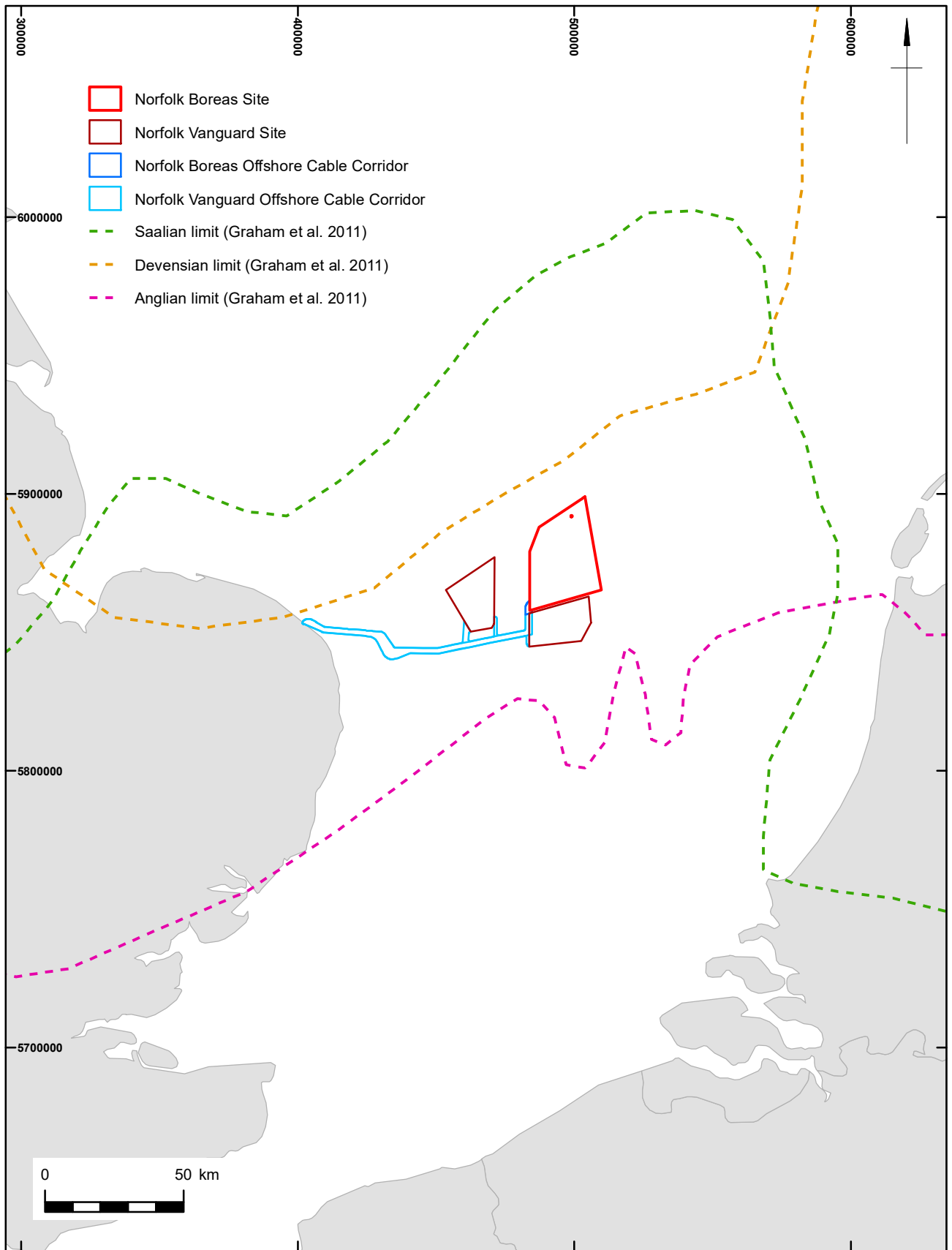
The figure presents information derived from several references: the global sea-level curve is from Lisiecki and Raymo (2005) and Jelgersma (1979). Details on the geology and archaeology were provided by Dix and Westley (2004); Funnel (1995); Gibbard and van Kolfschoten (2004); Kukla et al. (2002); Lee et al. (2006); Lowe and Walker (1997) and Wymer (1999).


This material is for client report only © Wessex Archaeology. No unauthorised reproduction.

Date:	30/01/2019	Revision Number:	0
Scale:	N/A	Illustrator:	RAM
Path:	W:\Projects\117122\GIS\Figs\MXD\Geoarch_St4\2019_01_30		

Chronostratigraphic timeline for the last 1 million years

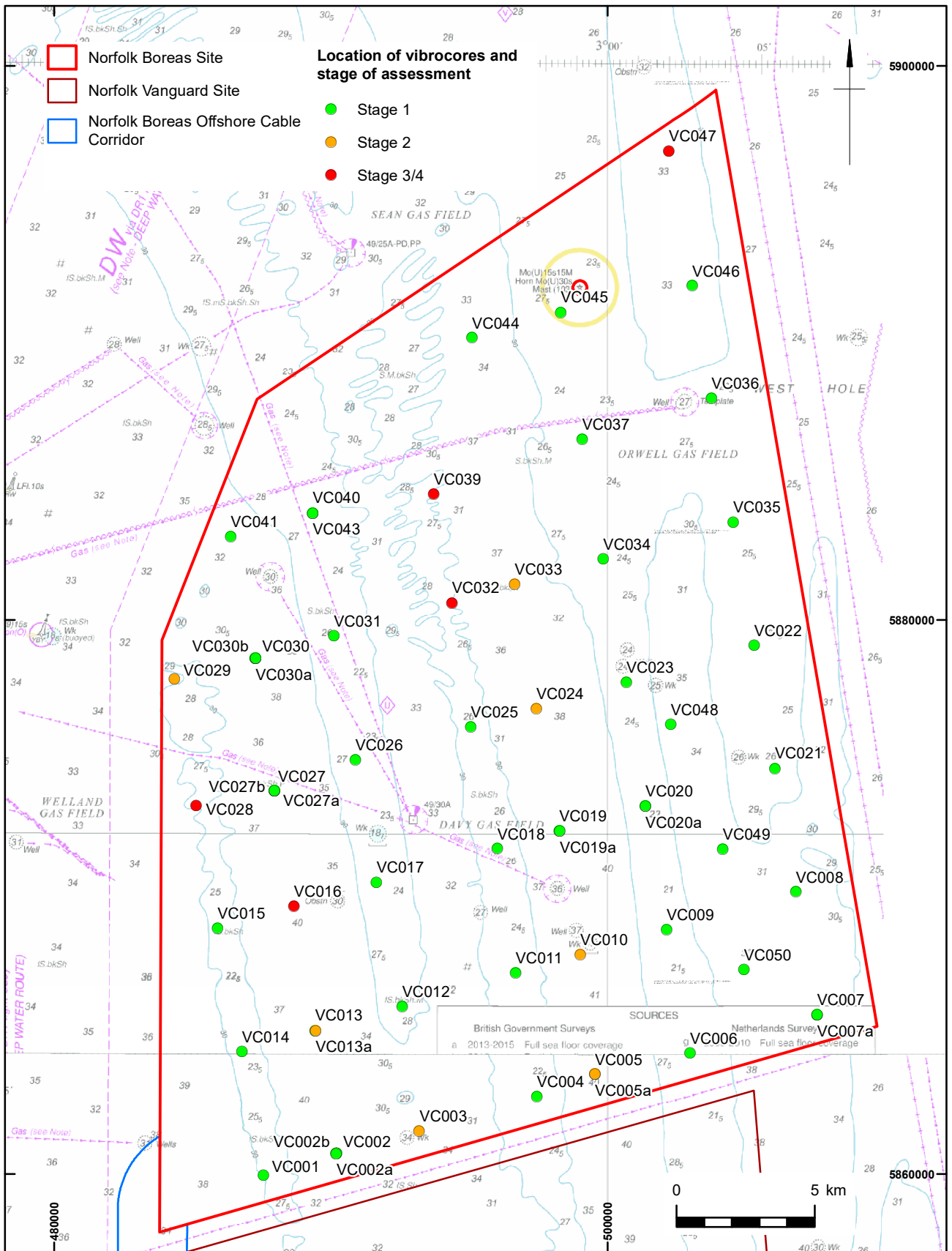
Figure 2




 Coordinate system: ETRS1989 UTM Z31N	Made with Natural Earth. Free vector and raster map data @ naturalearthdata.com .			
	This material is for client report only © Wessex Archaeology. No unauthorised reproduction.			
	Date:	18/03/2019	Revision Number:	1
	Scale:	1:2,000,000 at A4	Illustrator:	KJF/ND
Path:		W:\Projects\117122\GIS\FigsMXD\Geoarch_St4\2019_03_18		

Pleistocene ice limits

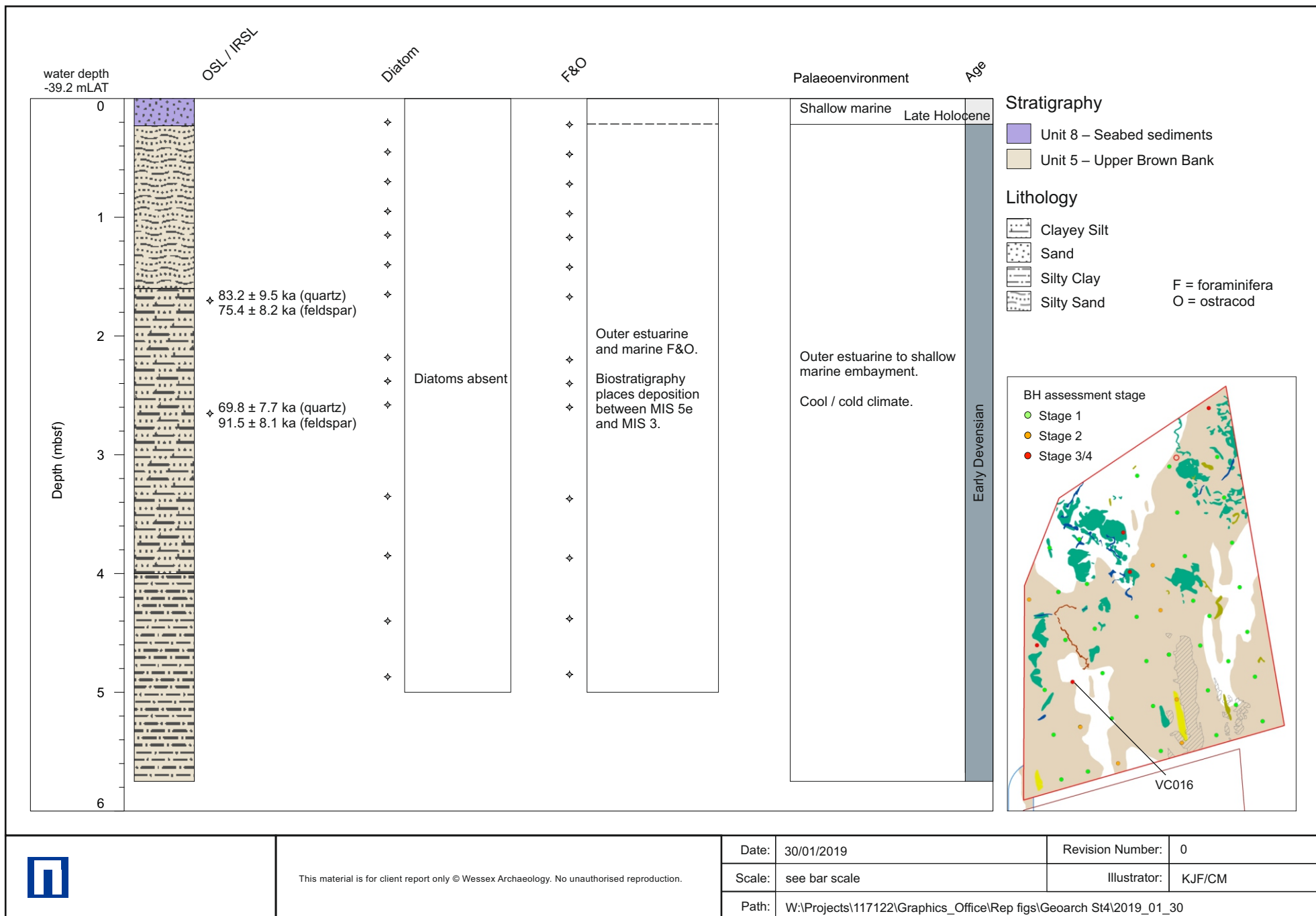
Figure 4



 <p>Coordinate system: ETRS1989 UTM Z31N</p>	Charts from MarineFIND.co.uk. © Crown Copyright 2019. All rights reserved. Licence No. EK001-0582-MF0050.			
	This material is for client report only © Wessex Archaeology. No unauthorised reproduction.			
	Date:	18/03/2019	Revision Number:	1
	Scale:	1:200,000 at A4	Illustrator:	KJF
Path:		W:\Projects\117122\GIS\FigsMXD\Geoarch_St4\2019_03_18		

Location of vibrocores and stage of assessment

Figure 5



This material is for client report only © Wessex Archaeology. No unauthorised reproduction.

Date: 30/01/2019

Revision Number: 0

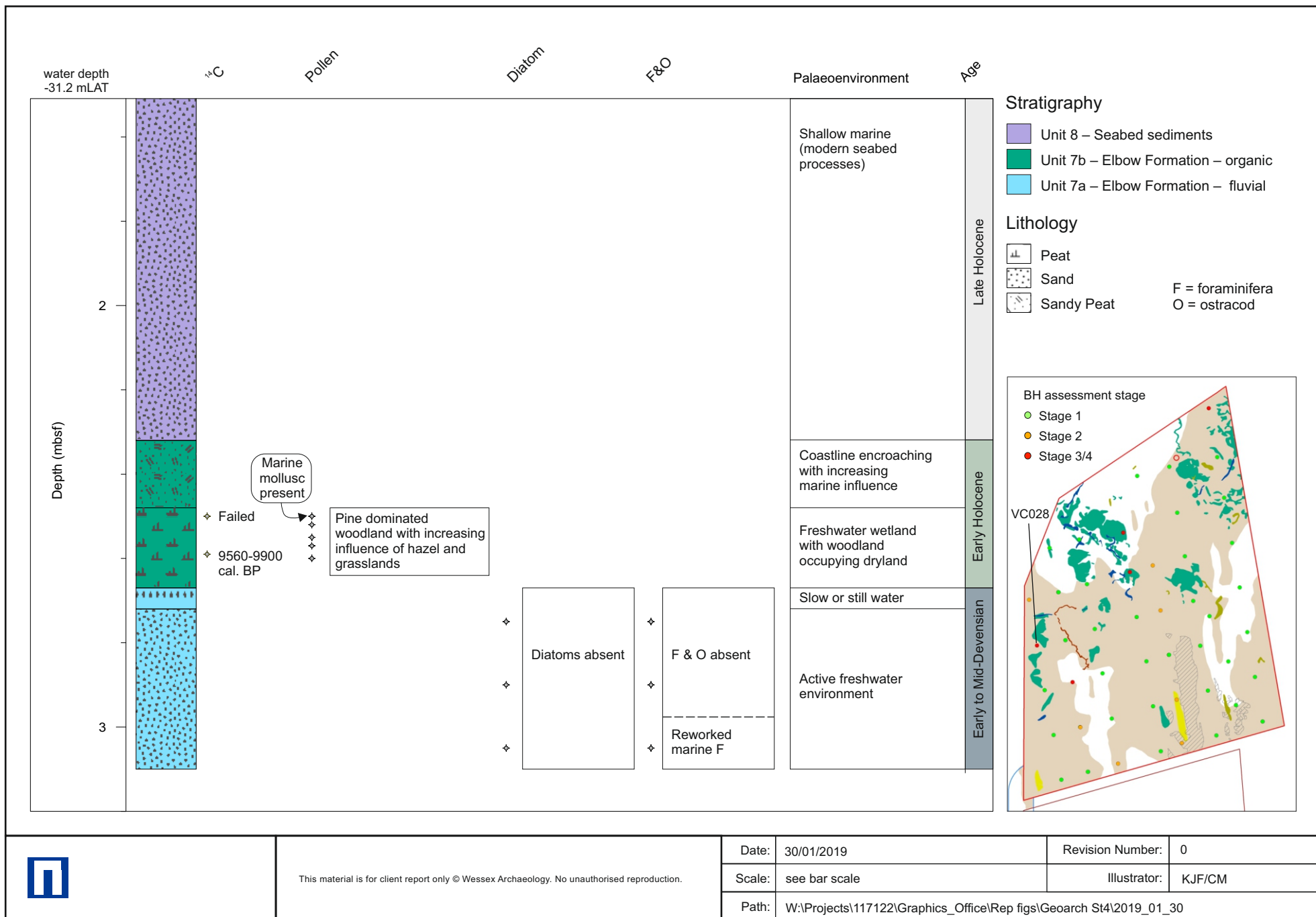
Scale: see bar scale

Illustrator: KJF/CM

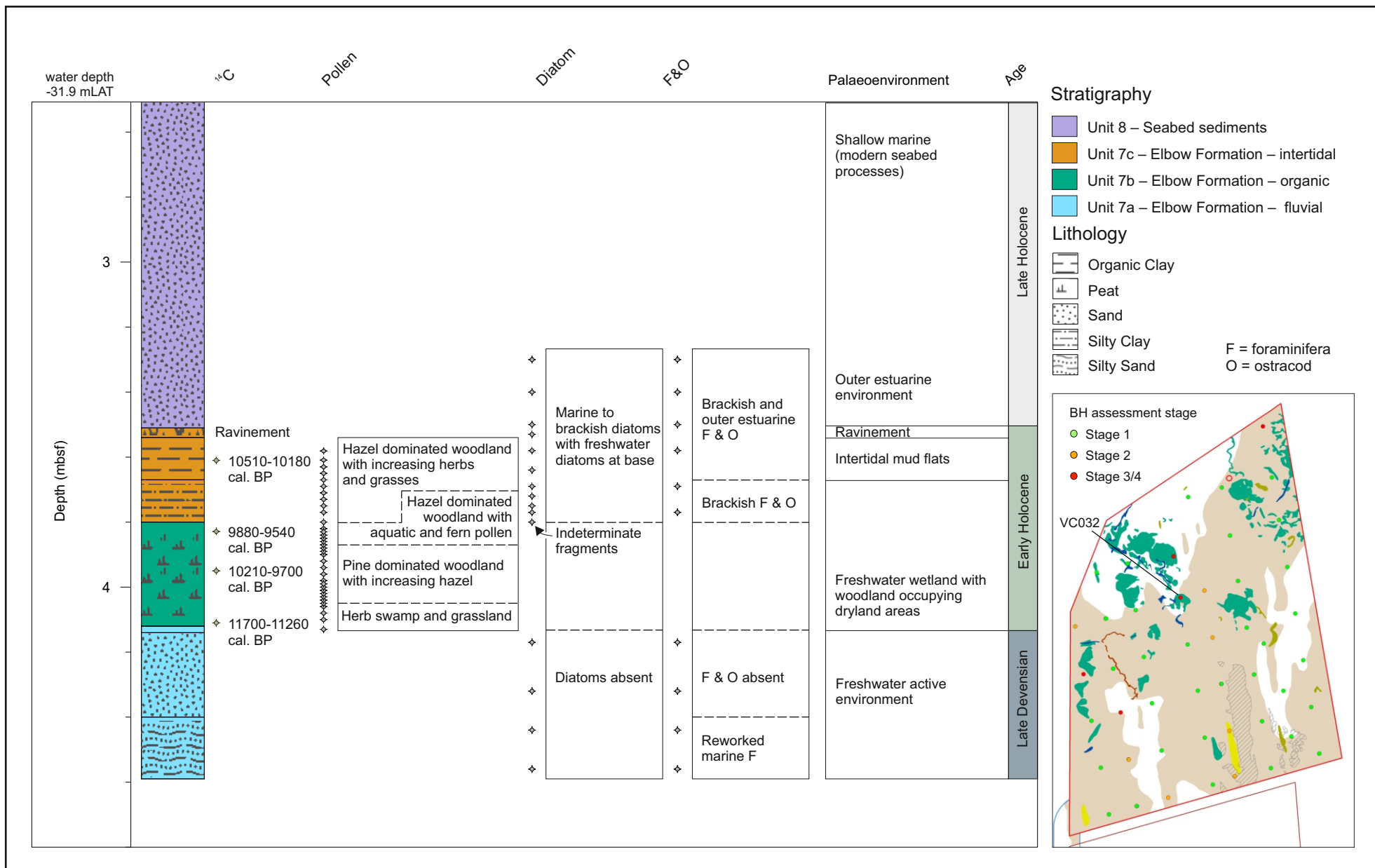
Path: W:\Projects\117122\Graphics_Office\Rep figs\Geoarch St4\2019_01_30

Vibrocore log and geophysical palaeolandscapes assessment showing palaeoenvironmental and dating, results and interpretation, for VC016

Figure 6



Vibrocore log and geophysical palaeolandscapes assessment showing palaeoenvironmental and dating, results and interpretation, for VC028



This material is for client report only © Wessex Archaeology. No unauthorised reproduction.

Date: 28/01/2019

Revision Number: 0

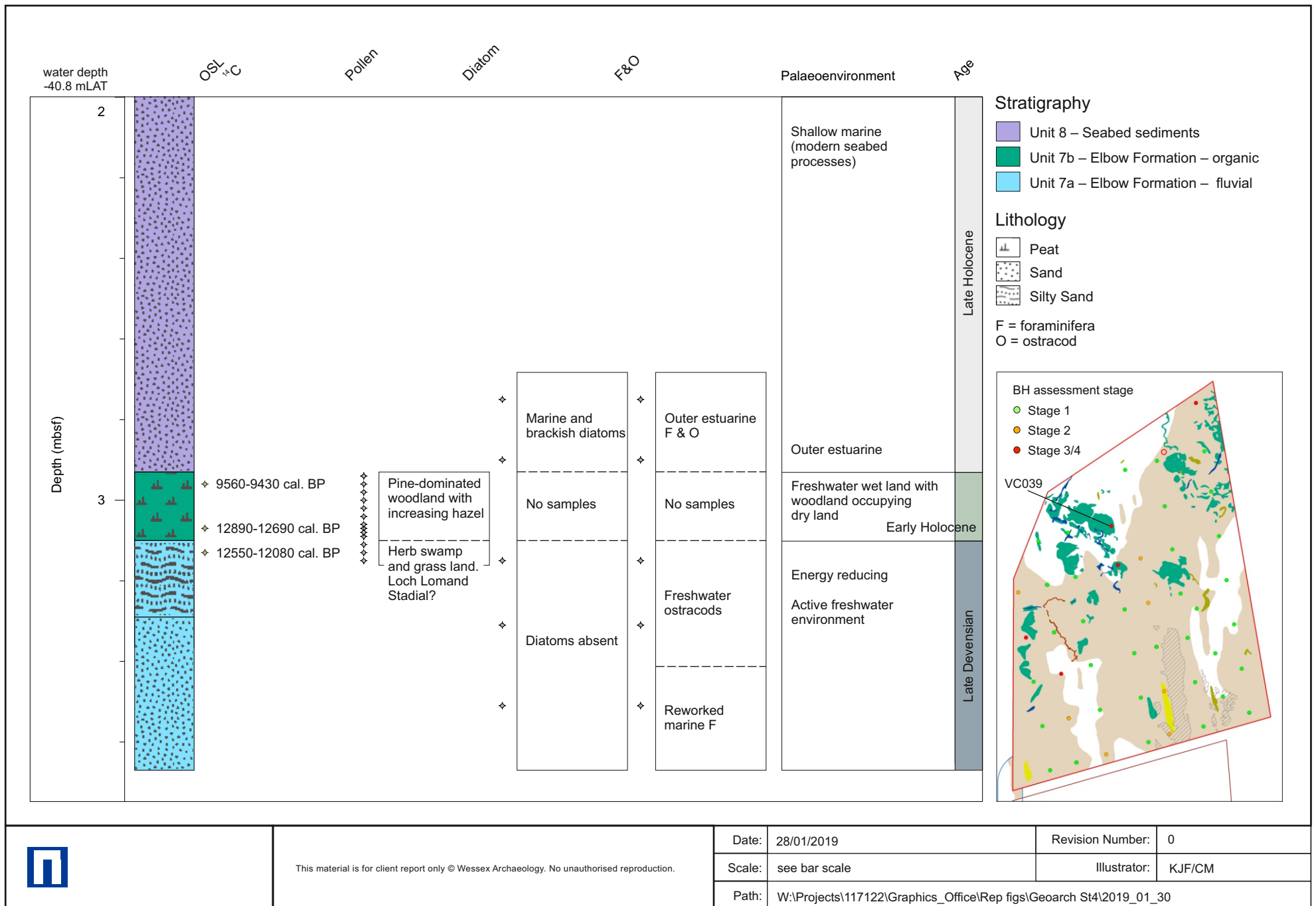
Scale: see bar scale

Illustrator: KJF/CM

Path: W:\Projects\117122\Graphics_Office\Rep figs\Geoarch St4\2019_01_30

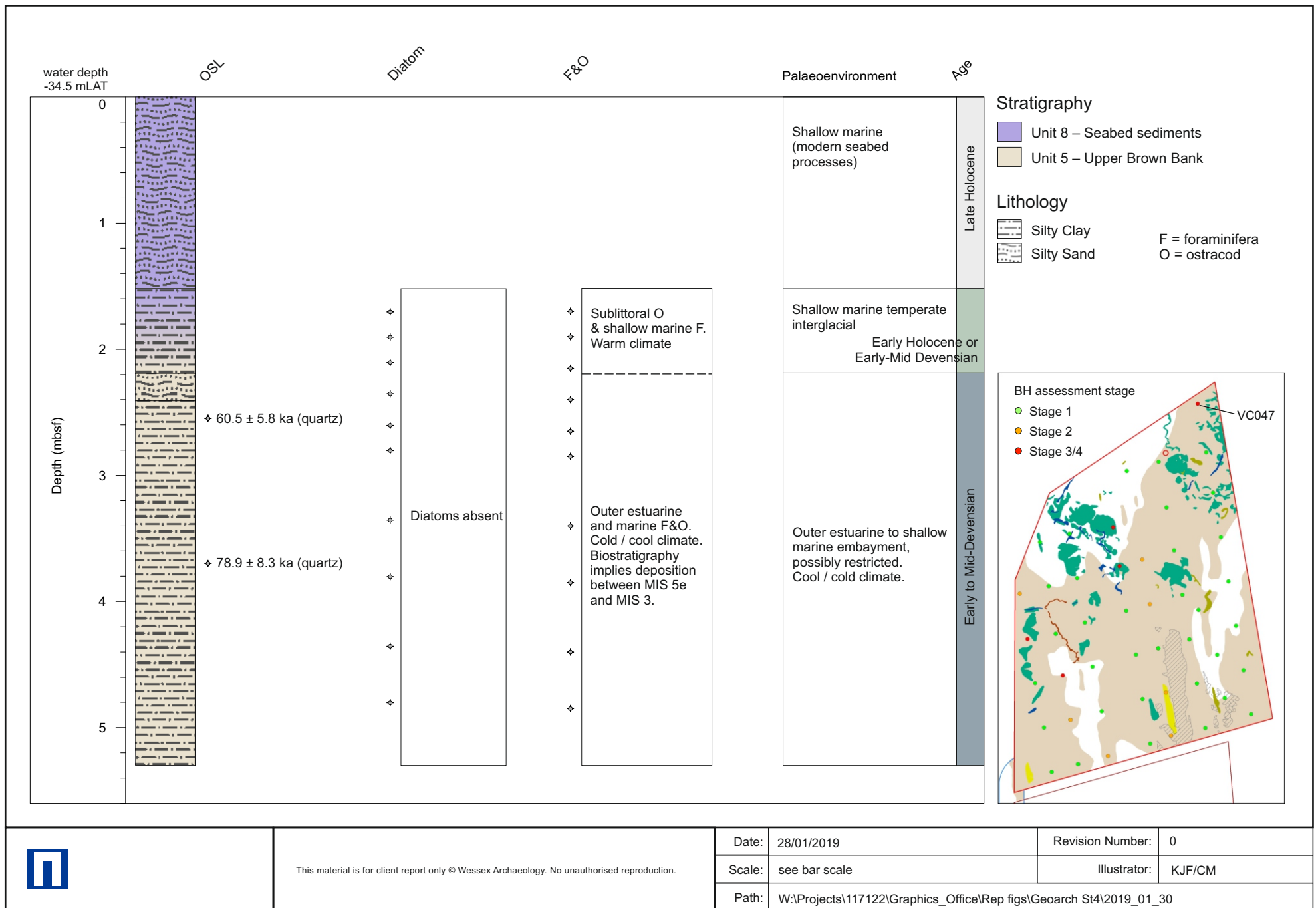
Vibrocore log and geophysical palaeolandscapes assessment showing palaeoenvironmental and dating, results and interpretation, for VC032

Figure 8

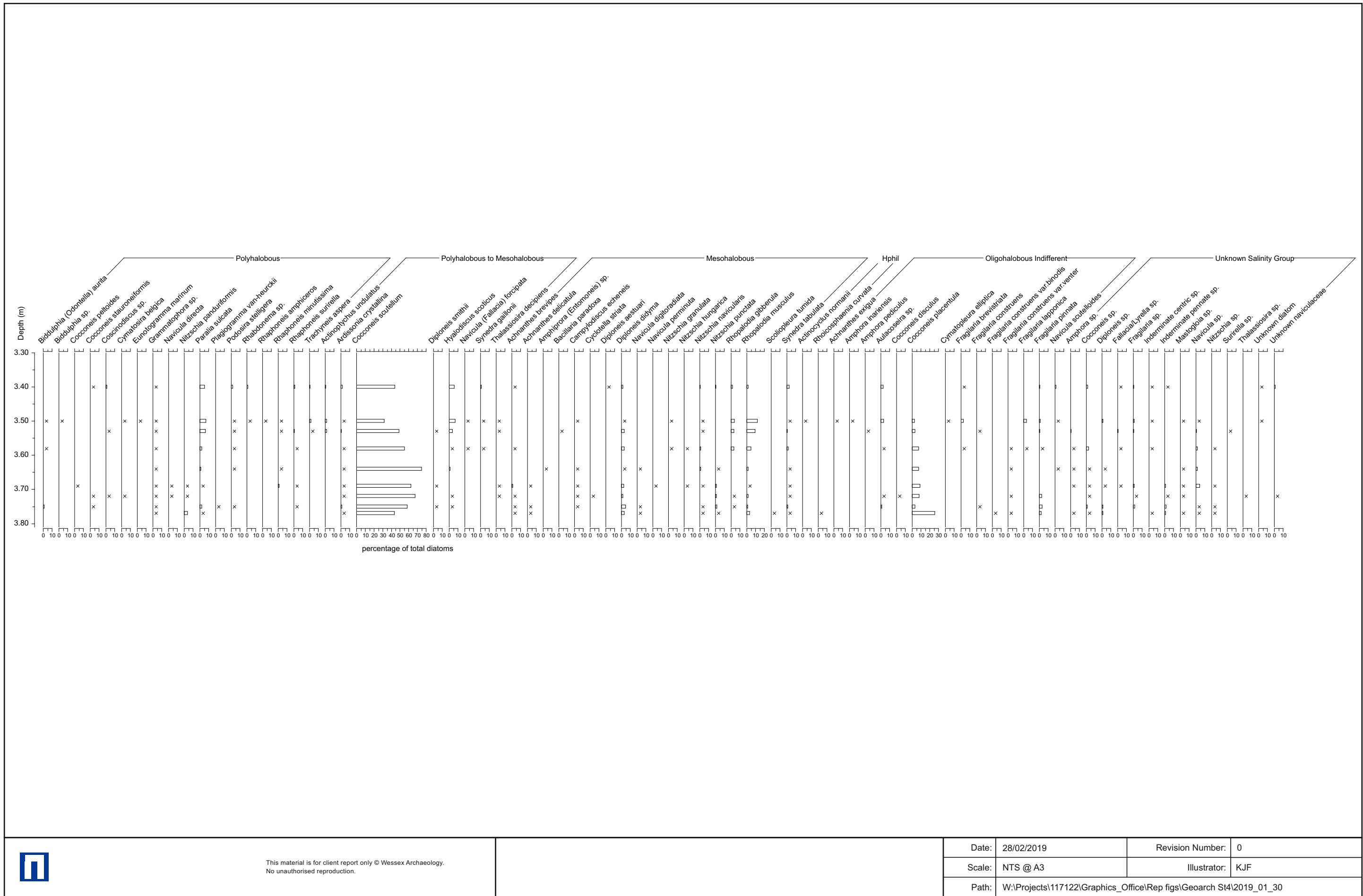


Vibrocore log and geophysical palaeolandscapes assessment showing palaeoenvironmental and dating, results and interpretation, for VC039

Figure 9

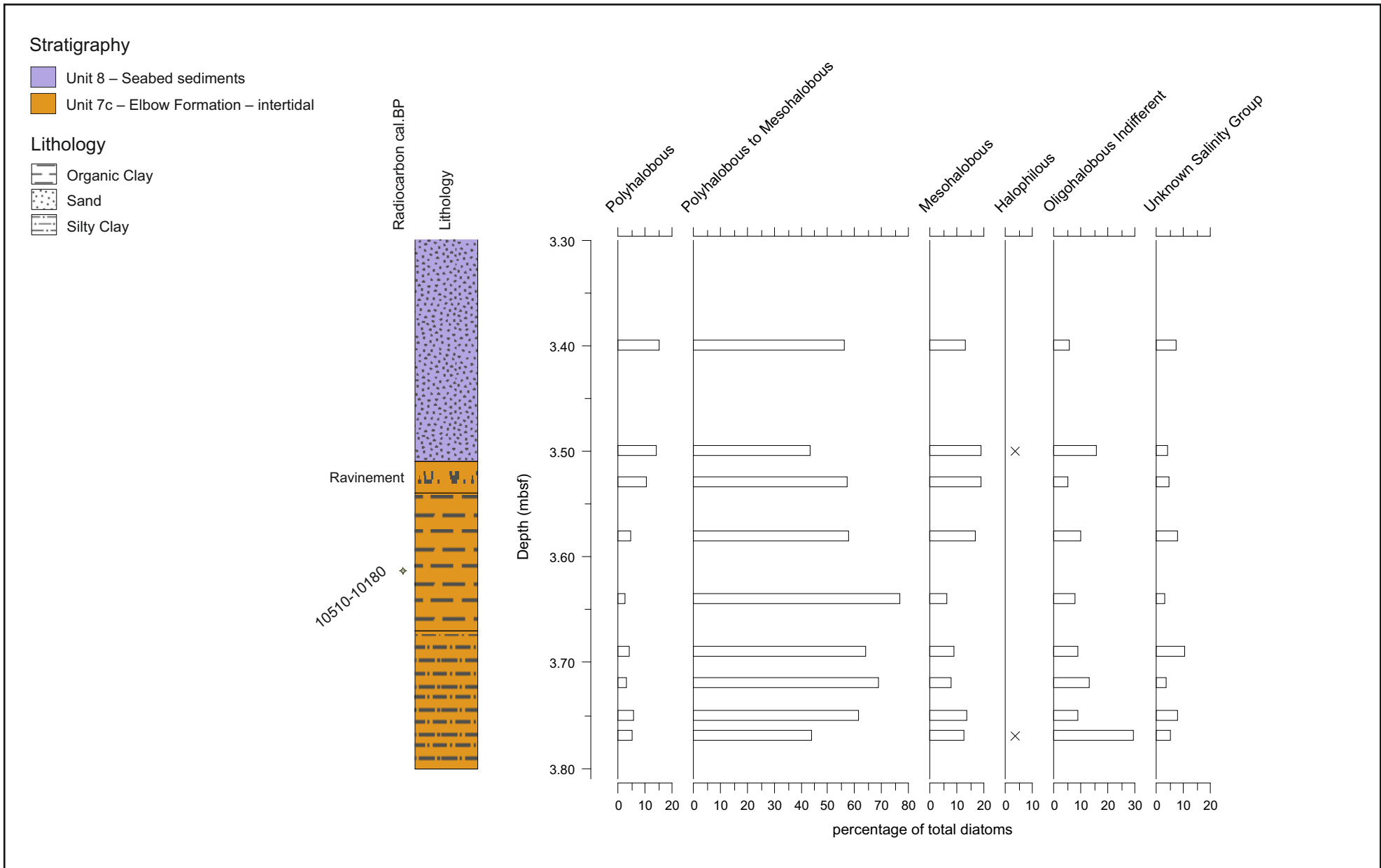



Vibrocore log and geophysical palaeolandscapes assessment showing palaeoenvironmental and dating, results and interpretation, for VC047



This material is for client report only © Wessex Archaeology.
No unauthorised reproduction.

Date:	28/02/2019	Revision Number:	0
Scale:	NTS @ A3	Illustrator:	KJF
Path:	W:\Projects\117122\Graphics_Office\Rep figs\Georch St4\2019_01_30		



	This material is for client report only © Wessex Archaeology. No unauthorised reproduction.	Date: 28/02/2019	Revision Number: 0
		Scale: see bar scale	Illustrator: KJF/CM
		Path: W:\Projects\117122\Graphics_Office\Rep figs\Geoarch St4\2019_01_30	

Percentage of total diatoms within each halobian (salinity) group, VC032

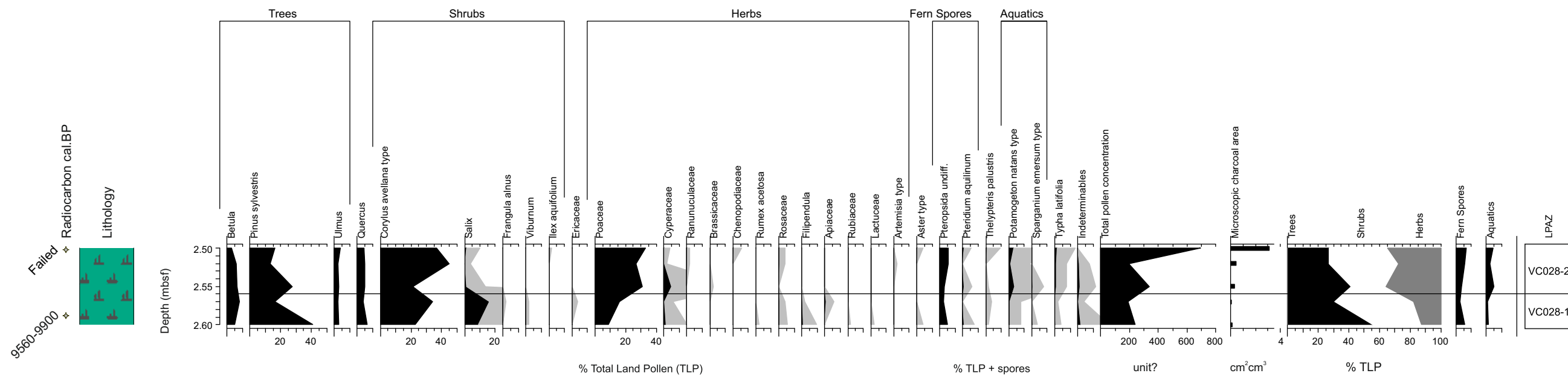
Figure 12

Stratigraphy

Unit 7b – Elbow Formation – organic

Lithology

Peat



This material is for client report only © Wessex Archaeology.
No unauthorised reproduction.

Date:	28/02/2019	Revision Number:	0
Scale:	NTS @ A3	Illustrator:	KJF
Path:	W:\Projects\117122\Graphics_Office\Rep figs\Georch St4\2019_01_30		

Pollen diagram VC028

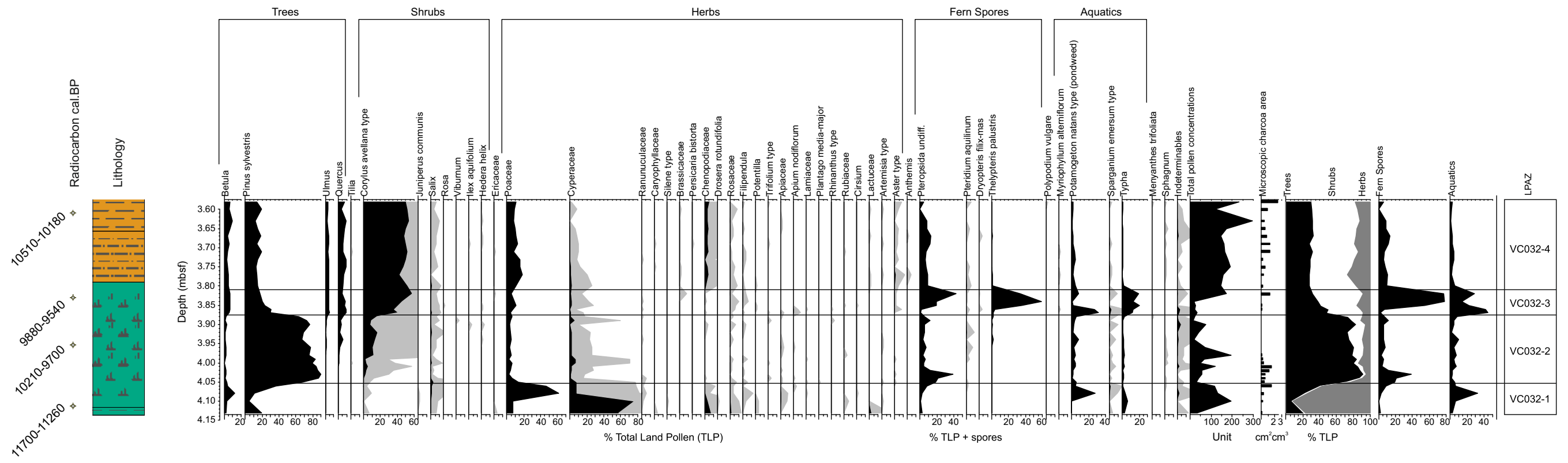
Figure 13

Stratigraphy

- Unit 7c – Elbow Formation – intertidal
- Unit 7b – Elbow Formation – organic

Lithology

- Organic Clay
- Peat
- Silty Clay



This material is for client report only © Wessex Archaeology.
No unauthorised reproduction.

Date:	28/02/2019	Revision Number:	0
Scale:	NTS @ A3	Illustrator:	KJF
Path:	W:\Projects\117122\Graphics_Office\Rep figs\Georch St4\2019_01_30		

Pollen diagram VC032

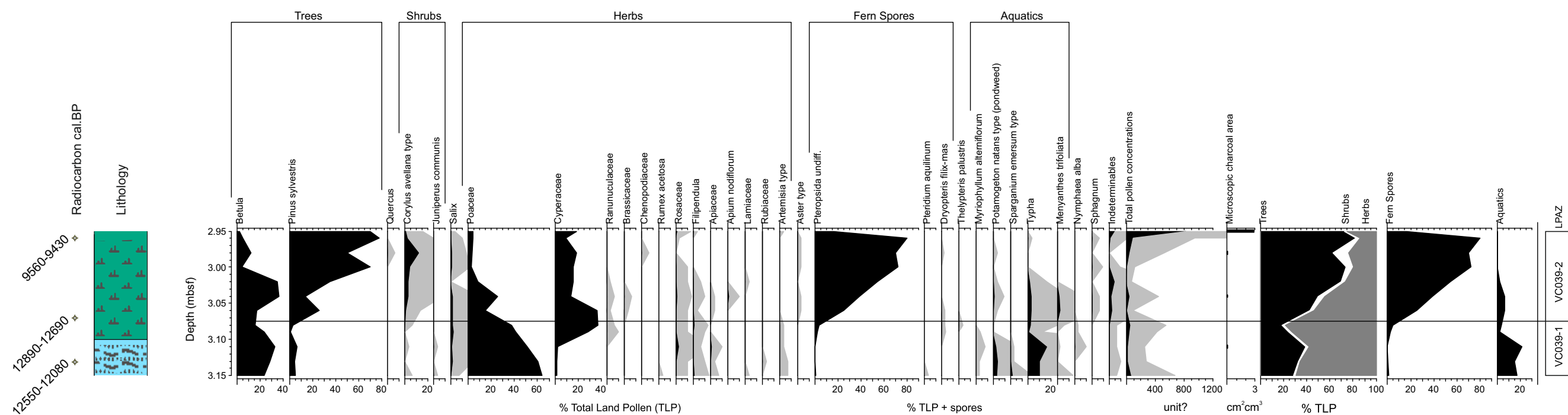
Figure 14

Stratigraphy

- Unit 7b – Elbow Formation – organic
- Unit 7a – Elbow Formation – fluvial

Lithology

- Peat
- Silty Sand

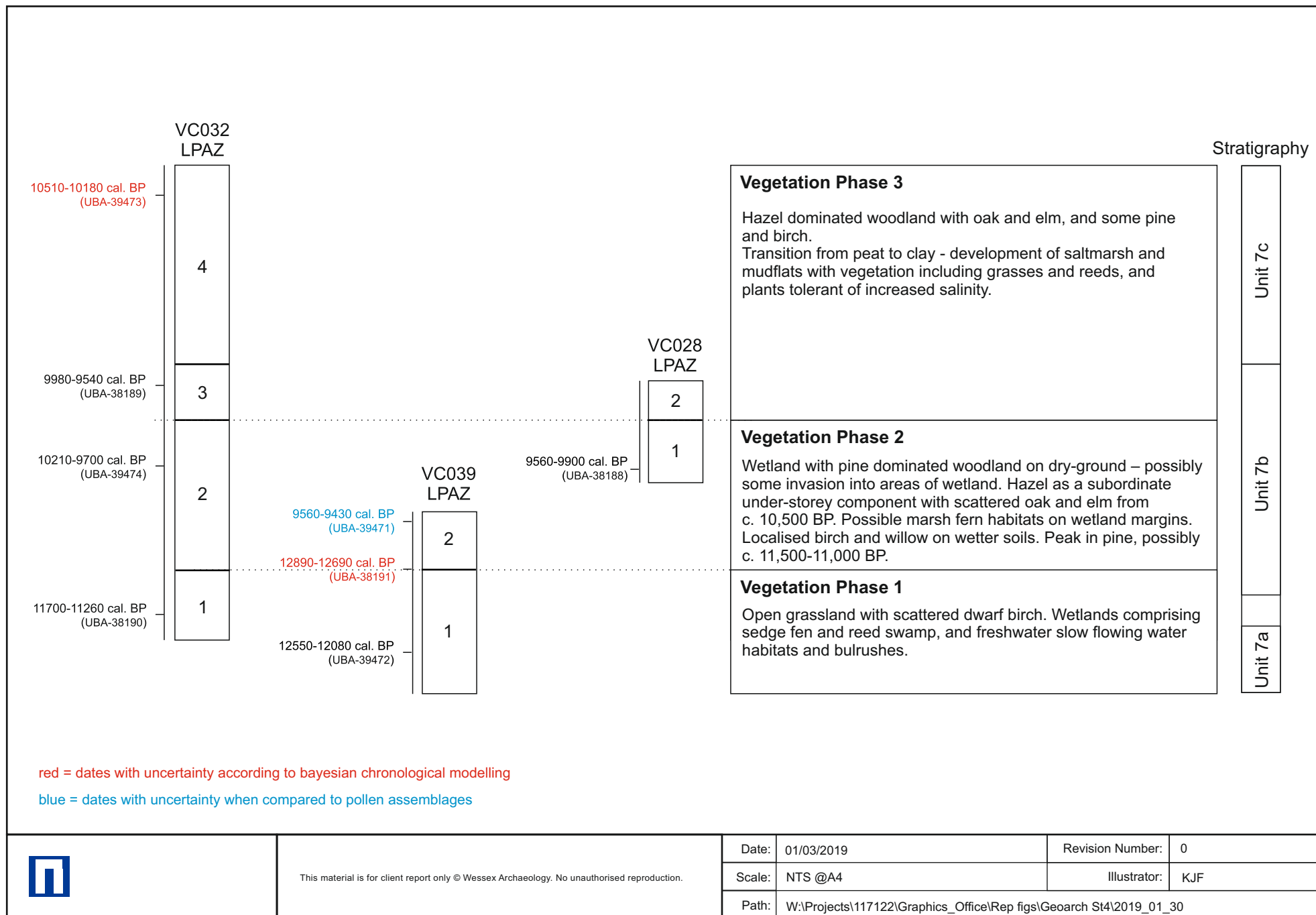


This material is for client report only © Wessex Archaeology.
No unauthorised reproduction.

Date:	28/02/2019	Revision Number:	0
Scale:	NTS @ A3	Illustrator:	KJF
Path:	W:\Projects\117122\Graphics_Office\Rep figs\Georch St4\2019_01_30		

Pollen diagram VC039

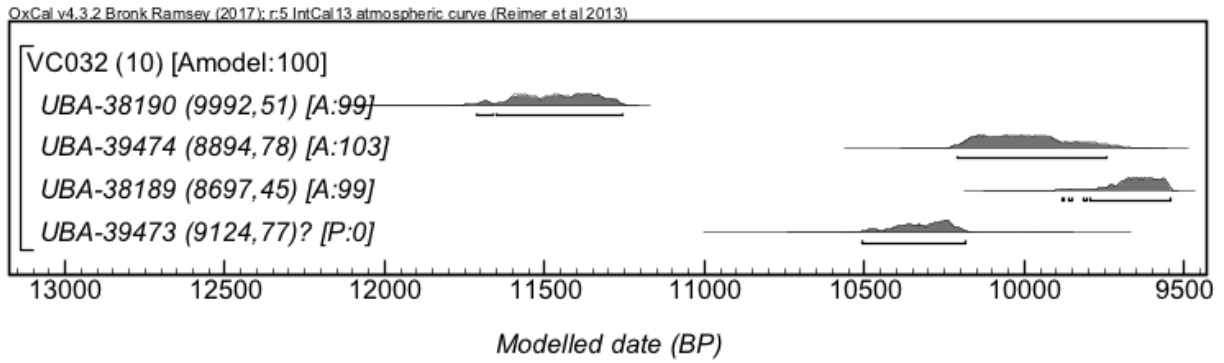
Figure 15



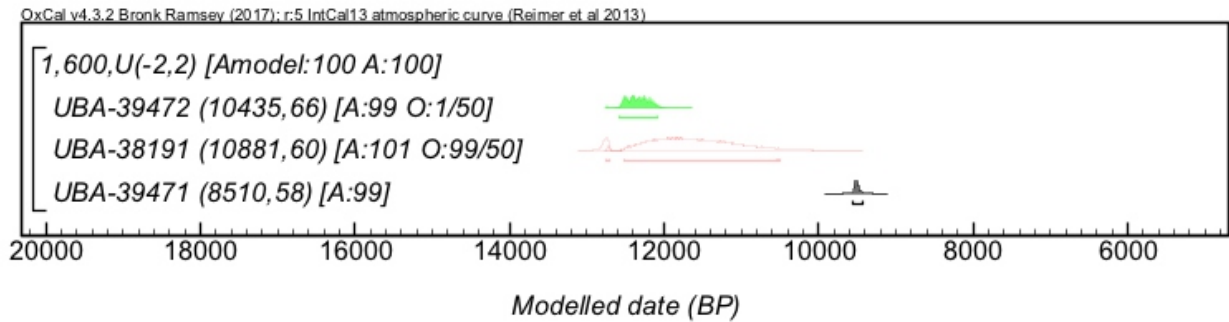
Composite diagram showing relationship between pollen assemblages in VC028, VC032 and VC039, and key vegetation phases

Figure 16

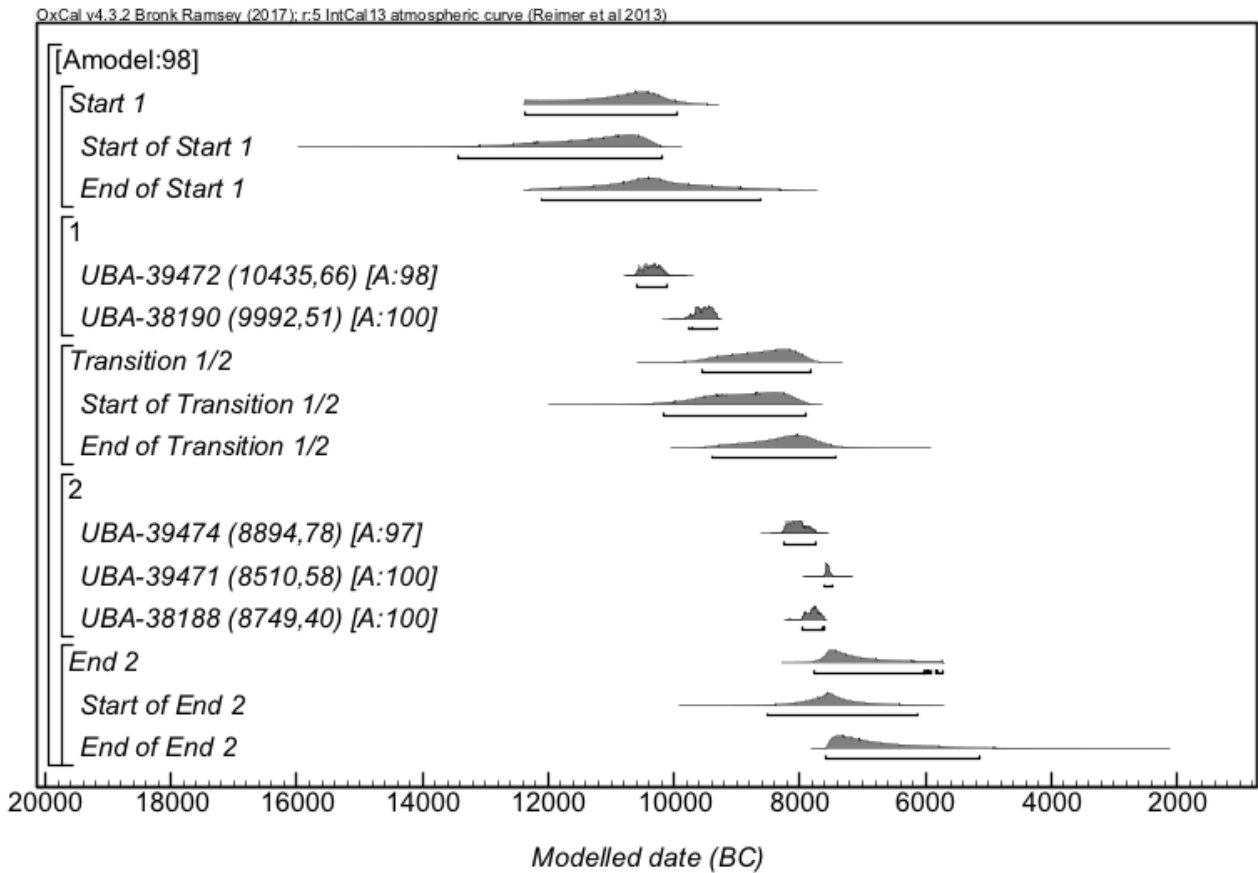
A. VC032 with UBA-39473 outlier




B. VC039 all dates



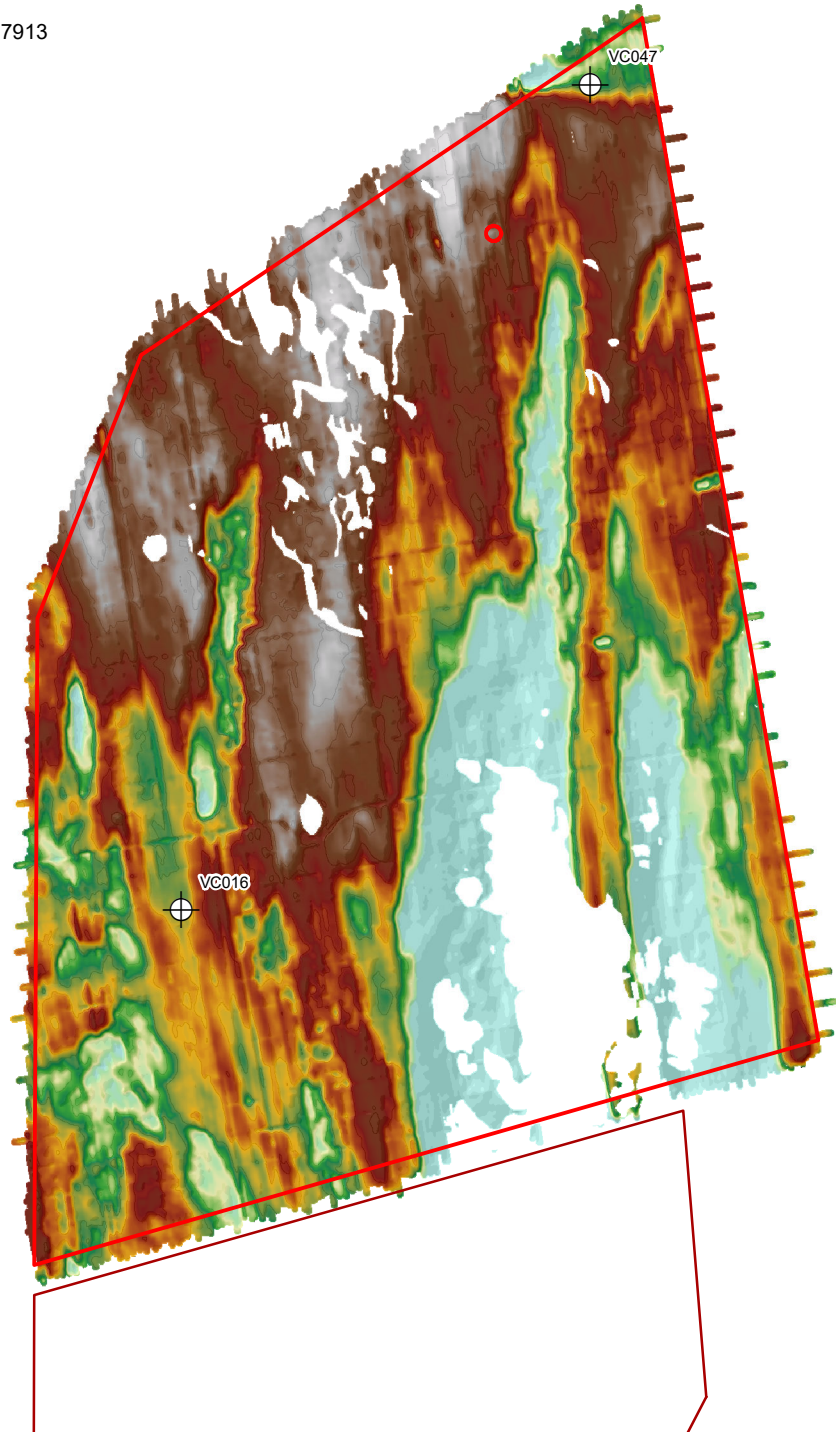
C. Modelled Vegetation Phases



	This material is for client report only © Wessex Archaeology. No unauthorised reproduction.			
	Date:	28/02/2019	Revision Number:	0
	Scale:	N/A	Illustrator:	CM/KJF
	Path:	W:\Projects\117122\Graphics_Office\Rep figs\Geoarch St4\2019_01_30		

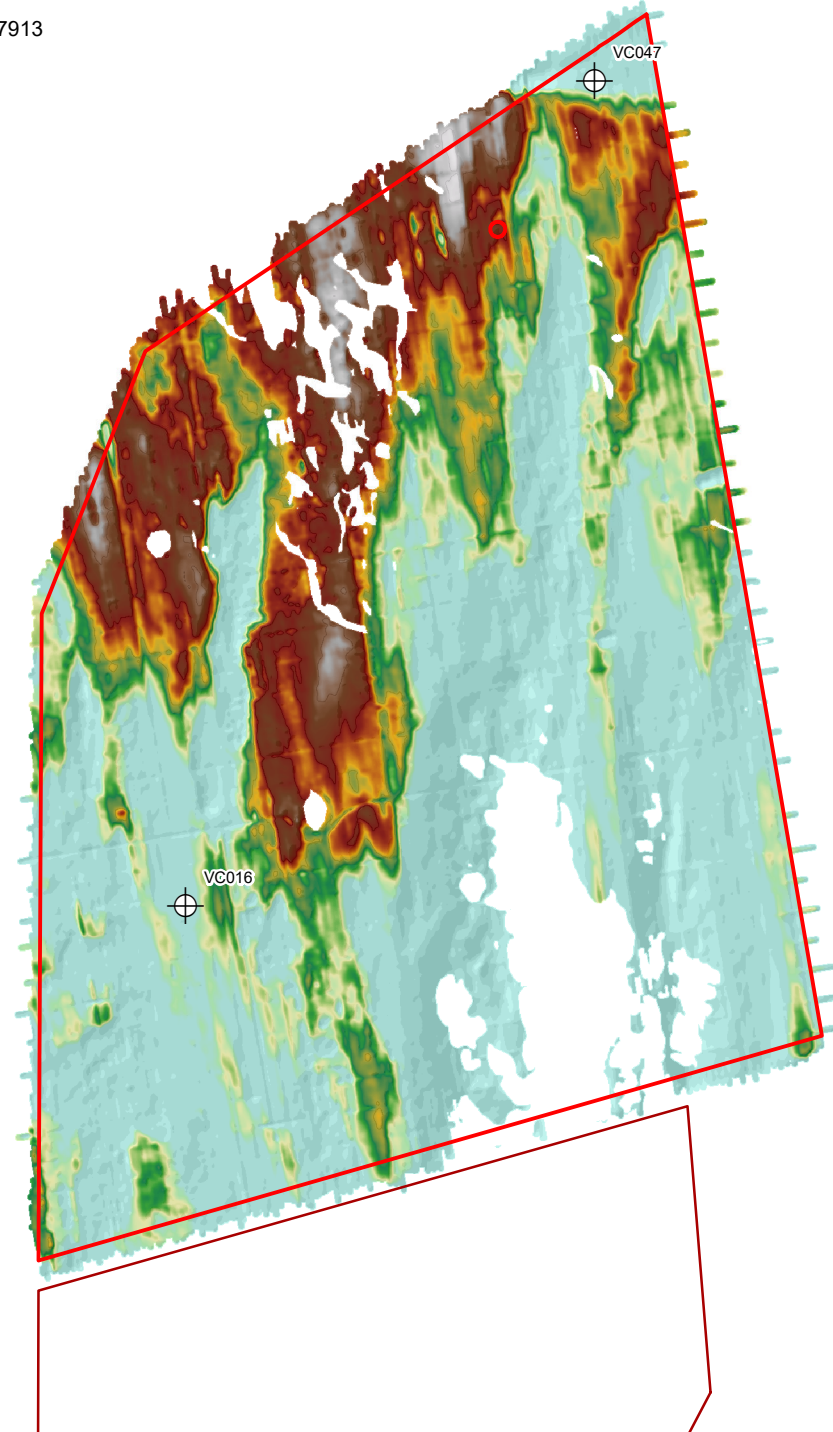
Scenario A ~115 ka (MIS 5d)
MSL -46 m

mLAT High : -38.7913
Low : -48



Scenario B ~80 ka (MIS 5b)
MSL -42 m

mLAT High : -38.7913
Low : -48

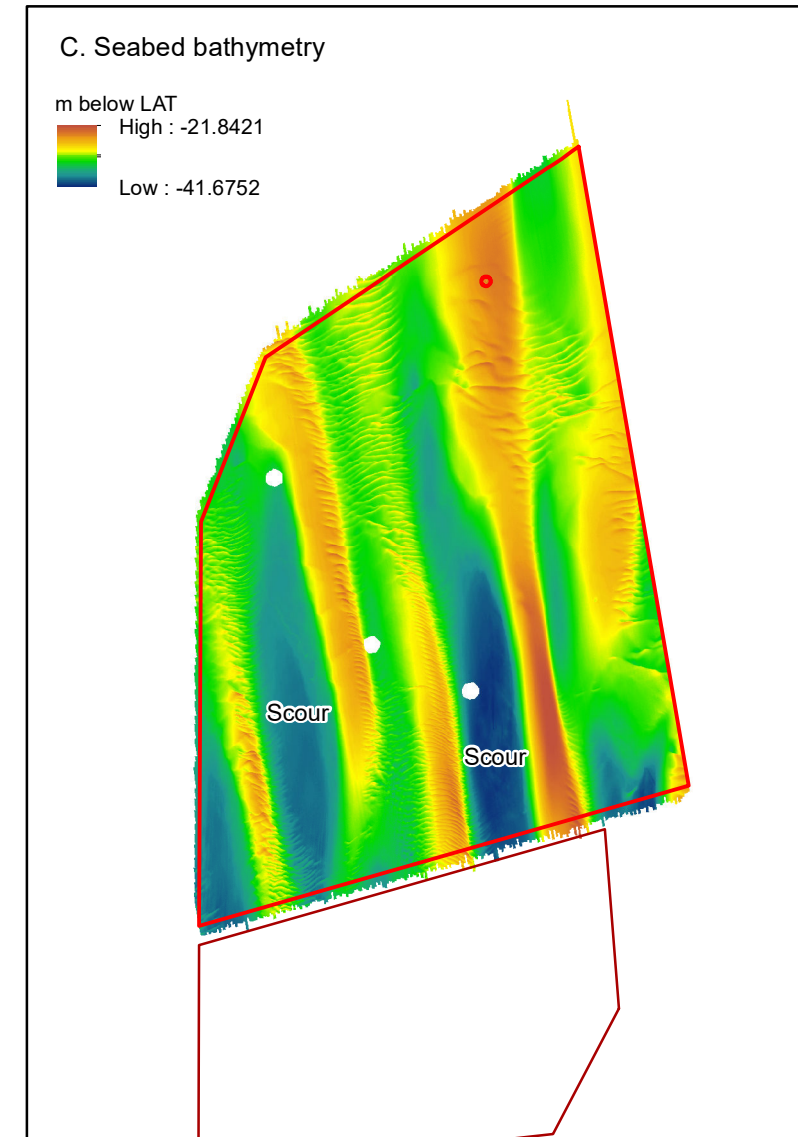
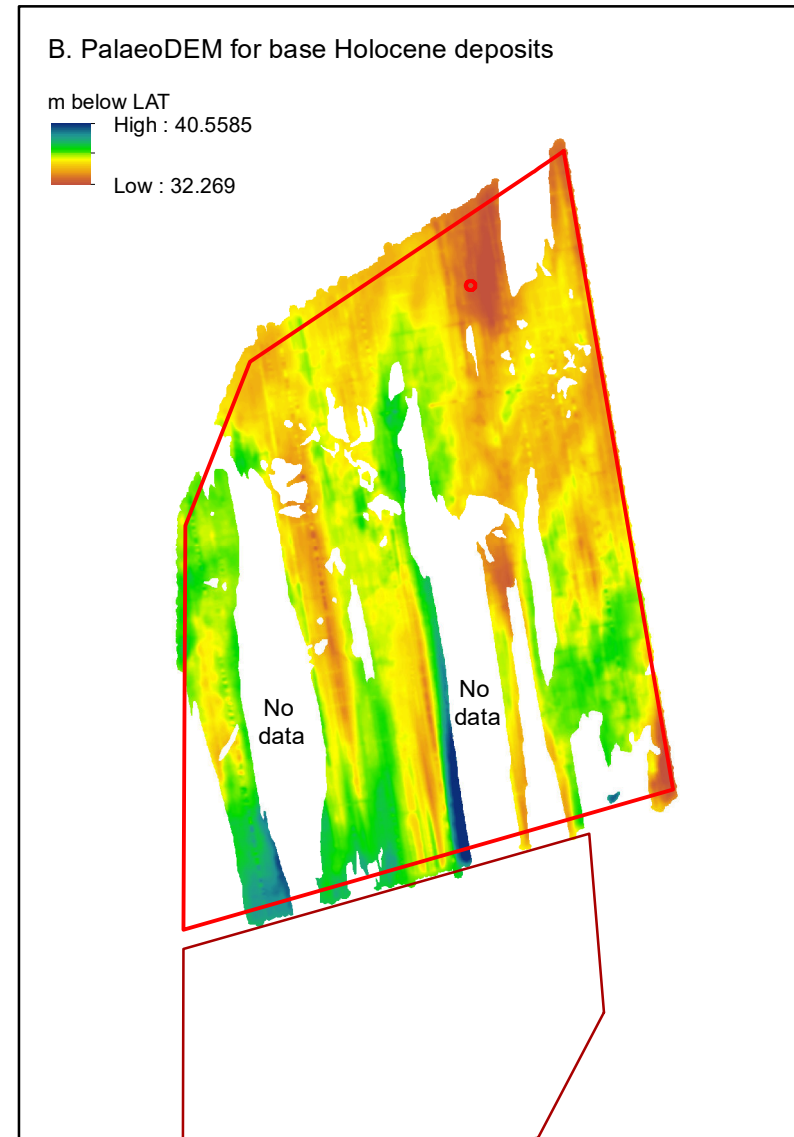
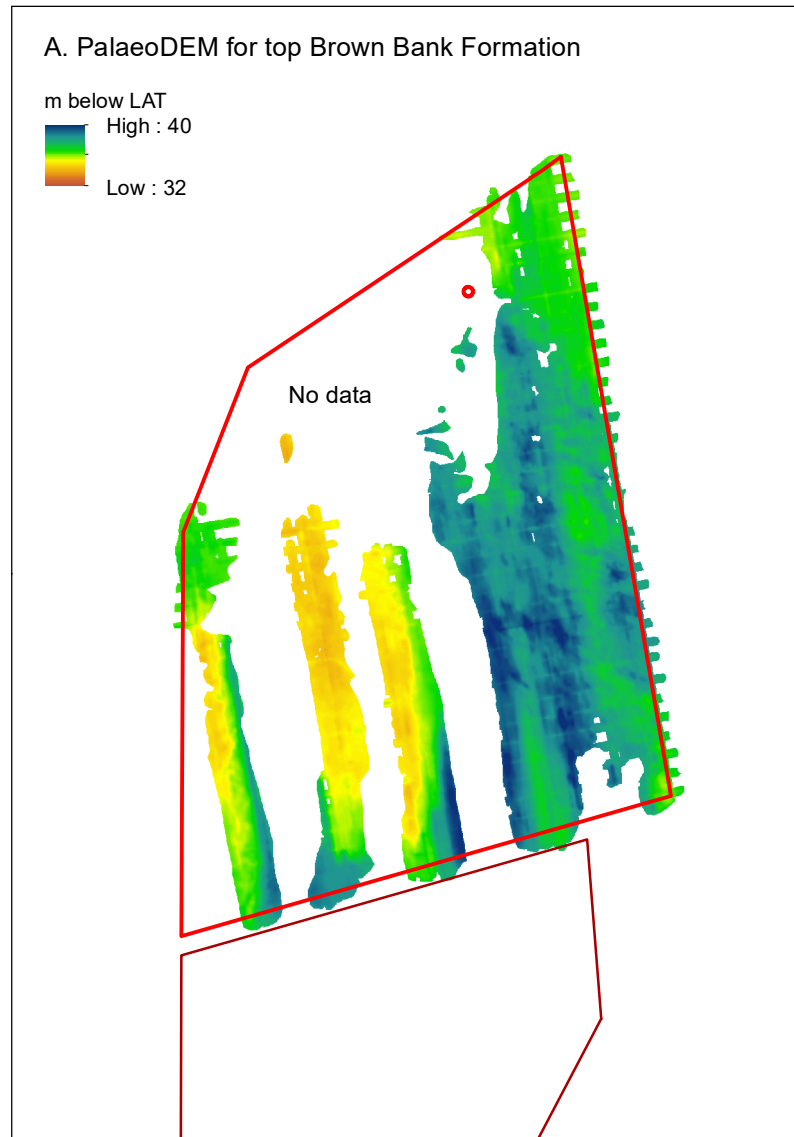


Norfolk Boreas Site
 Norfolk Vanguard Site
 VC016 and VC047

Coordinate system:
ETRS 1989 UTM Z31N

This material is for client report only © Wessex Archaeology. No unauthorised reproduction.

Date:	18/03/2019	Revision Number:	1
Scale:	1:250,000 at A3	Illustrator:	KJF
Path:	W:\Projects\117122\GIS\FigsMXD\Geoarch_St4\2019_03_18		

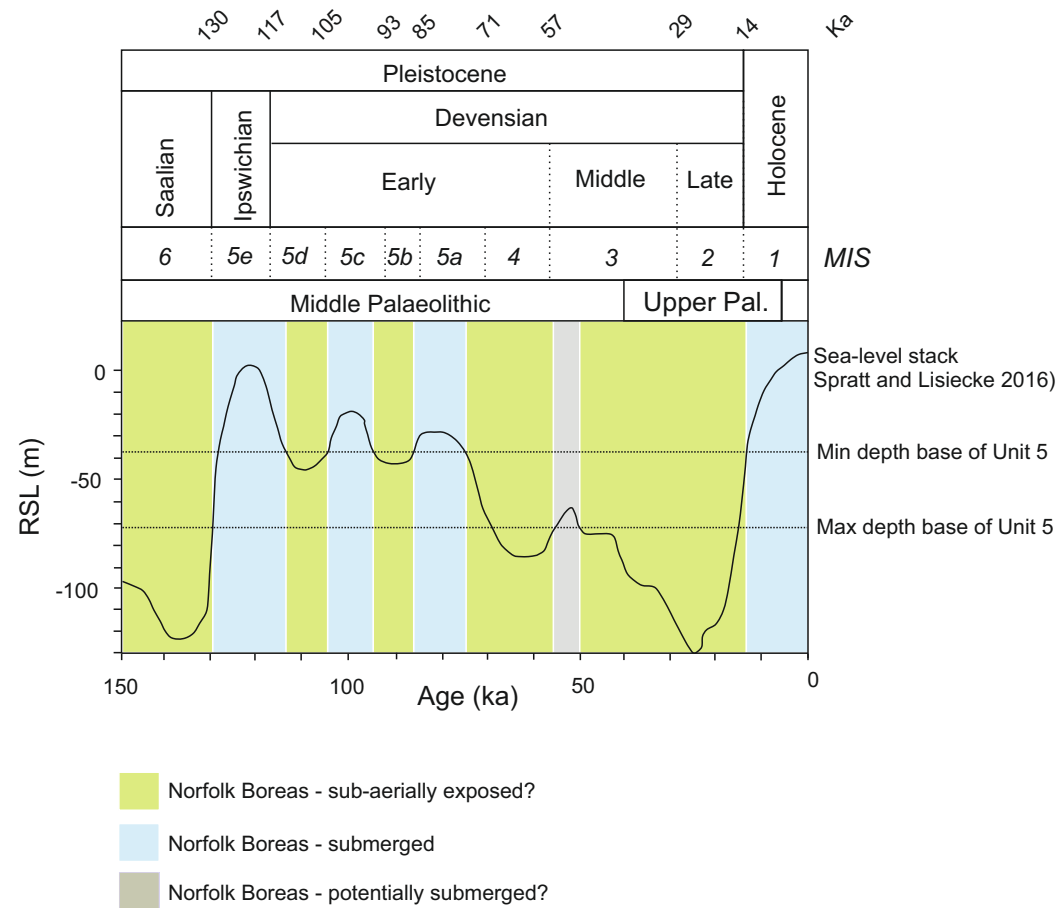



- Norfolk Boreas Site
- Norfolk Vanguard Site



Coordinate system:
 ETRS 1989 UTM Z31N
 This material is for client report only © Wessex Archaeology. No unauthorised reproduction.

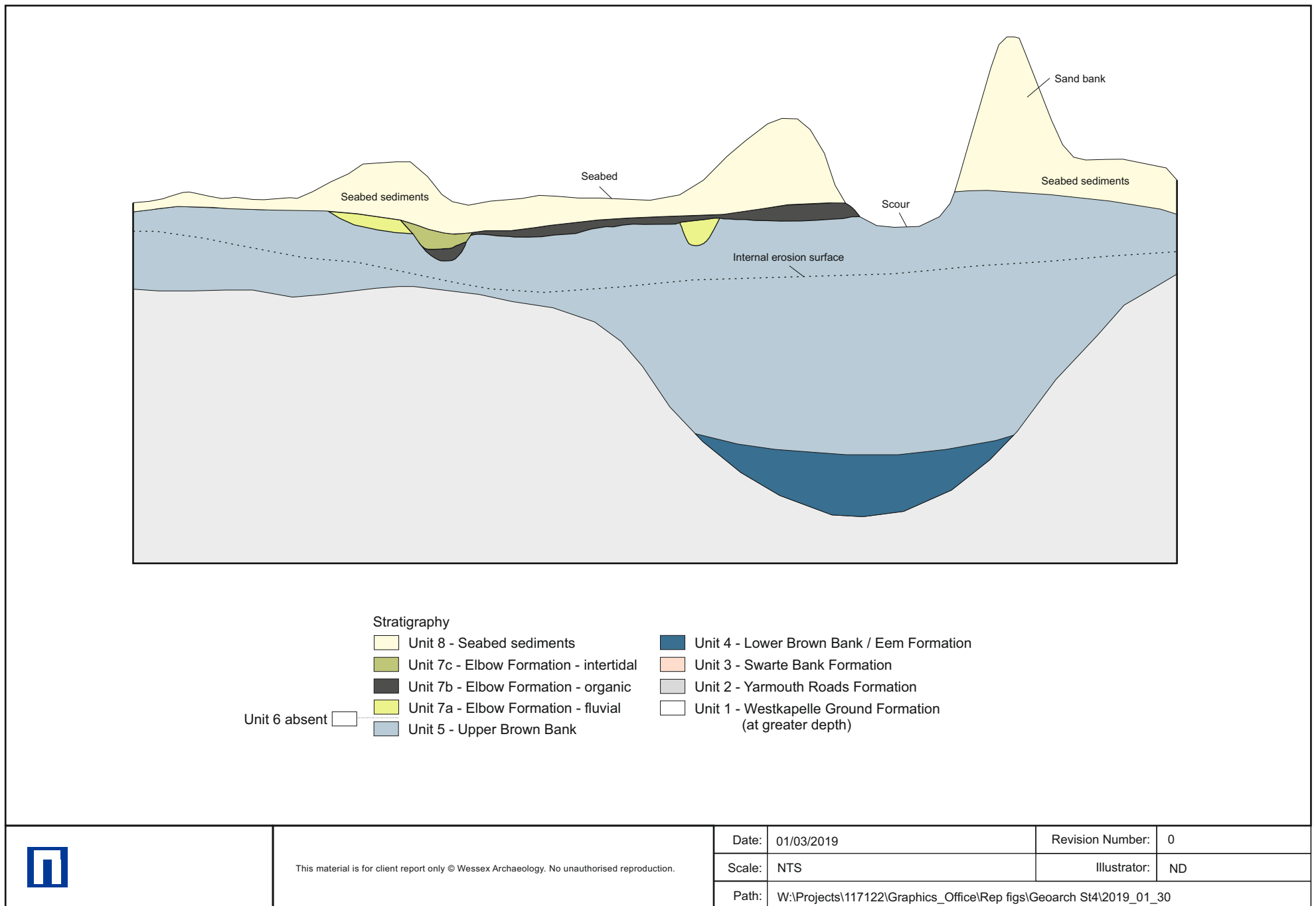
Date:	18/03/2019	Revision Number:	1
Scale:	1:400,000 at A3	Illustrator:	KJF
Path:	W:\Projects\117122\GIS\FigsMXD\Geoarch_St4\2019_03_18		



	This material is for client report only © Wessex Archaeology. No unauthorised reproduction.	Date: 01/03/2019	Revision Number: 0
		Scale: NTS	Illustrator: CM/KJF
		Path: W:\Projects\117122\Graphics_Office\Rep figs\Geoarch St4\2019_01_30	

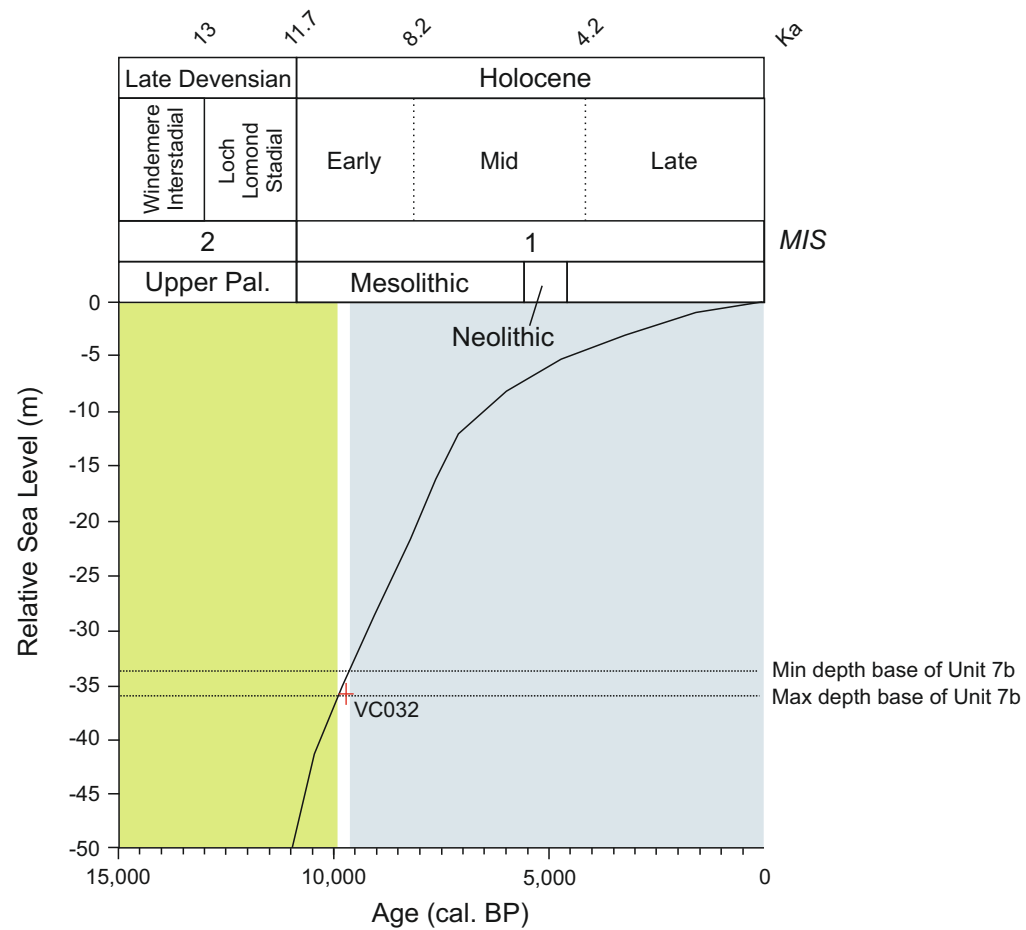
Middle to Upper Palaeolithic sea-level and palaeolandscape history of Norfolk Boreas

Figure 20



Schematic cross section of site stratigraphy (deposit model)

Figure 21



- Norfolk Vanguard West - sub-aerially exposed
- Norfolk Vanguard West - submerged
- + Sea level index point



This material is for client report only © Wessex Archaeology. No unauthorised reproduction.

Date:	01/03/2019	Revision Number:	0
Scale:	NTS	Illustrator:	CM/KJF
Path:	W:\Projects\117122\Graphics_Office\Rep figs\Geoarch St4\2019_01_30		

Upper Palaeolithic to Mesolithic sea-level and palaeolandscape history of Norfolk Boreas

Figure 22



Wessex Archaeology Ltd registered office Portway House, Old Sarum Park, Salisbury, Wiltshire SP4 6EB
Tel: 01722 326867 Fax: 01722 337562 info@wessexarch.co.uk www.wessexarch.co.uk

